EFFECT OF ROCK TRANSVERSE ISOTROPY ON STRESS DISTRIBUTION AND WELLBORE FRACTURE

A Thesis

by

CHUNYANG LU

Submitted to the Office of Graduate Studies of
Texas A&M University
in partial fulfillment of the requirements for the degree of

MASTER OF SCIENCE

Chair of Committee,	Ahmad Ghassemi
Committee Members,	Eduardo Gildin
	Peter P. Valko
	Charles Aubeny
Head of Department,	Daniel Hill

August 2013

Major Subject: Petroleum Engineering

ABSTRACT

Unconventional oil and gas, which is of major interest in petroleum industry, often occur in reservoirs with transversely isotropic rock properties such as shales. Overlooking transverse isotropy may result in deviation in stress distribution around wellbore and inaccurate estimation of fracture initiation pressure which may jeopardize safe drilling and efficient fracturing treatment.

In this work, to help understand the behavior of transversely isotropic reservoirs during drilling and fracturing, the principle of generalized plane-strain finite element formulation of anisotropic poroelastic problems is explained and a finite element model is developed from a plane-strain isotropic poroelastic model. Two numerical examples are simulated and the finite element results are compared with a closed form solution and another FE program. The validity of the developed finite element model is demonstrated. Using the validated finite element model, sensitivity analysis is carried out to evaluate the effects of transverse isotropy ratios, well azimuth, and rock bedding dip on pore pressure and stress distribution around a horizontal well.

The results show that their effect cannot be neglected. The short term pore pressure distribution is sensitive to Young' modulus ratio, while the long term pore pressure distribution is only sensitive to permeability ratio. The total stress distribution generally is not sensitive to transverse isotropy ratios. The effective stress and fracture initiation are very sensitive to Young' modulus ratio. As the well rotates from minimum horizontal in-situ stress to maximum horizontal in-situ stress, the pore pressure and

stress distributions tend to be more unevenly distributed around the wellbore, making the wellbore easier to fracture. The pore pressure and stress distributions tend to "rotate" in correspondence with the rock bedding plane. The fracture initiation potential and position will alter when rock bedding orientation varies.

DEDICATION

I dedicate this thesis to my wife, Hongmin Zhou. Without your encouragement, I would not major in Petroleum Engineering.

To my two lovely daughters, Gina Lu and Lynna Lu. I always enjoy the time playing with you two in my study break.

ACKNOWLEDGEMENTS

I would like to express special thanks to my advisor, Dr. Ahmad Ghassemi, for his motivation, great patience, unlimited support and advice throughout the course of this research. Also my deep acknowledgement to my committee members, Dr. Aubeny, Dr. Gildin, and Dr. Valko, for their guidance in my research and useful comments that helped my thesis.

Special thanks to the Harold Vance Department of Petroleum Engineering faculty and staff for their help whenever I needed it. Thanks also go to Crisman Institute for the sponsorship all these years. I also want to extend my gratitude to my friends and colleagues, Jian, Sonia, Yawei, Kai, Junjing, Jixiang, Jihui, Chun, Alexander and Clotide. You make my time at Texas A&M University a great experience.

Finally, thanks to my mother and father for their unconditional support and to my wife Hongmin Zhou for her patience, encouragement, and love.

NOMENCLATURE

FE	Finite Element
FEA	Finite Element Analysis
FEM	Finite Element Method
GPS	Generalized Plane Strain
DoF	Degree of Freedom
σ_{ij}	Total stress tensor
ε_{ij}	Strain tensor
u_i	Displacement vector,
k_{ij}	Intrinsic permeability, tensor, $k_{ij} = k_{ji}$
α_{ij}	Biot's coefficient, tensor, $\alpha_{ij} = \alpha_{ji}$
δ_{ij}	Kronecker delta tensor,
p	Pore pressure, scalar,
M	Biot's modulus, scalar,
q_i	Specific flux in unit time, vector,
μ	Fluid viscosity, scalar,
ζ	Variation of fluid volume per pore volumn, scalar.
D_{ijkl}	Drained elastic modulus tensor, $D_{ijkl}=D_{klij.}$
E_x, E_y, E_z	Young's moduli in x,y,z direction

v_{xy}, v_{yz}, v_{xz}	Poisson's ratios in xy,yz,xz plane
G_{xy}, G_{yz}, G_{xz}	Shear moduli in xy,yz,xz plane
k_x, k_y, k_z	Permeability in x,y,z directions
$\alpha_x, \alpha_y, \alpha_z$	Biot's coefficient in x,y,z directions
U_i	Arbitrary weighting functions associated with displacements
P	Arbitrary weighting functions associated with pore pressure
Ω	Entire integration domain
Γ	Boundary of domain Ω,
n_i	Outward normal unit vector at boundary Γ.
t_i	Surface traction vector on boundary Γ,
Q	Specific flux in unit time normal to the boundary Γ.
θ	Time step weighting coefficient. $0 \le \theta \le 1$.
X_g, Y_g, Z_g	Axes of the global coordinate system
X_m, Y_m, Z_m	Axes of the material coordinate system
X_w, Y_w, Z_w	Axes of the wellbore coordinate system
$[\lambda]$	Transformation matrix.
$l_{X'}, m_{X'}, n_{X'}$	Direction cosines of axes X' in X,Y,Z coordinate system
$l_{Y'}, m_{Y'}, n_{Y'}$	Direction cosines of axes Y' in X,Y,Z coordinate system
$l_{Z'}, m_{Z'}, n_{Z'}$	Direction cosines of axes Z' in X,Y,Z coordinate system
ϕ_{m1}, ϕ_{m2}, ϕ_{m3}	Angles rotating about z, x, y axes sequentially to transform global coordinate system to material coordinate system

ϕ_{w1}, ϕ_{w2}, ϕ_{w3}	Angles rotating about z, x, y axes sequentially to transform global coordinate system to wellbore coordinate system
p_0	Initial pore pressure
σ_H	Maximum horizontal in-situ stress
σ_h	Minimum horizontal in-situ stress
σ_v	Vertical in-situ stress
p_{mud}	Mud Pressure in wellbore
$\boldsymbol{r}$	Distance to the center of the wellbore
$\boldsymbol{R}$	Radius of the wellbore
$\boldsymbol{t}$	Surface traction vector
$\boldsymbol{n}$	Direction cosine vector of the normal to the plane on which the traction $\boldsymbol{t}$ acts.
$\boldsymbol{\sigma}_{in\text{-}situ}$	In-situ stresses matrix in wellbore coordinate system

TABLE OF CONTENTS

Page

Page

LIST OF FIGURES

Page

Page

Page

Page

Page

Page

Page

Page

LIST OF TABLES

Page

1. INTRODUCTIONAND LITERATURE REVIEW

Unconventional oil and gas have become more and more important in petroleum industry due to the increasing scarcity of conventional oil reserves in the past decades. However, unconventional petroleum resources often occur in anisotropic rocks, which imply directionally dependent properties. Comparing to isotropic cases, anisotropic rock properties can cause difficulty in estimation of the safe mud weight during drilling and the fracture initiation pressure during fracturing treatment. However, nowadays, it is still almost impossible to get all the parameters needed for a general anisotropic analysis from laboratory experiments or field tests. A practical way to consider rock anisotropy is to simplify it to one type of anisotropy - transverse isotropy which works for most laminated sedimentary rocks.

As a special case of anisotropy, a transversely isotropic material has an axis of symmetry which is normal to a plane of isotropy. Material properties on the plane of isotropy are the same in all directions. Take Young's Modulus as an example of directionally dependent properties in transversely isotropic materials. As shown in Fig. 1.1, direction 1 and direction 2 are in the plane of isotropy. Direction 3 is not in the plane of isotropy. Direction 4 is normal to the plane of isotropy. The relation among the Young's Modulus in these four directions (E1, E2, E3, E4) are $E1=E2 \neq E3 \neq E4$.

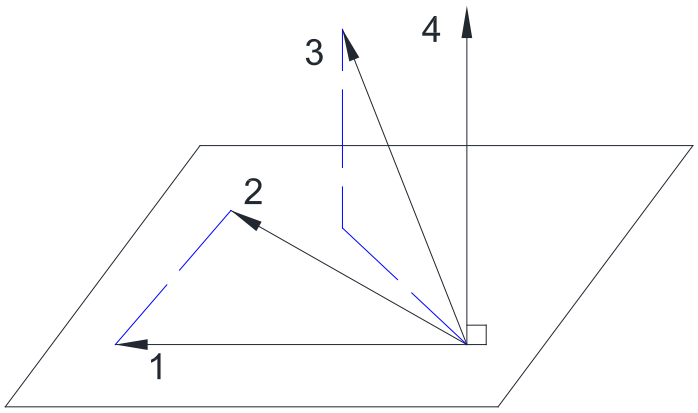

Fig. 1.1 Young's Moduli in different directions in transversely isotropic materials

Properties of most rocks vary with direction, especially for those laminated sedimentary rocks such as shales. For example, the Young's Modulus and permeability of shales are generally lower in the direction perpendicular to the bedding plane than in directions parallel to the bedding plane, which can be treated as a typical transversely isotropic material. In some cases, these directional variations in rock properties have a great influence on stress and pore pressure distribution and thus their effects should be considered. Obert and Duvall (Obert and Duval, 1967) used the Young's Modulus of oil shale, which are 1.8e6 psi perpendicular to the bedding plane and 3.1e6 psi parallel to the bedding plane, to calculate the tangential stress around a wellbore subjected to uniaxial applied stress. Their result shows that when the bedding is normal to the applied stress, the maximum tensile stress is increased by 32%, and the maximum compressive stress is decreased by 9% comparing to the isotropic case. If the applied stress is parallel to the bedding plane, the maximum tensile stress is decreased by 24%, and the maximum compressive stress is increased by 8% comparing to the isotropic case. Overlooking

transverse isotropy may result in deviation in stress distribution around wellbore and inaccurate estimation of fracture initiation pressure which may jeopardize safe drilling and efficient fracturing treatment.

Because wellbore stress distribution plays the most important role in determining fracture initiation pressure and position, a lot of studies on wellbore stress distribution have been done by scholars around the world. Their work can be generally divided into two categories: the analytical approach and the finite element approach.

The simplest and most widely used analytical solution is done by Kirsch (Kirsch 1898). It works for elastic and isotropic rocks. To take rock anisotropy into account, Amadei and Lekhnitskii solved the stress distribution around inclined boreholes in transversely isotropic rocks (Amadei 1983; Lekhnitskii 1963; Lekhnitskii 1981). Aadnoy provided the solution of stresses around horizontal boreholes drilled in sedimentary rocks (Aadnoy 1989). By examining the influence of pore pressure on the shear, effective compressive and tensile stresses around a borehole, researchers have revealed some critical pore pressure effects in rock mechanics (Cheng, Abousleiman, and Roegiers, 1993). To further consider the pore pressure, Detournay and Cheng solved the poroelastic response of a wellbore in a non-hydrostatic stress field (Detournay and Cheng, 1988). Cui, Cheng and Abousleiman further gave the poroelastic solution for an inclined borehole (Cui, Cheng and Abousleiman 1997a). Abousleiman and Cui provided a poro-elastic closed form solution for pore pressure and stress distribution around a wellbore perpendicular to the plane of isotropy drilled in transversely isotropic rock (Abousleiman and Cui 1998). Ghassemi, Diek, Roegiers and Tao also provided solutions

for stress distribution around a borehole (Ghassemi, Diek and Roegiers, 1998; Tao and Ghassemi, 2010).

Cui, Kaliakin, Abousleiman and Cheng developed a poroelastic generalized plane strain finite element model to solve pore pressure and stress distribution around a wellbore drilled in anisotropic rocks (Cui, Kaliakin, Abousleiman, and Cheng, 1997b). Zhou and Ghassemi developed a coupled chemo-poro-thermo-mechanical finite element program and analyzed the effects around a wellbore in swelling shale (Zhou and Ghassemi, 2009). Chen, Chenevert, Sharma and Yu developed of a model for determining wellbore stability considering the effects of mechanical forces and poroelasticity, as well as chemical and thermal effects (Chen, Chenevert, Sharma and Yu, 2003).

Besides studies discussed above, there are also a lot of interesting researches on dual-porosity poroelasticity (Bai, Abousleiman, Cui and Zhang, 1999), in-situ stress determination by hydraulic fracturing (Detournay, Cheng, Roegiers and McLennan, 1989), transversely isotropic poro-visco-elasticity (Hoang and Abousleiman, 2010), anisotropic poro-chemo-electro-elasticity (Tran and Abousleiman, 2013), wellbore stability with anisotropies and weak bedding planes (Zhang, 2013) and poroelastic response under various loading conditions (Kaewjuea, Senjuntichai and Rajapakse, 2011; Rémond and Naili, 2005).

In this study, the idea of generalized plane-strain proposed by Cui et al is adopted and the poroelastic plane-strain finite element model proposed by Zhou and Ghassemi is selected as the basis to develop the generalized plane-strain finite element model for

anisotropic poroelastic problems. Based on the newly developed model, rock transverse isotropy ratios, well azimuths, and rock bedding dips are selected as parameters in a sensitivity analysis for their effect on pore pressure and stress distribution around the horizontal well and the fracture initiation potential.

2. FINITE ELEMENT MODELING OF WELLBORE IN POROELASTIC ROCK

In this section, the principle of generalized plane-strain finite element formulation of anisotropic poroelastic problems is explained and a finite element model is developed from a plane-strain isotropic poroelastic model. Two numerical examples are simulated and the results are compared with a closed form solution and another FE program to demonstrate the validity of the developed finite element model.

2.1. Generalized Plane-Strain Finite Element Formulation of Anisotropic Poroelastic Problems

In this section, the principle of generalized plane-strain finite element formulation of anisotropic poroelastic problems is explained in steps. Firstly, the governing equations for poroelastic anisotropic problems is introduced. Secondly, the definition of generalized plane strain is explained. Thirdly, the weak forms of the governing equations are derived with Galerkin method and the finite element equations are developed. Then a discrete scheme in time domain is derived with Crank-Nicolson type of approximation. Finally, three coordinate systems are introduced to facilitate the parameter input and the transformation of material constants and stresses between different coordinate systems are explained.

2.1.1. Equations of Anisotropic Poroelasticity

The governing equations for poroelastic anisotropic model can be written as (compression positive):

$$\dot{\sigma}_{ij,j} = 0 \quad \text{..... (2.1)}$$

$$\dot{\varepsilon}_{ij} = \frac{1}{2}(\dot{u}_{i,j} + \dot{u}_{j,i}) \quad \text{..... (2.2)}$$

$$\dot{\sigma}_{ij} = D_{ijkl}\dot{\varepsilon}_{kl} + \alpha_{ij}\dot{p} \quad \text{..... (2.3)}$$

$$\dot{\zeta} = \alpha_{ij}\dot{\varepsilon}_{ij} + \frac{\dot{p}}{M} \quad \text{..... (2.4)}$$

$$q_i = -\frac{k_{ij}}{\mu} p_{,j} \quad \text{..... (2.5)}$$

$$\dot{\zeta} = -q_{i,i} \quad \text{..... (2.6)}$$

where

σ_{ij} : total stress tensor, $\sigma_{ij} = \sigma_{ji}$,

ε_{ij} : strain tensor, $\varepsilon_{ij} = \varepsilon_{ji}$,

u_i : displacement vector,

k_{ij} : intrinsic permeability, tensor, $k_{ij} = k_{ji}$,

α_{ij} : Biot's coefficient, tensor, $\alpha_{ij} = \alpha_{ji}$,

δ_{ij} : kronecker delta tensor,

p : pore pressure, scalar,

M: Biot's modulus, scalar,

q_i : specific flux in unit time, vector,

μ :fluid viscosity, scalar,

ζ : variation of fluid volume per pore volumn, scalar,

D_{ijkl} : drained elastic modulus tensor, $D_{ijkl}=D_{klij}$,

the over-dot indicates the time derivative.

2.1.1.1. Anisotropy

For the most general case in anisotropy, D_{ijkl} can be written into matrix form $[D]_{6x6}$ as:

$$[D]_{6\times6} = \begin{bmatrix} D_{1111} & D_{1122} & D_{1133} & D_{1123} & D_{1131} & D_{1112} \\ D_{2211} & D_{2222} & D_{2233} & D_{2223} & D_{2231} & D_{2212} \\ D_{3311} & D_{3322} & D_{3333} & D_{3323} & D_{3331} & D_{3312} \\ D_{2311} & D_{2322} & D_{2333} & D_{2323} & D_{2331} & D_{2312} \\ D_{3111} & D_{3122} & D_{3133} & D_{3123} & D_{3131} & D_{3112} \\ D_{1211} & D_{1222} & D_{1233} & D_{1223} & D_{1231} & D_{1212} \end{bmatrix} \quad \text{..... (2.7)}$$

where $D_{ijkl}=D_{klij}$

Note that the above matrix is symmetric, so the number of independent elastic material constants are 21.

Similarly, k_{ij} can be written into matrix form $[k]_{3x3}$ as:

$$[k]_{3\times3} = \begin{bmatrix} k_{11} & k_{12} & k_{13} \\ k_{21} & k_{22} & k_{23} \\ k_{31} & k_{32} & k_{33} \end{bmatrix} \quad \text{..... (2.8)}$$

where $k_{ij}=k_{ji}$

α_{ij} can be written as:

$$[\alpha]_{3\times3} = \begin{bmatrix} \alpha_{11} & \alpha_{12} & \alpha_{13} \\ \alpha_{21} & \alpha_{22} & \alpha_{23} \\ \alpha_{31} & \alpha_{32} & \alpha_{33} \end{bmatrix} \quad \text{..... (2.9)}$$

Since $\alpha_{ij} = \alpha_{ji}$, α_{ij} can also be written as:

$$[\alpha]_{6\times1} = [\alpha_{11}, \alpha_{22}, \alpha_{33}, \alpha_{12}, \alpha_{23}, \alpha_{13}]^T \quad \text{..... (2.10)}$$

2.1.1.2. Orthotropy

Due to the difficulty to get all 21 parameters from laboratory experiments or field tests, a practical way is to consider rock anisotropy as orthotropy, where the number of independent elastic material constants decrease to 9.For this case, D_{ijkl} can also be written into matrix form [D]. Instead of given [D], the inverse matrix, $[D]^{-1}$ is given hereby for simplicity:

$$[D]^{-1}_{6\times6} = \begin{bmatrix} \frac{1}{E_x} & -\frac{\nu_{yx}}{E_y} & -\frac{\nu_{zx}}{E_z} & 0 & 0 & 0 \\ -\frac{\nu_{xy}}{E_x} & \frac{1}{E_y} & -\frac{\nu_{zy}}{E_z} & 0 & 0 & 0 \\ -\frac{\nu_{xz}}{E_x} & -\frac{\nu_{yz}}{E_y} & \frac{1}{E_z} & 0 & 0 & 0 \\ 0 & 0 & 0 & \frac{1}{G_{xy}} & 0 & 0 \\ 0 & 0 & 0 & 0 & \frac{1}{G_{yz}} & 0 \\ 0 & 0 & 0 & 0 & 0 & \frac{1}{G_{xz}} \end{bmatrix} \quad \text{..... (2.11)}$$

where x, y, z axes coincide with the three principal directions of the material,

$$\frac{\nu_{xy}}{E_x} = \frac{\nu_{yx}}{E_y}, \frac{\nu_{xz}}{E_x} = \frac{\nu_{zx}}{E_z}, \frac{\nu_{yz}}{E_y} = \frac{\nu_{zy}}{E_z}$$

and the 9 independent elastic material constants can be taken as:

E_x, E_y, E_z: Young's moduli in x,y,z direction

ν_{xy}, ν_{yz}, ν_{xz}: Poisson's ratios in xy,yz,xz plane

G_{xy}, G_{yz}, G_{xz}: Shear moduli in xy,yz,xz plane

Similarly, k_{ij} can be written as:

$$[k]_{3\times3} = \begin{bmatrix} k_x & & \\ & k_y & \\ & & k_z \end{bmatrix} \quad \text{..... (2.12)}$$

where k_x, k_y, k_z are permeabilities in x,y,z directions.

α_{ij} can be written as:

$$[\alpha]_{3\times3} = \begin{bmatrix} \alpha_x & & \\ & \alpha_y & \\ & & \alpha_z \end{bmatrix} \quad \text{..... (2.13)}$$

Since $\alpha_{ij} = \alpha_{ji}$, α_{ij} can also be written as:

$$[\alpha]_{6\times1} = [\alpha_x, \alpha_y, \alpha_z, 0, 0, 0]^T \quad \text{..... (2.14)}$$

where $\alpha_x, \alpha_y, \alpha_z$ are Biot's coefficients in x,y,z directions.

2.1.1.3. Transverse Isotropy

The [D] for the transverse isotropy (assume x-y to be the isotropic plane) is the same as for orthotropy but with:

$E_x=E_y$, $v_{xy}=v_{yx}$, $v_{zx}=v_{zy}$, $v_{xz}=v_{yz}$, $G_{xz}=G_{yz}$, $G_{xy} = \dfrac{E_x}{2(1+v_{xy})}$, $k_x= k_y$, $\alpha_x = \alpha_y$

So the number of independent elastic material constants further decreases to 5, which can be taken as E_x, E_z, v_{xy}, v_{yz}, G_{xz}

2.1.2. Definition of Generalized Plane Strain

Consider a poro-elastic column with infinite length and arbitrary cross section. Assume the z-axis is parallel to the length of the infinite long column and x-y plane is

parallel to the cross section. If the material properties, boundary conditions, and initial state do not vary in z direction, we can assume that the stresses, strains and pore pressure are independent of the z coordinate and are functions of x, y and t only:

$$\varepsilon_x = \varepsilon_x(x,y,t), \varepsilon_y = \varepsilon_y(x,y,t), \varepsilon_z = \varepsilon_z(x,y,t)$$

$$\varepsilon_{xy} = \varepsilon_{xy}(x,y,t), \varepsilon_{yz} = \varepsilon_{yz}(x,y,t), \varepsilon_{xz} = \varepsilon_{xz}(x,y,t)$$

$$\sigma_x = \sigma_x(x,y,t), \sigma_y = \sigma_y(x,y,t), \sigma_z = \sigma_z(x,y,t) \quad \text{..... (2.15)}$$

$$\sigma_{xy} = \sigma_{xy}(x,y,t), \sigma_{yz} = \sigma_{yz}(x,y,t), \sigma_{xz} = \sigma_{xz}(x,y,t)$$

$$p = p(x,y,t)$$

Note that the strains in z direction (ε_z, ε_{xz}, ε_{yz}) are not necessarily zero, which is a fundamental difference between classic plane strain problem and generalized plane strain problem.

The displacements in x, y, z direction, u_x, u_y, u_z, are not necessarily functions of x, y and t only. We can derive the admissible form of u_x, u_y, u_z from equation (2.2) and (2.15). The derivation is shown below:

Expand kinematic equation (2.2) in 3D space:

$$\varepsilon_x = \frac{\partial u_x}{\partial x} \quad \text{..... (2.16)}$$

$$\varepsilon_y = \frac{\partial u_y}{\partial y} \quad \text{..... (2.17)}$$

$$\varepsilon_z = \frac{\partial u_z}{\partial z} \quad \text{..... (2.18)}$$

$$\varepsilon_{xy} = \frac{1}{2}\left(\frac{\partial u_x}{\partial y} + \frac{\partial u_y}{\partial x}\right) \quad \text{(2.19)}$$

$$\varepsilon_{yz} = \frac{1}{2}\left(\frac{\partial u_z}{\partial y} + \frac{\partial u_y}{\partial z}\right) \quad \text{(2.20)}$$

$$\varepsilon_{xz} = \frac{1}{2}\left(\frac{\partial u_x}{\partial z} + \frac{\partial u_z}{\partial x}\right) \quad \text{(2.21)}$$

Eliminating u_x, u_y, u_z from above equations, the Saint-Venant compatibility equations can be expressed as:

$$\frac{\partial^2 \varepsilon_x}{\partial y^2} + \frac{\partial^2 \varepsilon_y}{\partial x^2} = 2\frac{\partial^2 \varepsilon_{xy}}{\partial x \partial y} \quad \text{(2.22)}$$

$$\frac{\partial^2 \varepsilon_x}{\partial z^2} + \frac{\partial^2 \varepsilon_z}{\partial x^2} = 2\frac{\partial^2 \varepsilon_{xz}}{\partial x \partial z} \quad \text{(2.23)}$$

$$\frac{\partial^2 \varepsilon_z}{\partial y^2} + \frac{\partial^2 \varepsilon_y}{\partial z^2} = 2\frac{\partial^2 \varepsilon_{zy}}{\partial z \partial y} \quad \text{(2.24)}$$

$$\frac{\partial}{\partial x}\left(-\frac{\partial \varepsilon_{yz}}{\partial x} + \frac{\partial \varepsilon_{xz}}{\partial y} + \frac{\partial \varepsilon_{xy}}{\partial z}\right) = \frac{\partial^2 \varepsilon_x}{\partial y \partial z} \quad \text{(2.25)}$$

$$\frac{\partial}{\partial y}\left(\frac{\partial \varepsilon_{yz}}{\partial x} - \frac{\partial \varepsilon_{xz}}{\partial y} + \frac{\partial \varepsilon_{xy}}{\partial z}\right) = \frac{\partial^2 \varepsilon_y}{\partial x \partial z} \quad \text{(2.26)}$$

$$\frac{\partial}{\partial z}\left(\frac{\partial \varepsilon_{yz}}{\partial x} + \frac{\partial \varepsilon_{xz}}{\partial y} - \frac{\partial \varepsilon_{xy}}{\partial z}\right) = \frac{\partial^2 \varepsilon_z}{\partial x \partial y} \quad \text{(2.27)}$$

Utilizing equations (2.15), compatibility equations (2.33) can be simplified to:

$$\frac{\partial^2 \varepsilon_x}{\partial y^2} + \frac{\partial^2 \varepsilon_y}{\partial x^2} = \frac{\partial^2 \varepsilon_{xy}}{\partial x \partial y} \quad \text{(2.28)}$$

$$\frac{\partial^2 \varepsilon_z}{\partial x^2} = 0 \quad \text{..... (2.29)}$$

$$\frac{\partial^2 \varepsilon_z}{\partial y^2} = 0 \quad \text{..... (2.30)}$$

$$\frac{\partial^2 \varepsilon_{xz}}{\partial x \partial y} = \frac{\partial^2 \varepsilon_{yz}}{\partial x^2} \quad \text{..... (2.31)}$$

$$\frac{\partial^2 \varepsilon_{yz}}{\partial x \partial y} = \frac{\partial^2 \varepsilon_{xz}}{\partial y^2} \quad \text{..... (2.32)}$$

$$\frac{\partial^2 \varepsilon_z}{\partial x \partial y} = 0 \quad \text{..... (2.33)}$$

With compatibility equations (2.29), (2.30), (2.33), the form of ε_z can be narrowed down to: (Cheng 1998)

$$\varepsilon_z = A(t)x + B(t)y + C(t) \quad \text{..... (2.34)}$$

According to equation (2.18), integrating ε_z with respect to z, the displacement in z direction can be expressed as:

$$u_z = [A(t)x + B(t)y + C(t)]z + h(x, y, t) \quad \text{..... (2.35)}$$

Substituting (2.35) into equation (2.21), we have:

$$\varepsilon_{xz}(x, y, t) = \frac{1}{2}\left(\frac{\partial u_x}{\partial z} + A(t)z + \frac{\partial h(x, y, t)}{\partial x}\right) \quad \text{..... (2.36)}$$

Rearrange above equation:

$$\frac{\partial u_x}{\partial z} = -A(t)z + 2\varepsilon_{xz}(x, y, t) - \frac{\partial h(x, y, t)}{\partial x} \quad \text{..... (2.37)}$$

Integrating on both side of the equation with respect to z:

$$u_x = -\frac{A(t)}{2}z^2 + f_1(x,y,t)z + f_2(x,y,t) \quad \text{..... (2.38)}$$

Substituting equation (2.38) into (2.16), according to equation (2.15), we have:

$$\varepsilon_x(x,y,t) = \frac{\partial f_1(x,y,t)}{\partial x}z + \frac{\partial f_2(x,y,t)}{\partial x} \quad \text{..... (2.39)}$$

Apparently, $\frac{\partial f_1(x,y,t)}{\partial x} = 0$. In other words, $f_1(x,y,t)$ should not have any x term. Equation (2.38) should be rewritten as:

$$u_x = -\frac{A(t)}{2}z^2 + f_1(y,t)z + f_2(x,y,t) \quad \text{..... (2.40)}$$

Similarly, we can get:

$$u_y = -\frac{B(t)}{2}z^2 + f_3(x,t)z + f_4(x,y,t) \quad \text{..... (2.41)}$$

Substituting equation (2.40) and (2.41) into (2.19), according to equation (2.15), we have:

$$\varepsilon_{xy}(x,y,t) = \frac{1}{2}(z(\frac{\partial f_1\ (y,t)}{\partial y} + \frac{\partial f_3\ (x,t)}{\partial x}) + \frac{\partial f_2\ (x,y,t)}{\partial y} + \frac{\partial f_4\ (x,y,t)}{\partial x}) \quad \text{..... (2.42)}$$

Apparently, $\frac{\partial f_1(y,t)}{\partial y} + \frac{\partial f_3(x,t)}{\partial x} = 0$. In other words, the order of y term in $f_1(y,t)$ and the order of x term in $f_3(x,t)$ should not greater than one. The form of $f_1(y,t)$ and $f_3(x,t)$ should be:

$$f_1(y,t) = -D(t)y + F(t) \quad \text{..... (2.43)}$$

$$f_3(x,t) = D(t)x + H(t) \quad \text{..... (2.44)}$$

Substituting equations (2.43) and (2.44) into equations (2.40) and (2.41), respectively, the displacement in x, y direction can be expressed as:

$$u_x = -\frac{A(t)}{2} z^2 - D(t) yz + F(t) z + f(x, y, t) \quad \text{..... (2.45)}$$

$$u_y = -\frac{B(t)}{2} z^2 + D(t) xz + H(t) z + g(x, y, t) \quad \text{..... (2.46)}$$

Equations (2.35), (2.45) and (2.46) are the general form of equations for displacement in x, y, z direction in generalized plane strain problems. It can be shown that (Cheng 1998) A and B represent pure bending, C represents uniaxial loading, D represents torsion, F and H represent pure shear, h represents warping, f and g represent classic plane strain deformation (see Fig. 2.1 for illustration). Note that due to the lack of the volumetric deformation, the torsion, pure shear and warping will not generate pore pressure variation and the solution is purely elastic other than poroelastic.

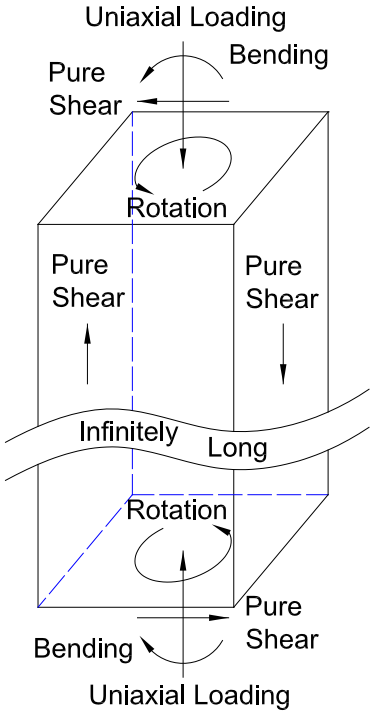

Fig. 2.1 A generalized plane strain geometry and the meaning of the constants in the general form of displacement equations

Furthermore, if A, B, C, D, E, F and H are time independent, which is common in geomechanical problems, the corresponding pure bending, uniaxial loading, torsion, pure shear can be treated as initial state and A, B, C, D, E, F, H can be treated as zero in incremental solution scheme:

$$\dot{u}_x = \frac{\partial u_x}{\partial t} = \frac{\partial f(x,y,t)}{\partial t} = \dot{u}_x(x,y,t) \quad \text{..... (2.47)}$$

$$\dot{u}_y = \frac{\partial u_y}{\partial t} = \frac{\partial g(x,y,t)}{\partial t} = \dot{u}_y(x,y,t) \quad \text{..... (2.48)}$$

$$\dot{u}_z = \frac{\partial u_z}{\partial t} = \frac{\partial h(x,y,t)}{\partial t} = \dot{u}_z(x,y,t) \quad \text{..... (2.49)}$$

2.1.3. Derivation of the Weak Form of Weighted Residual Statement of Governing Equations

Substitute equation (2.6) into equation (2.4):

$$q_{i,i} + \alpha_{ij}\dot{\varepsilon}_{ij} + \frac{\dot{p}}{M} = 0 \quad \text{..... (2.50)}$$

Assume U_i and P to be arbitrary weighting functions associated with displacements and pore pressure, respectively. Multiplying U_i with equation (2.1) and P with equation (2.50), and integrating over the entire domain Ω, we can get the equivalent integral form of equation (2.1) and (2.50):

$$\int_\Omega U_i \dot{\sigma}_{ij,j} d\Omega = 0 \quad \text{..... (2.51)}$$

$$\int_\Omega P(q_{i,i} + \alpha_{ij}\dot{\varepsilon}_{ij} + \frac{\dot{p}}{M}) d\Omega = 0 \quad \text{..... (2.52)}$$

The equation for integrating multivariate functions by parts is:

$$\int_\Omega u_{,i} v d\Omega = \int_\Gamma uvn_i d\Gamma - \int_\Omega uv_{,i} d\Omega \quad \text{..... (2.53)}$$

where Γ is the boundary of domain Ω, n_i is the outward normal unit vector at boundary Γ.

Expand equation (2.51):

$$\int_\Omega U_1\dot{\sigma}_{1j,j} + U_2\dot{\sigma}_{2j,j} + U_3\dot{\sigma}_{3j,j} d\Omega = 0 \quad \text{..... (2.54)}$$

Apply equation (2.53) to integrate equation (2.54) by parts:

$$\int_\Gamma (U_1\dot{\sigma}_{1j}n_j + U_2\dot{\sigma}_{2j}n_j + U_3\dot{\sigma}_{3j}n_j) d\Gamma - \int_\Omega U_{1,j}\dot{\sigma}_{1j} + U_{2,j}\dot{\sigma}_{2j} + U_{3,j}\dot{\sigma}_{3j} d\Omega = 0 \quad \text{..... (2.55)}$$

Simplify equation (2.55):

$$\int_\Gamma U_i \dot{\sigma}_{ij} n_j d\Gamma - \int_\Omega U_{i,j} \dot{\sigma}_{ij} d\Omega = 0 \quad \text{..... (2.56)}$$

Note that $\sigma_{ij} = \sigma_{ji}$,

$$U_{i,j}\dot{\sigma}_{ij} = \frac{1}{2}U_{i,j}\dot{\sigma}_{ij} + \frac{1}{2}U_{i,j}\dot{\sigma}_{ij} = \frac{1}{2}U_{i,j}\dot{\sigma}_{ij} + \frac{1}{2}U_{j,i}\dot{\sigma}_{ji}$$

$$= \frac{1}{2}U_{i,j}\dot{\sigma}_{ij} + \frac{1}{2}U_{j,i}\dot{\sigma}_{ij} = \frac{1}{2}(U_{i,j} + U_{j,i})\dot{\sigma}_{ij} \quad \text{..... (2.57)}$$

In light of equation (2.57), equation (2.56) can be rewritten as:

$$\int_\Gamma U_i \dot{\sigma}_{ij} n_j d\Gamma - \int_\Omega \frac{1}{2}(U_{i,j} + U_{j,i})\dot{\sigma}_{ij} d\Omega = 0 \quad \text{..... (2.58)}$$

Similarly, apply integration by parts to the first term of equation (2.52)

$$\int_\Gamma P q_i n_i d\Gamma + \int_\Omega (-P_{,i} q_i + P\alpha_{ij}\dot{\varepsilon}_{ij} + P\frac{\dot{p}}{M})d\Omega = 0 \quad \text{..... (2.59)}$$

Substitute equation (2.3) and (2.5) into equations (2.58) and (2.59) and rearrange:

$$\int_\Omega \frac{1}{2}(U_{i,j} + U_{j,i})D_{ijkl}\dot{\varepsilon}_{kl} d\Omega + \int_\Omega \frac{1}{2}(U_{i,j} + U_{j,i})\alpha_{ij}\dot{p} d\Omega - \int_\Gamma U_i \dot{\sigma}_{ij} n_j d\Gamma = 0 \quad \text{..... (2.60)}$$

$$\int_\Omega (-P_{,i}\frac{k_{ij}}{\mu} p_{,j} - P\alpha_{ij}\dot{\varepsilon}_{ij} - P\frac{\dot{p}}{M})d\Omega - \int_\Gamma P q_i n_i d\Gamma = 0 \quad \text{..... (2.61)}$$

On boundary Γ, we have:

$$t_i = \sigma_{ij} n_j \quad \text{..... (2.62)}$$

$$Q = q_i n_i \quad \text{..... (2.63)}$$

where

Γ is the boundary of domain Ω,

n_i is the outward normal unit vector at boundary Γ.

t_i is surface traction vector on boundary Γ,

Q is specific flux in unit time normal to the boundary Γ.

Substitute equation (2.62) and (2.63) into equations (2.60) and (2.61), we have:

$$\int_\Omega \frac{1}{2}(U_{i,j}+U_{j,i})D_{ijkl}\dot{\varepsilon}_{kl}d\Omega + \int_\Omega \frac{1}{2}(U_{i,j}+U_{j,i})\alpha_{ij}\dot{p}d\Omega - \int_\Gamma U_i \dot{t}_i d\Gamma = 0 \quad \text{..... (2.64)}$$

$$\int_\Omega (-P_{,i}\frac{k_{ij}}{\mu}p_{,j} - P\alpha_{ij}\dot{\varepsilon}_{ij} - P\frac{\dot{p}}{M})d\Omega - \int_\Gamma PQd\Gamma = 0 \quad \text{..... (2.65)}$$

2.1.4. Development of Finite Element Equations

Equation (2.2) can be expressed in matrix formation (Smith and Griffiths, 2004):

$$[\varepsilon]_{6\times1} = [A]_{6\times3}[u]_{3\times1} \quad \text{..... (2.66)}$$

where the subscript indicates the dimension of the matrix,

$$[\varepsilon]_{6\times1} = \begin{bmatrix} \varepsilon_x \\ \varepsilon_y \\ \varepsilon_z \\ \gamma_{xy} \\ \gamma_{yz} \\ \gamma_{xz} \end{bmatrix}, \; [A]_{6\times3} = \begin{bmatrix} \partial/\partial x & 0 & 0 \\ 0 & \partial/\partial y & 0 \\ 0 & 0 & \partial/\partial z \\ \partial/\partial y & \partial/\partial x & 0 \\ 0 & \partial/\partial z & \partial/\partial y \\ \partial/\partial z & 0 & \partial/\partial x \end{bmatrix}, \; [u]_{3\times1} = \begin{bmatrix} u_x \\ u_y \\ u_z \end{bmatrix}$$

$p_{,i}$ in Equation (2.5) can be expressed in matrix formation:

$$p_{,i} = \nabla p = \begin{bmatrix} \dfrac{\partial}{\partial x} \\ \dfrac{\partial}{\partial y} \\ \dfrac{\partial}{\partial z} \end{bmatrix}_{3\times1} p \quad \text{..... (2.67)}$$

The displacement and pore pressure are discretized independently as follows:

$$[u]_{3\times1} \cong [S_u]_{3\times3n_u}[\hat{u}]_{3n_u\times1} \quad \text{..... (2.68)}$$

$$p \cong [S_p]_{1\times n_p}[\hat{p}]_{n_p\times1} \quad \text{..... (2.69)}$$

where the subscript indicates the dimension of the matrix,

$[u]_{3\times1} = [u_x, u_y, u_z]^T$

u_x, u_y, u_z are the x, y, z displacements at a certain position in a given element,

$[\hat{u}]_{3n_u\times1} = [\hat{u}_x^1, \hat{u}_y^1, \hat{u}_z^1, \hat{u}_x^2, \hat{u}_y^2, \hat{u}_z^2, ..., \hat{u}_x^{n_u}, \hat{u}_y^{n_u}, \hat{u}_z^{n_u}]^T$,

$\hat{u}_x^i, \hat{u}_y^i, \hat{u}_z^i$ are the x, y, z displacements of node i in a given element,

n_u is the number of nodes with displacement DOFs in a given element,

p is the pore pressure at a certain position in a given element,

$[\hat{p}]_{n_p \times 1} = [\hat{p}^1, \hat{p}^2, ..., \hat{p}^{n_p}]^T$

$\hat{p}^i$ is the pore pressure of node i in a given element,

n_p is the number of nodes with pore pressure DOF in a given element,

$$[S_u]_{3\times 3n_u} = \begin{bmatrix} N_u^1 & 0 & 0 & N_u^2 & 0 & 0 & ... & N_u^{n_u} & 0 & 0 \\ 0 & N_u^1 & 0 & 0 & N_u^2 & 0 & ... & 0 & N_u^{n_u} & 0 \\ 0 & 0 & N_u^1 & 0 & 0 & N_u^2 & ... & 0 & 0 & N_u^{n_u} \end{bmatrix},$$

N_u^i is the shape function on node i for displacements discretization,

$[S_p]_{1\times n_p} = [N_p^1, N_p^2, ..., N_p^{n_p}]$,

N_p^i is the shape function on node i for pore pressure discretization.

Generally, N_u^i and N_p^i are functions of coordinate x, y, z for a 3D problem. However, for generalized plane strain problem, if incremental solution scheme is adopted and bending, torsion, pure shear, uniaxial loading are constant or can be neglected, N_u^i and N_p^i can be treated as functions of x, y only and independent of z. The shape functions work for classic plane strain problems still applies here.

Substitute equation (2.68) into (2.66),

$$[\varepsilon]_{6\times 1} \cong [B_u]_{6\times 3n_u} [\hat{u}]_{3n_u \times 1} \quad \text{..... (2.70)}$$

where

the subscript indicates the dimension of the matrix,

$$[B_u]_{6\times 3n_u} = [A]_{6\times 3}[S_u]_{3\times 3n_u}$$

$$= \begin{bmatrix} \frac{\partial N_u^1}{\partial x} & & & \frac{\partial N_u^2}{\partial x} & & & \cdots & \frac{\partial N_u^{n_u}}{\partial x} & 0 & 0 \\ & \frac{\partial N_u^1}{\partial y} & & & \frac{\partial N_u^2}{\partial y} & & \cdots & 0 & \frac{\partial N_u^{n_u}}{\partial y} & 0 \\ & & \frac{\partial N_u^1}{\partial z} & & & \frac{\partial N_u^2}{\partial z} & \cdots & 0 & 0 & \frac{\partial N_u^{n_u}}{\partial z} \\ \frac{\partial N_u^1}{\partial y} & \frac{\partial N_u^1}{\partial x} & & \frac{\partial N_u^2}{\partial y} & \frac{\partial N_u^2}{\partial x} & & \cdots & \frac{\partial N_u^{n_u}}{\partial y} & \frac{\partial N_u^{n_u}}{\partial x} & 0 \\ & \frac{\partial N_u^1}{\partial z} & \frac{\partial N_u^1}{\partial y} & & \frac{\partial N_u^2}{\partial z} & \frac{\partial N_u^2}{\partial y} & \cdots & 0 & \frac{\partial N_u^{n_u}}{\partial z} & \frac{\partial N_u^{n_u}}{\partial y} \\ \frac{\partial N_u^1}{\partial z} & & \frac{\partial N_u^1}{\partial x} & \frac{\partial N_1^x}{\partial z} & & \frac{\partial N_u^2}{\partial x} & \cdots & \frac{\partial N_u^{n_u}}{\partial z} & 0 & \frac{\partial N_u^{n_u}}{\partial x} \end{bmatrix}$$

Note that N_u^i is independent of z, so $\frac{\partial N_u^i}{\partial z}$=0, $[B_u]_{6\times 3n_u}$ can be simplified to:

$$[B_u]_{6\times 3n_u} = \begin{bmatrix} \frac{\partial N_u^1}{\partial x} & & & \frac{\partial N_u^2}{\partial x} & & & \cdots & \frac{\partial N_u^{n_u}}{\partial x} & 0 & 0 \\ & \frac{\partial N_u^1}{\partial y} & & & \frac{\partial N_u^2}{\partial y} & & \cdots & 0 & \frac{\partial N_u^{n_u}}{\partial y} & 0 \\ & & 0 & & & 0 & \cdots & 0 & 0 & 0 \\ \frac{\partial N_u^1}{\partial y} & \frac{\partial N_u^1}{\partial x} & & \frac{\partial N_u^2}{\partial y} & \frac{\partial N_u^2}{\partial x} & & \cdots & \frac{\partial N_u^{n_u}}{\partial y} & \frac{\partial N_u^{n_u}}{\partial x} & 0 \\ & 0 & \frac{\partial N_u^1}{\partial y} & & 0 & \frac{\partial N_u^2}{\partial y} & \cdots & 0 & 0 & \frac{\partial N_u^{n_u}}{\partial y} \\ 0 & & \frac{\partial N_u^1}{\partial x} & 0 & & \frac{\partial N_u^2}{\partial x} & \cdots & 0 & 0 & \frac{\partial N_u^{n_u}}{\partial x} \end{bmatrix}$$

Substitute equation (2.69) into (2.67),

$$p_{,i} = \nabla p \cong [B_p]_{3\times n_p}[\hat{p}]_{n_p\times 1} \quad \text{..... (2.71)}$$

where

the subscript indicates the dimension of the matrix,

$$[B_p]_{3\times n_p} = \begin{bmatrix} \frac{\partial}{\partial x} \\ \frac{\partial}{\partial y} \\ \frac{\partial}{\partial z} \end{bmatrix}_{3\times 1} [S_p]_{1\times n_p} = \begin{bmatrix} \frac{\partial N_p^1}{\partial x} & \frac{\partial N_p^2}{\partial x} & \cdots & \frac{\partial N_p^{n_p}}{\partial x} \\ \frac{\partial N_p^1}{\partial y} & \frac{\partial N_p^2}{\partial y} & \cdots & \frac{\partial N_p^{n_p}}{\partial y} \\ \frac{\partial N_p^1}{\partial z} & \frac{\partial N_p^2}{\partial z} & \cdots & \frac{\partial N_p^{n_p}}{\partial z} \end{bmatrix}$$

Note that N_p^i are independent of z, so $\frac{\partial N_p^i}{\partial z}$=0, $[B_p]_{3\times n_p}$ can be simplified to:

$$[B_p]_{3\times n_p} = \begin{bmatrix} \frac{\partial N_p^1}{\partial x} & \frac{\partial N_p^2}{\partial x} & \cdots & \frac{\partial N_p^{n_p}}{\partial x} \\ \frac{\partial N_p^1}{\partial y} & \frac{\partial N_p^2}{\partial y} & \cdots & \frac{\partial N_p^{n_p}}{\partial y} \\ 0 & 0 & \cdots & 0 \\ & & & \end{bmatrix}$$

According to Galerkin method, the arbitrary weighting functions U_i and P are discretized in the same way as the displacement and pore pressure:

$$[U]_{3\times 1} \cong [S_u]_{3\times 3n_u} [\hat{U}]_{3n_u\times 1} \quad \text{..... (2.72)}$$

$$P \cong [S_p]_{1\times n_p} [\hat{P}]_{n_p\times 1} \quad \text{..... (2.73)}$$

Note that $\frac{1}{2}(U_{i,j} + U_{j,i})$ in equation (2.64) is similar to equation (2.2), following the same procedure, we can get:

$$[\delta]_{6\times 1} \cong [B_u]_{6\times 3n_u} [\hat{U}]_{3n_u\times 1} \quad \text{..... (2.74)}$$

where

the subscript indicates the dimension of the matrix,

$$[\delta]_{6\times1} = [\delta_{11}, \delta_{22}, \delta_{33}, \delta_{12}, \delta_{23}, \delta_{13}]\ , \delta_{ij} = \frac{1}{2}(U_{i,j} + U_{j,i})$$

Substitute above equations into equation (2.64) and (2.65), we can obtain

$$[K]_{3n_u\times3n_u}[\dot{\hat{u}}]_{3n_u\times1} + [G]_{3n_u\times n_p}[\dot{\hat{p}}]_{n_p\times1} = [F\ ]_{3n_u\times1} \quad \text{..... (2.75)}$$

$$[G]^T_{n_p\times3n_u}[\dot{\hat{u}}]_{3n_u\times1} + [L]_{n_p\times n_p}[\dot{\hat{p}}]_{n_p\times1} + [H]_{n_p\times n_p}[\hat{p}]_{n_p\times1} = [Q\ ]_{n_p\times1} \quad \text{..... (2.76)}$$

where

$$[K]_{3n_u\times3n_u} = \int_\Omega [B_u]^T_{3n_u\times6}[D]_{6\times6}[B_u]_{6\times3n_u}\, d\Omega$$

$$[G]_{3n_u\times n_p} = -\int_\Omega [B_u]^T_{3n_u\times6}[\alpha]_{6\times1}[S_p]_{1\times n_p}\, d\Omega$$

$$[L]_{n_p\times n_p} = -\int_\Omega \frac{1}{M}[S_p]^T_{n_p\times1}[S_p]_{1\times n_p}\, d\Omega$$

$$[H]_{n_p\times n_p} = -\int_\Omega \frac{1}{\mu}[B_p]^T_{n_p\times3}[k]_{3\times3}[B_p]_{3\times n_p}\, d\Omega$$

$$[F\ ]_{3n_u\times1} = \int_\Gamma [S_u]^T_{3\times3n_u}[\dot{t}]_{3\times1}\, d\Gamma$$

$$[Q\ ]_{n_p\times1} = \int_\Gamma [S_p]^T_{n_p\times1} Q d\Gamma$$

Above is the element stiffness matrix from which the global stiffness matrix is later assembled. Note that sub-matrix [K] is singular which may cause problem in solution. Physically, this is caused by lack of displacement restraint so that the FE model is “free to move”. Proper displacement boundary condition must be introduced before solution.

2.1.5. Discretization in Time Domain

Due to the time-dependency of poro-elastic problems, the Crank-Nicolson type of approximation is adopted to discretize above equations in time domain.

The equations advancing the displacement and pore pressure solutions from t^n to t^{n+1} can be expressed as:

$$[\hat{u}]^{n+1} = [\hat{u}]^n + \Delta[\hat{u}] \quad \text{..... (2.77)}$$

$$[\hat{p}]^{n+1} = [\hat{p}]^n + \Delta[\hat{p}] \quad \text{..... (2.78)}$$

where

the superscript indicates the time step, e.g. $[\hat{u}]^{n+1}$ is the displacement vector at the beginning of t^{n+1},

$\Delta[\hat{u}]$ is the increment of displacement from t^n to t^{n+1},

$\Delta[\hat{p}]$ is the increment of pore pressure from t^n to t^{n+1}.

The increment of displacement and pore pressure from t^n to t^{n+1} can be expressed with a weighted average of the gradients at the beginning and end of the time interval:

$$\Delta[\hat{u}] = \Delta t((1-\theta)\dot{\hat{u}}^n + \theta\dot{\hat{u}}^{n+1}) \quad \text{..... (2.79)}$$

$$\Delta[\hat{p}] = \Delta t((1-\theta)\dot{\hat{p}}^n + \theta\dot{\hat{p}}^{n+1}) \quad \text{..... (2.80)}$$

where

$\Delta t = t^{n+1} - t^n$,

θ is a time step weighting coefficient. $0 \le \theta \le 1$.

$\theta = 0$: Explicit

$\theta = 0.5$: Crank-Nicolson

$\theta = 1$: Fully implicit

the over-dot indicates the time derivative.

Multiplying equation (2.75), (2.76) with $\Delta t(1-\theta)$, we have:

$$\Delta t(1-\theta)([K]_{3n_u\times 3n_u}[\dot{\hat{u}}]^n_{3n_u\times 1}+[G]_{3n_u\times n_p}[\dot{\hat{p}}]^n_{n_p\times 1}) = \Delta t(1-\theta)[F\ ]_{3n_u\times 1} \quad \text{..... (2.81)}$$

$$\Delta t(1-\theta)([G]^T_{n_p\times 3n_u}[\dot{\hat{u}}]^n_{3n_u\times 1}+[L]_{n_p\times n_p}[\dot{\hat{p}}]^n_{n_p\times 1}+[H]_{n_p\times n_p}[\hat{p}]^n_{n_p\times 1}) = \Delta t(1-\theta)[Q\ ]_{n_p\times 1} \quad \text{..... (2.82)}$$

Similarly, multiplying equation (2.75), (2.76) with $\Delta t\theta$, we have:

$$\Delta t\theta([K]_{3n_u\times 3n_u}[\dot{\hat{u}}]^{n+1}_{3n_u\times 1}+[G]_{3n_u\times n_p}[\dot{\hat{p}}]^{n+1}_{n_p\times 1}) = \Delta t\theta[F\ ]_{3n_u\times 1} \quad \text{..... (2.83)}$$

$$\Delta t\theta([G]^T_{n_p\times 3n_u}[\dot{\hat{u}}]^{n+1}_{3n_u\times 1}+[L]_{n_p\times n_p}[\dot{\hat{p}}]^{n+1}_{n_p\times 1}+[H]_{n_p\times n_p}[\hat{p}]^{n+1}_{n_p\times 1}) = \Delta t\theta[Q\ ]_{n_p\times 1} \quad \text{..... (2.84)}$$

Adding equation (2.81) and (2.83), equation (2.82) and (2.84), and substituting equation (2.79) and (2.80) in to eliminate time derivatives, equation (2.75) and (2.76) are discretized in time domain t^n to t^{n+1} as:

$$[K]_{3n_u\times 3n_u}\Delta[\hat{u}]_{3n_u\times 1}+[G]_{3n_u\times n_p}\Delta[\hat{p}]_{n_p\times 1} = \Delta t[F\ ]_{3n_u\times 1} \quad \text{..... (2.85)}$$

$$[G]^T_{n_p\times 3n_u}\Delta[\hat{u}]^n_{3n_u\times 1}+[L]_{n_p\times n_p}\Delta[\hat{p}]_{n_p\times 1}+[H]_{n_p\times n_p}\Delta t([\hat{p}]^n_{n_p\times 1}+\theta\Delta[\hat{p}]_{n_p\times 1}) = \Delta t[Q\ ]_{n_p\times 1} \quad \text{.. (2.86)}$$

The right hand side terms of above equations can be written as:

$$\Delta t[F\ ]_{3n_u\times 1} = \int_\Gamma [S_u]^T_{3\times 3n_u}[\dot{t}]_{3\times 1}\Delta t d\Gamma = \int_\Gamma [S_u]^T_{3\times 3n_u}\Delta[t]_{3\times 1}d\Gamma$$

$$\Delta t[Q\ ]_{n_p\times 1} = \int_\Gamma [S_p]^T_{n_p\times 1}Q\Delta t d\Gamma = \int_\Gamma [S_p]^T_{n_p\times 1}\Delta Q d\Gamma$$

where

$\Delta[t]_{3\times1}$ is the change of surface traction vector on boundary Γ from t^n to t^{n+1},

ΔQ is the change of specific flux normal to the boundary Γ from t^n to t^{n+1}.

Marking $\Delta t[F\ ]_{3n_u\times1}$, $\Delta t[Q\ ]_{n_p\times1}$ as $\Delta[F\ ]_{3n_u\times1}$, $\Delta[Q\ ]_{n_p\times1}$ respectively, and rearranging equation (2.85) and (2.86) into matrix form, we have the incremental solution scheme from t^n to t^{n+1}:

$$\begin{bmatrix} [K]_{3n_u\times3n_u} & [G]_{3n_u\times n_p} \\ [G]^T_{n_p\times3n_u} & [L]_{n_p\times n_p}+\theta\Delta t[H]_{n_p\times n_p} \end{bmatrix} \begin{Bmatrix} \Delta[\hat{u}]_{3n_u\times1} \\ \Delta[\hat{p}]_{n_p\times1} \end{Bmatrix} = \begin{Bmatrix} \Delta F_{3n_u\times1} \\ \Delta Q_{n_p\times1}-\Delta t[H]_{n_p\times n_p}[\hat{p}]^n_{n_p\times1} \end{Bmatrix} \quad \text{..... (2.87)}$$

where,

$$[K]_{3n_u\times3n_u}=\int_\Omega [B_u]^T_{3n_u\times6}[D]_{6\times6}[B_u]_{6\times3n_u}\,d\Omega$$

$$[G]_{3n_u\times n_p}=-\int_\Omega [B_u]^T_{3n_u\times6}[\alpha]_{6\times1}[S_p]_{1\times n_p}\,d\Omega$$

$$[L]_{n_p\times n_p}=-\int_\Omega \frac{1}{M}[S_p]^T_{n_p\times1}[S_p]_{1\times n_p}\,d\Omega$$

$$[H]_{n_p\times n_p}=-\int_\Omega \frac{1}{\mu}[B_p]^T_{n_p\times3}[k]_{3\times3}[B_p]_{3\times n_p}\,d\Omega$$

$$\Delta[F\ ]_{3n_u\times1}=\int_\Gamma [S_u]^T_{3\times3n_u}\Delta[t]_{3\times1}\,d\Gamma$$

$$\Delta[Q\ ]_{n_p\times1}=\int_\Gamma [S_p]^T_{n_p\times1}\Delta Q\,d\Gamma$$

2.1.6. Transformation of Material Constants and Stresses Between Coordinate Systems

As seen in equation (2.11) to (2.14), the material constants such as elastic modulus, permeability and Biot's coefficient are defined in material principal directions. The in-situ stresses are usually given in horizontal and vertical directions. The well can be drilled along arbitrary direction. To clearly present above three sets of directions, three different coordinate systems are defined in this study (Fig. 2.2):

-X_g,Y_g,Z_g is the global coordinate system where the in-situ stresses is defined

-X_m,Y_m,Z_m is the material coordinate system where the material constants are defined.

-X_w,Y_w,Z_w is the wellbore coordinate system whose z-axis the well is drilled along

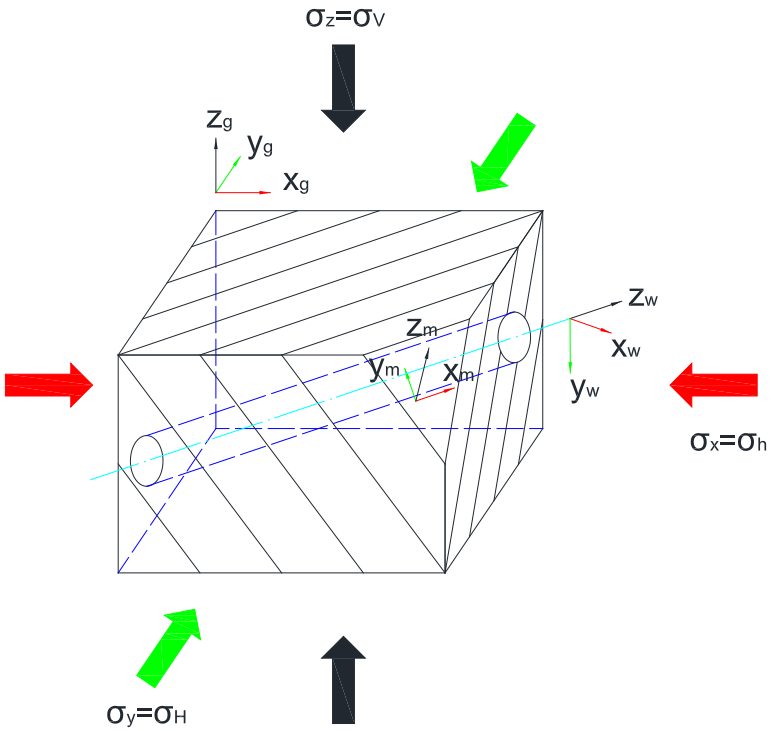

Fig. 2.2 Geometry and coordinate systems setup for borehole problems

Since the orientations of both the rock bedding and the wellbore can be arbitrary, above three sets of coordinate systems generally does not coincide with each other, and the transformation of material constants and stresses is necessary. Due to the nature of generalized plane strain condition, the problem has to be solved under wellbore coordinate system X_w,Y_w,Z_w , which means the in-situ stresses and material constants need to be transformed into wellbore coordinate system X_w,Y_w,Z_w .

The following scheme is made to associate different coordinate systems and convert stress, strain and material constants in different coordinate systems:

The direction cosines of coordinate system X', Y', Z', in X,Y,Z coordinate system can be written in matrix form:

$$[\lambda]=\begin{bmatrix} l_{X'} & m_{X'} & n_{X'} \\ l_{Y'} & m_{Y'} & n_{Y'} \\ l_{Z'} & m_{Z'} & n_{Z'} \end{bmatrix} \quad \text{..... (2.88)}$$

where

$[\lambda]$ is the transformation matrix.

$l_{X'}, m_{X'}, n_{X'}$ is the direction cosines of axes X' in X,Y,Z coordinate system

$l_{X'}=\cos(X,X')$, $m_{X'}=\cos(Y,X')$, $n_{X'}=\cos(Z,X')$

$l_{Y'}, m_{Y'}, n_{Y'}$ is the direction cosines of axes Y' in X,Y,Z coordinate system

$l_{Y'}=\cos(X,X')$, $m_{Y'}=\cos(Y,X')$, $n_{Y'}=\cos(Z,X')$

$l_{Z'}, m_{Z'}, n_{Z'}$ is the direction cosines of axes Z' in X,Y,Z coordinate system

$l_{Z'}=\cos(X,X')$, $m_{Z'}=\cos(Y,X')$, $n_{Z'}=\cos(Z,X')$

It can be proved that $[\lambda]$ is orthogonal matrix, which means following equation holds:

$$[\lambda]^T = [\lambda]^{-1} \quad \text{..... (2.89)}$$

The stress, strain, permeability, Biot's coefficient in X', Y', Z' and X,Y,Z coordinate systems have following relation:

$$[\sigma]'_{3\times3} = [\lambda][\sigma]_{3\times3}[\lambda]^T \quad \text{..... (2.90)}$$

$$[\sigma]_{3\times3} = [\lambda]^T[\sigma]'_{3\times3}[\lambda] \quad \text{..... (2.91)}$$

$$[\varepsilon]'_{3\times3} = [\lambda][\varepsilon]_{3\times3}[\lambda]^T \quad \text{..... (2.92)}$$

$$[\varepsilon]_{3\times3} = [\lambda]^T[\varepsilon]'_{3\times3}[\lambda] \quad \text{..... (2.93)}$$

$$[k]'_{3\times3} = [\lambda][k]_{3\times3}[\lambda]^T \quad \text{..... (2.94)}$$

$$[k]_{3\times3} = [\lambda]^T[k]'_{3\times3}[\lambda] \quad \text{..... (2.95)}$$

$$[\alpha]'_{3\times3} = [\lambda][\alpha]_{3\times3}[\lambda]^T \quad \text{..... (2.96)}$$

$$[\alpha]_{3\times3} = [\lambda]^T[\alpha]'_{3\times3}[\lambda] \quad \text{..... (2.97)}$$

where

$$[\sigma]_{3\times3} = \begin{bmatrix} \sigma_x & \sigma_{xy} & \sigma_{yz} \\ \sigma_{xy} & \sigma_y & \sigma_{xz} \\ \sigma_{yz} & \sigma_{xz} & \sigma_z \end{bmatrix}, \quad [\varepsilon]_{3\times3} = \begin{bmatrix} \varepsilon_x & \varepsilon_{xy} & \varepsilon_{yz} \\ \varepsilon_{xy} & \varepsilon_y & \varepsilon_{xz} \\ \varepsilon_{yz} & \varepsilon_{xz} & \varepsilon_z \end{bmatrix} = \begin{bmatrix} \varepsilon_x & \frac{1}{2}\gamma_{xy} & \frac{1}{2}\gamma_{yz} \\ \frac{1}{2}\gamma_{xy} & \varepsilon_y & \frac{1}{2}\gamma_{xz} \\ \frac{1}{2}\gamma_{yz} & \frac{1}{2}\gamma_{xz} & \varepsilon_z \end{bmatrix}$$

$$[k]_{3\times3}=\begin{bmatrix}k_{11} & k_{12} & k_{13}\\ k_{21} & k_{22} & k_{23}\\ k_{31} & k_{32} & k_{33}\end{bmatrix},\ [\alpha]_{3\times3}=\begin{bmatrix}\alpha_{11} & \alpha_{12} & \alpha_{13}\\ \alpha_{21} & \alpha_{22} & \alpha_{23}\\ \alpha_{31} & \alpha_{32} & \alpha_{33}\end{bmatrix}$$

However, we still need to transform stiffness matrix between different coordinate systems. Expand equation (2.90), (2.92) and rearrange in matrix form, we have:

$$[\sigma]'_{6\times1}=[T_1]_{6\times6}[\sigma]_{6\times1} \quad \text{..... (2.98)}$$

$$[\sigma]_{6\times1}=[T_2]^T_{6\times6}[\sigma]'_{6\times1} \quad \text{..... (2.99)}$$

$$[\varepsilon]'_{6\times1}=[T_2]_{6\times6}[\varepsilon]_{6\times1} \quad \text{..... (2.100)}$$

$$[\varepsilon]_{6\times1}=[T_1]^T_{6\times6}[\varepsilon]'_{6\times1} \quad \text{..... (2.101)}$$

where

$$[\varepsilon]_{6\times1}=\begin{bmatrix}\varepsilon_x\\ \varepsilon_y\\ \varepsilon_z\\ \gamma_{xy}\\ \gamma_{yz}\\ \gamma_{xz}\end{bmatrix},\ [\sigma]_{6\times1}=\begin{bmatrix}\sigma_x\\ \sigma_y\\ \sigma_z\\ \sigma_{xy}\\ \sigma_{yz}\\ \sigma_{xz}\end{bmatrix}$$

$$[T_1]_{6\times6}=\begin{bmatrix}l_{X'}^2 & m_{X'}^2 & n_{X'}^2 & 2l_{X'}m_{X'} & 2m_{X'}n_{X'} & 2n_{X'}l_{X'}\\ l_{Y'}^2 & m_{Y'}^2 & n_{Y'}^2 & 2l_{Y'}m_{Y'} & 2m_{Y'}n_{Y'} & 2n_{Y'}l_{Y'}\\ l_{Z'}^2 & m_{Z'}^2 & n_{Z'}^2 & 2l_{Z'}m_{Z'} & 2m_{Z'}n_{Z'} & 2n_{Z'}l_{Z'}\\ l_{X'}l_{Y'} & m_{X'}m_{Y'} & n_{X'}n_{Y'} & l_{X'}m_{Y'}+l_{Y'}m_{X'} & m_{X'}n_{Y'}+m_{Y'}n_{X'} & n_{X'}l_{Y'}+n_{Y'}l_{X'}\\ l_{Y'}l_{Z'} & m_{Y'}m_{Z'} & n_{Y'}n_{Z'} & l_{Y'}m_{Z'}+l_{Z'}m_{Y'} & m_{Y'}n_{Z'}+m_{Z'}n_{Y'} & n_{Y'}l_{Z'}+n_{Z'}l_{Y'}\\ l_{Z'}l_{X'} & m_{Z'}m_{X'} & n_{Z'}n_{X'} & l_{Z'}m_{X'}+l_{X'}m_{Z'} & m_{Z'}n_{X'}+m_{X'}n_{Z'} & n_{Z'}l_{X'}+n_{X'}l_{Z'}\end{bmatrix}$$

$$[T_2]_{6\times6} = \begin{bmatrix} l_{X'}^2 & m_{X'}^2 & n_{X'}^2 & l_{X'}m_{X'} & m_{X'}n_{X'} & n_{X'}l_{X'} \\ l_{Y'}^2 & m_{Y'}^2 & n_{Y'}^2 & l_{Y'}m_{Y'} & m_{Y'}n_{Y'} & n_{Y'}l_{Y'} \\ l_{Z'}^2 & m_{Z'}^2 & n_{Z'}^2 & l_{Z'}m_{Z'} & m_{Z'}n_{Z'} & n_{Z'}l_{Z'} \\ 2l_{X'}l_{Y'} & 2m_{X'}m_{Y'} & 2n_{X'}n_{Y'} & l_{X'}m_{Y'}+l_{Y'}m_{X'} & m_{X'}n_{Y'}+m_{Y'}n_{X'} & n_{X'}l_{Y'}+n_{Y'}l_{X'} \\ 2l_{Y'}l_{Z'} & 2m_{Y'}m_{Z'} & 2n_{Y'}n_{Z'} & l_{Y'}m_{Z'}+l_{Z'}m_{Y'} & m_{Y'}n_{Z'}+m_{Z'}n_{Y'} & n_{Y'}l_{Z'}+n_{Z'}l_{Y'} \\ 2l_{Z'}l_{X'} & 2m_{Z'}m_{X'} & 2n_{Z'}n_{X'} & l_{Z'}m_{X'}+l_{X'}m_{Z'} & m_{Z'}n_{X'}+m_{X'}n_{Z'} & n_{Z'}l_{X'}+n_{X'}l_{Z'} \end{bmatrix}$$

Note that following equation holds:

$$[T_2]_{6\times6} = [A]_{6\times6}[T_1]_{6\times6}[A]_{6\times6}^{-1} \quad \text{..... (2.102)}$$

where

$$[A]_{6\times6} = \begin{bmatrix} 1 & & & & & \\ & 1 & & & & \\ & & 1 & & & \\ & & & 2 & & \\ & & & & 2 & \\ & & & & & 2 \end{bmatrix}$$

From equation (2.98) and (2.99), it is obvious that:

$$[T_2]_{6\times6}^T = [T_1]_{6\times6}^{-1} \quad \text{..... (2.103)}$$

Substituting $[\sigma]_{6\times1} = [D]_{6\times6}[\varepsilon]_{6\times1}$ and then equation (2.101) into equation (2.98), we can write:

$$[\sigma]'_{6\times1} = [T_1]_{6\times6}[D]_{6\times6}[T_1]_{6\times6}^T[\varepsilon]'_{6\times1} \quad \text{..... (2.104)}$$

So the stiffness matrix in X', Y', Z' coordinate system can be expressed in X,Y,Z coordinate system as:

$$[D]'_{6\times6} = [T_1]_{6\times6}[D]_{6\times6}[T_1]_{6\times6}^T \quad \text{..... (2.105)}$$

Note that equation (2.100), (2.101) is expressed in engineering shear strain. If expressed in shear strain, equation (2.100), (2.101) can be rewritten as:

$$[\varepsilon_\varepsilon]'_{6\times1} = [T_1]_{6\times6}[\varepsilon_\varepsilon]_{6\times1} \quad \text{..... (2.106)}$$

$$[\varepsilon_\varepsilon]_{6\times1} = [T_2]^T_{6\times6}[\varepsilon_\varepsilon]'_{6\times1} \quad \text{..... (2.107)}$$

where

$$[\varepsilon_\varepsilon]_{6\times1} = \begin{bmatrix} \varepsilon_x \\ \varepsilon_y \\ \varepsilon_z \\ \varepsilon_{xy} \\ \varepsilon_{yz} \\ \varepsilon_{xz} \end{bmatrix}$$

Similar to equation (2.104), substituting stress-strain relation and then equation (2.106) or (2.107) into equation (2.98), we can write:

$$[\sigma]'_{6\times1} = [T_1]_{6\times6}[D_\varepsilon]_{6\times6}[T_1]^{-1}_{6\times6}[\varepsilon_\varepsilon]'_{6\times1} = [T_1]_{6\times6}[D_\varepsilon]_{6\times6}[T_2]^T_{6\times6}[\varepsilon_\varepsilon]'_{6\times1} \quad \text{..... (2.108)}$$

where $[D_\varepsilon]_{6\times6}$ is the stiffness matrix coincide with $[\varepsilon_\varepsilon]_{6\times1}$

Similar to equation(2.105), the stiffness matrix in X', Y', Z' coordinate system can be expressed in X,Y,Z coordinate system as:

$$[D_\varepsilon]'_{6\times6} = [T_1]_{6\times6}[D_\varepsilon]_{6\times6}[T_1]^{-1}_{6\times6} = [T_1]_{6\times6}[D_\varepsilon]_{6\times6}[T_2]^T_{6\times6} \quad \text{..... (2.109)}$$

Note that $[\varepsilon_\varepsilon]_{6\times1} \neq [\varepsilon]_{6\times1}$ and $[D_\varepsilon]_{6\times6} \neq [D]_{6\times6}$.Their relation can be expressed as:

$$[\varepsilon_\varepsilon]_{6\times1} = [A]^{-1}_{6\times6}[\varepsilon]_{6\times1} \quad \text{..... (2.110)}$$

$$[D_\varepsilon]_{6\times1} = [D]_{6\times1}[A]_{6\times6} \quad \text{..... (2.111)}$$

Usually, it is not convenient and straightforward to calculate transformation matrix with equation (2.88). Following scheme is applied in this FE code to get transformation matrix from a series of coordinate system rotation.

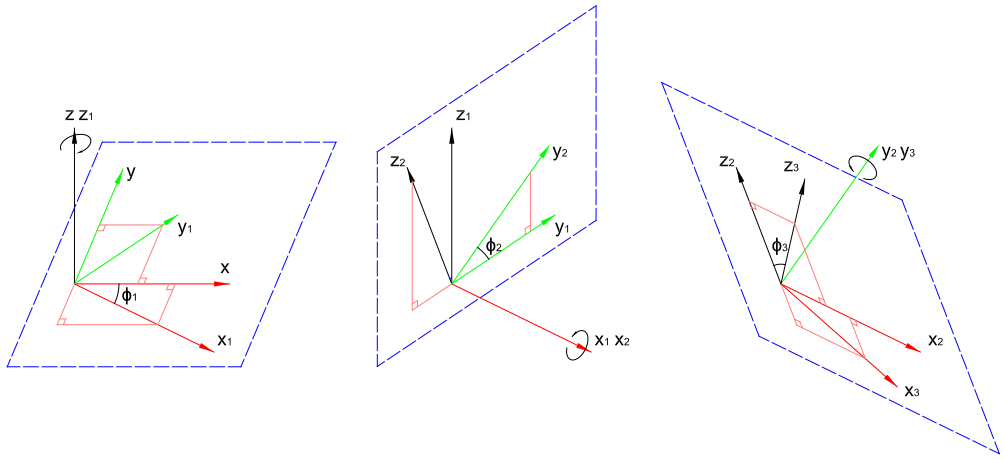

Step1 **Step2** **Step3**

Fig. 2.3 Rotating coordinate system in three steps

As shown in Fig. 2.3, the final transformed axes are achieved by rotating coordinate system about Z, X, Y axes respectively in three sequential steps: first, rotate the original x-y-z axes by an angle (ϕ_1) about the z-axis to obtain a new frame we may call x1-y1-z1. Next, rotate this new frame by an angle (ϕ_2) about the x1 axis to obtain another frame we can call x2-y2-z2. Finally, rotate this frame by an angle (ϕ_3) about the x3 axis to obtain the final frame x3-y3-z3. These three transformations correspond to the following transformation matrix:

$$[\lambda]=\begin{bmatrix}\cos\phi_1 & \sin\phi_1 & 0\\ -\sin\phi_1 & \cos\phi_1 & 0\\ 0 & 0 & 1\end{bmatrix}\begin{bmatrix}1 & 0 & 0\\ 0 & \cos\phi_2 & \sin\phi_2\\ 0 & -\sin\phi_2 & \cos\phi_2\end{bmatrix}\begin{bmatrix}\cos\phi_3 & 0 & \sin\phi_3\\ 0 & 1 & 0\\ -\sin\phi_3 & 0 & \cos\phi_3\end{bmatrix} \quad \text{..... (2.112)}$$

Two sets of rotation angles are specified as input to facilitate the definition of different coordinate systems:

ϕ_{m1}, ϕ_{m2}, ϕ_{m3}: Angles rotating about z, x, y axes sequentially to transform global coordinate system to material coordinate system

ϕ_{w1}, ϕ_{w2}, ϕ_{w3}: Angles rotating about z, x, y axes sequentially to transform global coordinate system to wellbore coordinate system

As mentioned in the beginning of this session, the in-situ stresses and material constants need to be transformed into wellbore coordinate system X_w,Y_w,Z_w .According to equation (2.112) and (2.90), the transformation of in-situ stresses from global coordinate system to wellbore coordinate system can be completed by:

$$[\lambda]_{G2W}=\begin{bmatrix}\cos\phi_{w1} & \sin\phi_{w1} & 0\\ -\sin\phi_{w1} & \cos\phi_{w1} & 0\\ 0 & 0 & 1\end{bmatrix}\begin{bmatrix}1 & 0 & 0\\ 0 & \cos\phi_{w2} & \sin\phi_{w2}\\ 0 & -\sin\phi_{w2} & \cos\phi_{w2}\end{bmatrix}\begin{bmatrix}\cos\phi_{w3} & 0 & \sin\phi_{w3}\\ 0 & 1 & 0\\ -\sin\phi_{w3} & 0 & \cos\phi_{w3}\end{bmatrix} \quad \text{... (2.113)}$$

$$[\sigma]^W_{3\times3}=[\lambda]_{G2W}[\sigma]^G_{3\times3}[\lambda]^T_{G2W} \quad \text{..... (2.114)}$$

The transformation of material constants from material coordinate system to wellbore coordinate system can be treated as two steps: first, transform from material coordinate system to global coordinate system. Then, transform from global coordinate system to wellbore coordinate system. According to equation (2.112), (2.94) and (2.96), the transformation of permeability and Biot's coefficient from material coordinate system to wellbore coordinate system can be completed by:

$$[\lambda]_{G2M} = \begin{bmatrix} \cos\phi_{m1} & \sin\phi_{m1} & 0 \\ -\sin\phi_{m1} & \cos\phi_{m1} & 0 \\ 0 & 0 & 1 \end{bmatrix} \begin{bmatrix} 1 & 0 & 0 \\ 0 & \cos\phi_{m2} & \sin\phi_{m2} \\ 0 & -\sin\phi_{m2} & \cos\phi_{m2} \end{bmatrix} \begin{bmatrix} \cos\phi_{m3} & 0 & \sin\phi_{m3} \\ 0 & 1 & 0 \\ -\sin\phi_{m3} & 0 & \cos\phi_{m3} \end{bmatrix}. \quad (2.115)$$

$$[\lambda]_{M2G} = [\lambda]_{G2M}^{T} \quad (2.116)$$

$$[\lambda]_{M2W} = [\lambda]_{G2W}[\lambda]_{M2G} \quad (2.117)$$

$$[k]_{3\times3}^{W} = [\lambda]_{M2W}[k]_{3\times3}^{M}[\lambda]_{M2W}^{T} \quad (2.118)$$

$$[\alpha]_{3\times3}^{W} = [\lambda]_{M2W}[\alpha]_{3\times3}^{M}[\lambda]_{M2W}^{T} \quad (2.119)$$

The stiffness matrix in wellbore coordinate system can be found by calculating $[T_1]_{6\times6}$ from the elements of $[\lambda]_{M2W}$ and then substituting $[T_1]_{6\times6}$ into equation (2.105).

2.2. Numerical Examples and Verification Using Analytical and Numerical Results

To verify the proposed finite element model, two examples are simulated and the finite element results are compared with a closed form solution and another FE program.

2.2.1. Example I and Verification Using Closed Form Solution

Abousleiman and Cui (Abousleiman and Cui 1998) proposed a closed form solution for an inclined well drilled perpendicular to the isotropic plane of a transversely isotropic poro-elastic formation.

In this section, an example case is simulated using the anisotropic generalized plane-strain model, and the results are compared to above closed form solution provided by Abousleiman and Cui. The pore pressure and stress distribution in the domain near the wellbore are compared.

2.2.1.1. Problem Statement

An inclined well is drilled in transversely isotropic reservoir. The well axis is perpendicular to the isotropic plane. The borehole radius is R=0.1 m.

The loading and geometry are shown in Fig. 2.4. The definition and notation of coordinate systems are the same as described before. The in-situ stresses σ_H, σ_h, σ_v are defined in global coordinate system and thus are also denoted as σ_x^g, σ_y^g, σ_z^g.

The well coordinate system, which denotes the well orientation, is rotated from global coordinate system position following the steps described in section 2.1.6: Assume the well coordinate system initially coincide with the global coordinate system. In first step, rotate the initial well coordinate system an azimuth angle $\phi_{azimuth}$ (which is 30° here) about its z-axis to get a new well coordinate system. In second step, rotate the new well coordinate system a zenith angle ϕ_{zenith} (which is 60° here) about its y axis toward the x_w-axis. The in situ stresses are converted to the well coordinate system and denoted as σ_x^g, σ_y^g, σ_z^g, σ_{xy}^g, σ_{yz}^g, σ_{zx}^g. Since the well is perpendicular to the isotropic plane, the material coordinate system is the same as well coordinate system.

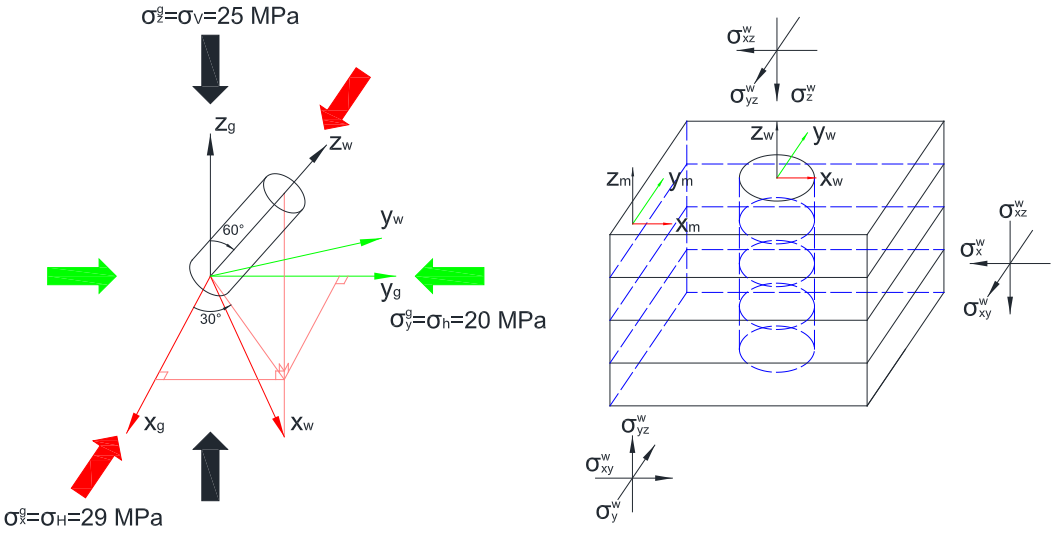

Fig. 2.4 Definition sketch of an inclined borehole problem

The reservoir properties are presented as follows:

Angles rotating about z, x, y axes sequentially to transform global coordinate system to material coordinate system and wellbore coordinate system:

- To material c.s.: ϕ_{m1} =30°, ϕ_{m2}=0°, ϕ_{m3}=-60°
- To wellbore c.s.: ϕ_{w1}=30°, ϕ_{w2}=0°, ϕ_{w3}=-60°

Initial state (in global coordinate system):

- Initial Pore Pressure: p_0=9.8 MPa
- In-situ Stresses: σ_H=29 MPa, σ_h=20 MPa, σ_v=25 MPa
- Mud Pressure: p_{mud}=0 MPa (instantaneous excavation)

Transversely isotropic rock properties (in material coordinate system):

- Biot Coefficient: $\alpha_x=\alpha_y$=0.626, α_z=0.575
- Permeability: $K_x=K_y=K_z$=1.01325e-7 darcy
- Young's Modulus: $E_x=E_y=E_z$ =20.6 GPa

- Poisson's Ratio: $\nu_{xy}=0.189$, $\nu_{yz}=\nu_{zx}=0.378$
- Shear Modulus: $G_{xy}=G_{yz}=G_{zx}= 8.66$ GPa
- Fluid viscosity: $\mu=0.001$Pa.s
- Biot Modulus: M=15.8 GPa

2.2.1.2. Finite Element Model

Fig. 2.5 shows the finite element mesh, which consists of 8000 nodes and 2624 quadrilateral eight-noded elements. To approximate the infinite domain, a square region bounded by x = ± 6 m and y = ± 6 m is used.

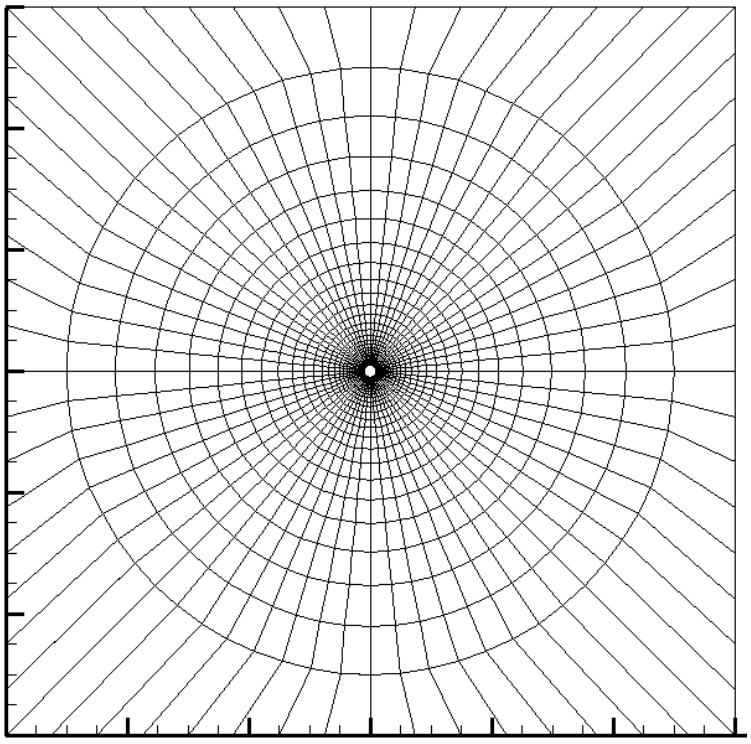

Fig. 2.5 Finite element mesh

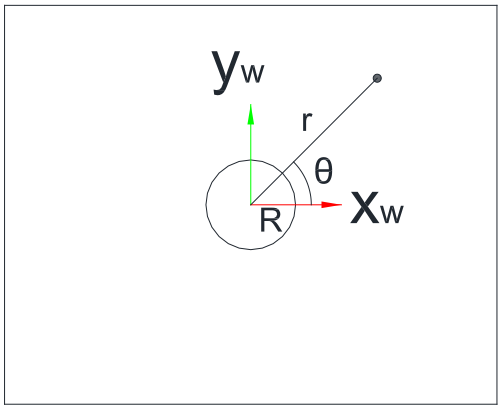

Fig. 2.6 Definition of θ, R and r

The boundary conditions are presented in Table 2.1,

Table 2.1. Boundary Conditions

	Wellbore Wall (r=R)	Infinity/Far Distance (r->∞)
Force/Displacement	T=0: $\boldsymbol{t}=-\boldsymbol{\sigma}_{\text{in-situ}}\,\boldsymbol{n}$ T>0: $\boldsymbol{t}=p_{mud}\,\boldsymbol{n}$	Displacements in x, y and z directions are zero.
Pore Pressure/Flux	T=0: $p=p_0$ T>0: $p=p_{mud}$	No Flow Boundary

where

r: distance to the center of the wellbore, see Fig. 2.6 for the illustration of r,

R: radius of the wellbore,

t: vector, surface traction,

$\boldsymbol{t} = \{t_x, t_y, t_z\}$

n: vector, direction cosines (in wellbore coordinate system) of the normal to the plane on which the traction ***t*** acts.

$\boldsymbol{n} = \{n_x, n_y, n_z\} = \{\cos\theta, \sin\theta, 1\}$

$\boldsymbol{\sigma}_{\text{in-situ}}$: 3x3 matrix, in-situ stresses (in wellbore coordinate system),

$$\boldsymbol{\sigma} = \begin{bmatrix} \sigma_x^w & \sigma_{xy}^w & \sigma_{xz}^w \\ \sigma_{xy}^w & \sigma_y^w & \sigma_{yz}^w \\ \sigma_{xz}^w & \sigma_{yz}^w & \sigma_z^w \end{bmatrix}$$

2.2.1.3. Results

Pore pressure and total stress in different direction near the wellbore at 1 second and 3 days from both finite element analysis and closed form solution are presented for comparison. As seen in Fig. 2.7 and Fig. 2.8, the FEA results make a very good match with closed form solution.

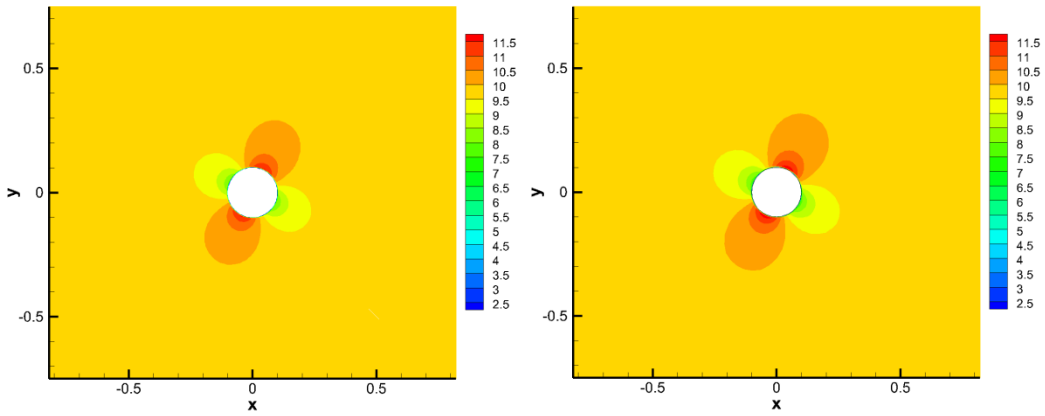

Closed Form Solution **FEA Results**

(a) Pore Pressure

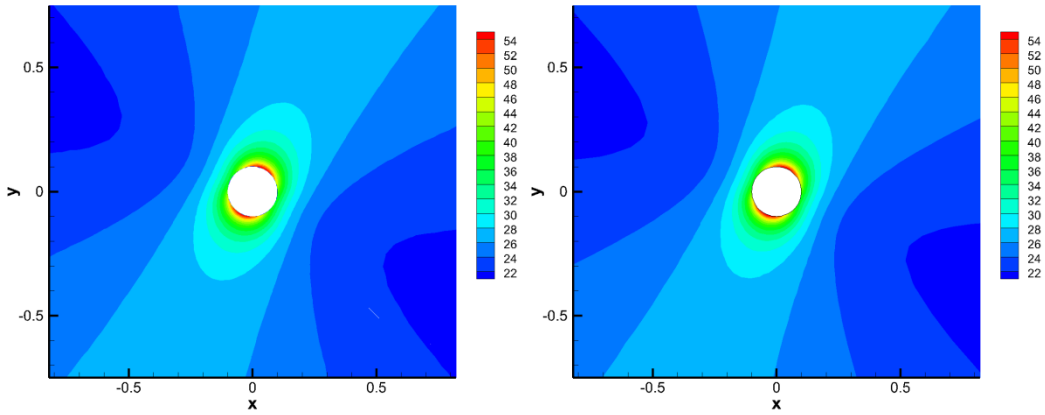

Closed Form Solution **FEA Results**

(b) Tangential Total Stress

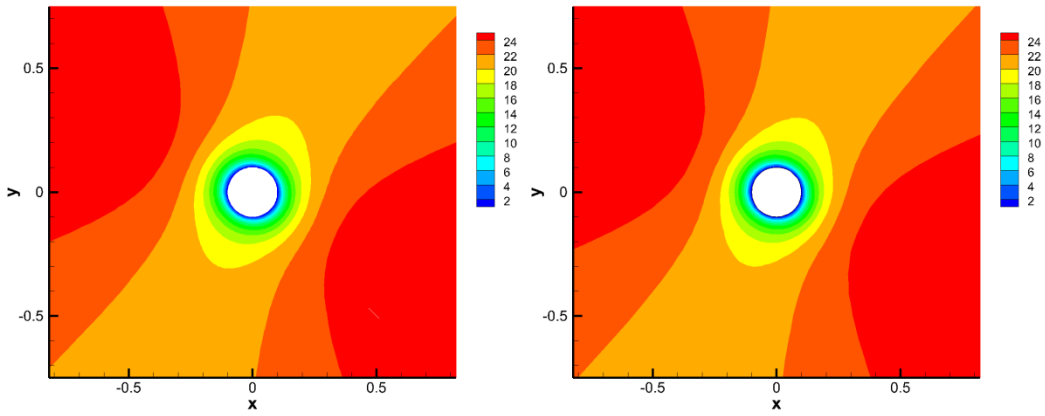

Closed Form Solution **FEA Results**

(c) Radial Total Stress

Fig. 2.7 Results at t=1 second from closed form solution and FEA

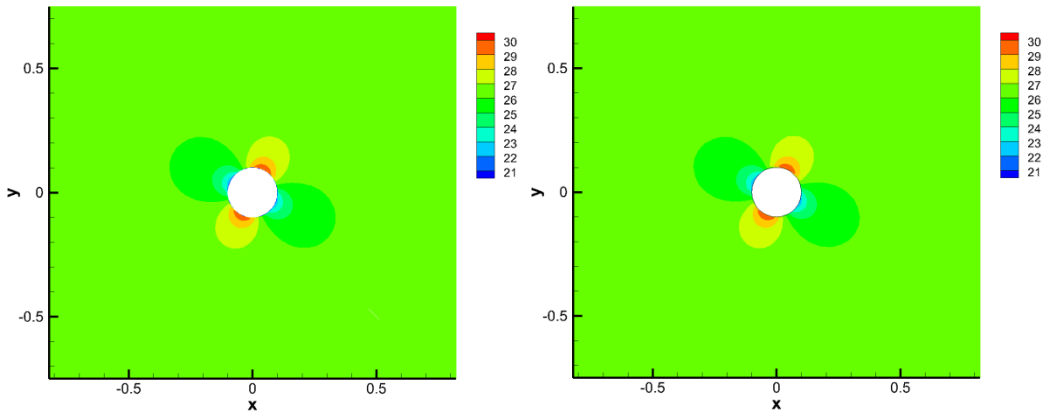

Closed Form Solution **FEA Results**

(d) Z Direction Total Stress

Fig. 2.7 Continued

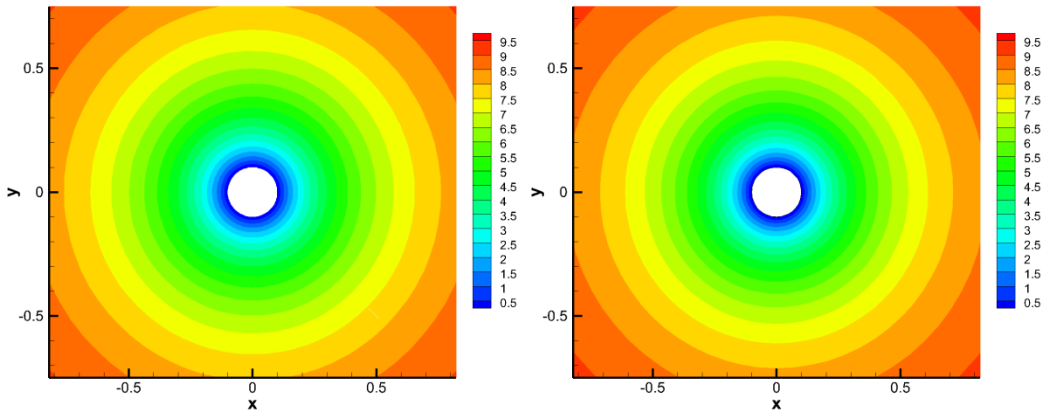

Closed Form Solution **FEA Results**

(a) Pore Pressure

Fig. 2.8 Results at t=3 days from closed form solution and FEA

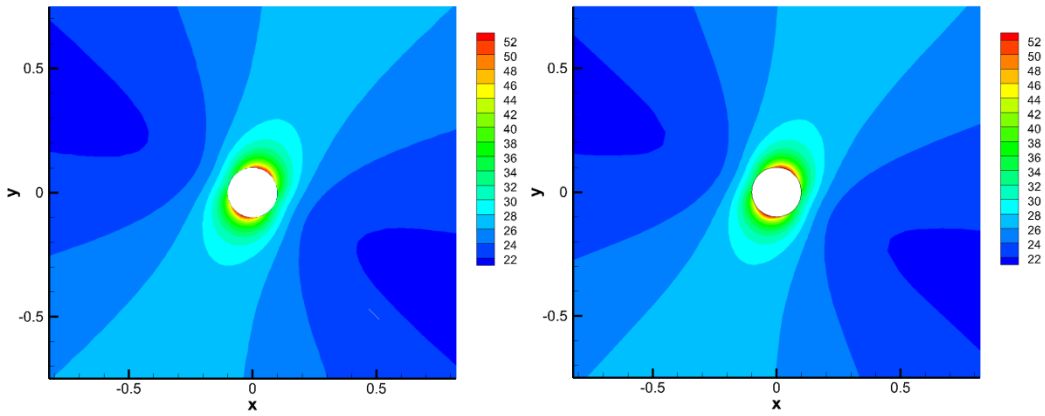

Closed Form Solution **FEA Results**

(b) Tangential Total Stress

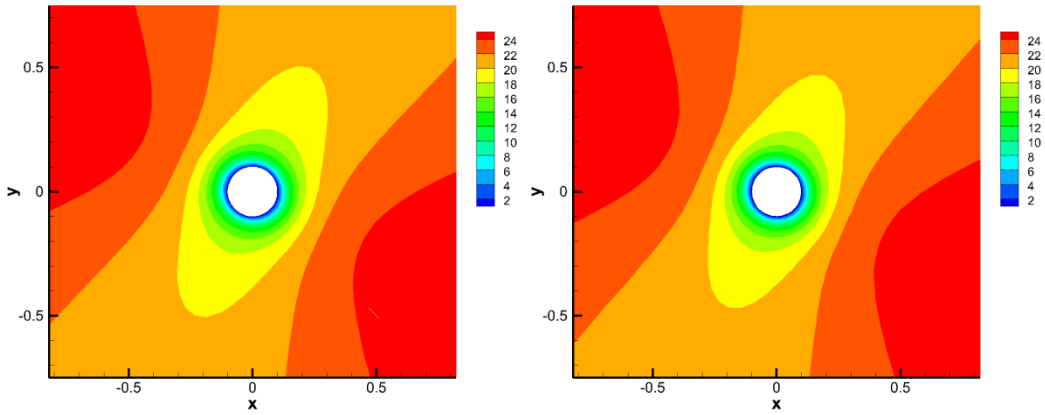

Closed Form Solution **FEA Results**

(c) Radial Total Stress

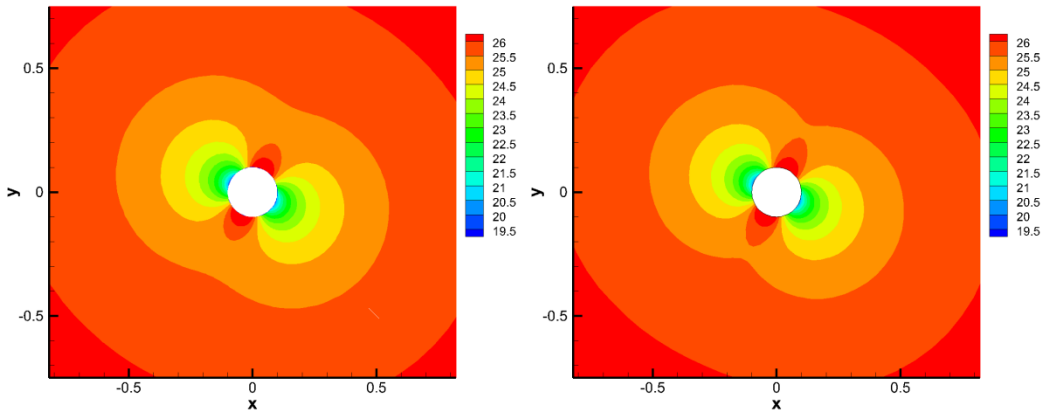

Closed Form Solution **FEA Results**

(d) Z Direction Total Stress

Fig. 2.8 Continued

2.2.2. Example II and Verification Using Finite Element Program

Cui, Kaliakin, Abousleiman, and Cheng (Cui, Cheng, Kaliakin, and Abousleiman 1996, Cui, Kaliakin, Abousleiman, and Cheng, 1997b) investigated an inclined well drilled in anisotropic poroelatic formation with a generalized plane strain finite element they developed. Although the source codes are not released, their simulation results are presented in several published papers.

In this section, another example case is simulated and the results are compared to the results provided by Cui, Kaliakin, Abousleiman, and Cheng. The pore pressure and stress distribution along the 0 degree path and the 90 degree path will be compared.

2.2.2.1. Problem Statement

An inclined well is drilled in transversely isotropic reservoir of which the isotropic plane is horizontal. The borehole radius is R=0.1 m.

The loading and geometry are shown in Fig. 2.9. The definition and notation of coordinate systems are the same as described before. The in-situ stresses σ_H, σ_h, σ_v are defined in global coordinate system and thus are also denoted as σ_x^g, σ_y^g, σ_z^g.

The well is drilled in x_g- z_g plane with an inclination angle of 70°. The well coordinate system, which denotes the well orientation, is rotated from global coordinate system position following the steps described in section 2.1.6: Assume the well coordinate system initially coincide with the global coordinate system. In first step, rotate the initial well coordinate system an azimuth angle $\phi_{azimuth}$ (which is 0° here) about its z-axis to get a new well coordinate system. In second step, rotate the new well coordinate system a zenith angle ϕ_{zenith} (which is 70° here) about its y axis toward the x_w-

axis. The in situ stresses are converted to the well coordinate system and denoted as σ_x^g, σ_y^g, σ_z^g, σ_{xy}^g, σ_{yz}^g, σ_{zx}^g. Since the isotropic plane is horizontal, the material coordinate system is the same as global coordinate system.

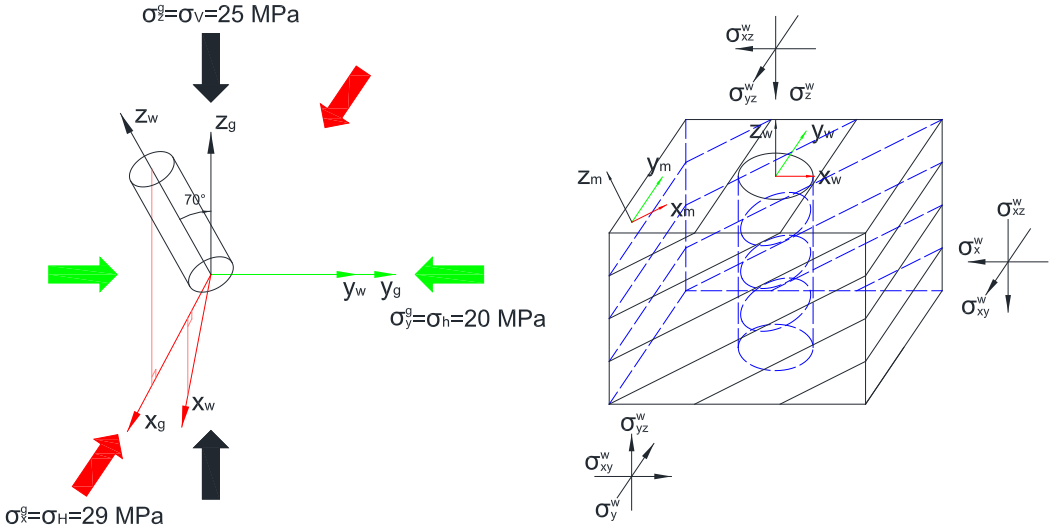

Fig. 2.9 Definition sketch of an inclined borehole problem

The reservoir properties are presented as follows:

Angles rotating about z, x, y axes sequentially to transform global coordinate system to material coordinate system and wellbore coordinate system:

- To material c.s.: ϕ_{m1} =0°, ϕ_{m2}=0°, ϕ_{m3}=0°
- To wellbore c.s.: ϕ_{w1}=0°, ϕ_{w2}=0°, ϕ_{w3}=-70°

Initial state (in global coordinate system):

- Initial Pore Pressure: p_0=10 MPa
- In-situ Stresses: σ_H=29 MPa, σ_h=20 MPa, σ_v=25 MPa

- Mud Pressure: p_{mud}=0 MPa (instantaneous excavation)

Transversely isotropic rock properties (in material coordinate system):

- Biot Coefficient: $\alpha_x=\alpha_y=0.733$, $\alpha_z=0.749$
- Permeability: $K_x=K_y$=1.0e-7 darcy, K_z=1.0e-8 darcy
- Young's Modulus: $E_x=E_y$= 20.6 GPa, E_z =17.3 GPa
- Poisson's Ratio: $\nu_{xy}=0.189$, $\nu_{yz}=\nu_{zx}=0.246$
- Shear Modulus: $G_{xy}=G_{yz}=G_{zx}$= 8.66 GPa
- Fluid viscosity: μ=0.001Pa.s
- Biot Modulus: M=15.8 GPa

The finite element model is the same as example I.

2.2.2.2. Results

Pore pressure, tangential stress, radial stress and z-direction stress along two different radial paths at two different time steps from Cui's model and the model proposed in this thesis are presented for comparison. The two radial paths are at the radial angle θ=5.7° and θ=84.4° respectively (see Fig. 2.6 for the illustration of θ). The selection of the two angles 5.7° and 84.4°, rather than 0° and 90° is dictated by the nodal location of the FE mesh (Cui, Cheng, Kaliakin, and Abousleiman 1996). As seen in Fig. 2.10 to Fig. 2.15, the proposed model in this thesis make a very good match with the FEA results provided by Cui et al.

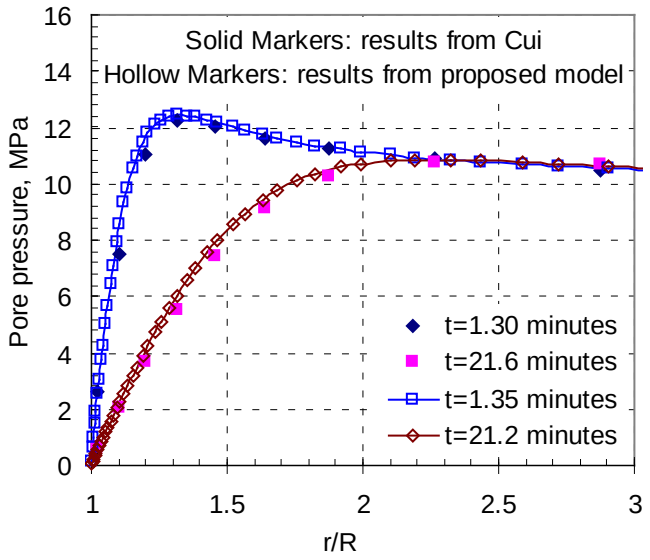

Fig. 2.10 Pore pressure around the wellbore at θ=84.4°

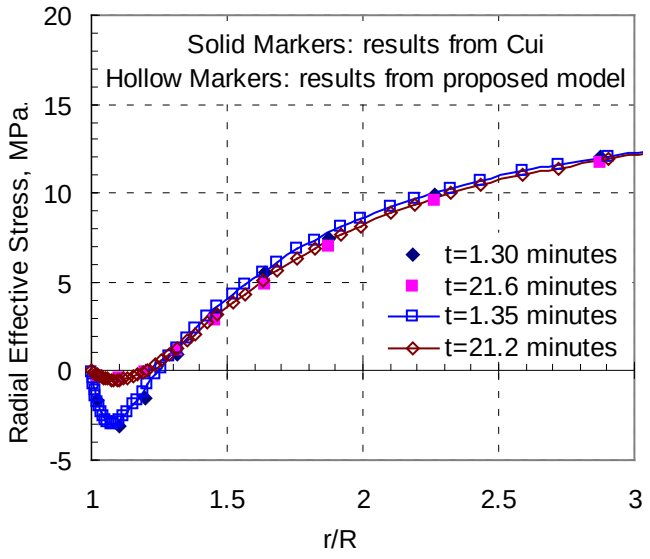

Fig. 2.11 Radial Terzaghi's effective stress around the wellbore at θ=5.7°

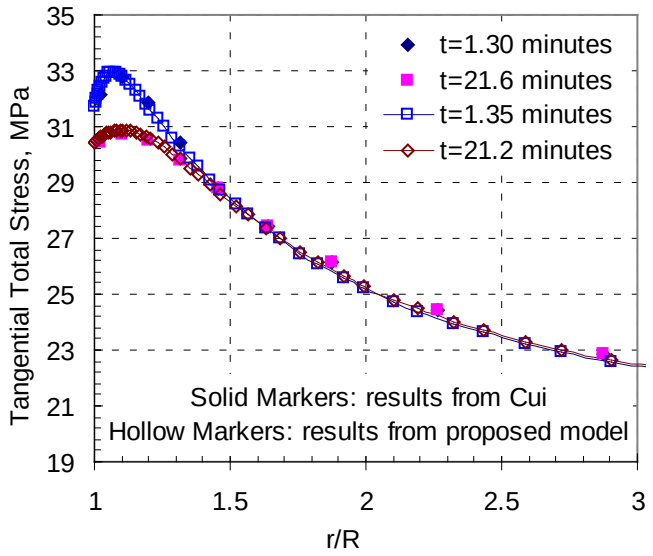

Fig. 2.12 Tangential total stress around the wellbore at θ=5.7°

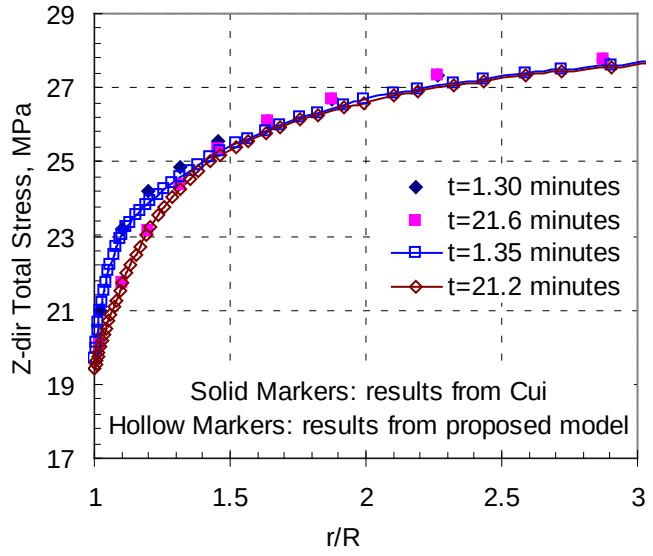

Fig. 2.13 Z direction total stress around the wellbore at θ=5.7°

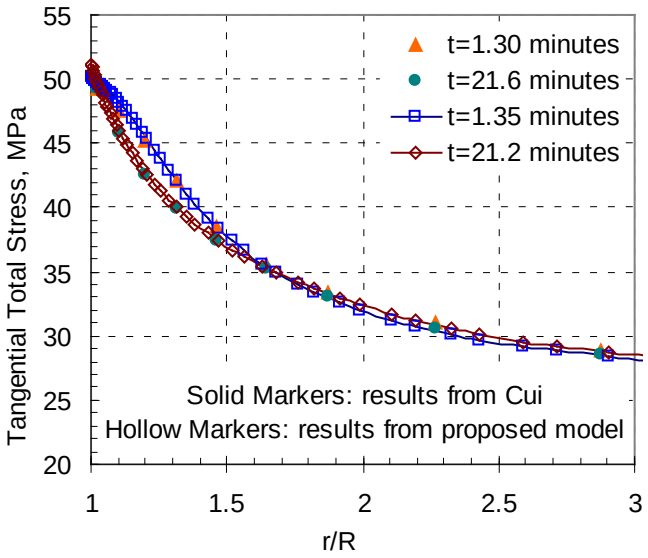

Fig. 2.14 Tangential total stress around the wellbore at θ=84.4°

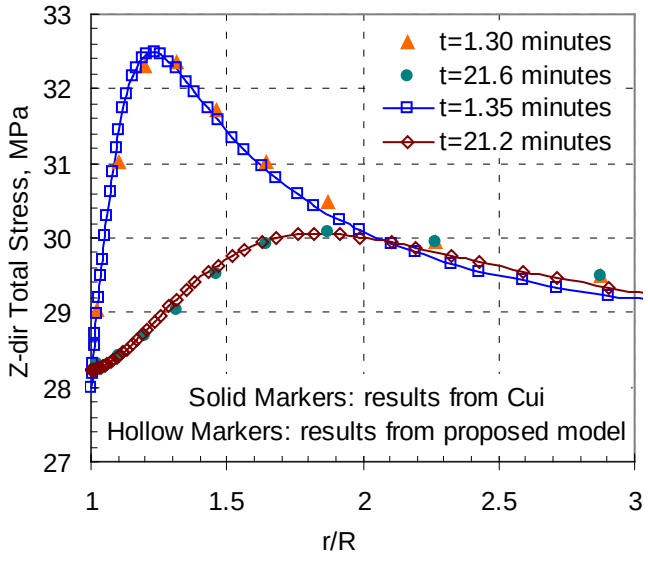

Fig. 2.15 Z direction total stress around the wellbore at θ=84.4°

3. SENSITIVITY STUDY OF THE PORE PRESSURE AND STRESS DISTRIBUTION AROUND THE HORIZONTAL WELL

In last section, the principle of generalized plane-strain finite element formulation of anisotropic poroelastic problems is explained and the validity of the developed finite element model is demonstrated. In this section, using the validated finite element model, sensitivity analysis is carried out to evaluate the effects of transverse isotropy ratios, well azimuth, and rock bedding dip on pore pressure distribution, total and effective stress distribution and possibility of fracture initiation. Twelve cases are simulated.

3.1. Effect of Different Rock Transverse Isotropy Ratios

In this section, a horizontal well drilled in horizontal rock bedding is assumed. The effects of different horizontal-to-vertical ratios of Young's modulus, poisson's ratio, permeability on the pore pressure and stress distribution are studied. The effect of different rock transverse isotropy ratios on possibility of fracture initiation is discussed.

3.1.1. Problem Statement

A horizontal well is drilled along the minimum horizontal in-situ stress in transversely isotropic reservoir. The isotropic plane (see Fig. 3.1) is also horizontal. The borehole radius is R=0.1 m.

The loading and geometry are shown in Fig. 3.2. The definition and notation of coordinate systems are the same as described before. The in-situ stresses σ_H, σ_h, σ_v are defined in global coordinate system and thus are also denoted as σ_x^g, σ_y^g, σ_z^g.

The well coordinate system, which denotes the well orientation, is rotated from global coordinate system position following the steps described in section 2.1.6: Assume the well coordinate system initially coincide with the global coordinate system. In first step, rotate the initial well coordinate system 90° about its z-axis to get a new well coordinate system. In second step, rotate the new well coordinate system 90° about its x axis. The in situ stresses are converted to the well coordinate system and denoted as σ_x^g, σ_y^g, σ_z^g, σ_{xy}^g, σ_{yz}^g, σ_{zx}^g. Since the isotropic plane is horizontal, the material coordinate system is the same as global coordinate system.

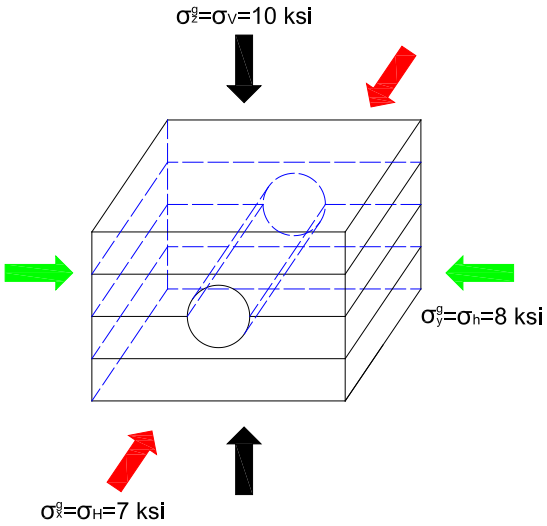

Fig. 3.1 Case 1-4: horizontal well and rock bedding position

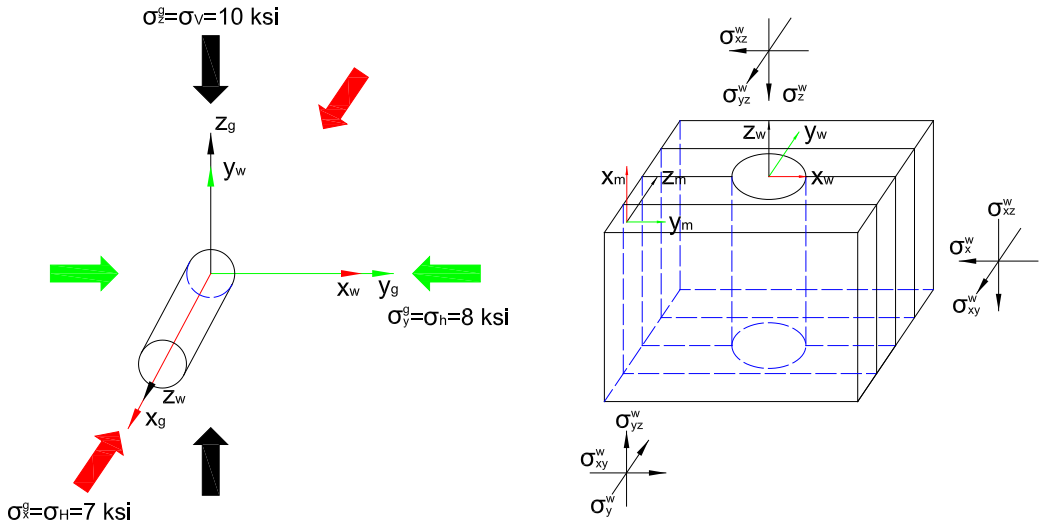

Fig. 3.2 Case 1-4: definition sketch of an horizontal borehole problem

To study the effects of transverse isotropy ratios, four cases are simulated in this section. In case 1, isotropic reservoir properties are used. In case 2, only the Young's modulus in horizontal and vertical direction is different ($E_h/E_v=3$). In case 3, only the Poisson's ratio parallel and perpendicular to the isotropic plane is different ($v_v/v_h=4$). In case 4, only the permeability in horizontal and vertical direction is different ($K_h/K_v=10$).

Note that Biot's coefficient or Biot's modulus is not included in this sensitivity analysis as an independent parameter. Based on the assumption of microisotropy, which states that the material is isotropic at the grain level and the macroscopic anisotropy is the manifestation of the directionality of the skeleton or pore and grain structure (Cui, Cheng, Kaliakin and Abousleiman, 1996) , the Biot's coefficient and Biot's modulus are not independent material parameters and can be defined from solid grain bulk modulus, fluid bulk modulus, porosity, Young's modulus and Poisson's ratio (Cheng, 1997):

$$\alpha_x = 1 - \frac{D_{11} + D_{12} + D_{13}}{3K_s} \quad \text{..... (3.1)}$$

$$\alpha_y = 1 - \frac{D_{12} + D_{22} + D_{23}}{3K_s} \quad \text{..... (3.2)}$$

$$\alpha_z = 1 - \frac{D_{13} + D_{23} + D_{33}}{3K_s} \quad \text{..... (3.3)}$$

$$M = \frac{K_f K_s}{K_s \phi + K_f (\frac{\alpha_x + \alpha_y + \alpha_z}{3} - \phi)} \quad \text{..... (3.4)}$$

where,

K_s is the solid grain bulk modulus,

K_f is the fluid bulk modulus,

ϕ is the porosity,

$\alpha_x, \alpha_y, \alpha_z$: Biot's coefficient in x,y,z directions,

M: Biot's modulus,

D_{ij} is the corresponding element in the 6 by 6 drained elastic modulus matrix [D]

The common reservoir properties in four cases are presented as follows:

Angles rotating about z, x, y axes sequentially to transform global coordinate system to material coordinate system and wellbore coordinate system:

- To material c.s.: ϕ_{m1} =0°, ϕ_{m2}=0°, ϕ_{m3}=0°
- To wellbore c.s.: ϕ_{w1}=90°, ϕ_{w2}=90°, ϕ_{w3}=0°

Initial state (in global coordinate system):

- Initial Pore Pressure: p_0=6 ksi

- In-situ Stresses: σ_H=8 ksi, σ_h=7 ksi, σ_v=10 ksi
- Mud Pressure: p_{mud}=8 ksi
- Fluid viscosity: μ=0.001Pa.s

Different transversely isotropic rock properties in four cases are listed as follows (in material coordinate system):

Case 1: Isotropic case

- Permeability: $K_x=K_y=K_z$=1.0e-7 darcy
- Young's Modulus: $E_x=E_y=E_z$ =1.4e3 ksi
- Poisson's Ratio: $\nu_{xy}=\nu_{yz}=\nu_{zx}$=0.25
- Shear Modulus: $G_{xy}=G_{yz}=G_{zx}$= 0.56e3 ksi
- Biot Coefficient: $\alpha_x=\alpha_y=\alpha_z$=0.866
- Biot Modulus: M=2.36e3 ksi

Case 2: E_h/E_v=3

- Permeability: $K_x=K_y=K_z$=1.0e-7 darcy
- Young's Modulus: $E_x=E_y$=4.2e3 ksi, E_z =1.4e3 ksi
- Poisson's Ratio: $\nu_{xy}=\nu_{yz}=\nu_{zx}$=0.25
- Shear Modulus: G_{xy}=1.68e3 ksi, $G_{yz}=G_{zx}$= 0.56e3 ksi
- Biot Coefficient: $\alpha_x=\alpha_y$=0.332, α_z=0.599
- Biot Modulus: M=2.78e3 ksi

Case 3: v_v/v_h=4

- Permeability: $K_x=K_y=K_z$=1.0e-7 darcy
- Young's Modulus: $E_x=E_y=E_z$ =1.4e3 ksi

- Poisson's Ratio: ν_{xy}=0.0625, $\nu_{yz}=\nu_{zx}$=0.25
- Shear Modulus: G_{xy}=0.658e3 ksi, $G_{yz}=G_{zx}$= 0.56e3 ksi
- Biot Coefficient: $\alpha_x=\alpha_y$=0.897, α_z=0.882
- Biot Modulus: M=2.34e3 ksi

Case 4: K_h/K_v=10

- Permeability: $K_x=K_y$=1.0e-6 darcy, K_z=1.0e-7 darcy
- Young's Modulus: $E_x=E_y=E_z$ =1.4e3 ksi
- Poisson's Ratio: $\nu_{xy}= \nu_{yz}=\nu_{zx}$=0.25
- Shear Modulus: $G_{xy}=G_{yz}=G_{zx}$= 0.56e3 ksi
- Biot Coefficient: $\alpha_x=\alpha_y=\alpha_z$=0.866
- Biot Modulus: M=2.36e3 ksi

3.1.2. Results

Pore pressure, Biot effective stress and total stress in different directions (tangential, radial and z-direction) near the wellbore and tangential Terzaghi's effective stress around wellbore at three time steps (1 second, 30 minutes and 3 days) from all four cases are presented in Fig. 3.3-Fig. 3.34.

3.1.2.1. Case 1: E_h/E_v=1, v_v/v_h=1, K_h/K_v=1

Case 1 is the base of all four cases. Case 2, 3 and 4 is compared to case 1 to study the effect of different transverse isotropy ratios.

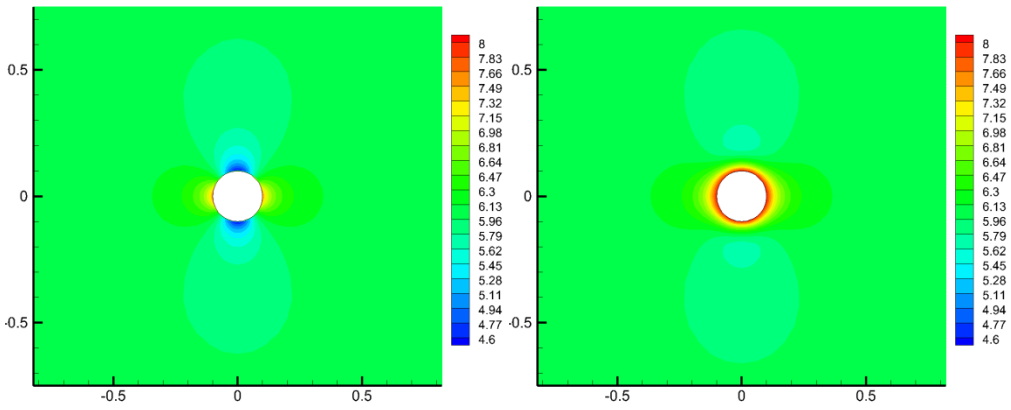

(a) t=1 second **(b) t=30 minutes**

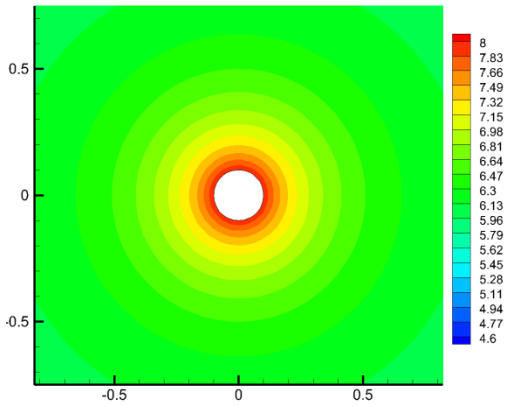

(c) t=3 days

Fig. 3.3 Case 1: pore pressure distribution

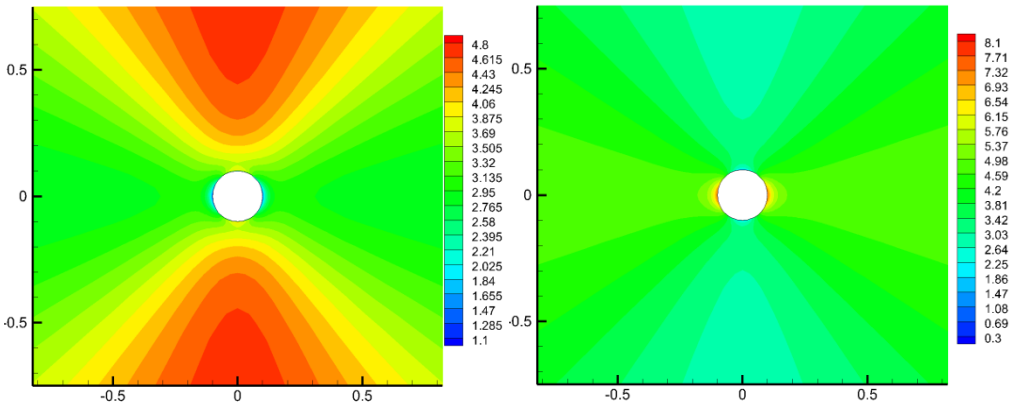

(a) Radial Stress **(b) Tangential Stress**

Fig. 3.4 Case 1: Biot's effective stress distribution at t=1 second

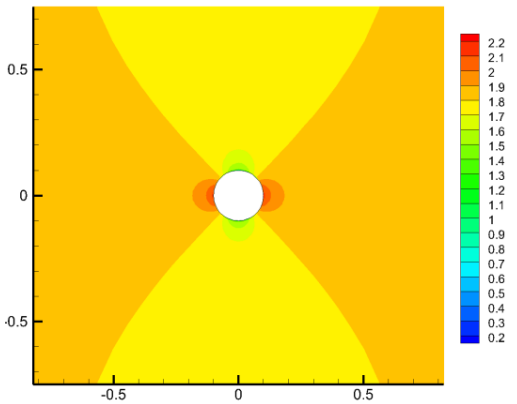

(c) Z Direction Stress

Fig. 3.4 Continued

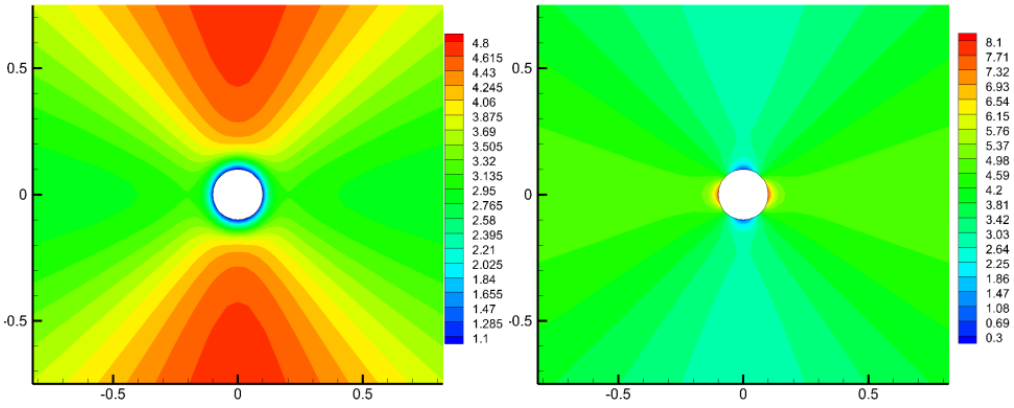

(a) Radial Stress **(b) Tangential Stress**

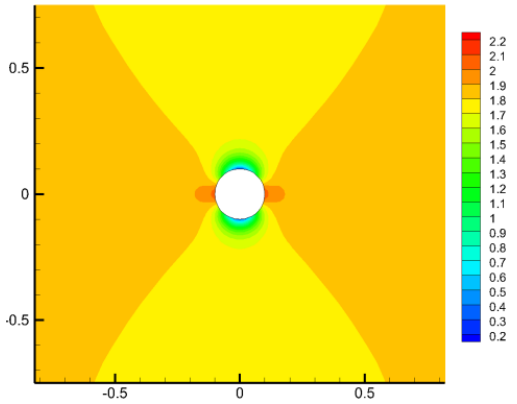

(c) Z Direction Stress

Fig. 3.5 Case 1: Biot's effective stress distribution at t=30 minutes

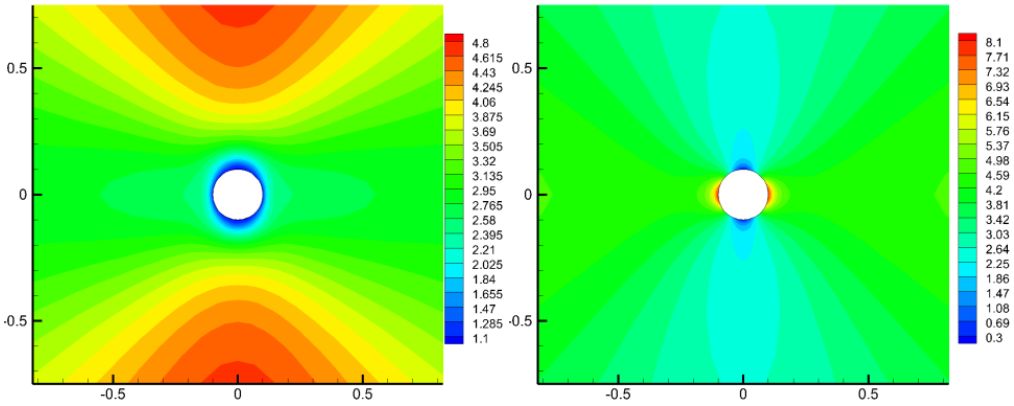

(a) Radial Stress **(b) Tangential Stress**

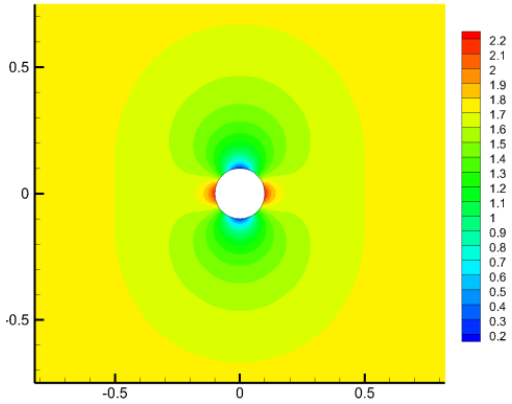

(c) Z Direction Stress

Fig. 3.6 Case 1: Biot's effective stress distribution at t=3 days

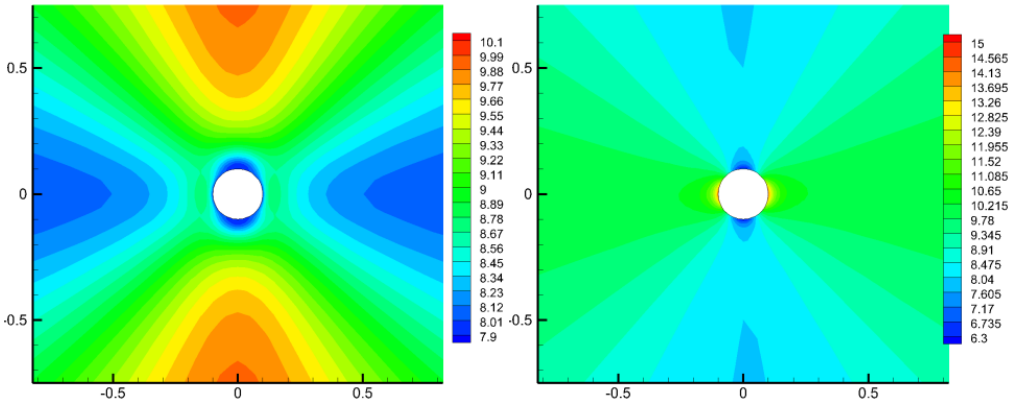

(a) Radial Stress **(b) Tangential Stress**

Fig. 3.7 Case 1: total stress distribution at t=1 second

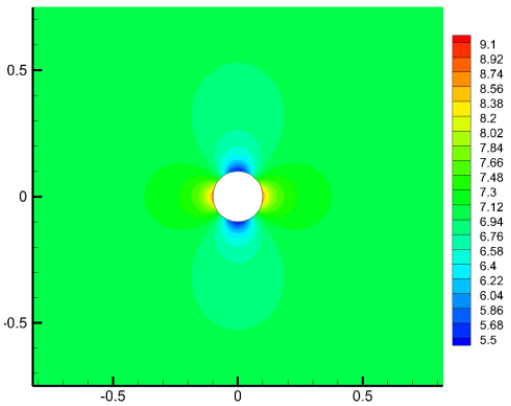

(c) Z Direction Stress

Fig. 3.7 Continued

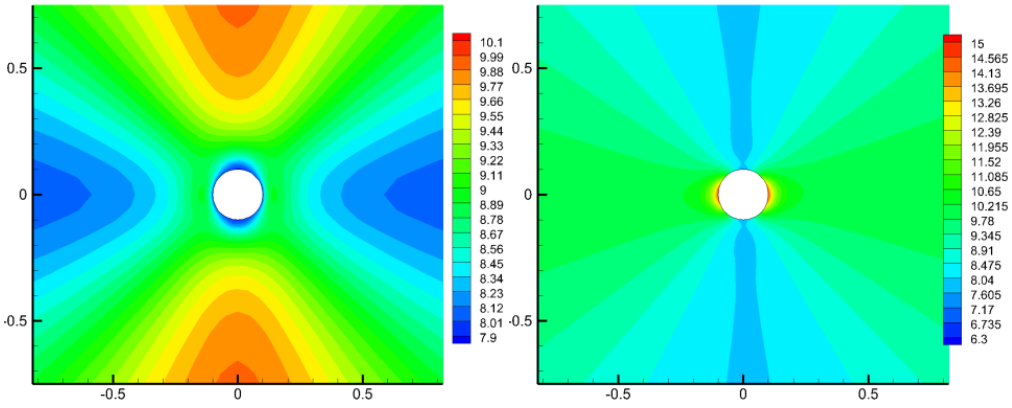

(a) Radial Stress **(b) Tangential Stress**

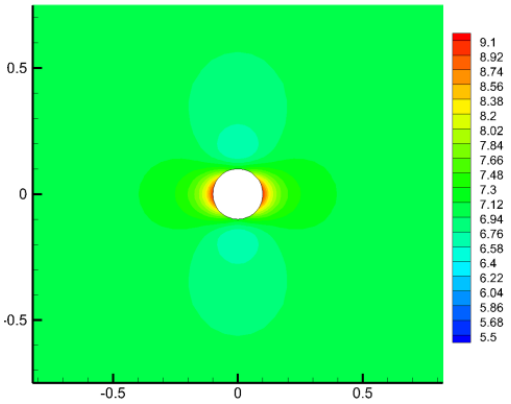

(c) Z Direction Stress

Fig. 3.8 Case 1: total stress distribution at t=30 minutes

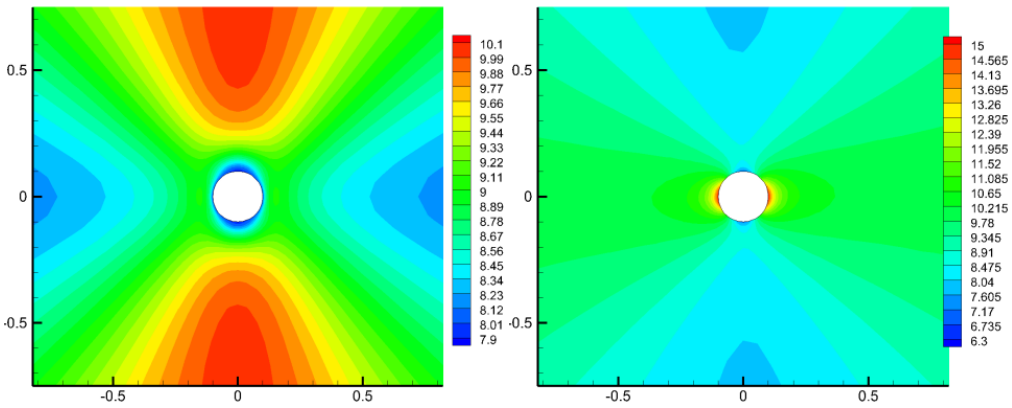

(a) Radial Stress **(b) Tangential Stress**

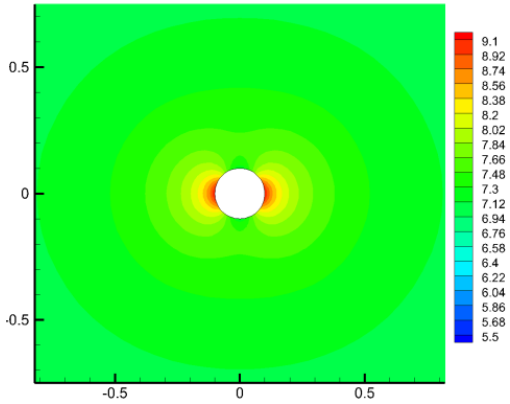

(c) Z Direction Stress

Fig. 3.9 Case 1: total stress distribution at t=3 days

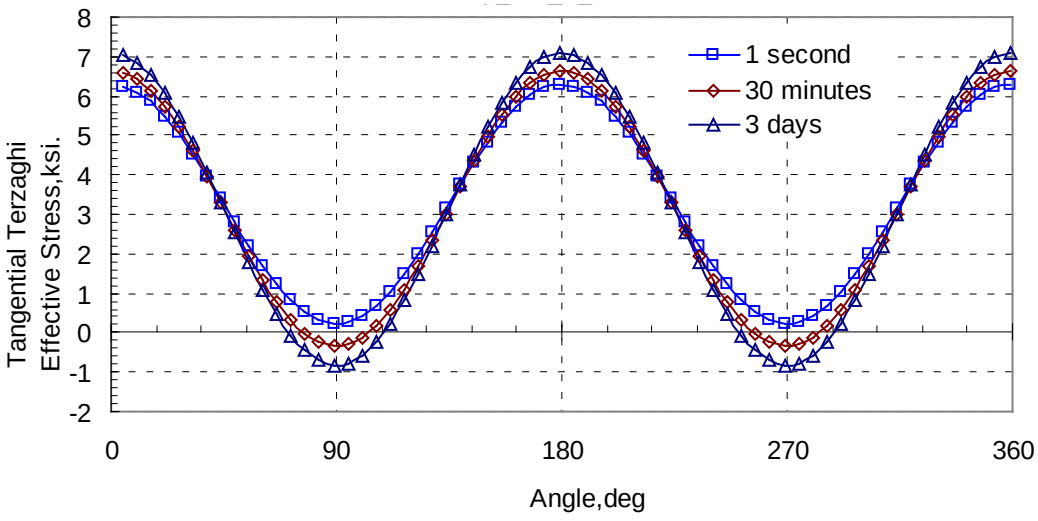

Fig. 3.10 Case 1: tangential Terzaghi's effective stress around wellbore

3.1.2.2. Case 2: $E_h/E_v=3$, $v_v/v_h=1$, $K_h/K_v=1$

Compared to case 1, Case 2 shows the effect of different horizontal and vertical Young's modulus ratio.

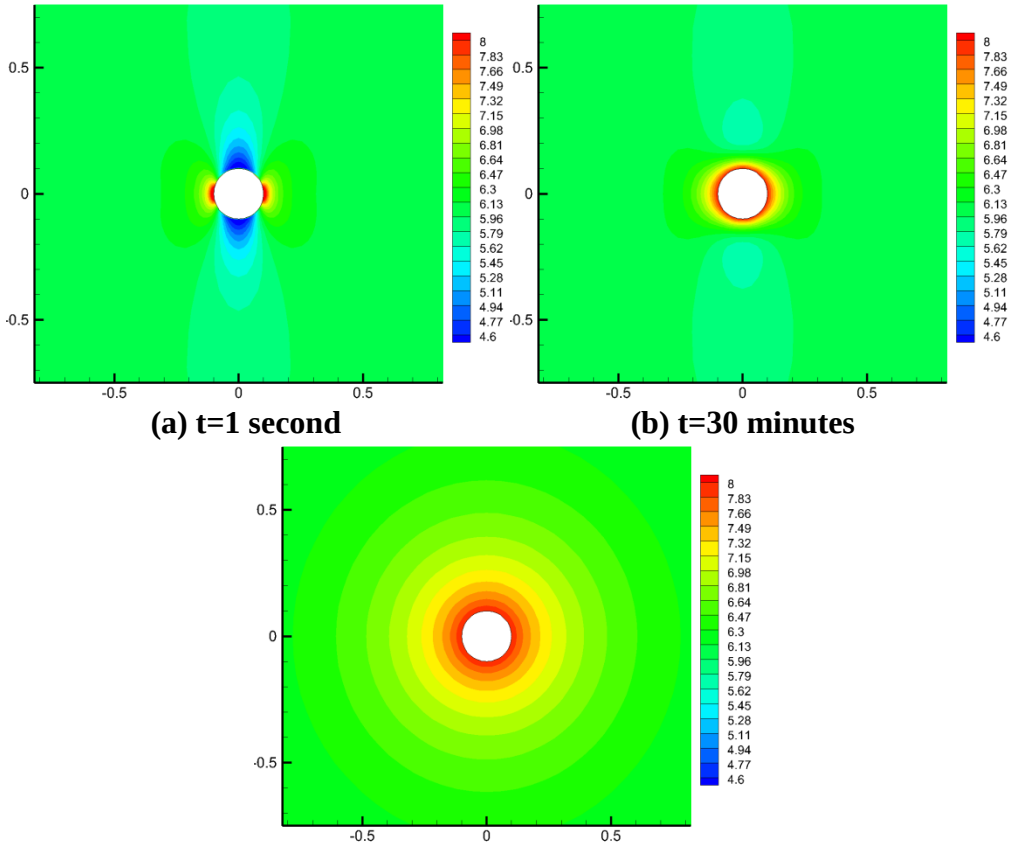

(a) t=1 second **(b) t=30 minutes**

(c) t=3 days

Fig. 3.11 Case 2: pore pressure distribution

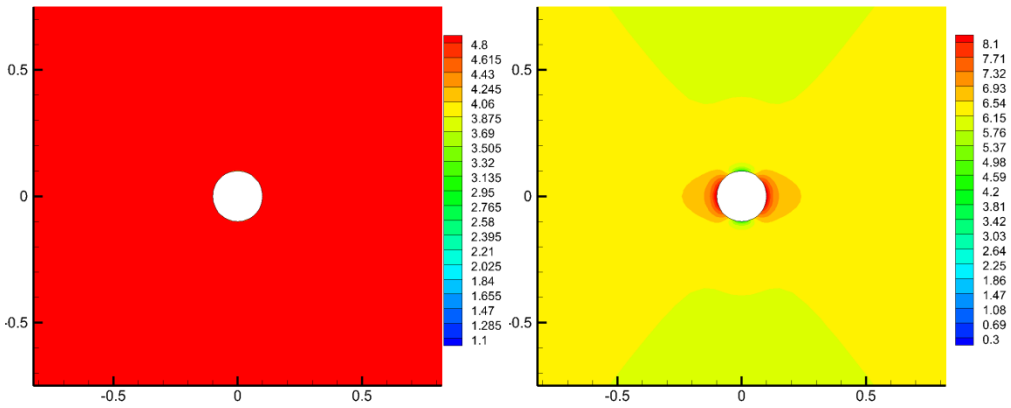

(a) Radial Stress **(b) Tangential Stress**

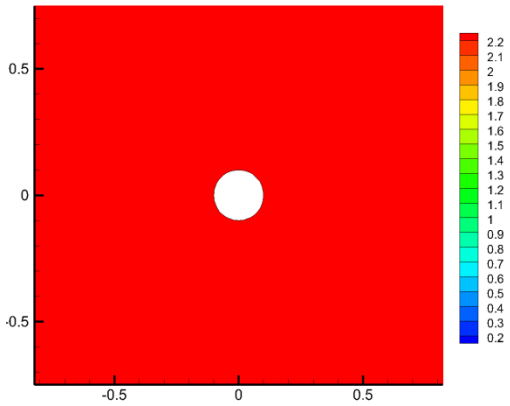

(c) Z Direction Stress

Fig. 3.12 Case 2: Biot's effective stress distribution at t=1 second

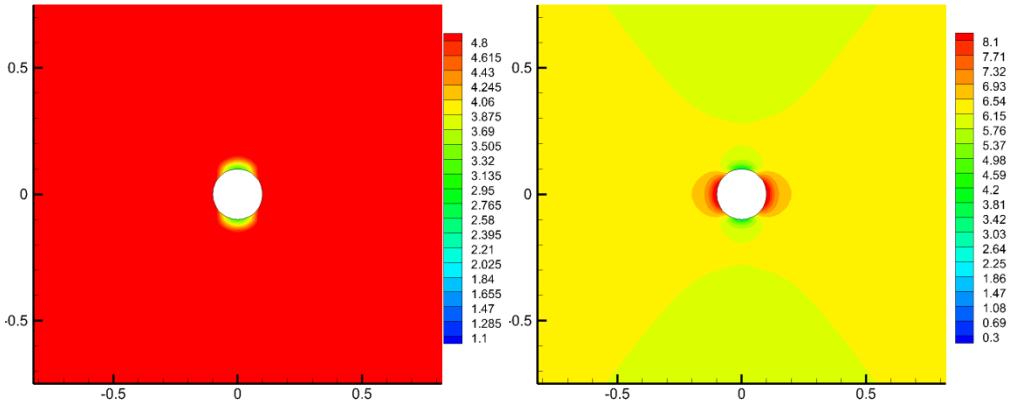

(a) Radial Stress **(b) Tangential Stress**

Fig. 3.13 Case 2: Biot's effective stress distribution at t=30 minutes

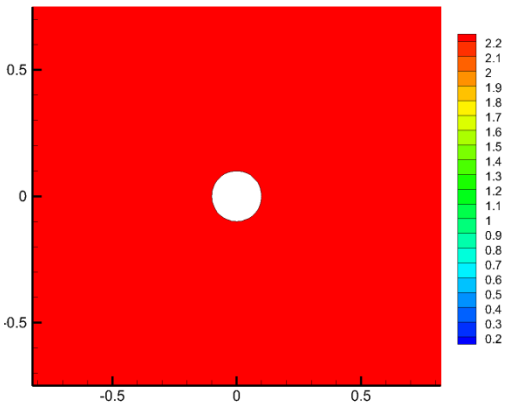

(c) Z Direction Stress

Fig. 3.13 Continued

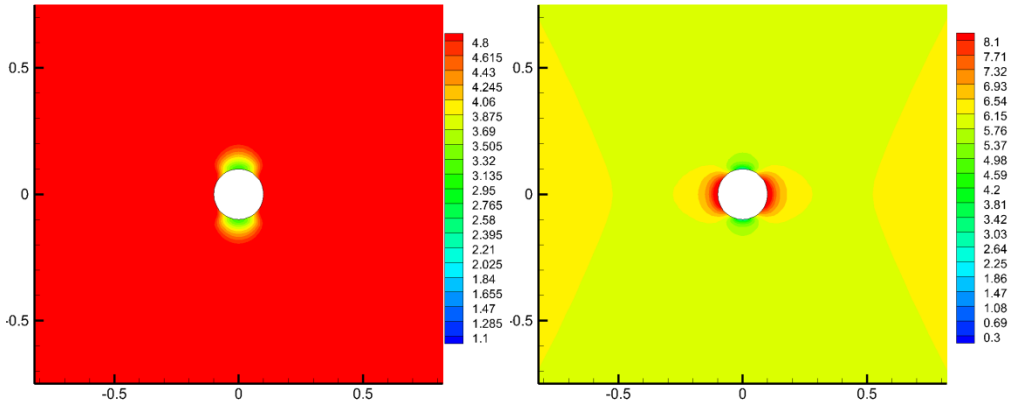

(a) Radial Stress **(b) Tangential Stress**

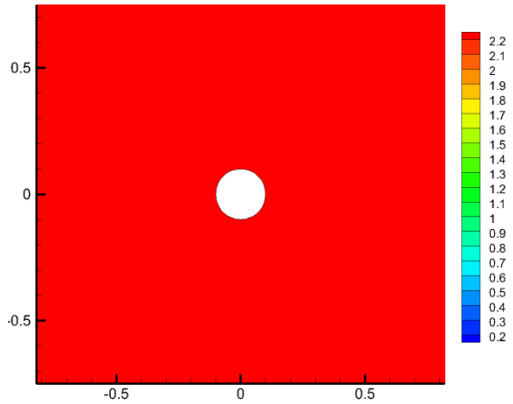

(c) Z Direction Stress

Fig. 3.14 Case 2: Biot's effective stress distribution at t=3 days

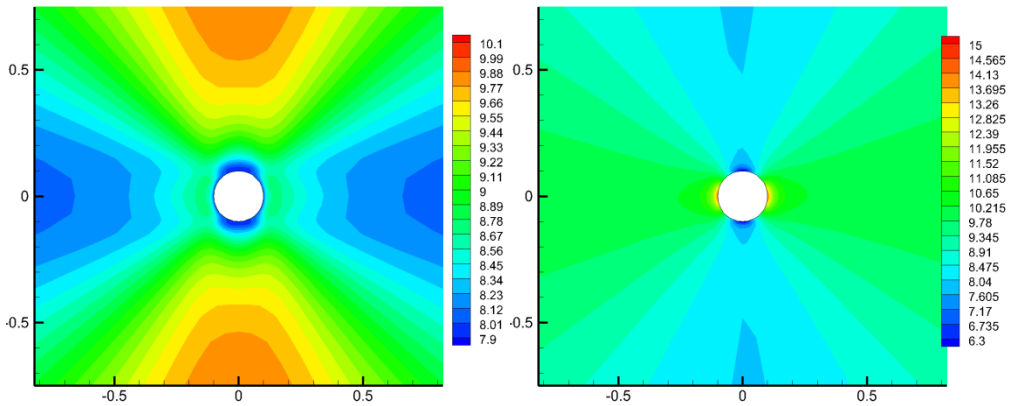

(a) Radial Stress **(b) Tangential Stress**

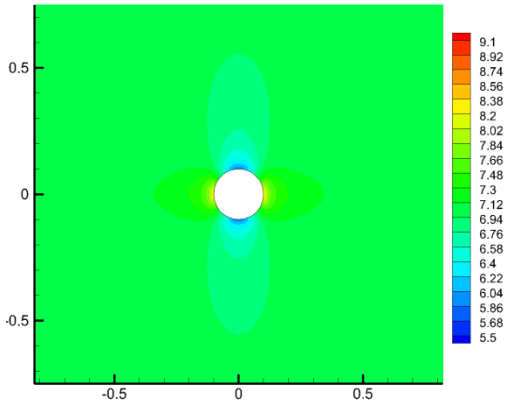

(c) Z Direction Stress

Fig. 3.15 Case 2: total stress distribution at t=1 second

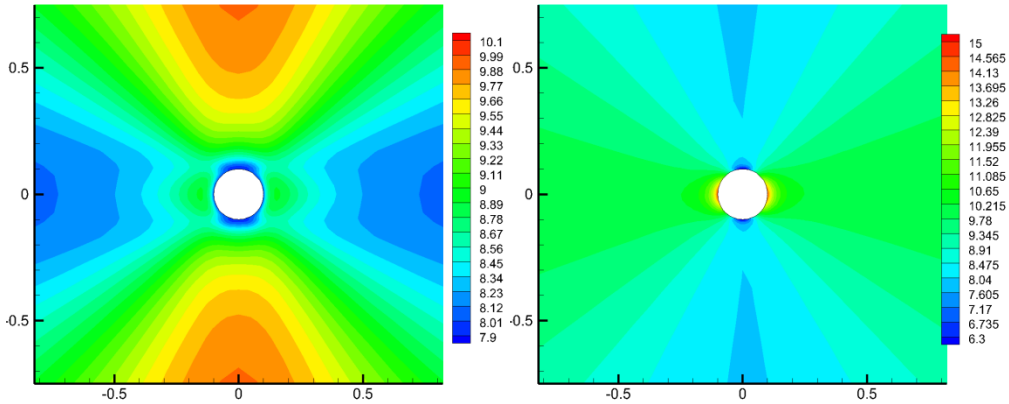

(a) Radial Stress **(b) Tangential Stress**

Fig. 3.16 Case 2: total stress distribution at t=30 minutes

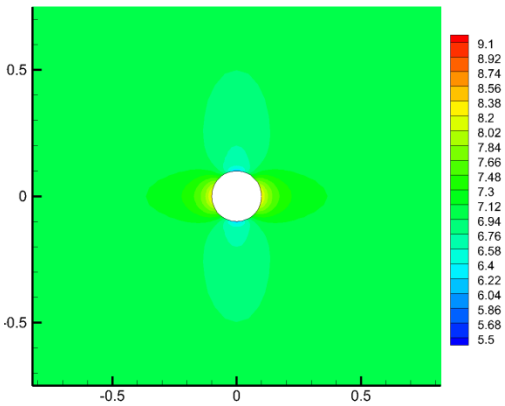

(c) Z Direction Stress

Fig. 3.16 Continued

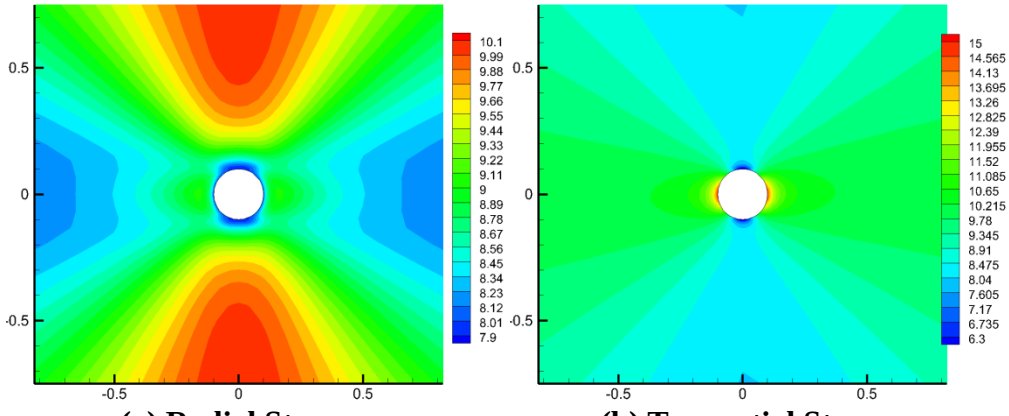

(a) Radial Stress **(b) Tangential Stress**

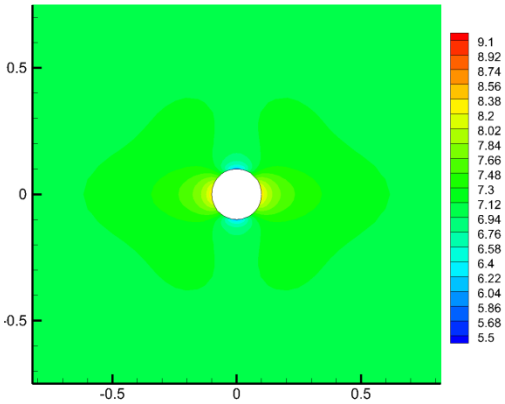

(c) Z Direction Stress

Fig. 3.17 Case 2: total stress distribution at t=3 days

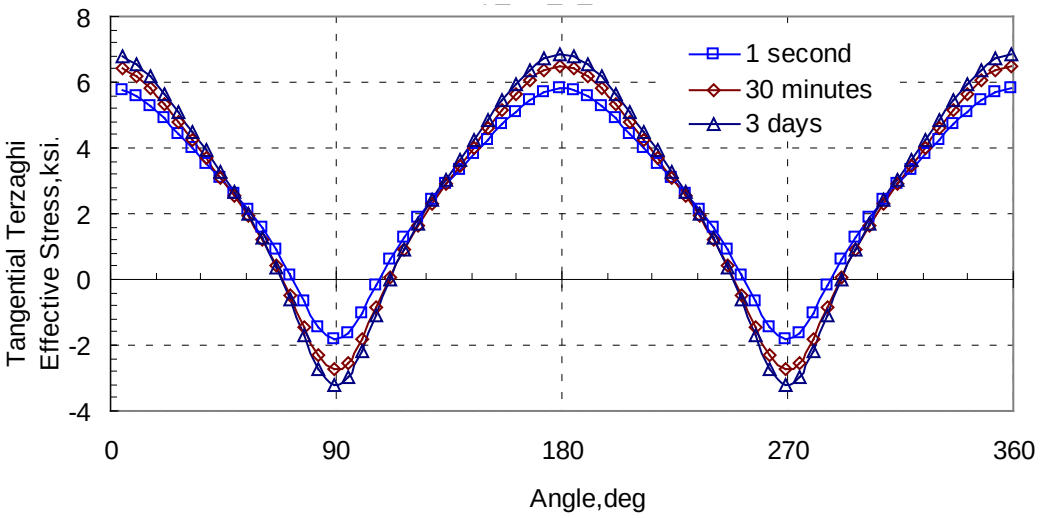

Fig. 3.18 Case 2: tangential Terzaghi's effective stress around wellbore

3.1.2.3. Case 3: $E_h/E_v=1$, $v_h/v_v=4$, $K_h/K_v=1$

Compared to case 1, Case 3 shows the effect of different horizontal and vertical Poisson's ratio.

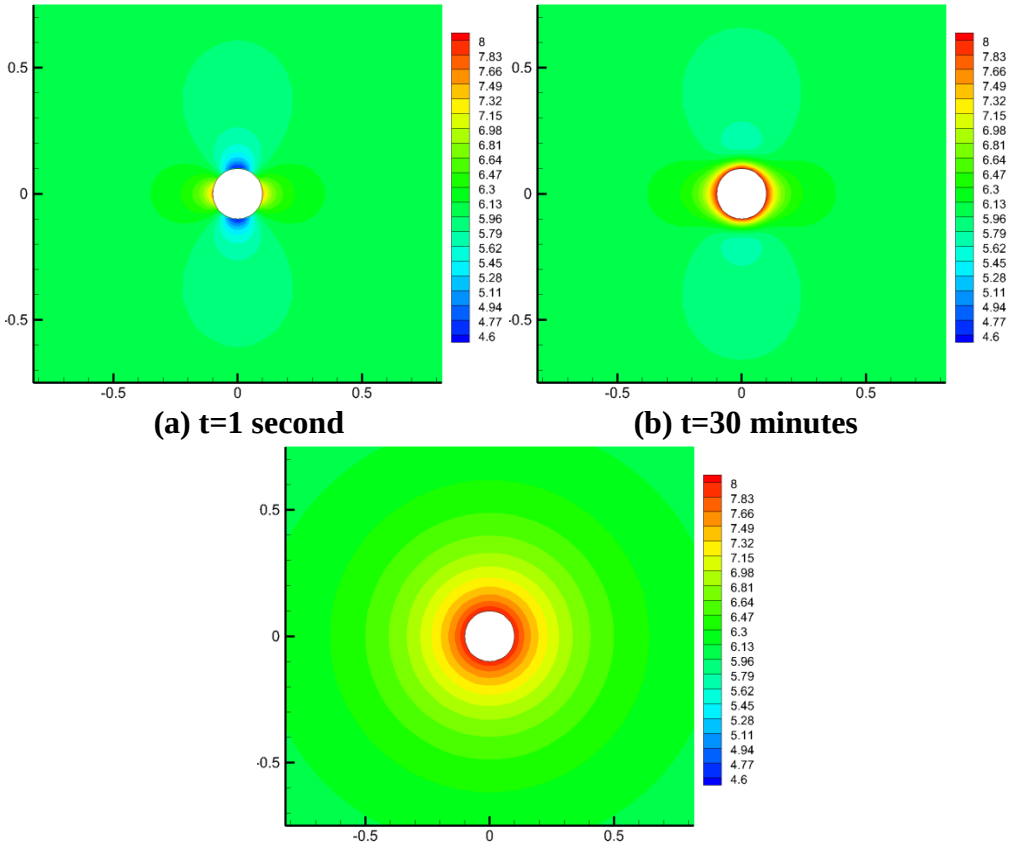

(a) t=1 second **(b) t=30 minutes**

(c) t=3 days

Fig. 3.19 Case 3: pore pressure distribution

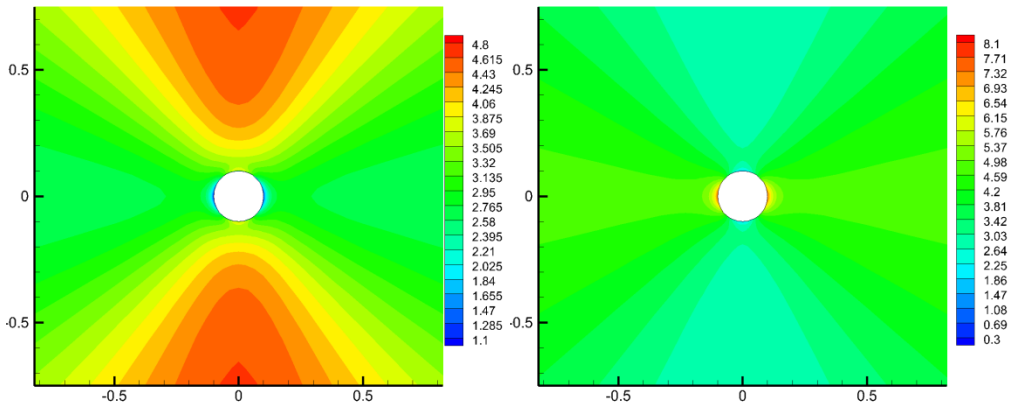

(a) Radial Stress **(b) Tangential Stress**

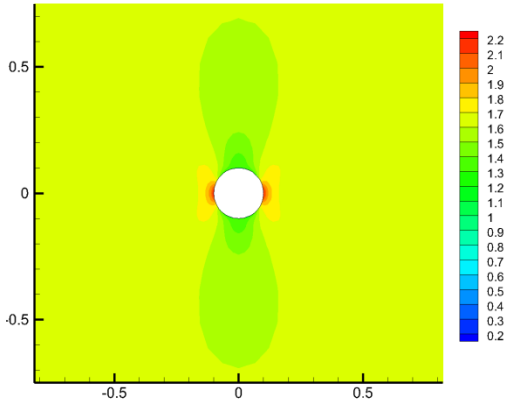

(c) Z Direction Stress

Fig. 3.20 Case 3: Biot's effective stress distribution at t=1 second

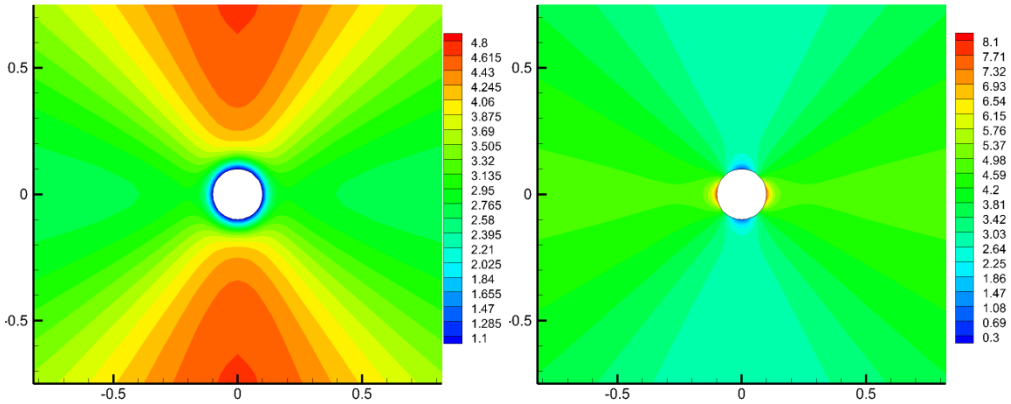

(a) Radial Stress **(b) Tangential Stress**

Fig. 3.21 Case 3: Biot's effective stress distribution at t=30 minutes

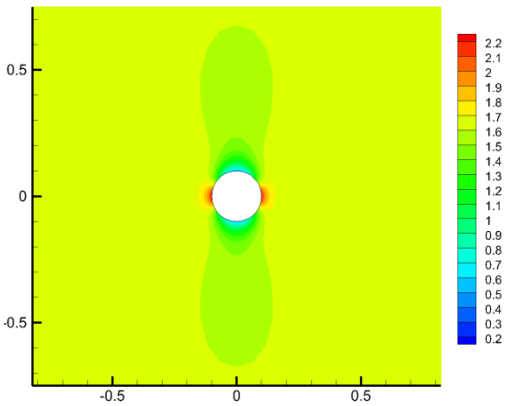

(c) Z Direction Stress

Fig. 3.21 Continued

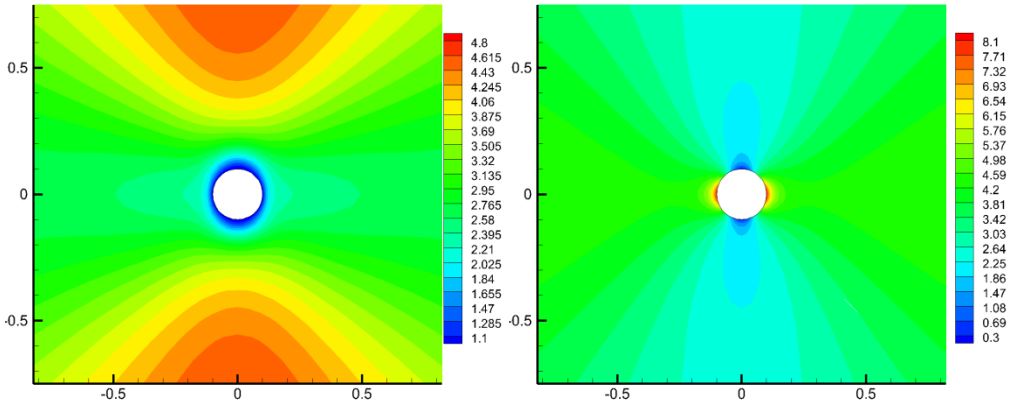

(a) Radial Stress **(b) Tangential Stress**

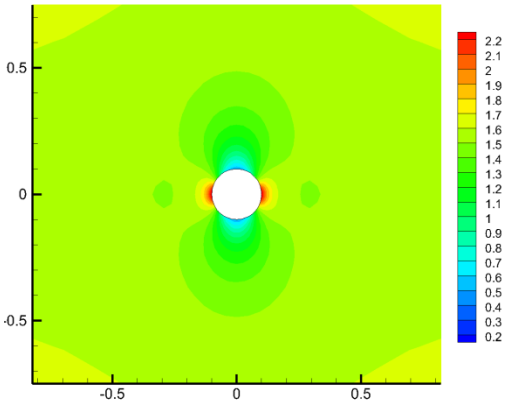

(c) Z Direction Stress

Fig. 3.22 Case 3: Biot's effective stress distribution at t=3 days

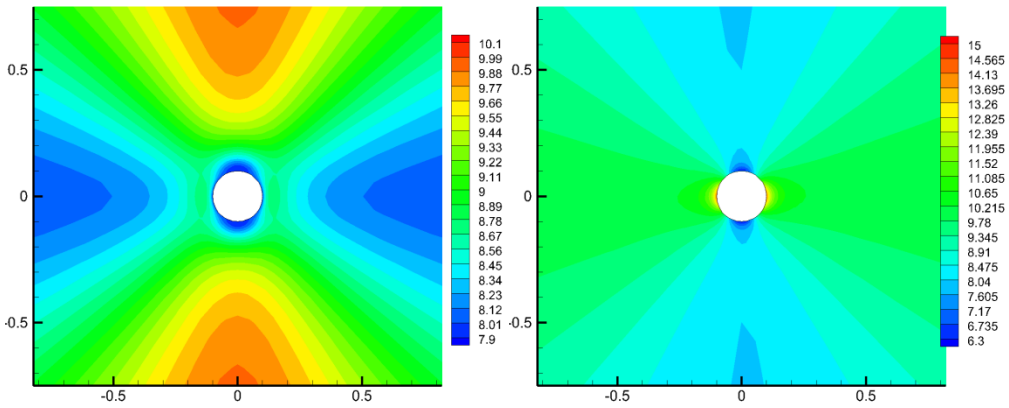

(a) Radial Stress **(b) Tangential Stress**

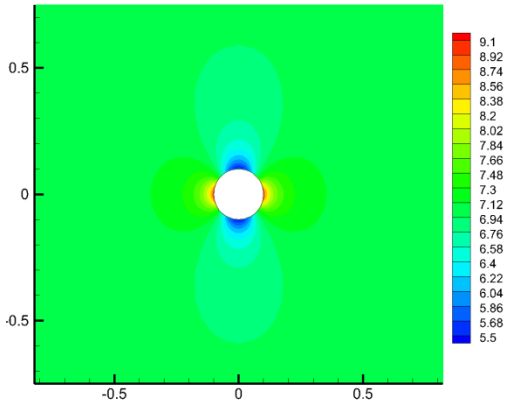

(c) Z Direction Stress

Fig. 3.23 Case 3: total stress distribution at t=1 second

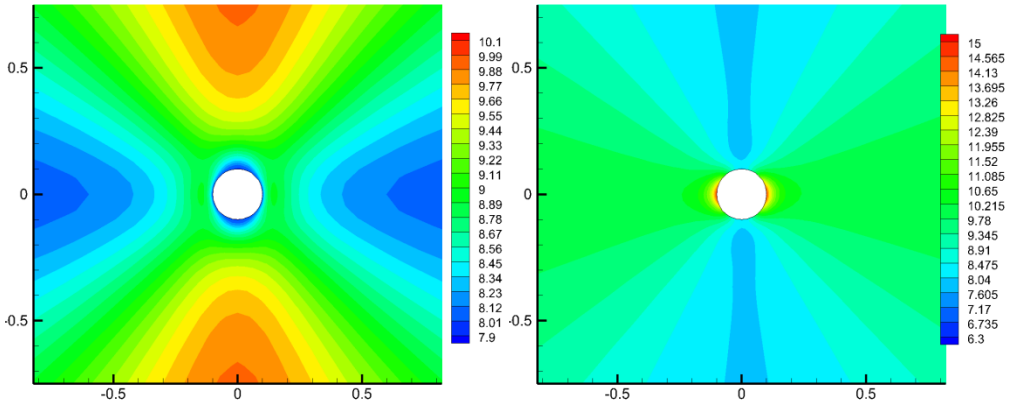

(a) Radial Stress **(b) Tangential Stress**

Fig. 3.24 Case 3: total stress distribution at t=30 minutes

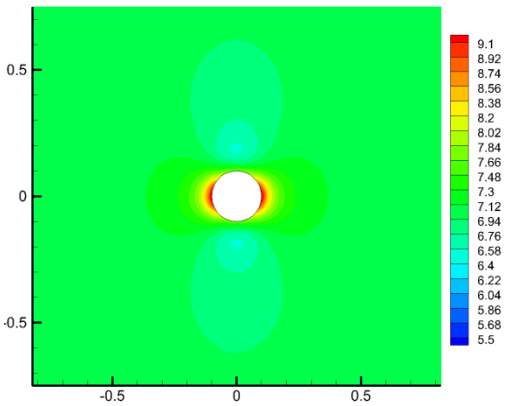

(c) Z Direction Stress

Fig. 3.24 Continued

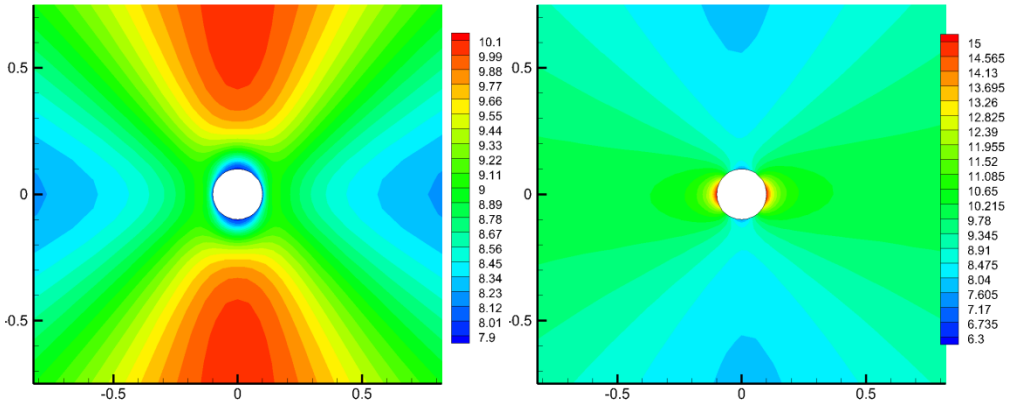

(a) Radial Stress **(b) Tangential Stress**

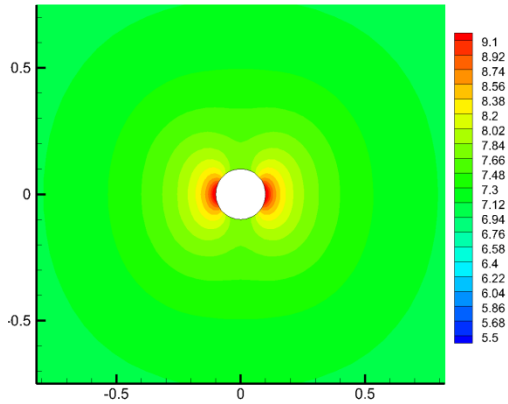

(c) Z Direction Stress

Fig. 3.25 Case 3: total stress distribution at t=3 days

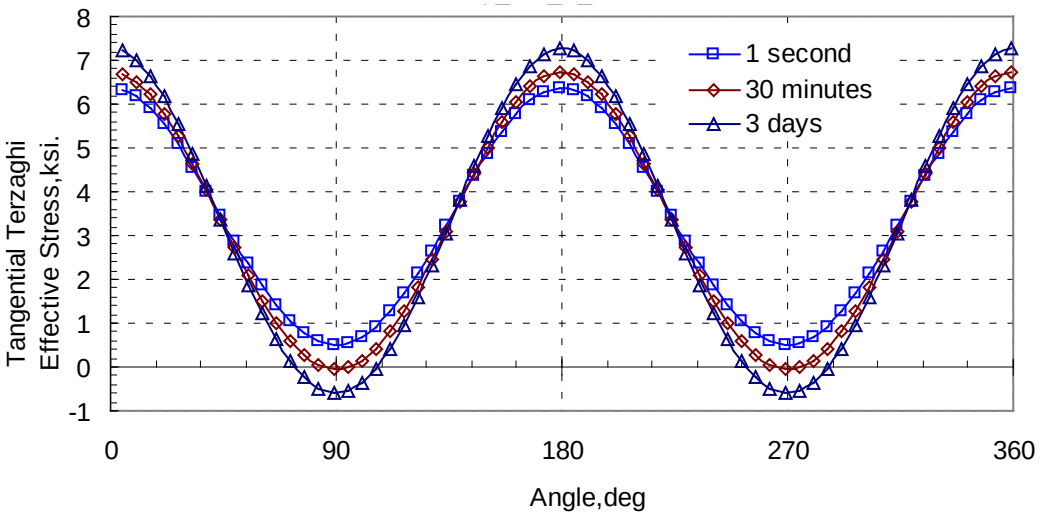

Fig. 3.26 Case 3: tangential Terzaghi's effective stress around wellbore

3.1.2.4. Case 4 $E_h/E_v=1$, $v_h/v_v=1$, $K_h/K_v=10$

Compared to case 1, Case 4 shows the effect of different horizontal and vertical permeability ratio.

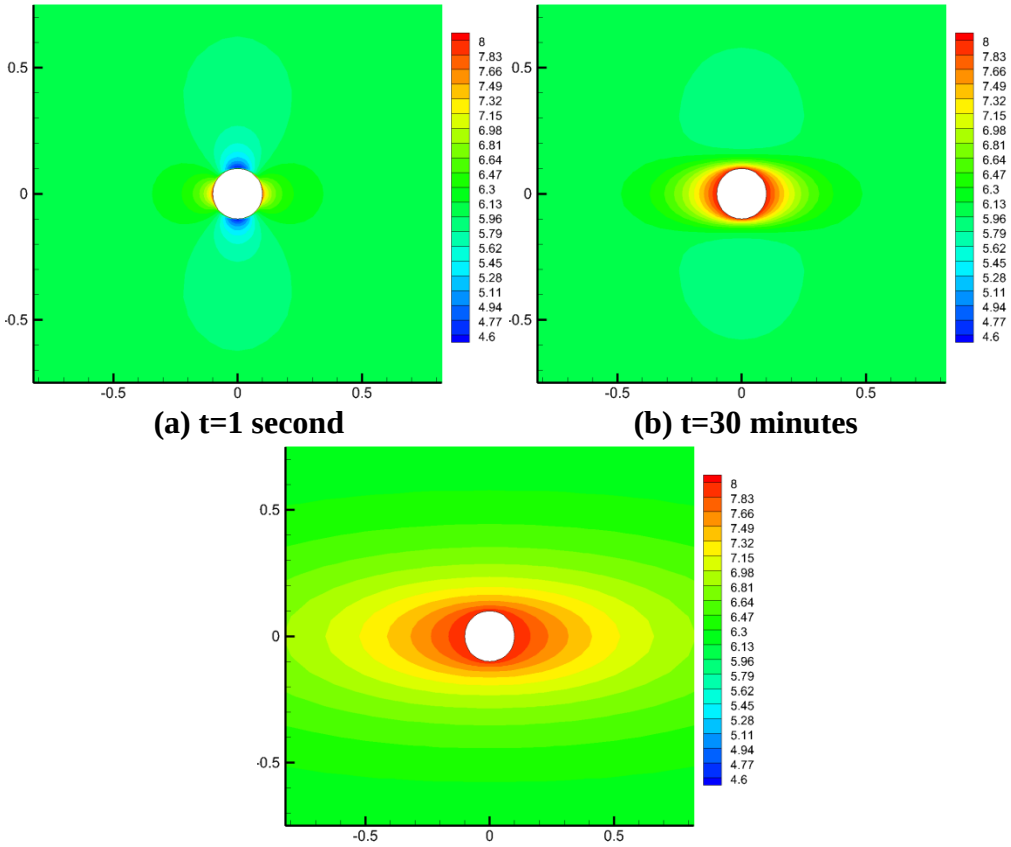

(a) t=1 second **(b) t=30 minutes**

(c) t=3 days

Fig. 3.27 Case 4: pore pressure distribution

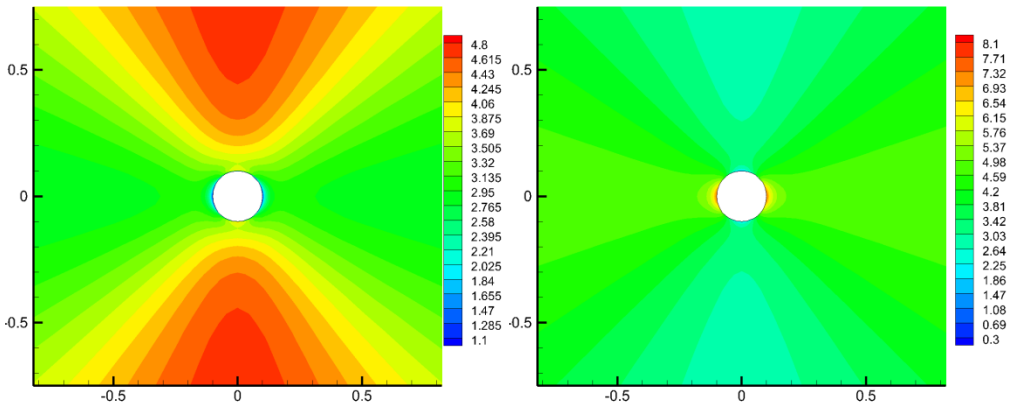

(a) Radial Stress **(b) Tangential Stress**

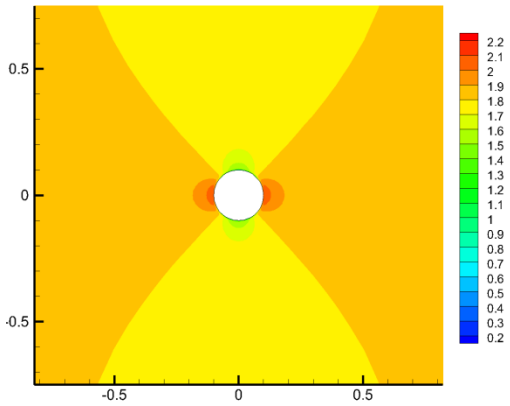

(c) Z Direction Stress

Fig. 3.28 Case 4: Biot's effective stress distribution at t=1 second

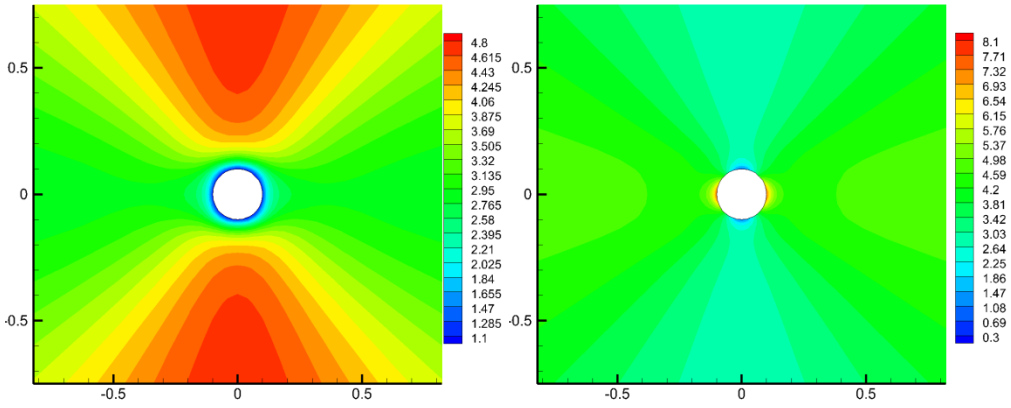

(a) Radial Stress **(b) Tangential Stress**

Fig. 3.29 Case 4: Biot's effective stress distribution at t=30 minutes

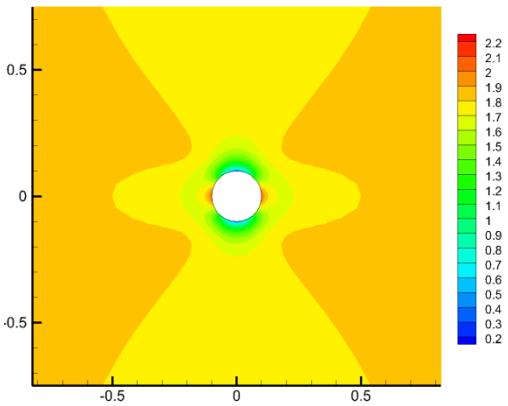

(c) Z Direction Stress

Fig. 3.29 Continued

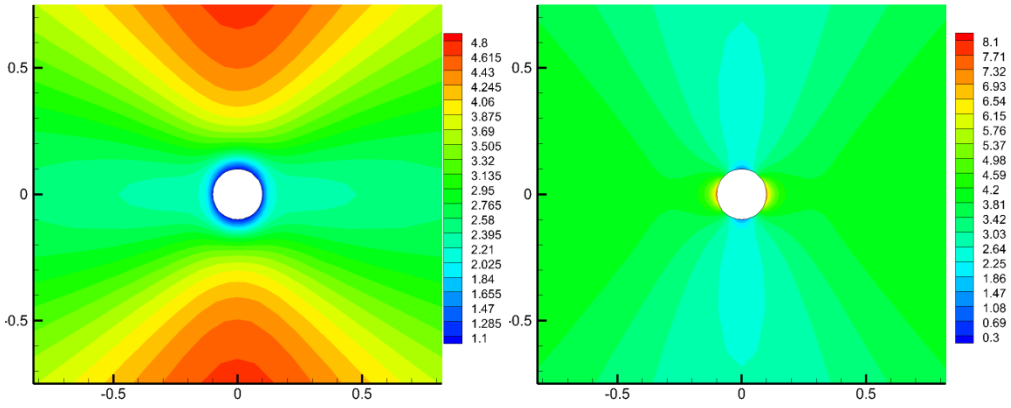

(a) Radial Stress **(b) Tangential Stress**

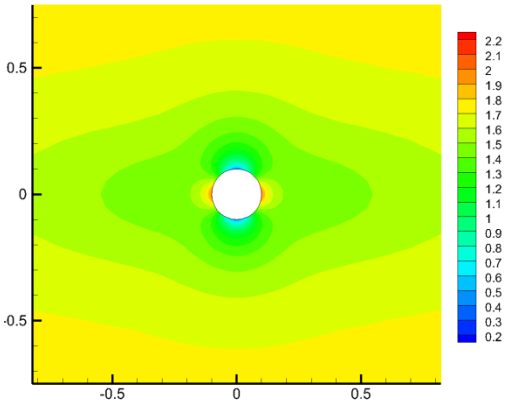

(c) Z Direction Stress

Fig. 3.30 Case 4: Biot's effective stress distribution at t=3 days

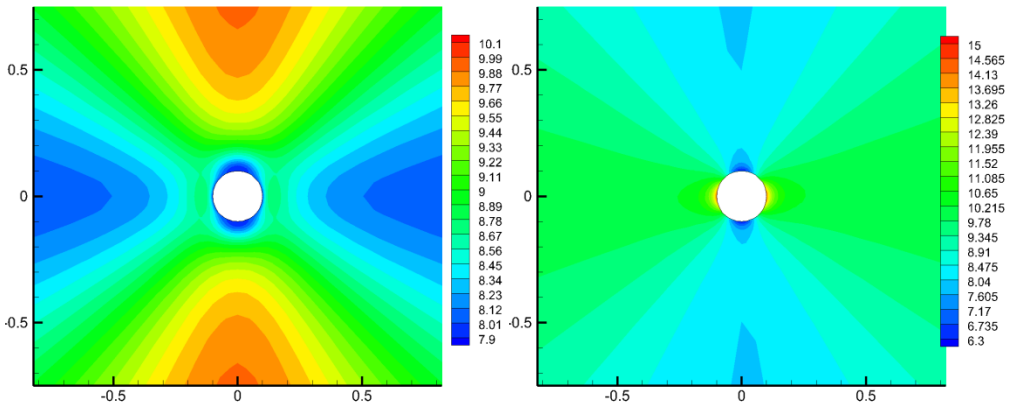

(a) Radial Stress **(b) Tangential Stress**

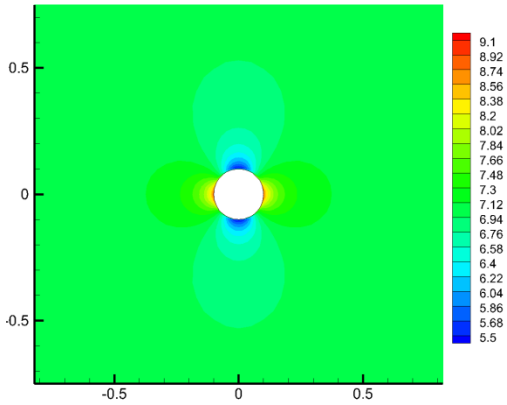

(c) Z Direction Stress

Fig. 3.31 Case 4: total stress distribution at t=1 second

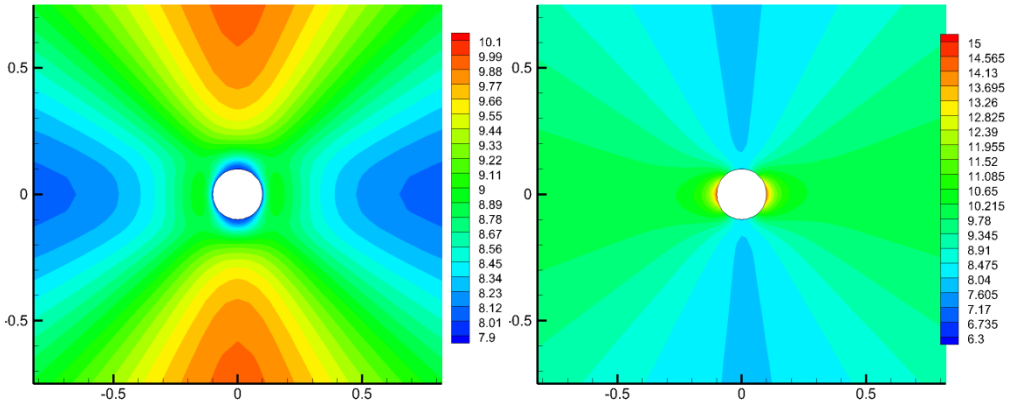

(a) Radial Stress **(b) Tangential Stress**

Fig. 3.32 Case 4: total stress distribution at t=30 minutes

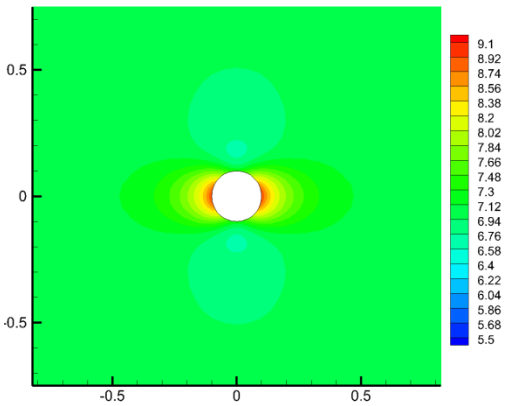

(c) Z Direction Stress

Fig. 3.32 Continued

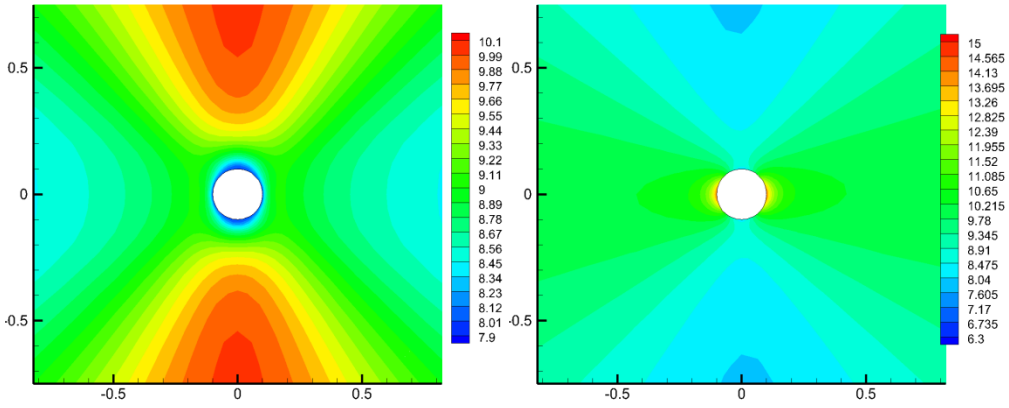

(a) Radial Stress **(b) Tangential Stress**

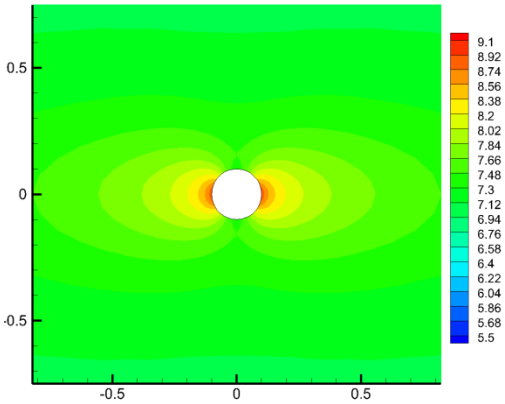

(c) Z Direction Stress

Fig. 3.33 Case 4: total stress distribution at t=3 days

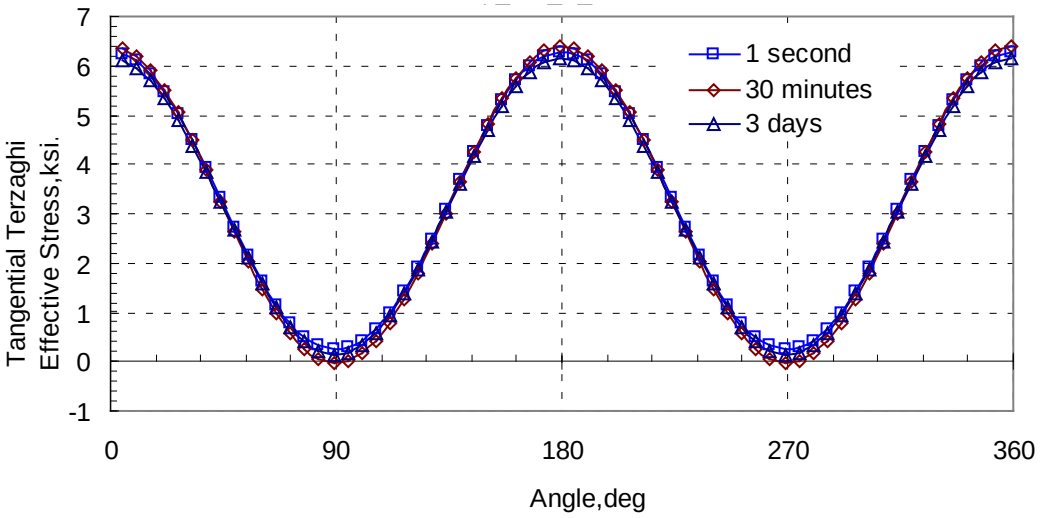

Fig. 3.34 Case 4: tangential Terzaghi's effective stress around wellbore

3.1.3. Summary

Comparing case 2, 3 and 4 with case 1, we found some interesting results discussed as follows.

Different horizontal and vertical Young's modulus ratio significantly changes the short term pore pressure distribution, which is due to the excavation of the wellbore. However, it has limited effect on long term pore pressure distribution. It influences total stress distribution, but the effect is not very prominent. Nevertheless, it has significant influence on the effective stress distribution as well as the fracture initiation. As E_h/E_v increases, the effective stress decreases and the well is more likely to be fractured. One possible reason to this is the dramatic change of Biot's coefficient caused by different Young's modulus ratio.

Different horizontal and vertical Poisson's ratio has almost no effect on pore pressure distribution. It influences the z-direction component of both effective and total stress. Comparing the tangential Terzaghi's effective stress of case 1 and 3, we can notice that its influence on fracture initiation is not very prominent.

Different horizontal and vertical permeability has little effect on short term pore pressure distribution, but very significant effect on long term pore pressure distribution. It has very limited influence on total stress distribution, but due to the effect of pore pressure, it influences the long term effective stress distribution as well as fracture initiation.

In summary, the study shows that the short term pore pressure distribution is sensitive to both E_v/E_h ratio and K_v/K_h ratio, while the long term pore pressure

distribution is only sensitive to K_v/K_h ratio. Restrained by equilibrium condition, the total stress distribution generally is not very sensitive to transverse isotropy ratios, but the effective stress and fracture initiation is very sensitive to E_v/E_h ratio. ν_v/ν_h ratio only has large effect on z-direction stress.

3.2. Effect of Different Well Azimuth

In this section, a horizontal well drilled in horizontal rock bedding is assumed. The horizontal well is oriented at different azimuth. The effects of different well orientation on the pore pressure, stress distribution and possibility of fracture initiation are studied.

3.2.1. Problem Statement

A horizontal well is drilled at different azimuth to the direction of minimum horizontal in-situ stress in transversely isotropic reservoir. The isotropic plane (see Fig. 3.35) is also horizontal. The borehole radius is R=0.1 m.

The loading and geometry are shown in Fig. 3.36. The definition and notation of coordinate systems are the same as described before. The in-situ stresses σ_H, σ_h, σ_v are defined in global coordinate system and thus are also denoted as σ_x^g, σ_y^g, σ_z^g.

The well coordinate system, which denotes the well orientation, is rotated from global coordinate system position following the steps described in section 2.1.6: Assume the well coordinate system initially coincide with the global coordinate system. In first step, rotate the initial well coordinate system 90° about its z-axis to get a new well coordinate system (WCS'). In second step, rotate the new well coordinate system 90° about its x axis to get another new well coordinate system (WCS''). In third step, rotate the WCS'' an azimuth angle $\phi_{azimuth}$ (which is the parameter in this section) about its y axis. The in situ stresses are converted to the well coordinate system and denoted as σ_x^g, σ_y^g, σ_z^g, σ_{xy}^g, σ_{yz}^g, σ_{zx}^g. Since the isotropic plane is horizontal, the material coordinate system is the same as global coordinate system.

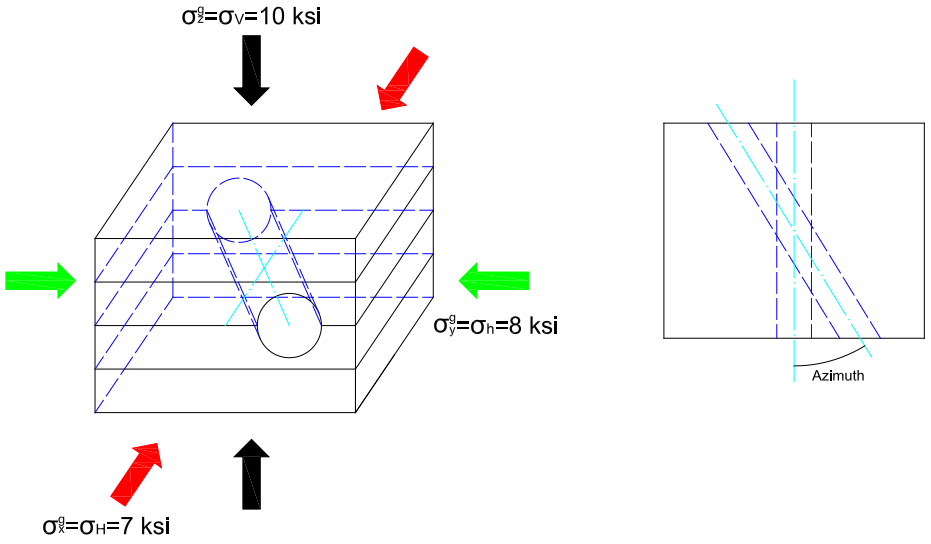

Fig. 3.35 Case 5-8: horizontal well and rock bedding position

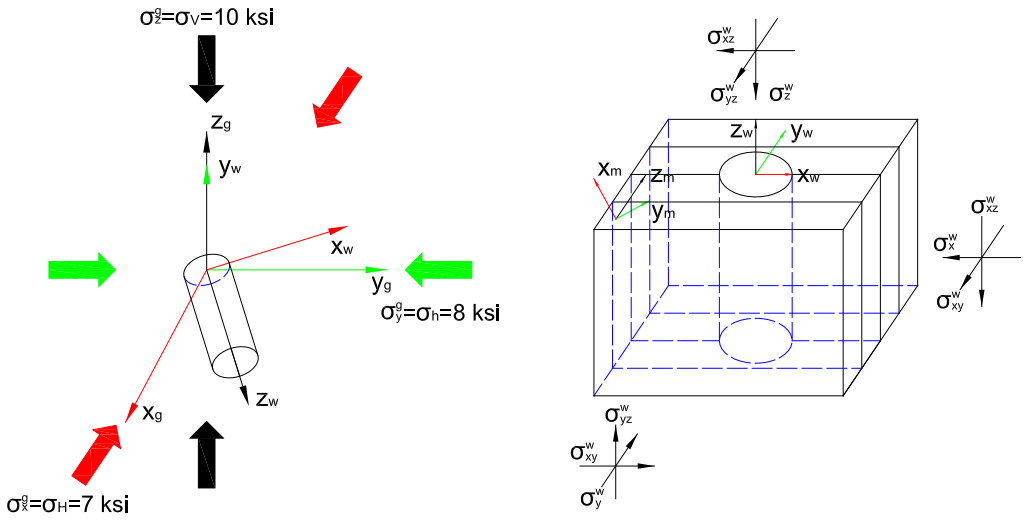

Fig. 3.36 Case 5-8: definition sketch of an deviated horizontal borehole problem

To study the effects of well azimuth, four cases are simulated in this section. In case 5, the horizontal well is drilled along the direction of minimum horizontal in-situ stress. In case 6, the horizontal well is drilled at 30° to the direction of minimum

horizontal in-situ stress. In case 7, the horizontal well is drilled at 60° to the direction of minimum horizontal in-situ stress. In case 8, the horizontal well is drilled 90° to the direction of minimum horizontal in-situ stress.

The common reservoir properties in four cases are presented as follows:

Angles rotating about z, x, y axes sequentially to transform global coordinate system to material coordinate system: ϕ_{m1} =0°, ϕ_{m2}=0°, ϕ_{m3}=0°

Initial state (in global coordinate system):

- Initial Pore Pressure: p_0=6 ksi
- In-situ Stresses: σ_H=8 ksi, σ_h=7 ksi, σ_v=10 ksi
- Mud Pressure: p_{mud}=8 ksi
- Fluid viscosity: μ=0.001Pa.s

Transversely isotropic rock properties (in material coordinate system):

- Permeability: K_x=K_y=1.0e-6 darcy, K_z=1.0e-7 darcy (K_h/K_v=10)
- Young's Modulus: E_x=E_y=4.2e3 ksi, E_z =1.4e3 ksi (E_h/E_v=3)
- Poisson's Ratio: ν_{xy}= ν_{yz}=ν_{zx}=0.25
- Shear Modulus: G_{xy}=1.68e3 ksi, G_{yz}=G_{zx}= 0.56e3 ksi
- Biot Coefficient: α_x=α_y=0.332, α_z=0.599
- Biot Modulus: M=2.78e3 ksi

Angles rotating about z, x, y axes sequentially to transform global coordinate system to wellbore coordinate system in four cases are listed as follows:

- Case 5, azimuth=0°: ϕ_{w1}=90°, ϕ_{w2}=90°, ϕ_{w3}=0°
- Case 6, azimuth=30°: ϕ_{w1}=90°, ϕ_{w2}=90°, ϕ_{w3}=30°

- Case 7, azimuth=60°: ϕ_{w1}=90°, ϕ_{w2}=90°, ϕ_{w3}=60°
- Case 8, azimuth=90°: ϕ_{w1}=90°, ϕ_{w2}=90°, ϕ_{w3}=90°

3.2.2. Results

Pore pressure, Biot's effective stress and total stress in different directions (tangential, radial and z-direction) near the wellbore and tangential Terzaghi's effective stress around wellbore at three time steps (1 second, 30 minutes and 3 days) from all four cases are presented in Fig. 3.3-Fig. 3.34.

3.2.2.1. Case 5: azimuth=0°

Case 5 is the base of all these four cases. Case 6, 7 and 8 is compared to case 5 to study the effect of different well azimuth.

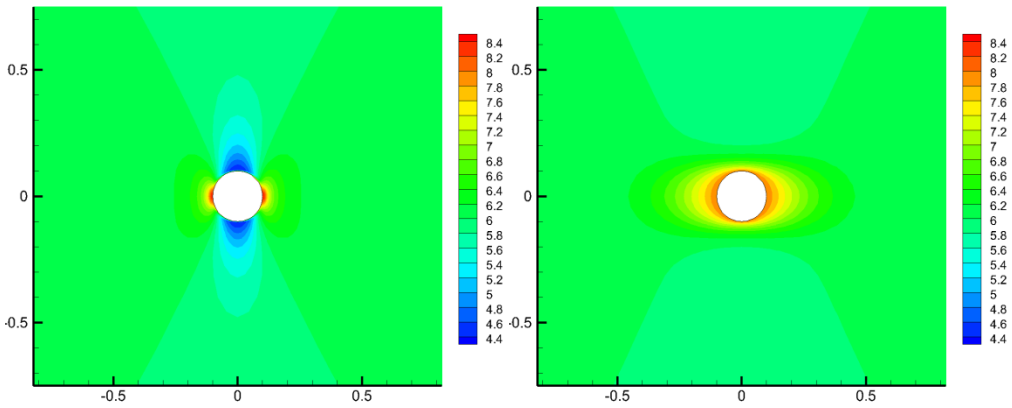

(a) t=1 second **(b) t=30 minutes**

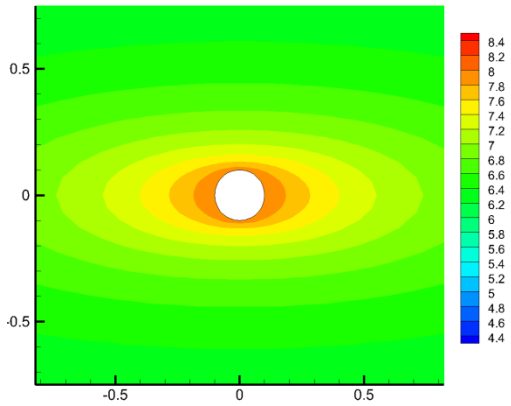

(c) t=3 days

Fig. 3.37 Case 5: pore pressure distribution

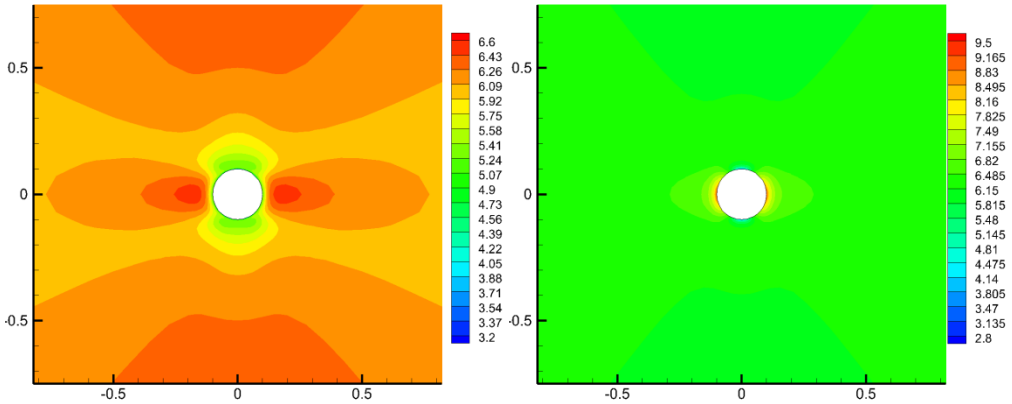

(a) Radial Stress **(b) Tangential Stress**

Fig. 3.38 Case 5: Biot's effective stress distribution at t=1 second

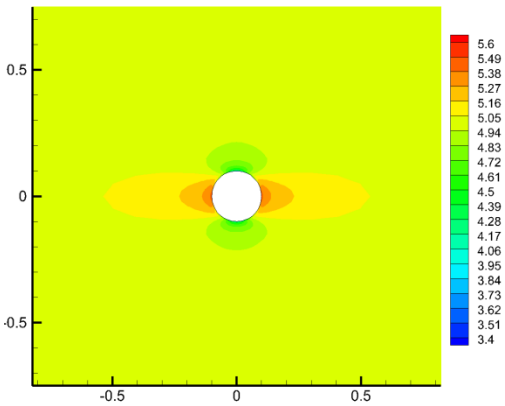

(c) Z Direction Stress

Fig. 3.38 Continued

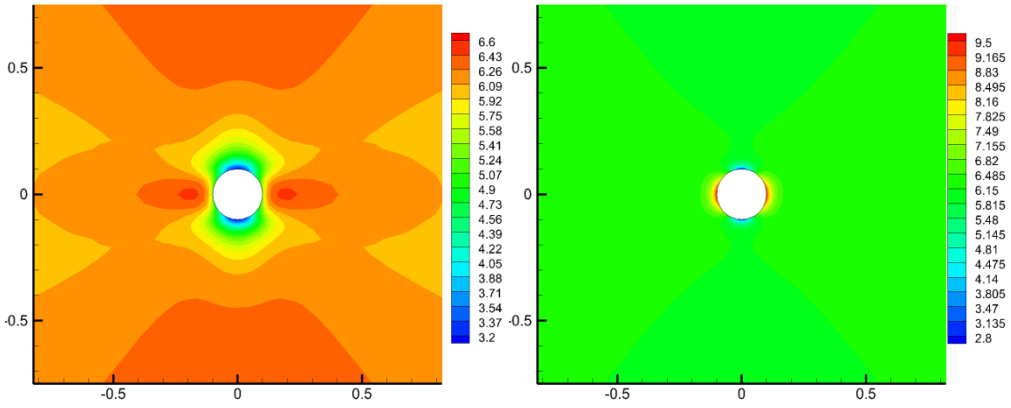

(a) Radial Stress **(b) Tangential Stress**

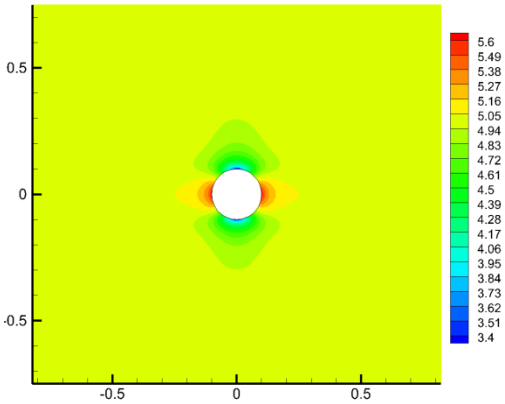

(c) Z Direction Stress

Fig. 3.39 Case 5: Biot's effective stress distribution at t=30 minutes

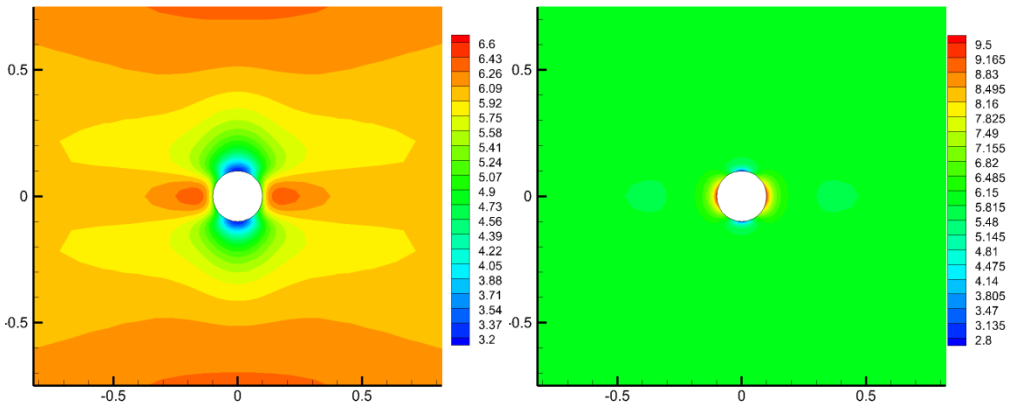

(a) Radial Stress **(b) Tangential Stress**

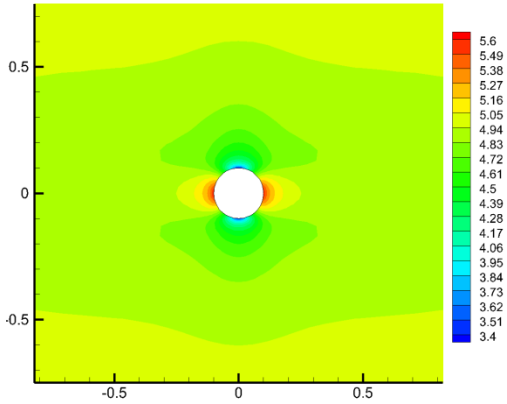

(c) Z Direction Stress

Fig. 3.40 Case 5: Biot's effective stress distribution at t=3 days

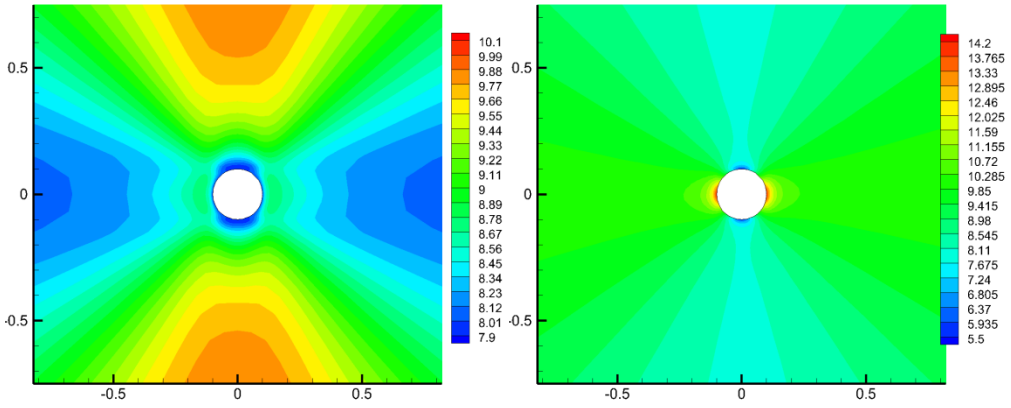

(a) Radial Stress **(b) Tangential Stress**

Fig. 3.41 Case 5: total stress distribution at t=1 second

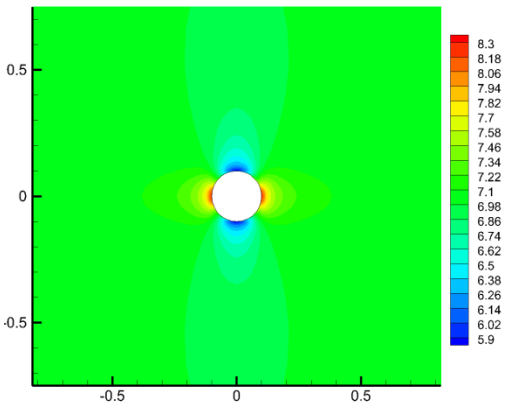

(c) Z Direction Stress

Fig. 3.41 Continued

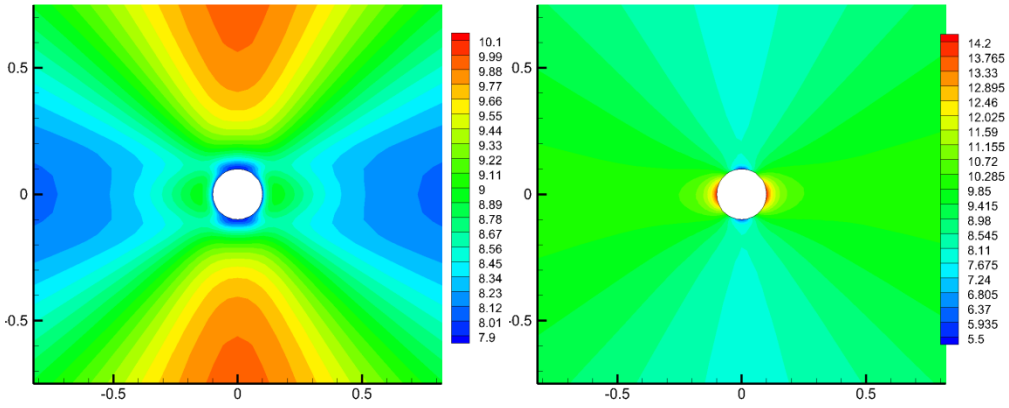

(a) Radial Stress **(b) Tangential Stress**

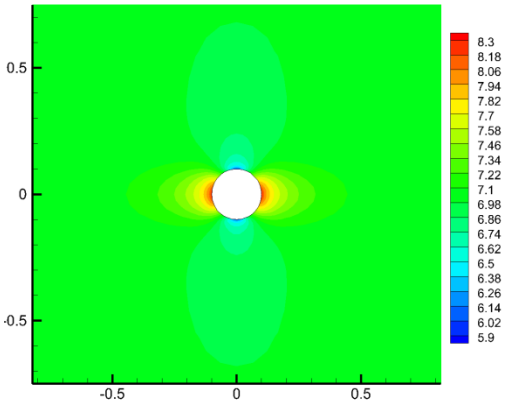

(c) Z Direction Stress

Fig. 3.42 Case 5: total stress distribution at t=30 minutes

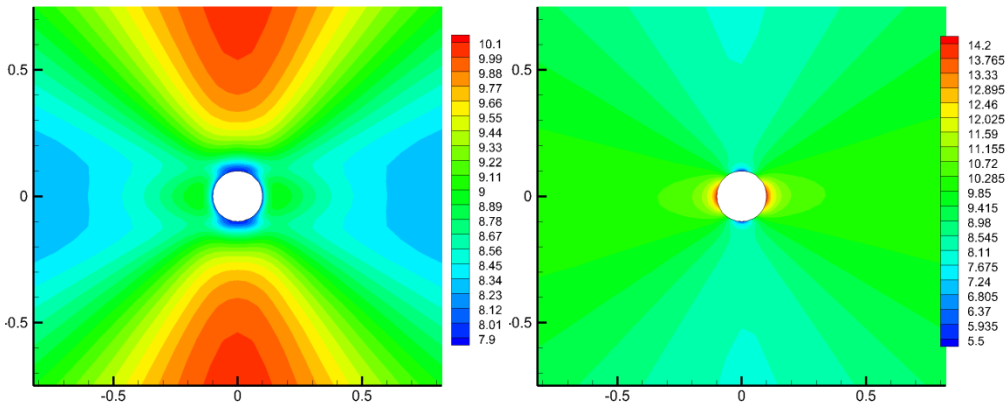

(a) Radial Stress **(b) Tangential Stress**

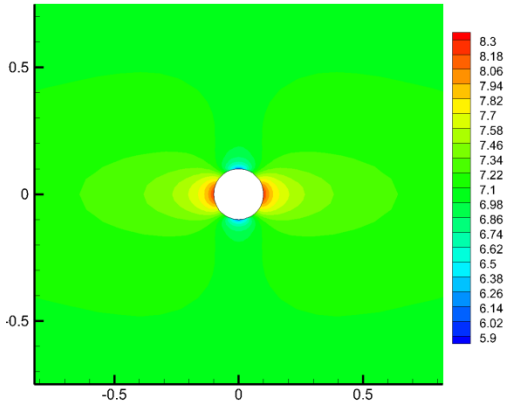

(c) Z Direction Stress

Fig. 3.43 Case 5: total stress distribution at t=3 days

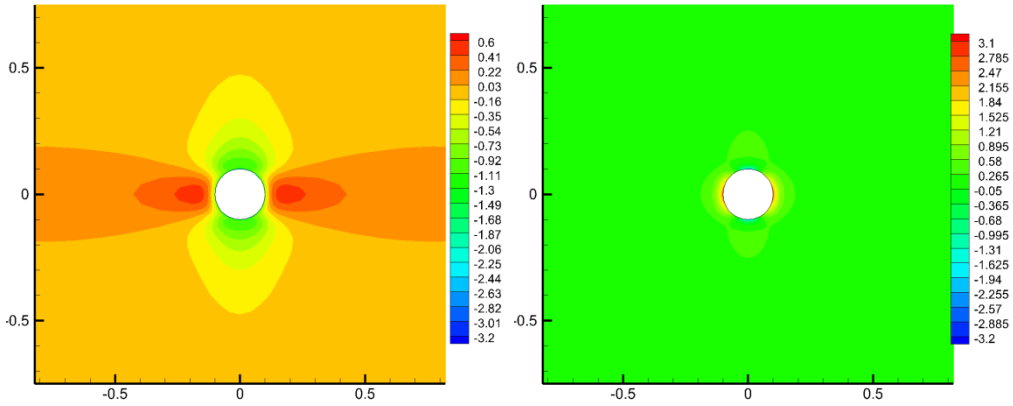

(a) Radial Stress **(b) Tangential Stress**

Fig. 3.44 Case 5: induced Biot's effective stress distribution at t=1 second

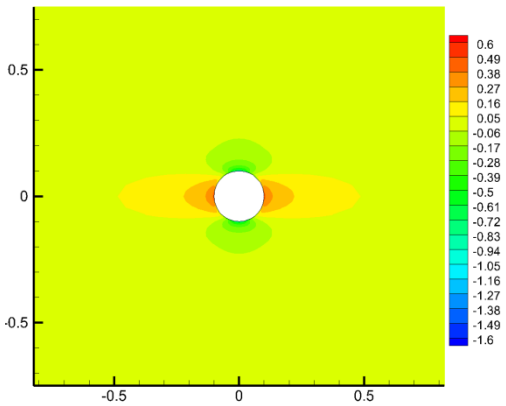

(c) Z Direction Stress

Fig. 3.44 Continued

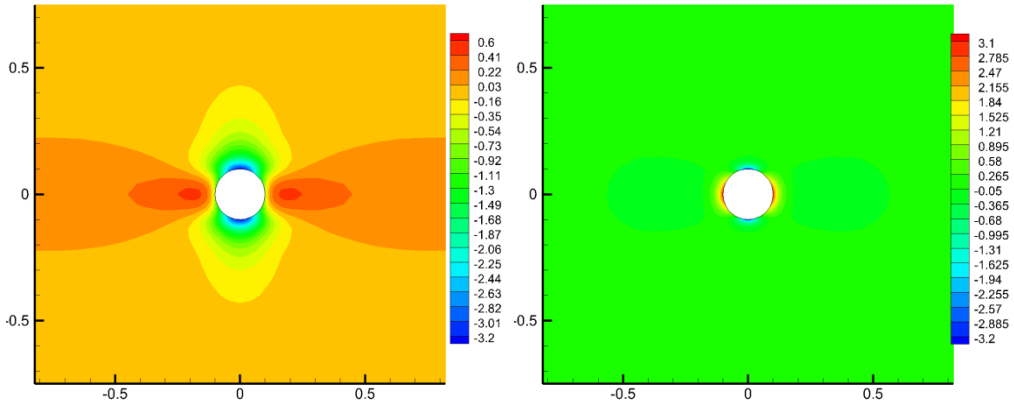

(a) Radial Stress **(b) Tangential Stress**

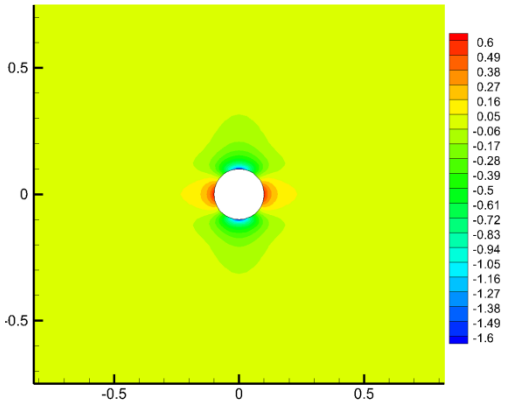

(c) Z Direction Stress

Fig. 3.45 Case 5: induced Biot's effective stress distribution at t=30 minutes

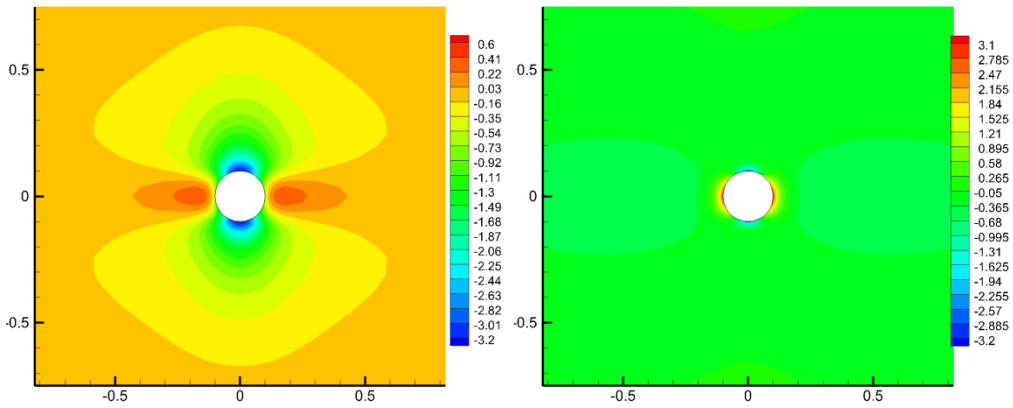

(a) Radial Stress **(b) Tangential Stress**

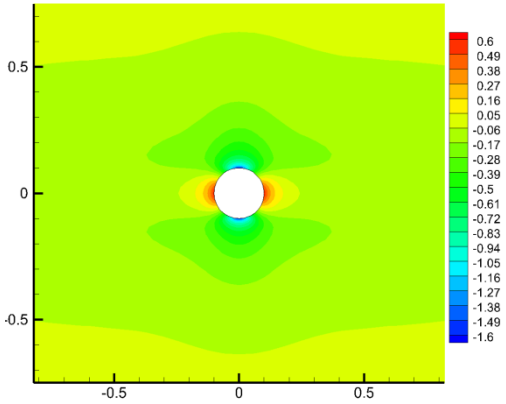

(c) Z Direction Stress

Fig. 3.46 Case 5: induced Biot's effective stress distribution at t=3 days

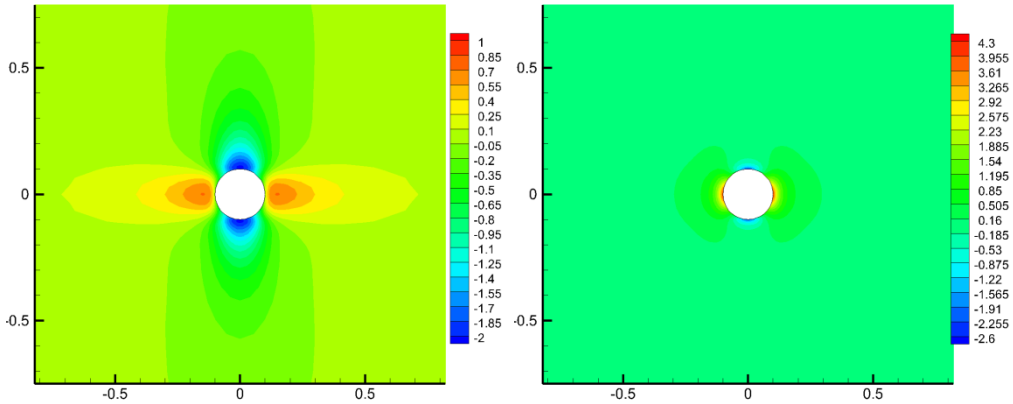

(a) Radial Stress **(b) Tangential Stress**

Fig. 3.47 Case 5: induced total stress distribution at t=1 second

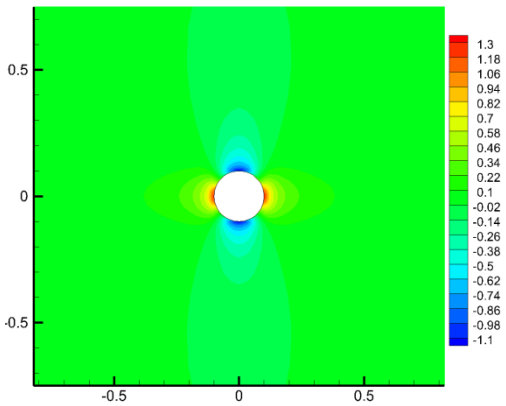

(c) Z Direction Stress

Fig. 3.47 Continued

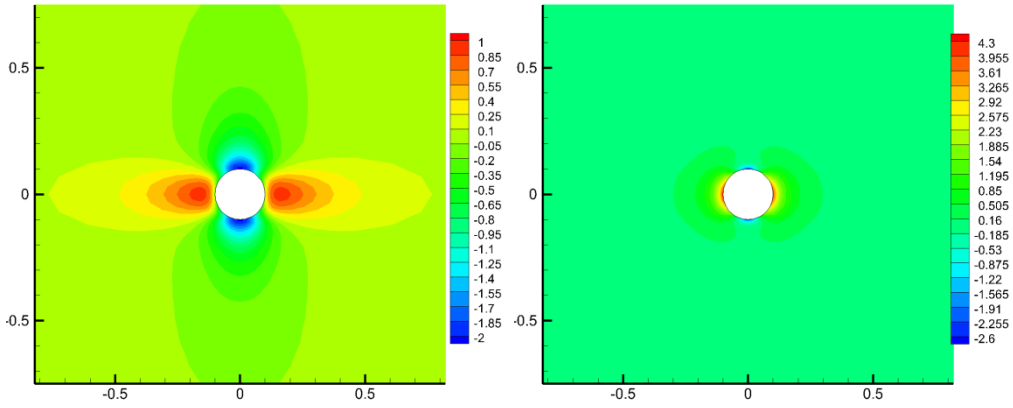

(a) Radial Stress **(b) Tangential Stress**

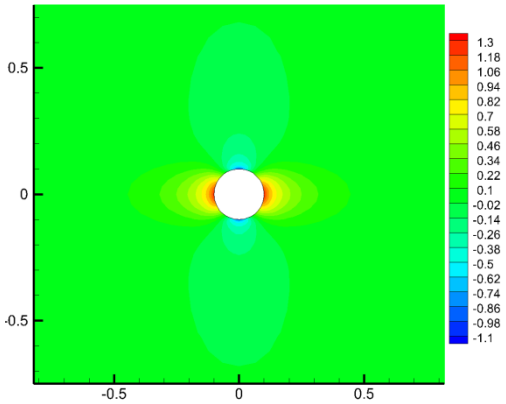

(c) Z Direction Stress

Fig. 3.48 Case 5: induced total stress distribution at t=30 minutes

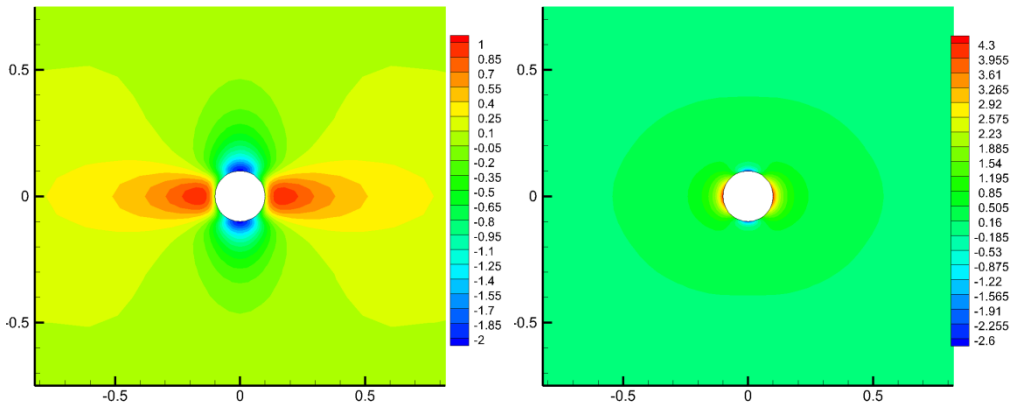

(a) Radial Stress **(b) Tangential Stress**

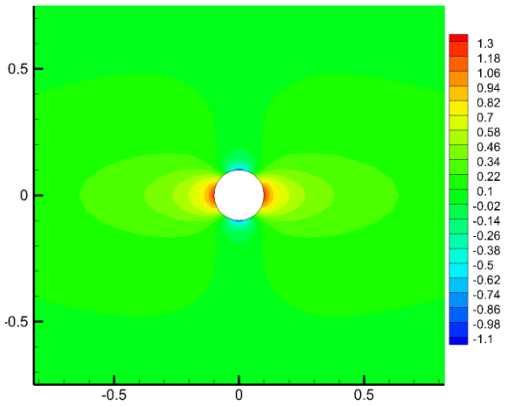

(c) Z Direction Stress

Fig. 3.49 Case 5: induced total stress distribution at t=3 days

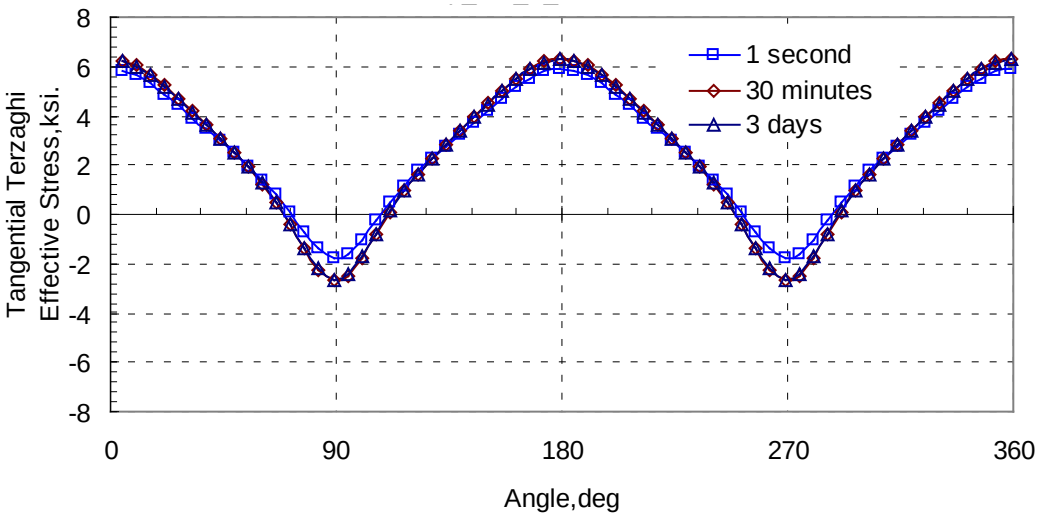

Fig. 3.50 Case 5: Tangential Terzaghi's Effective Stress around Wellbore

3.2.2.2. Case 6: azimuth=30°

Compared to Case 5, Case 6 shows the effect of 30° well azimuth.

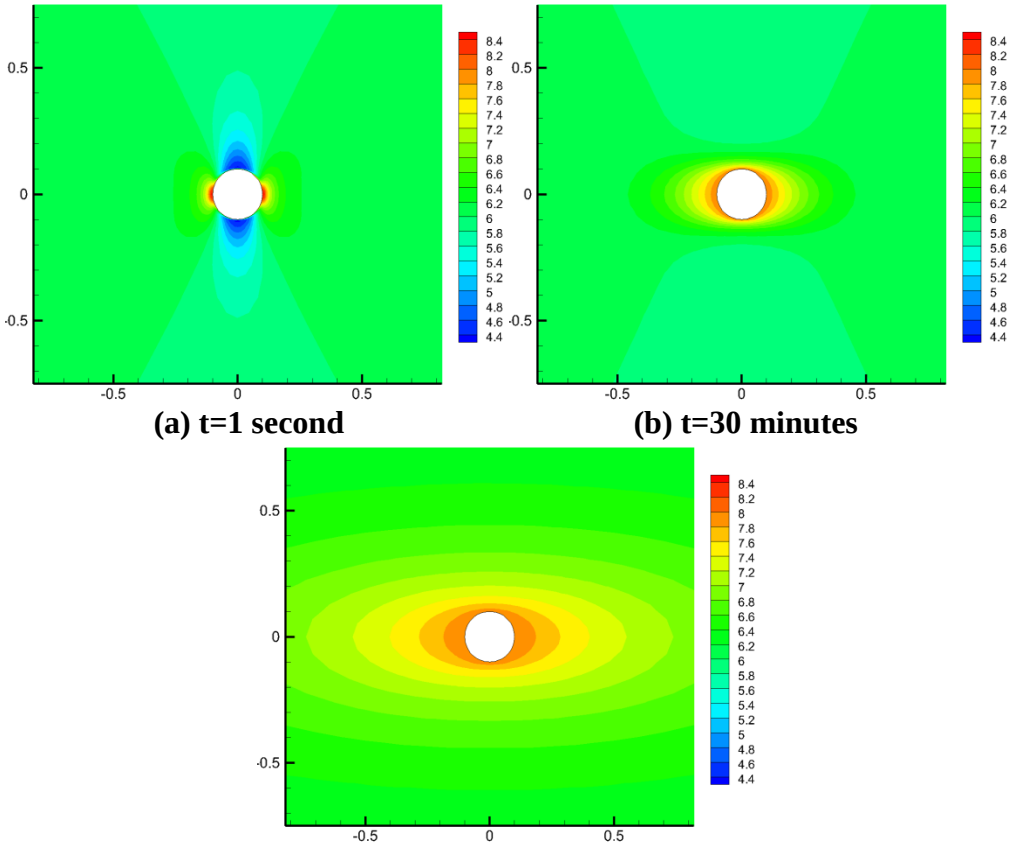

(a) t=1 second **(b) t=30 minutes**

(c) t=3 days

Fig. 3.51 Case 6: pore pressure distribution

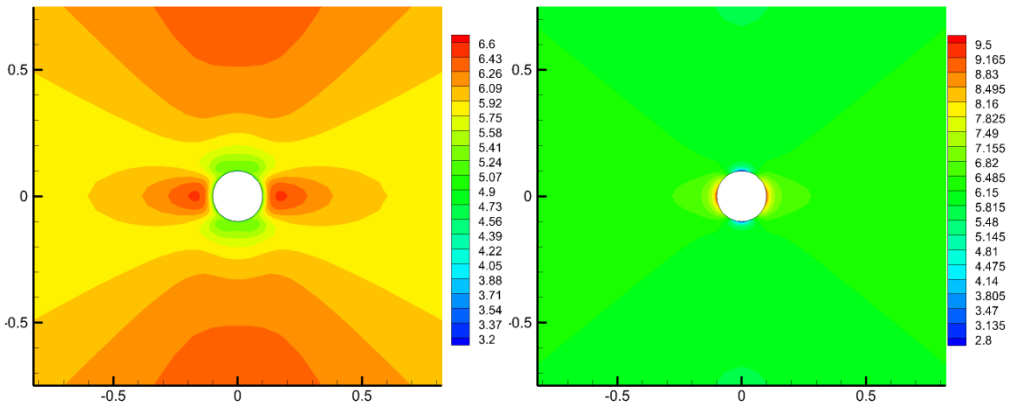

(a) Radial Stress **(b) Tangential Stress**

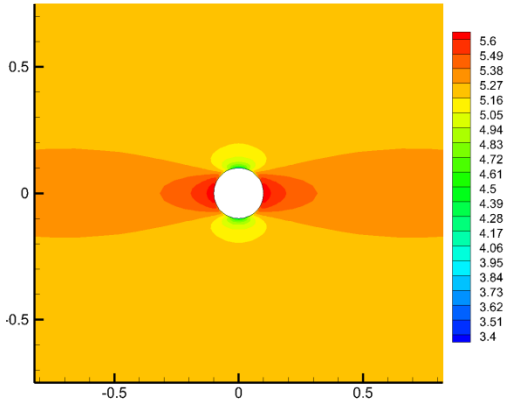

(c) Z Direction Stress

Fig. 3.52 Case 6: Biot's effective stress distribution at t=1 second

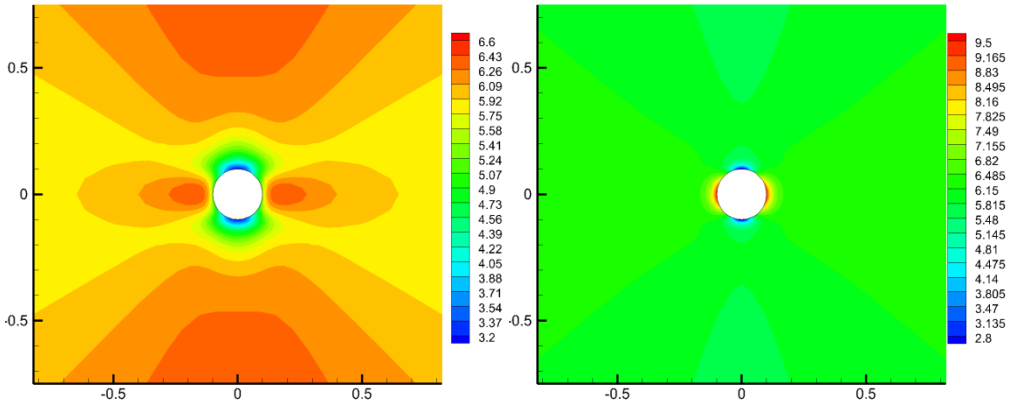

(a) Radial Stress **(b) Tangential Stress**

Fig. 3.53 Case 6: Biot's effective stress distribution at t=30 minutes

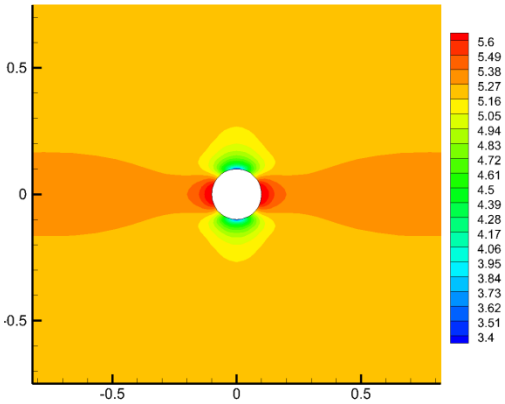

(c) Z Direction Stress

Fig. 3.53 Continued

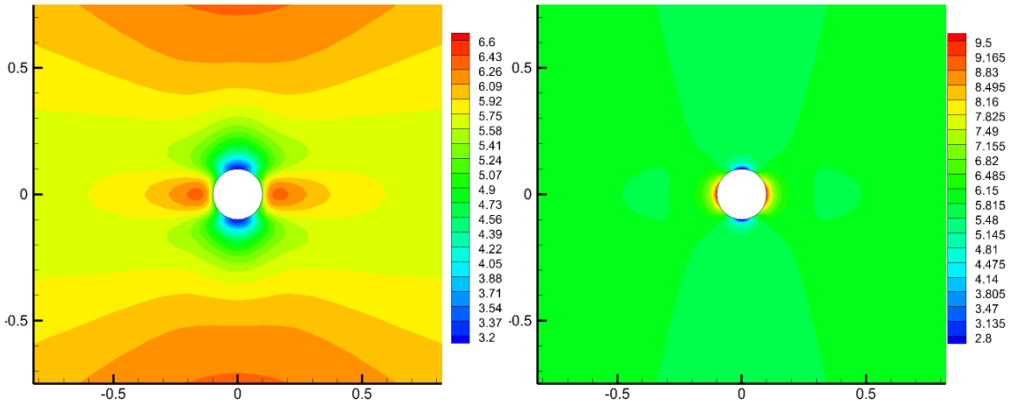

(a) Radial Stress **(b) Tangential Stress**

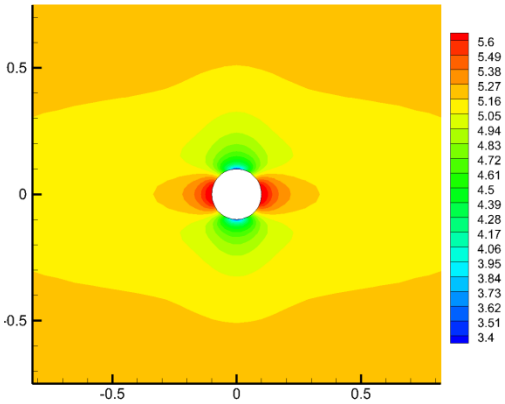

(c) Z Direction Stress

Fig. 3.54 Case 6: Biot's effective stress distribution at t=3 days

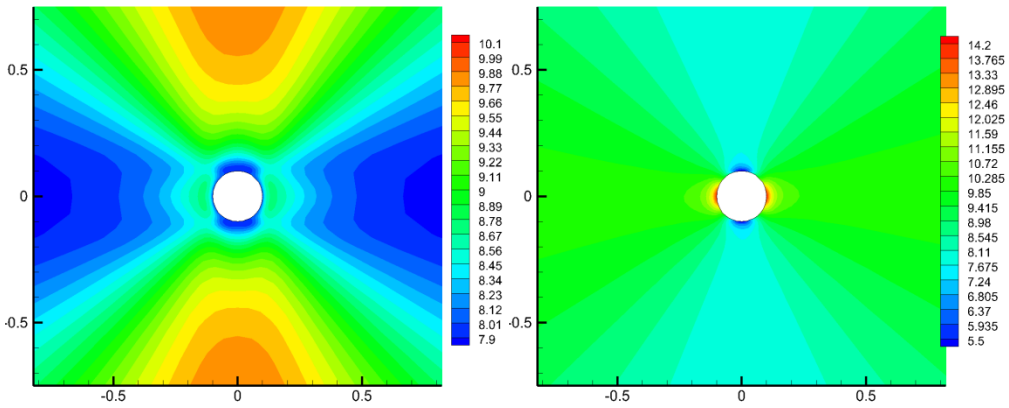

(a) Radial Stress **(b) Tangential Stress**

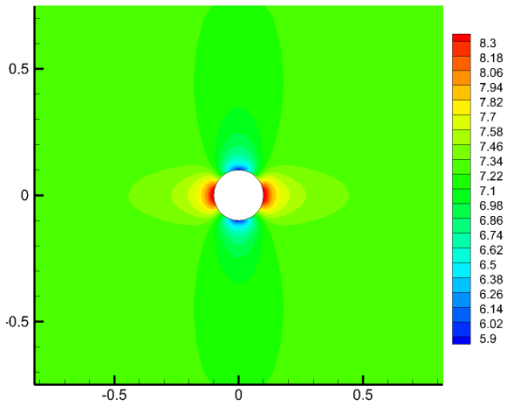

(c) Z Direction Stress

Fig. 3.55 Case 6: total stress distribution at t=1 second

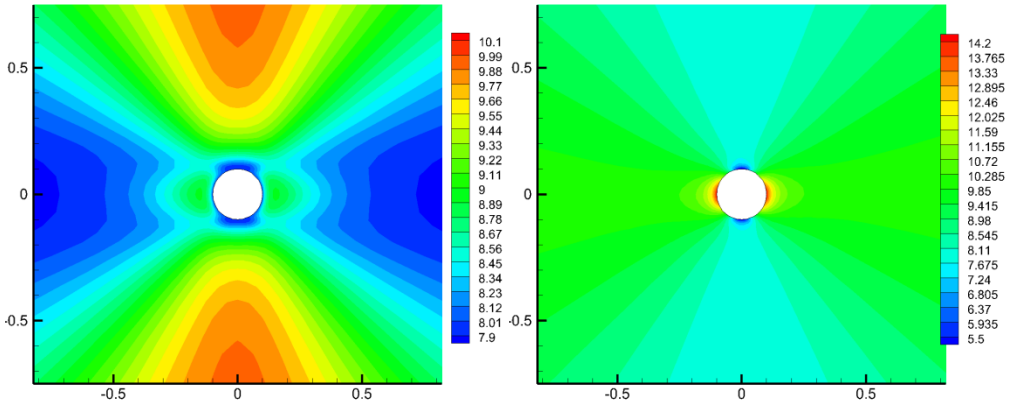

(a) Radial Stress **(b) Tangential Stress**

Fig. 3.56 Case 6: total stress distribution at t=30 minutes

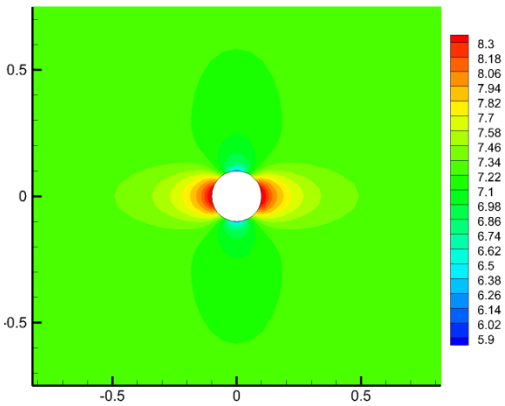

(c) Z Direction Stress

Fig. 3.56 Continued

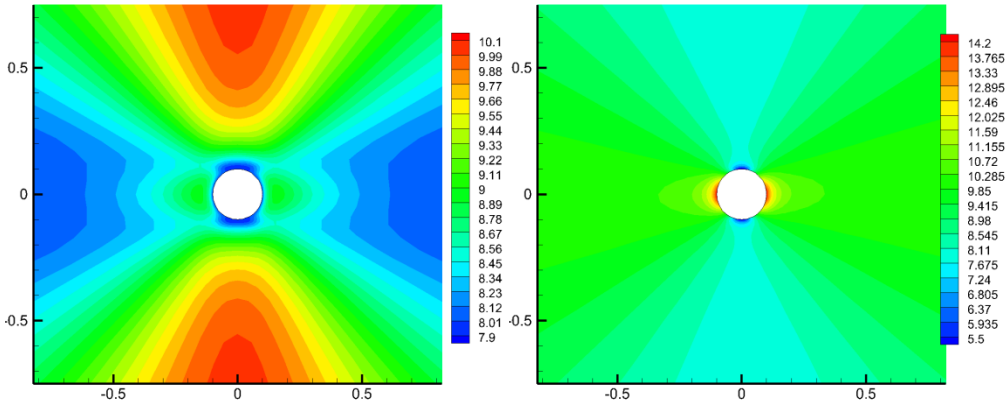

(a) Radial Stress **(b) Tangential Stress**

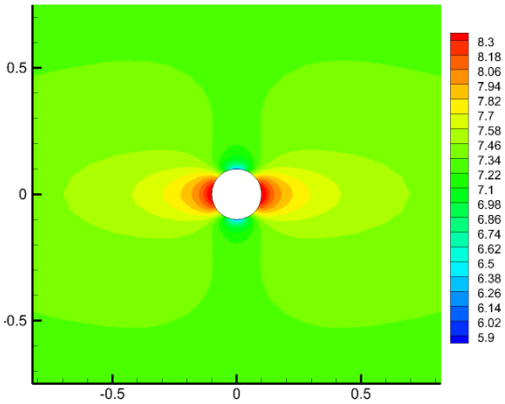

(c) Z Direction Stress

Fig. 3.57 Case 6: total stress distribution at t=3 days

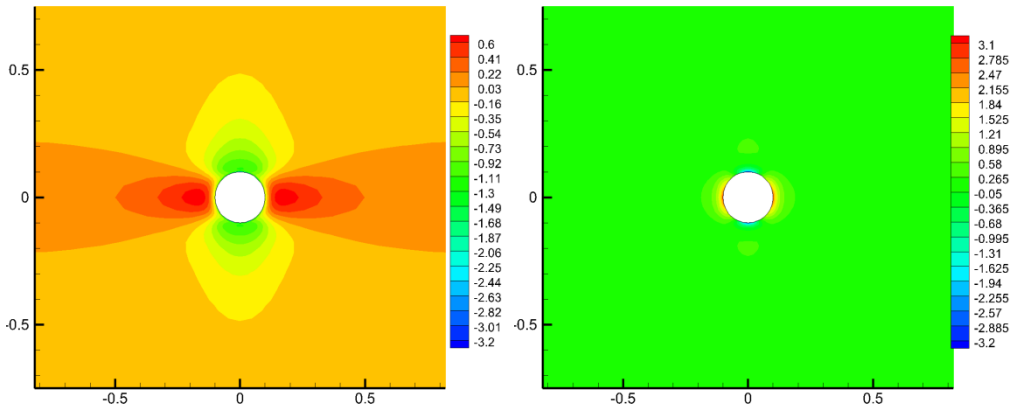

(a) Radial Stress **(b) Tangential Stress**

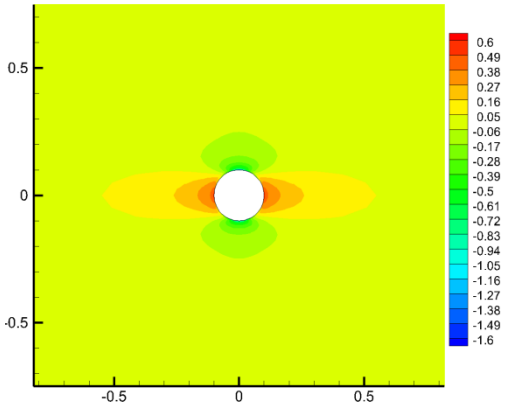

(c) Z Direction Stress

Fig. 3.58 Case 6: induced Biot's effective stress distribution at t=1 second

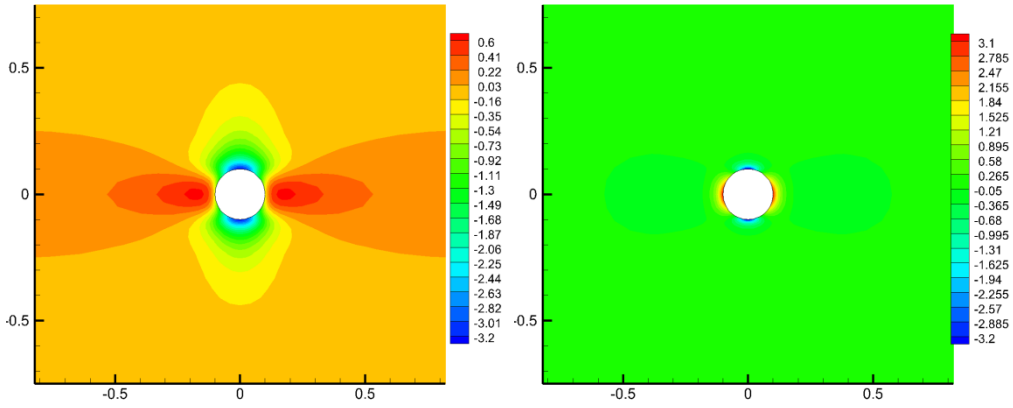

(a) Radial Stress **(b) Tangential Stress**

Fig. 3.59 Case 6: induced Biot's effective stress distribution at t=30 minutes

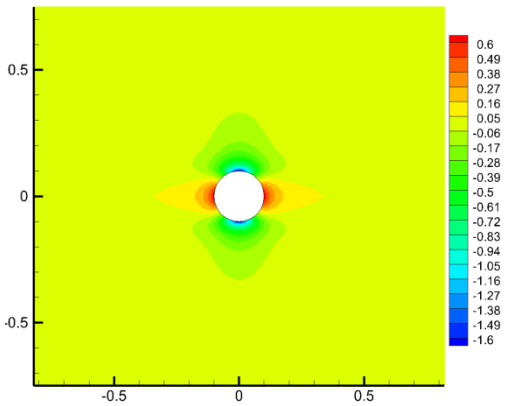

(c) Z Direction Stress

Fig. 3.59 Continued

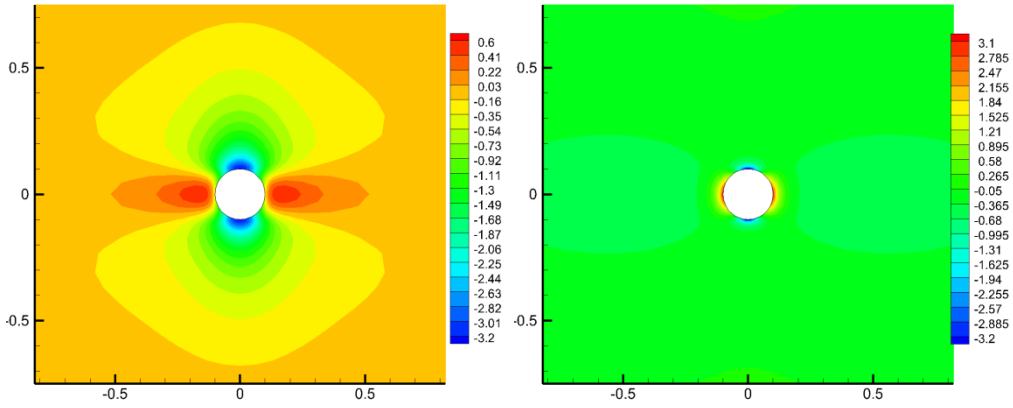

(a) Radial Stress **(b) Tangential Stress**

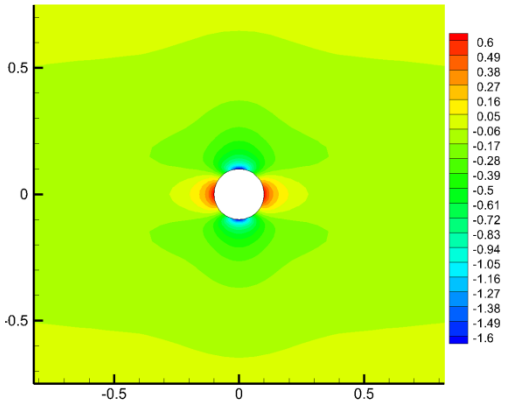

(c) Z Direction Stress

Fig. 3.60 Case 6: induced Biot's effective stress distribution at t=3 days

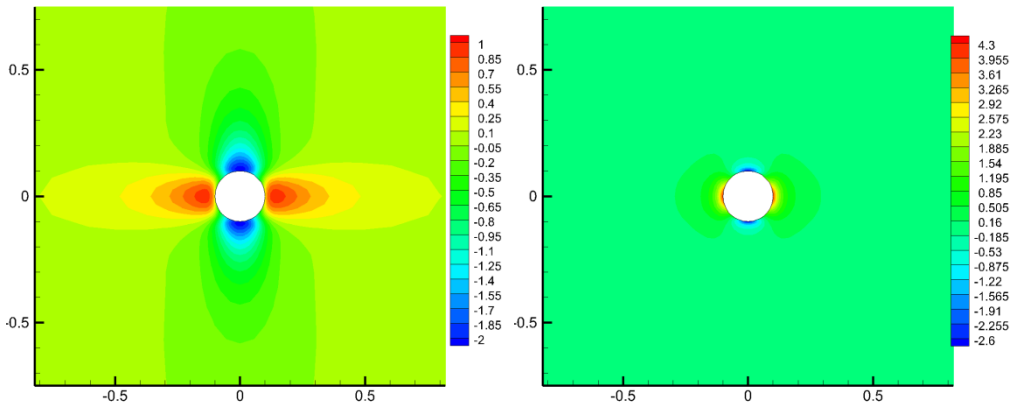

(a) Radial Stress **(b) Tangential Stress**

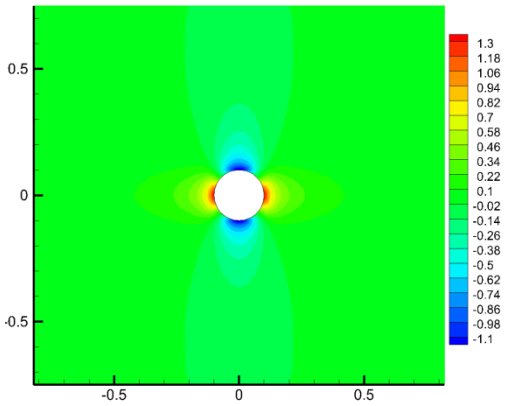

(c) Z Direction Stress

Fig. 3.61 Case 6: induced total stress distribution at t=1 second

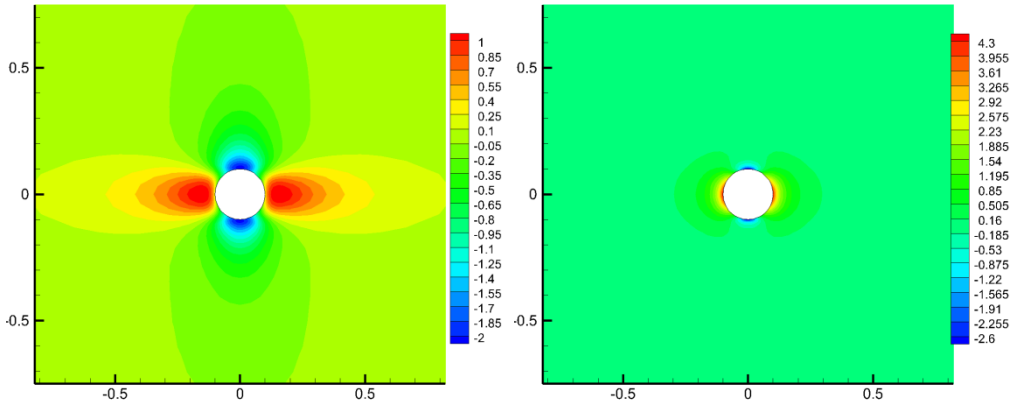

(a) Radial Stress **(b) Tangential Stress**

Fig. 3.62 Case 6: induced total stress distribution at t=30 minutes

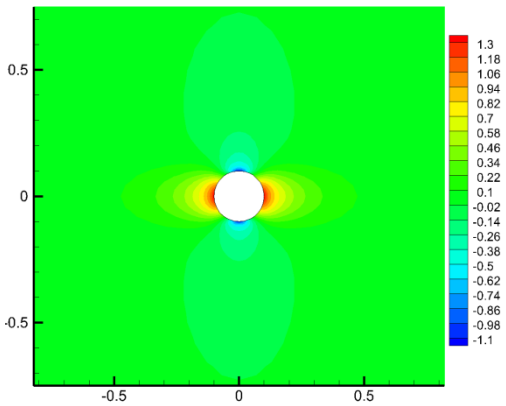

(c) Z Direction Stress

Fig. 3.62 Continued

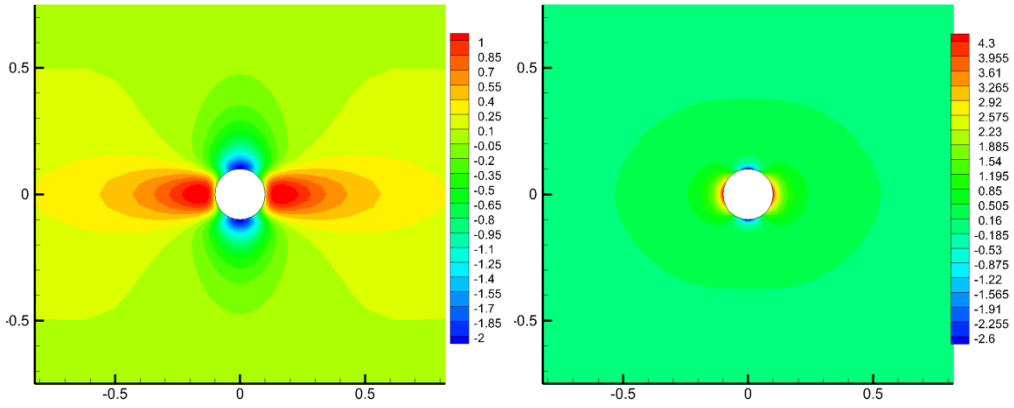

(a) Radial Stress **(b) Tangential Stress**

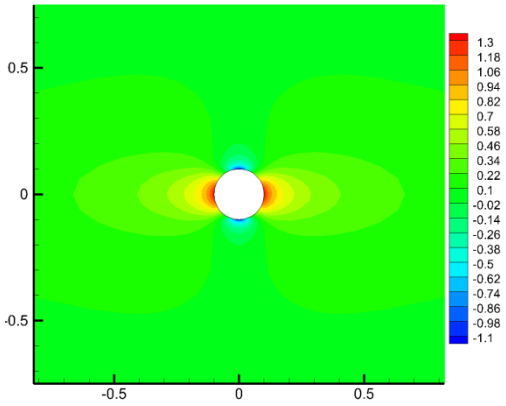

(c) Z Direction Stress

Fig. 3.63 Case 6: induced total stress distribution at t=3 days

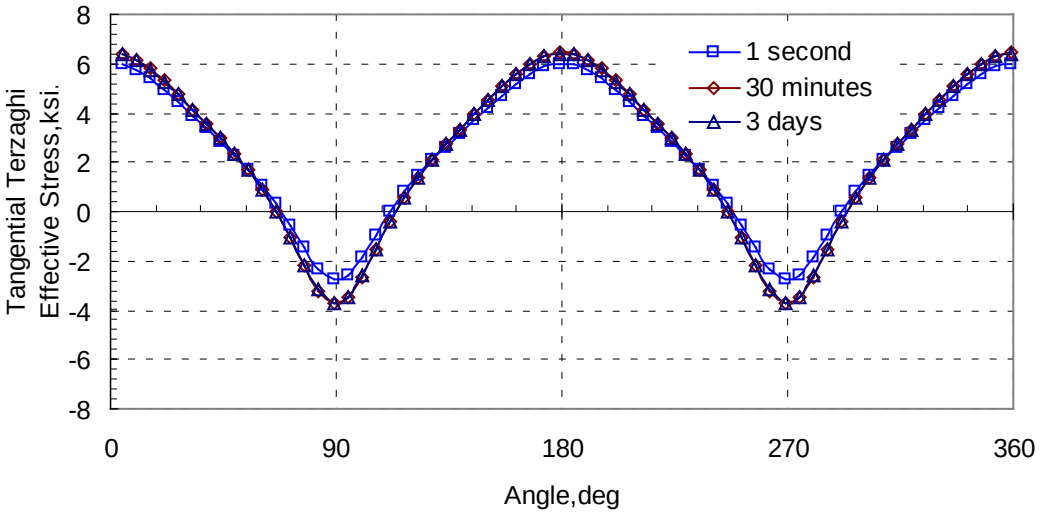

Fig. 3.64 Case 6: tangential Terzaghi's effective stress around wellbore

3.2.2.3. Case 7: azimuth=60°

Compared to Case 5, Case 7 shows the effect of 60° well azimuth.

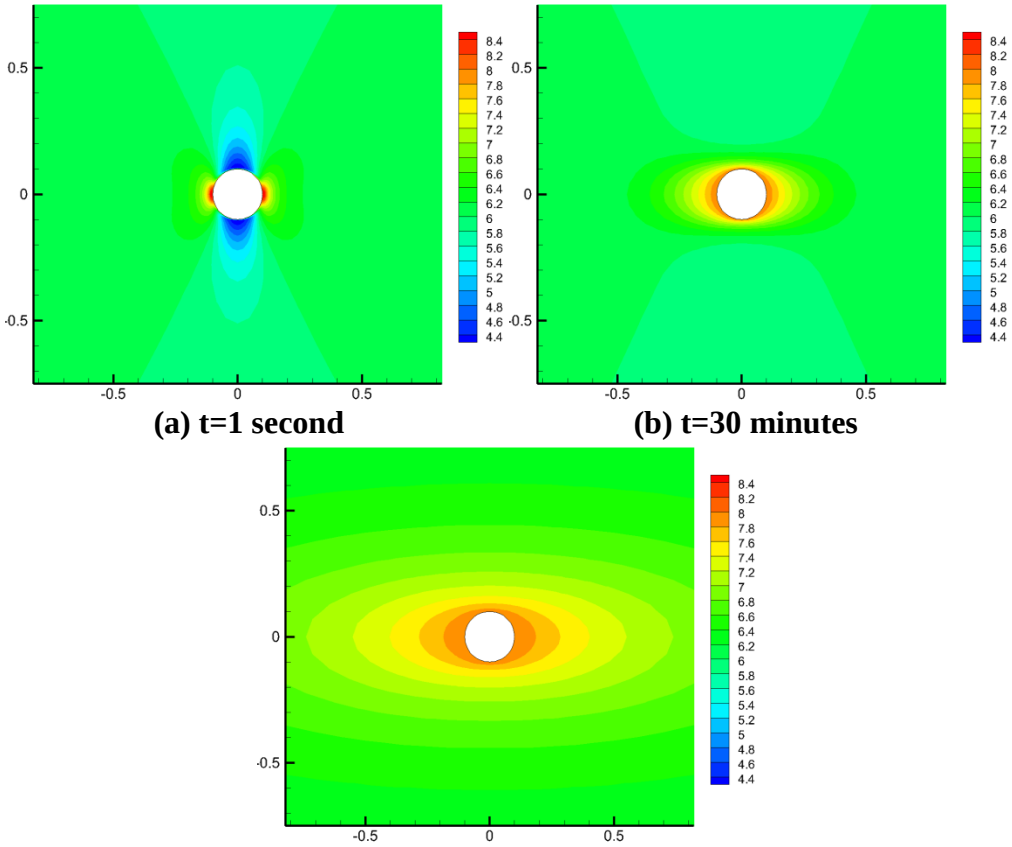

(a) t=1 second **(b) t=30 minutes**

(c) t=3 days

Fig. 3.65 Case 7: pore pressure distribution

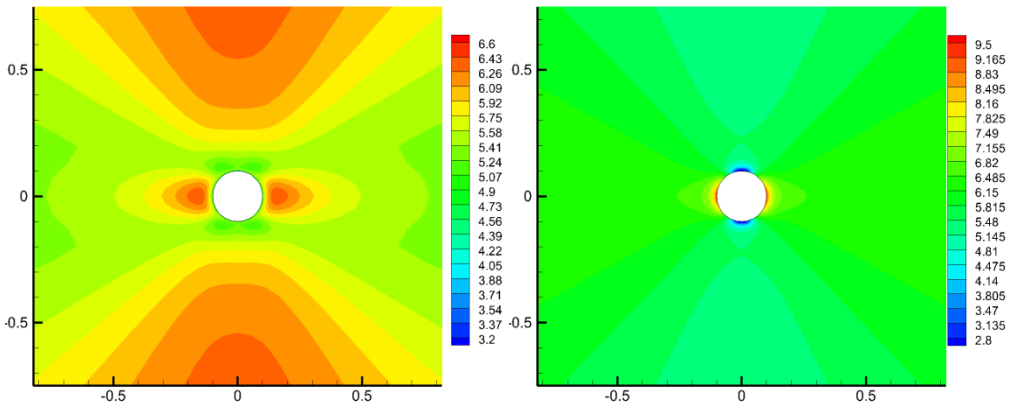

(a) Radial Stress **(b) Tangential Stress**

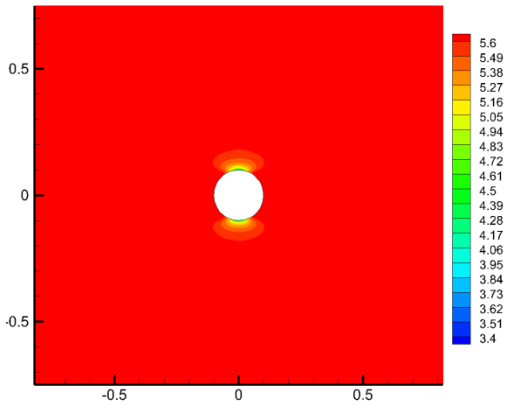

(c) Z Direction Stress

Fig. 3.66 Case 7: Biot's effective stress distribution at t=1 second

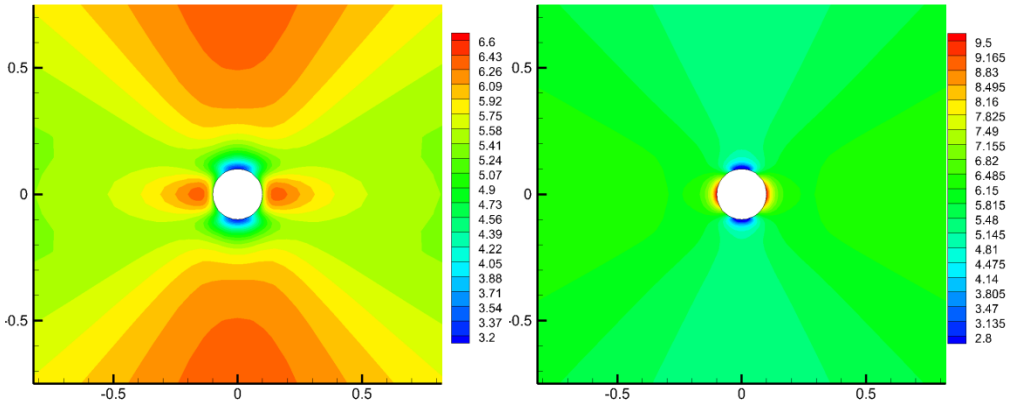

(a) Radial Stress **(b) Tangential Stress**

Fig. 3.67 Case 7: Biot's effective stress distribution at t=30 minutes

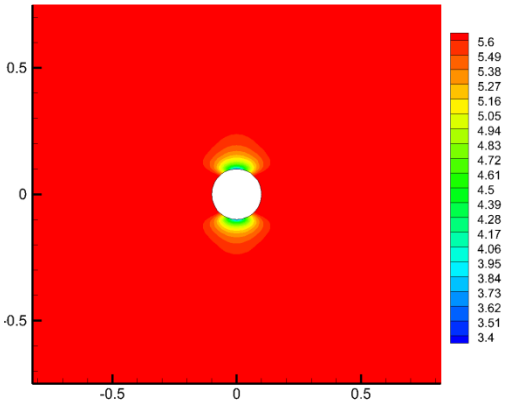

(c) Z Direction Stress

Fig. 3.67 Continued

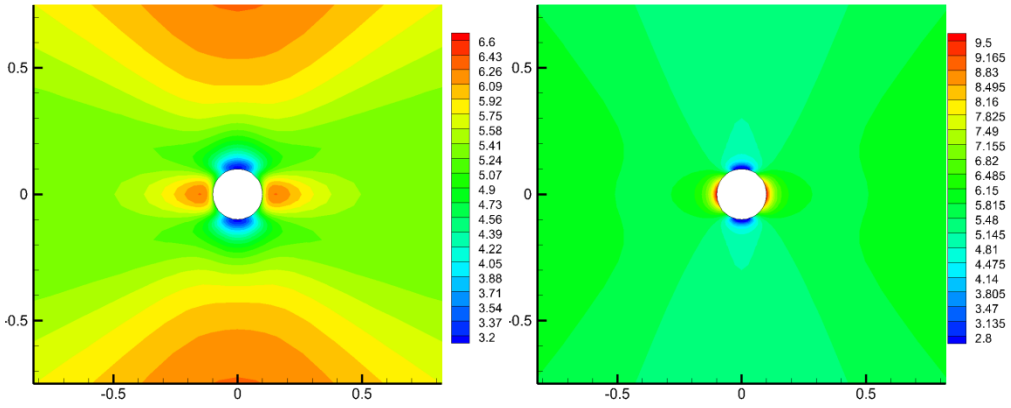

(a) Radial Stress **(b) Tangential Stress**

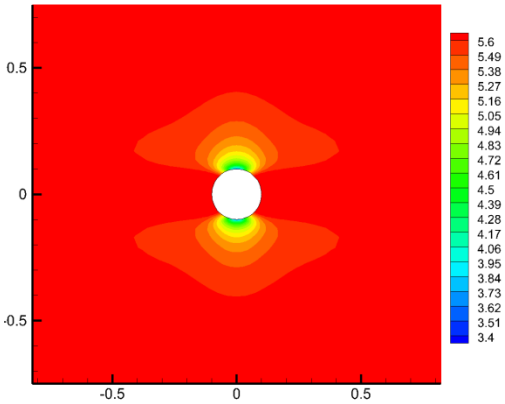

(c) Z Direction Stress

Fig. 3.68 Case 7: Biot's effective stress distribution at t=3 days

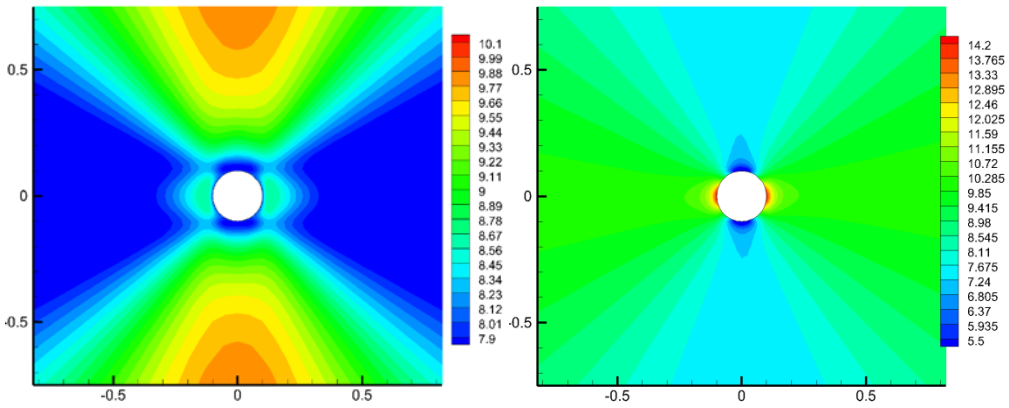

(a) Radial Stress **(b) Tangential Stress**

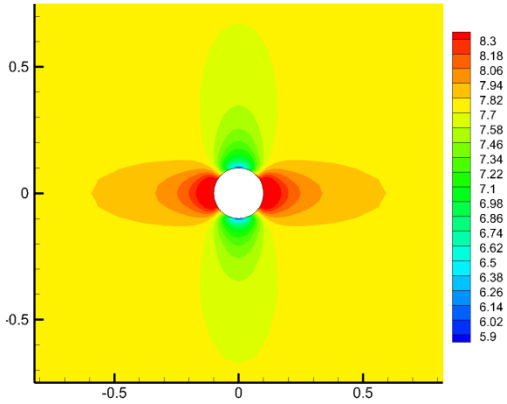

(c) Z Direction Stress

Fig. 3.69 Case 7: total stress distribution at t=1 second

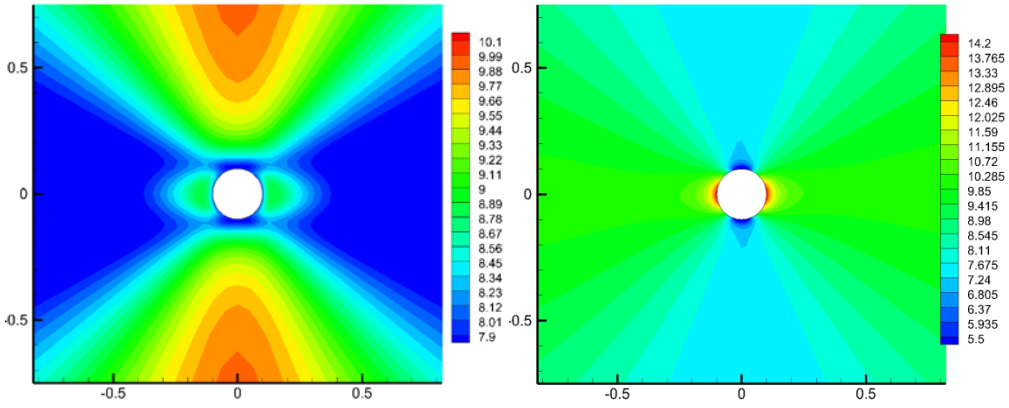

(a) Radial Stress **(b) Tangential Stress**

Fig. 3.70 Case 7: total stress distribution at t=30 minutes

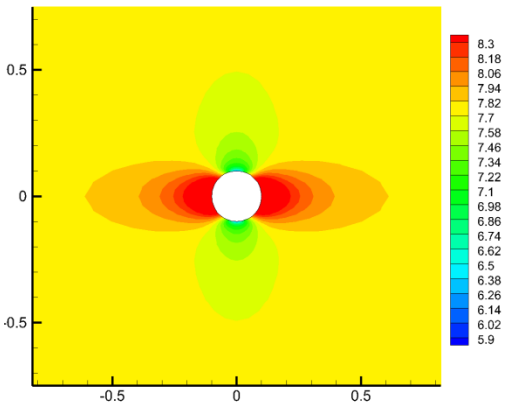

(c) Z Direction Stress

Fig. 3.70 Continued

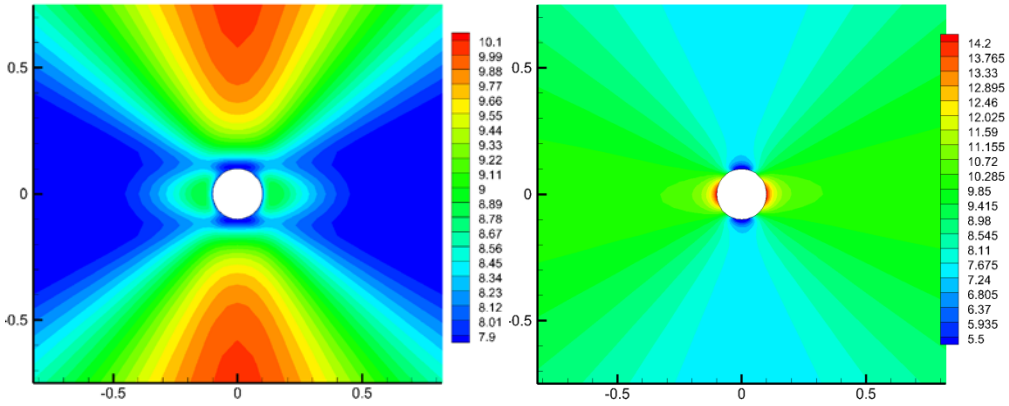

(a) Radial Stress **(b) Tangential Stress**

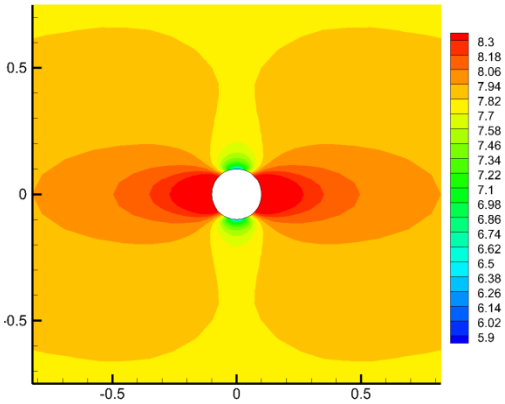

(c) Z Direction Stress

Fig. 3.71 Case 7: total stress distribution at t=3 days

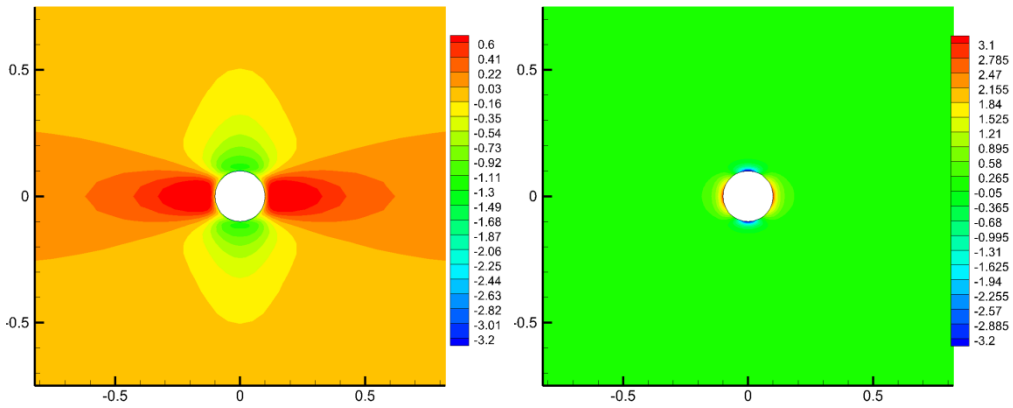

(a) Radial Stress **(b) Tangential Stress**

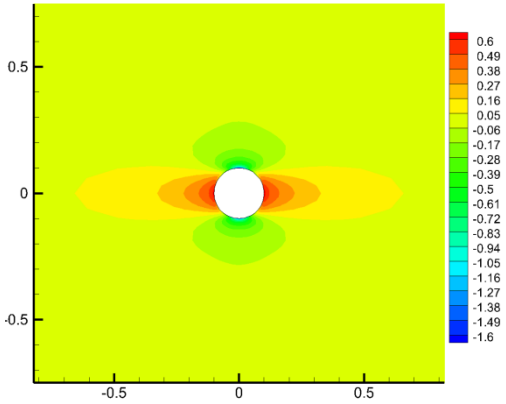

(c) Z Direction Stress

Fig. 3.72 Case 7: induced Biot's effective stress distribution at t=1 second

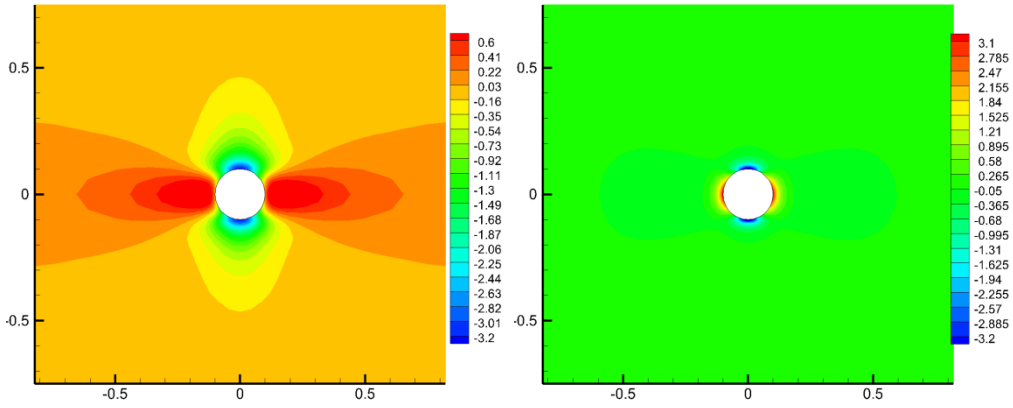

(a) Radial Stress **(b) Tangential Stress**

Fig. 3.73 Case 7: induced Biot's effective stress distribution at t=30 minutes

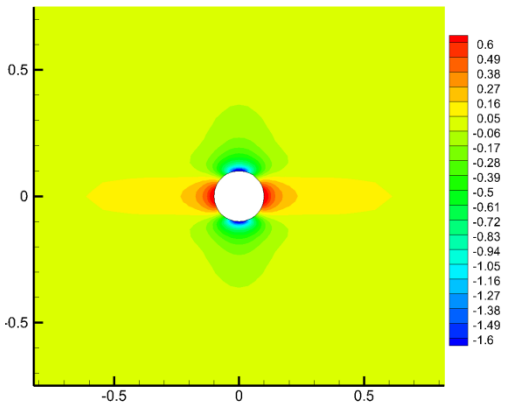

(c) Z Direction Stress

Fig. 3.73 Continued

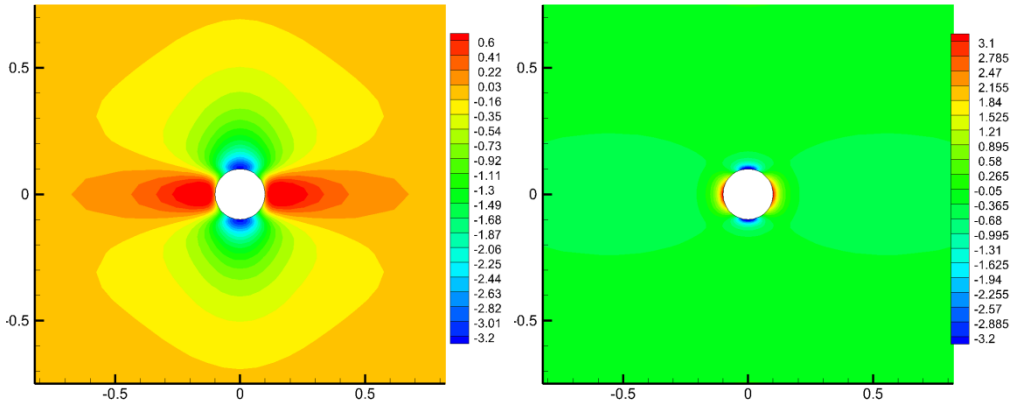

(a) Radial Stress **(b) Tangential Stress**

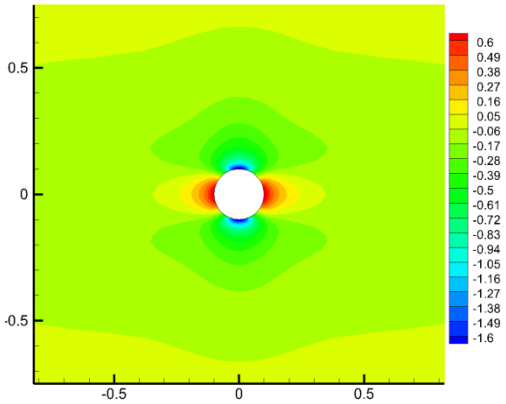

(c) Z Direction Stress

Fig. 3.74 Case 7: induced Biot's effective stress distribution at t=3 days

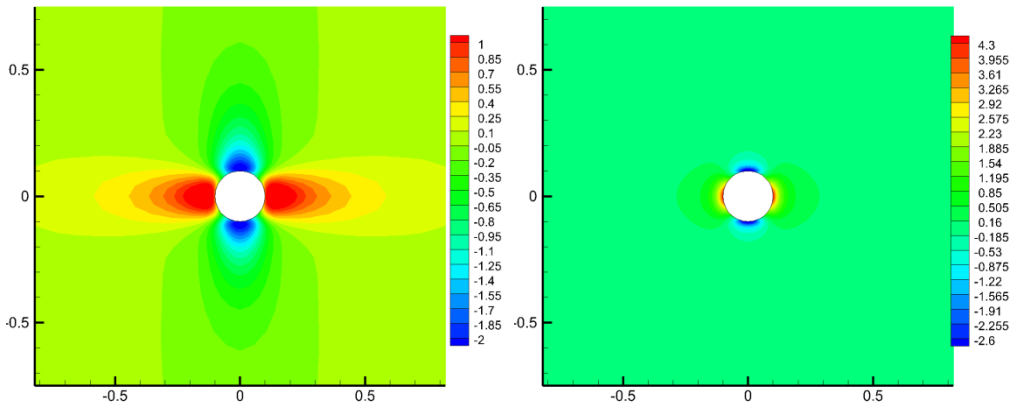

(a) Radial Stress **(b) Tangential Stress**

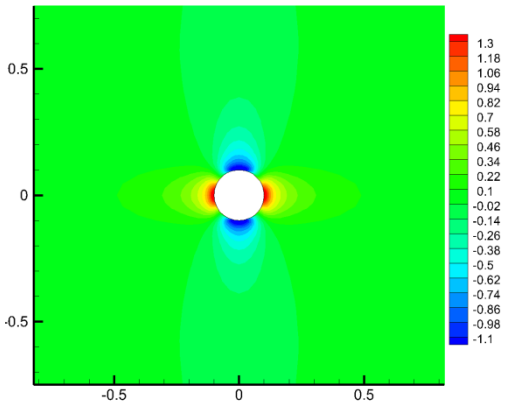

(c) Z Direction Stress

Fig. 3.75 Case 7: induced total stress distribution at t=1 second

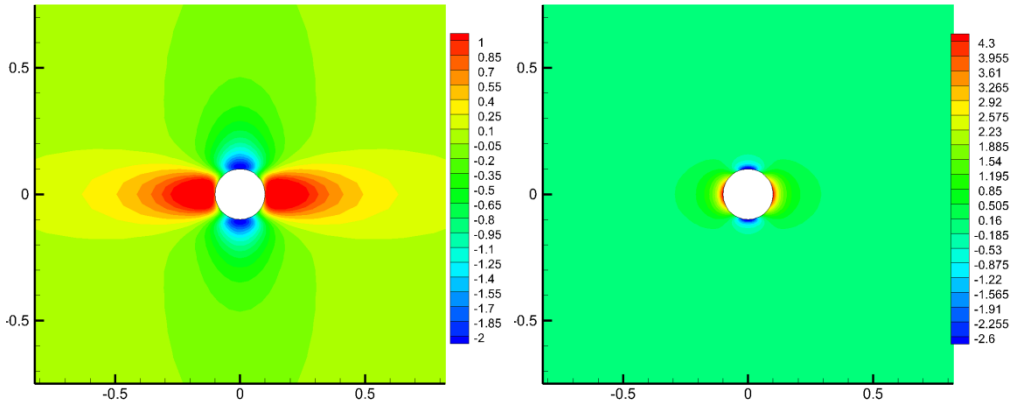

(a) Radial Stress **(b) Tangential Stress**

Fig. 3.76 Case 7: induced total stress distribution at t=30 minutes

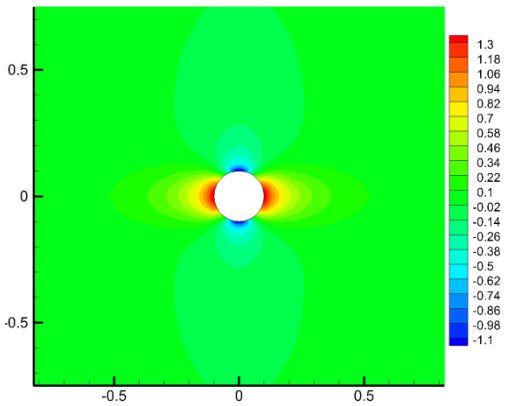

(c) Z Direction Stress

Fig. 3.76 Continued

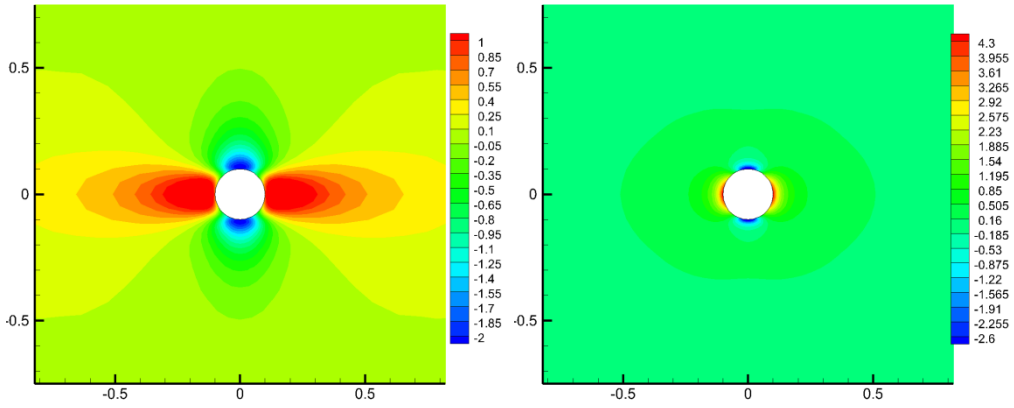

(a) Radial Stress **(b) Tangential Stress**

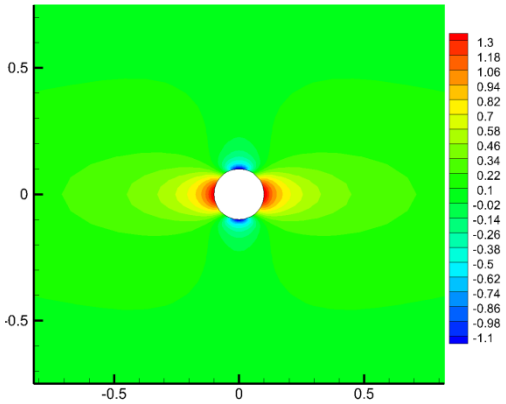

(c) Z Direction Stress

Fig. 3.77 Case 7: induced total stress distribution at t=3 days

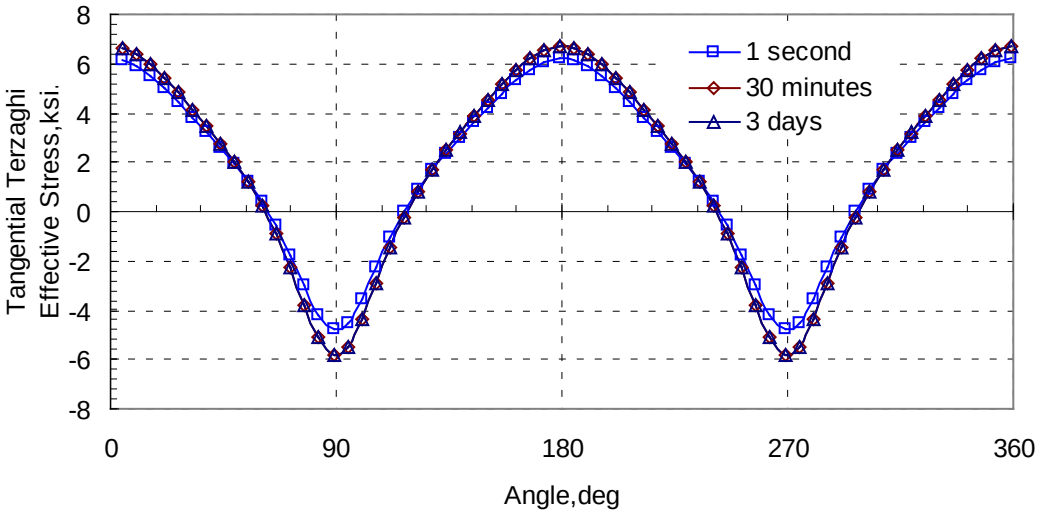

Fig. 3.78 Case 7: tangential Terzaghi's effective stress around wellbore

3.2.2.4. Case 8: azimuth=90°

Compared to Case 5, Case 8 shows the effect of 90° well azimuth.

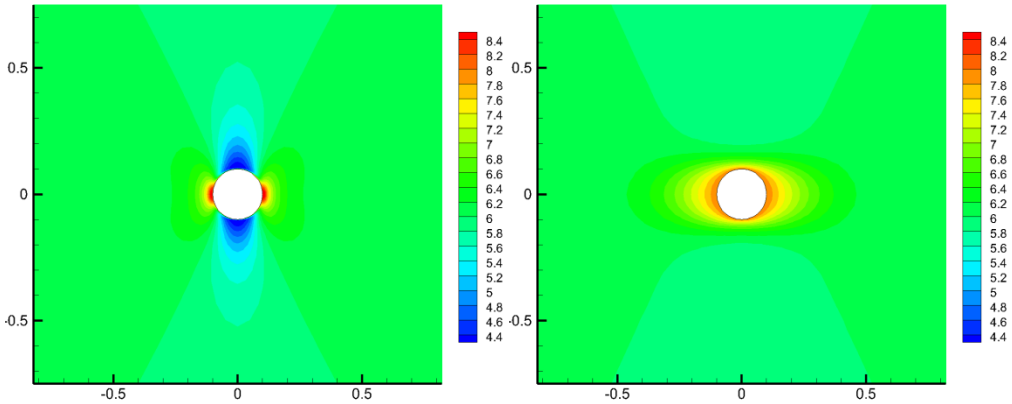

(a) t=1 second **(b) t=30 minutes**

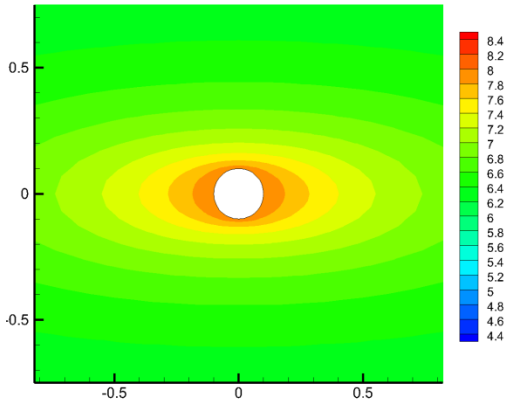

(c) t=3 days

Fig. 3.79 Case 8: pore pressure distribution

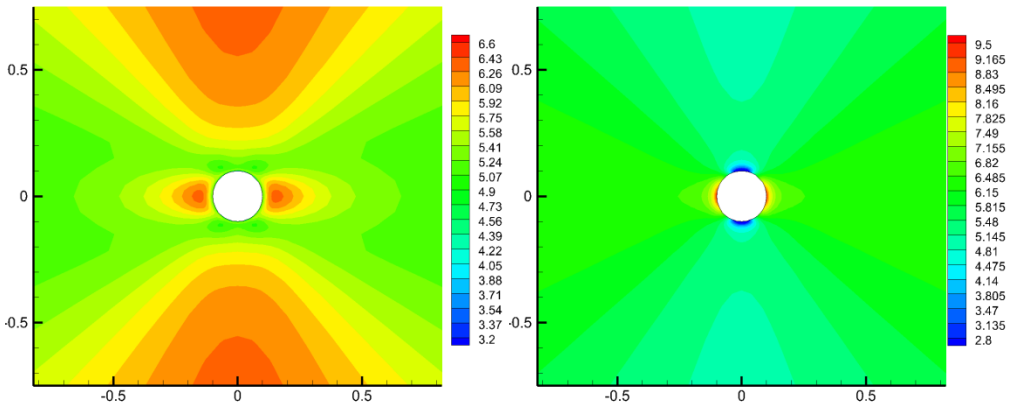

(a) Radial Stress **(b) Tangential Stress**

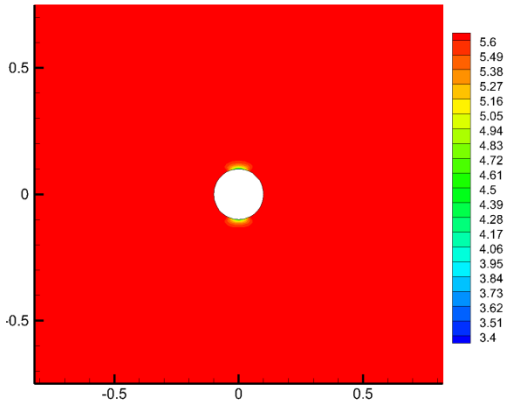

(c) Z Direction Stress

Fig. 3.80 Case 8: Biot's effective stress distribution at t=1 second

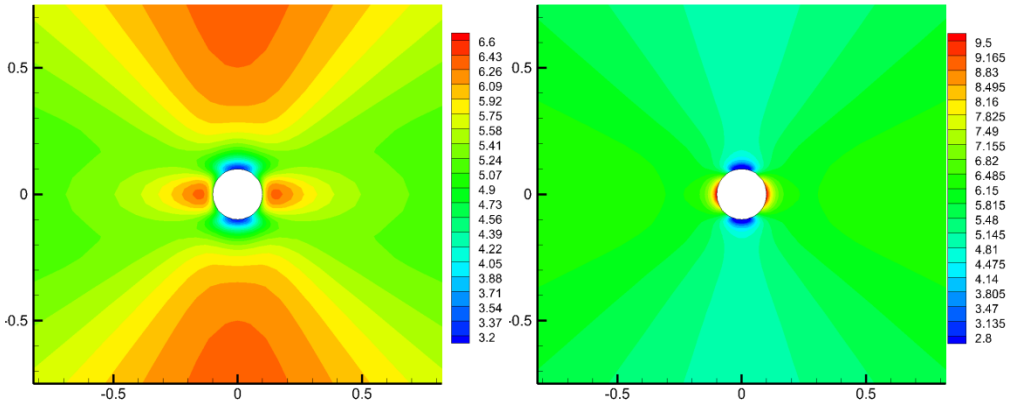

(a) Radial Stress **(b) Tangential Stress**

Fig. 3.81 Case 8: Biot's effective stress distribution at t=30 minutes

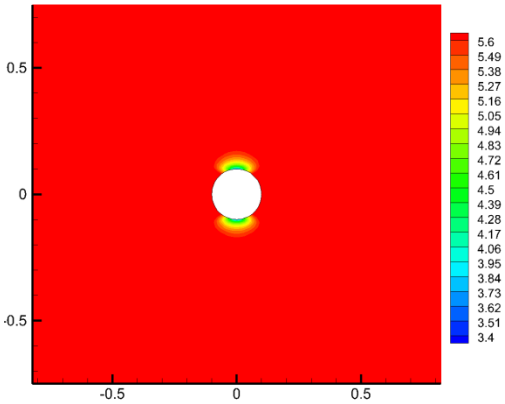

(c) Z Direction Stress

Fig. 3.81 Continued

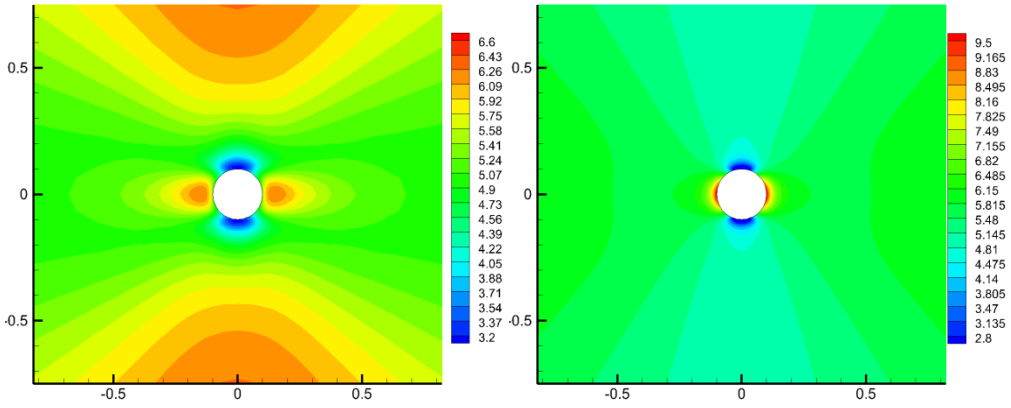

(a) Radial Stress **(b) Tangential Stress**

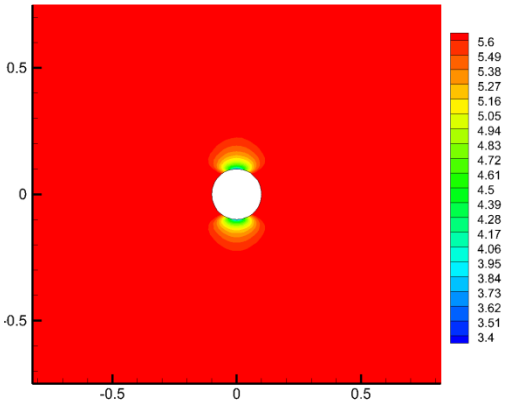

(c) Z Direction Stress

Fig. 3.82 Case 8: Biot's effective stress distribution at t=3 days

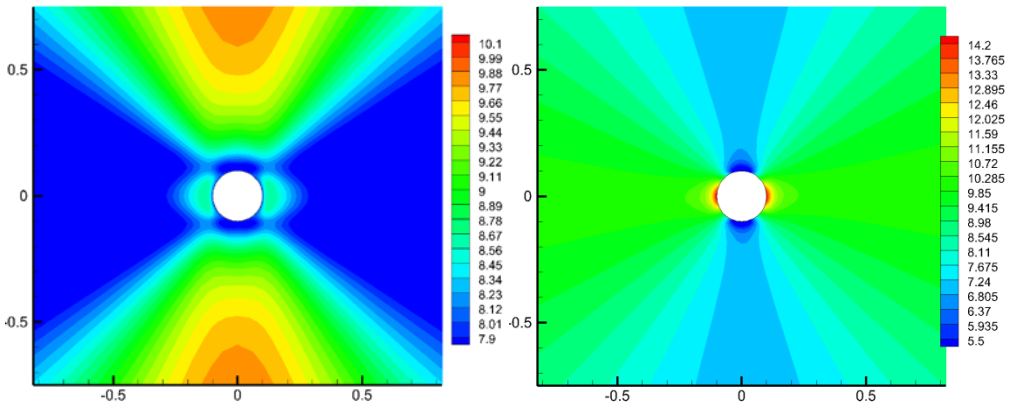

(a) Radial Stress **(b) Tangential Stress**

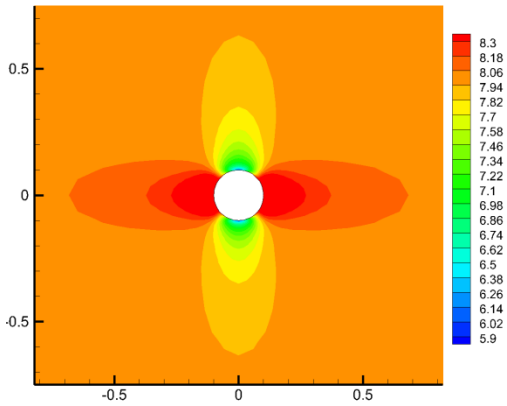

(c) Z Direction Stress

Fig. 3.83 Case 8: total stress distribution at t=1 second

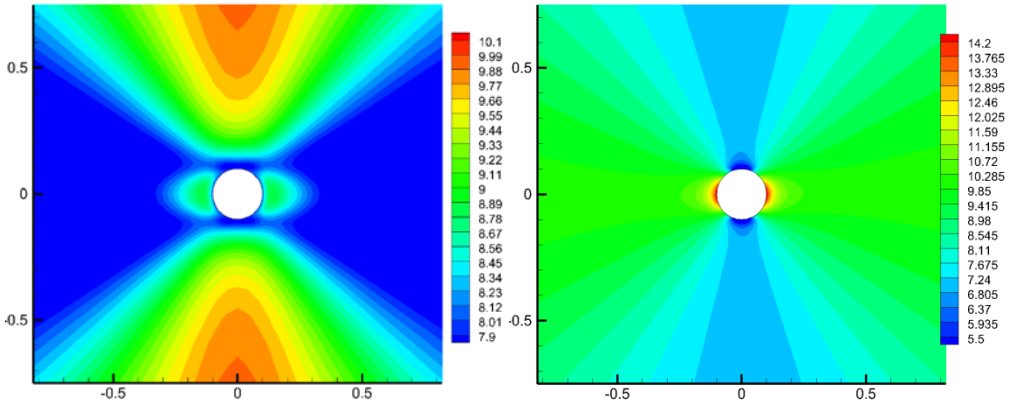

(a) Radial Stress **(b) Tangential Stress**

Fig. 3.84 Case 8: total stress distribution at t=30 minutes

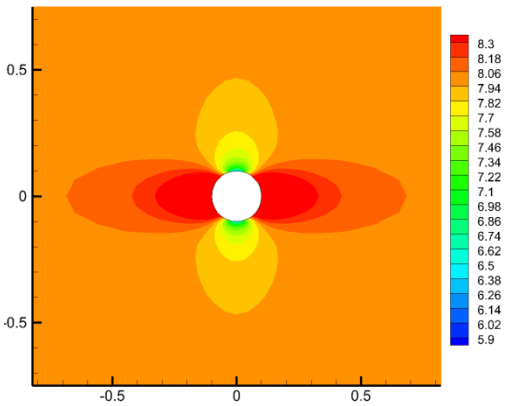

(c) Z Direction Stress

Fig. 3.84 Continued

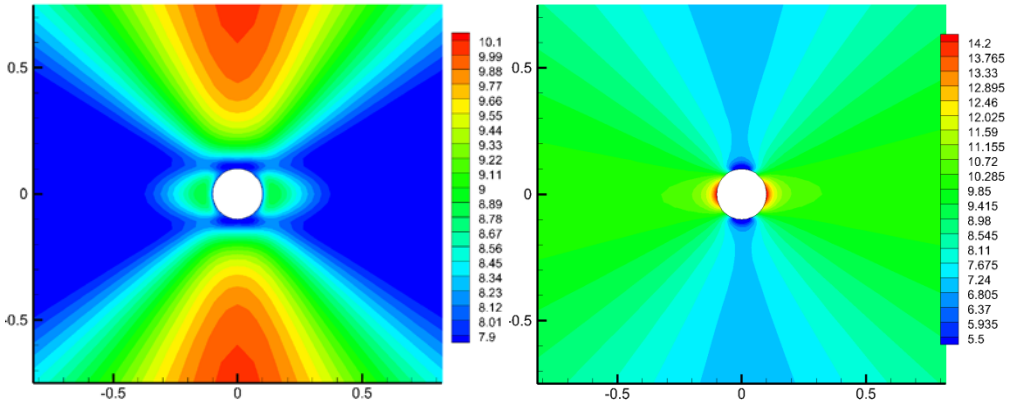

(a) Radial Stress **(b) Tangential Stress**

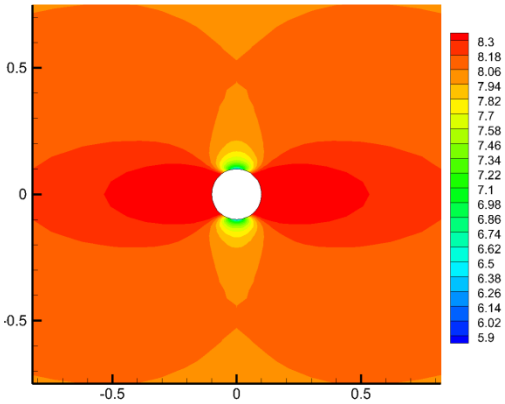

(c) Z Direction Stress

Fig. 3.85 Case 8: total stress distribution at t=3 days

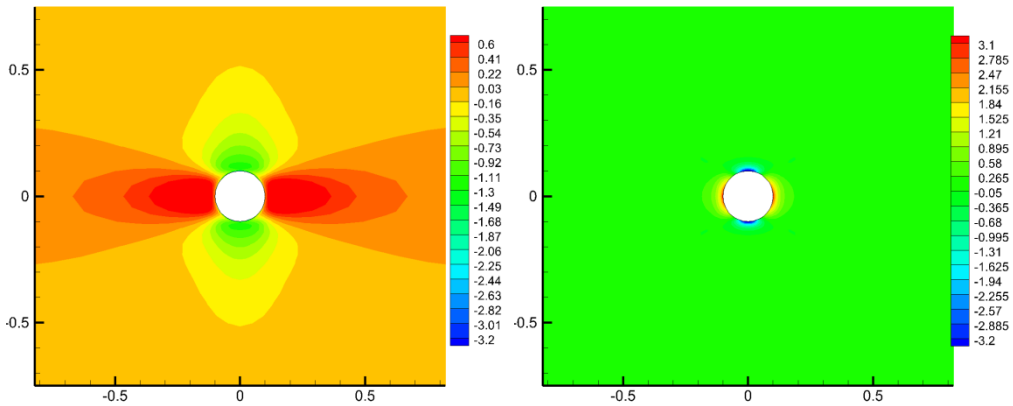

(a) Radial Stress **(b) Tangential Stress**

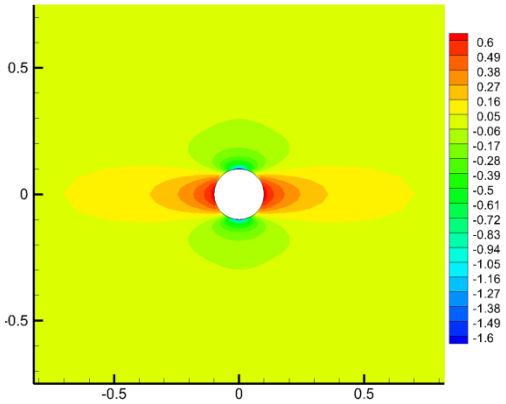

(c) Z Direction Stress

Fig. 3.86 Case 8: induced Biot's effective stress distribution at t=1 second

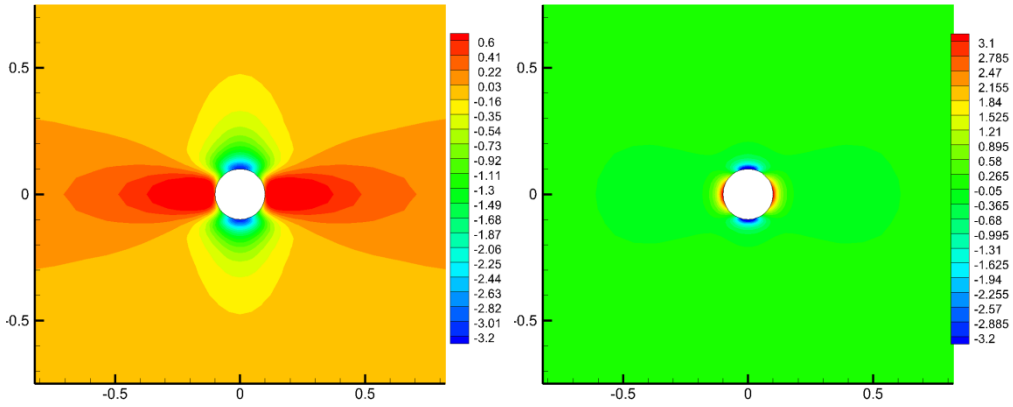

(a) Radial Stress **(b) Tangential Stress**

Fig. 3.87 Case 8: induced Biot's effective stress distribution at t=30 minutes

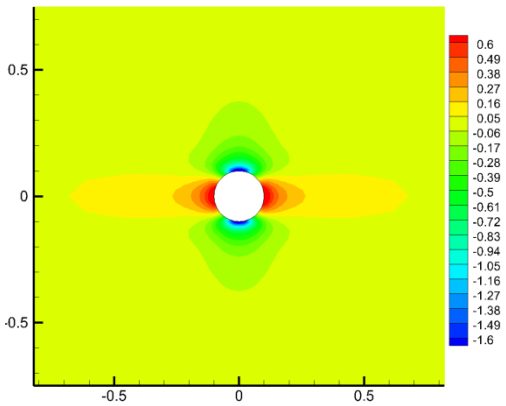

(c) Z Direction Stress

Fig. 3.87 Continued

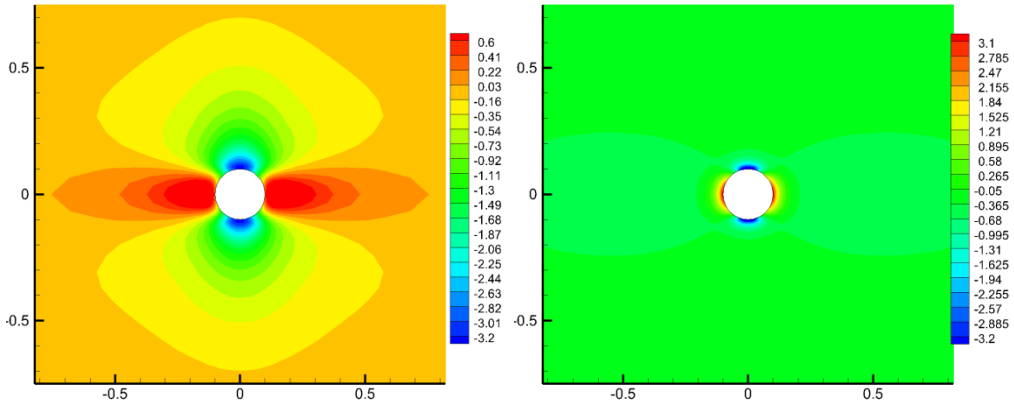

(a) Radial Stress **(b) Tangential Stress**

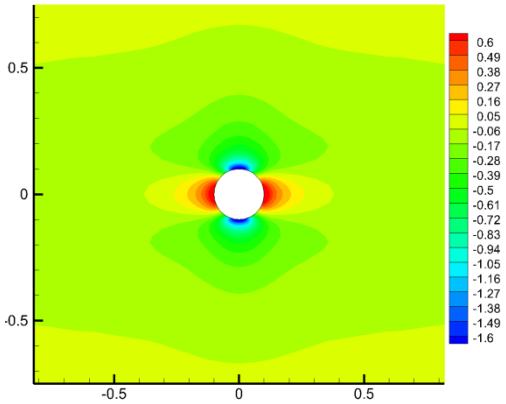

(c) Z Direction Stress

Fig. 3.88 Case 8: induced Biot's effective stress distribution at t=3 days

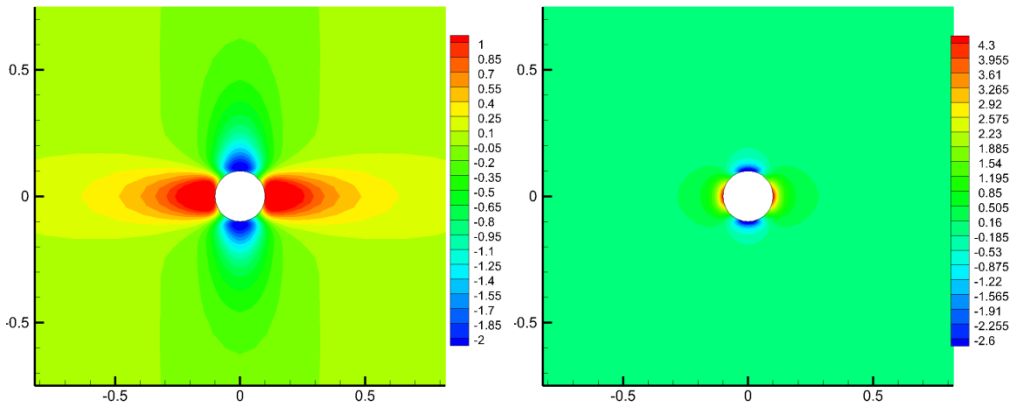

(a) Radial Stress **(b) Tangential Stress**

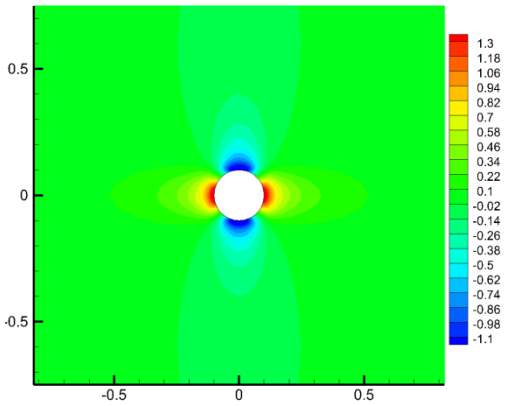

(c) Z Direction Stress

Fig. 3.89 Case 8: induced total stress distribution at t=1 second

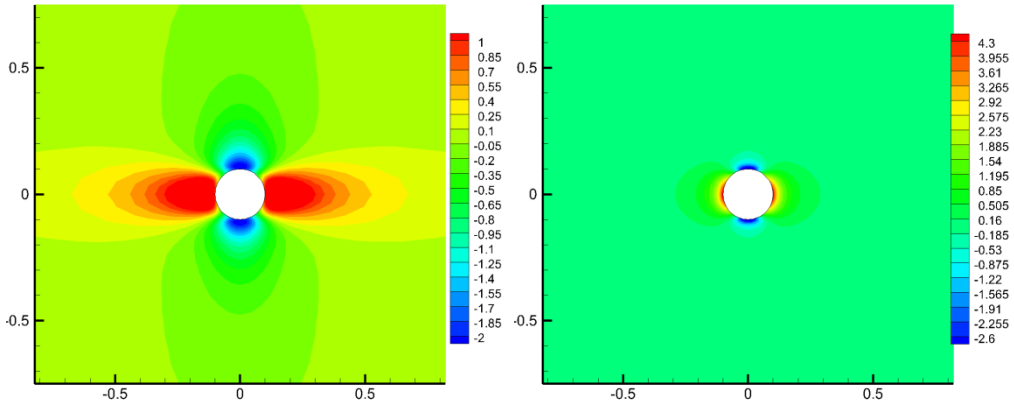

(a) Radial Stress **(b) Tangential Stress**

Fig. 3.90 Case 8: induced total stress distribution at t=30 minutes

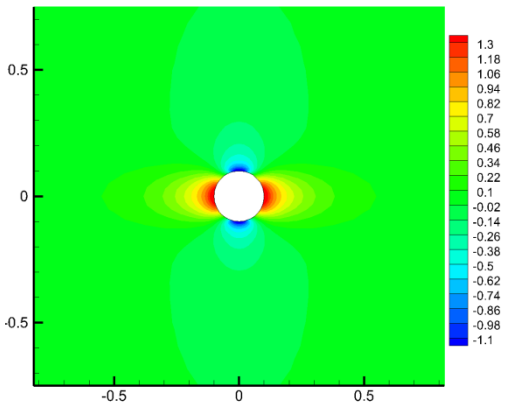

(c) Z Direction Stress

Fig. 3.90 Continued

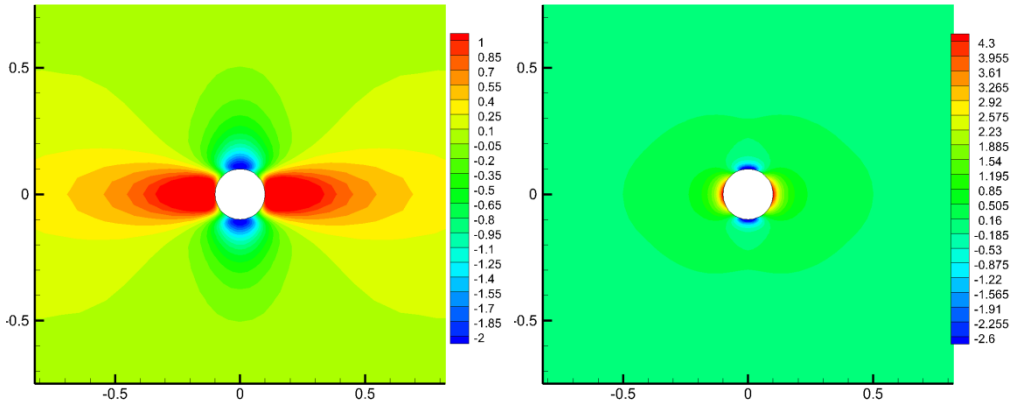

(a) Radial Stress **(b) Tangential Stress**

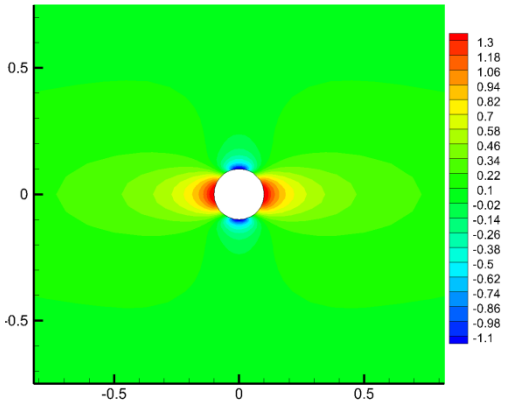

(c) Z Direction Stress

Fig. 3.91 Case 8: induced total stress distribution at t=3 days

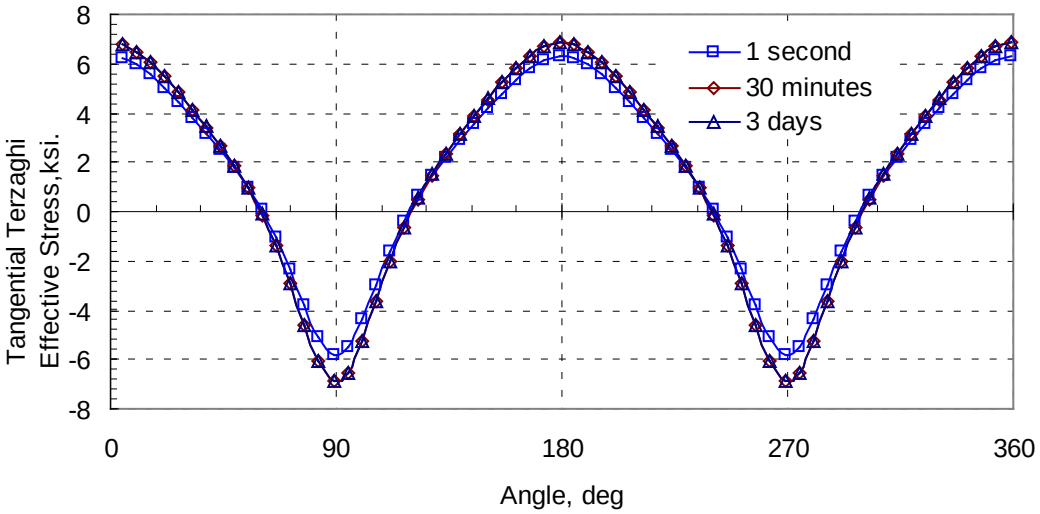

Fig. 3.92 Case 8: tangential Terzaghi's effective stress around wellbore

3.2.3. Summary

Comparing Case 6, 3 and 4 with Case 5, we found some interesting results discussed as follows.

As the well azimuth rotates from the direction of minimum horizontal stress to the direction of maximum horizontal stress, the in-situ stresses in well coordinate system changes: The x-direction in-situ stress decreases, the z-direction in-situ stress increases, and the y-direction in-situ stress remains the same. Obviously, the difference between x direction and y direction in-situ stress further increases. Due to the wellbore excavation, this enlarged stress difference makes the maximum value at horizontal position near the wellbore further increases and the minimum value at vertical position near the wellbore further decrease in both the induced effective stress distribution and the induced total stress distribution. In other words, the induced stress distributions become more uneven around the wellbore.

Since the actual stresses can be treated as a superposition of induced stresses and initial in-situ stresses, the actual total stress and effective stress distributions exhibit similar enlarged difference between minimum and maximum values around the wellbore. Expressing x, y direction in-situ stresses in cylindrical coordinate system and assuming the positive direction of x axis to be the reference direction, we can find that the radial in-situ stress decreases at $\theta=0°$ and 180° (horizontal position) and remains the same at $\theta=90°$ and 270° (vertical position) while the tangential in-situ stress remains the same at $\theta=0°$, 90°, 180° and 270° (both horizontal and vertical position). Further considering the change of in-situ stresses in well coordinate system, we can find that in the actual total

stress and effective stress distribution, the maximum values of z direction components increase, minimum values of radial components decrease, minimum values of tangential components decrease, and maximum values of tangential components increase as the well azimuth rotates from the direction of minimum horizontal stress to the direction of maximum horizontal stress

Different well azimuth makes the short term pore pressure around the wellbore more unevenly distributed. Similarly, this is also caused by the enlarged difference between x direction and y direction in-situ stresses. However, the well azimuth has almost no effect on long term pore pressure distribution.

The shapes of the tangential Terzaghi's effective stress around the wellbore are similar under different well azimuth, but the minimum value decreases as well azimuth increase from 0° to 90°. This means the well is more likely to be fractured as the well rotates from minimum horizontal in-situ stress to maximum horizontal in-situ stress.

In summary, the study shows that the effect of well azimuth cannot be neglected. As the well rotates from minimum horizontal in-situ stress to maximum horizontal in-situ stress, the pore pressure and stress distributions tend to be more unevenly distributed around the wellbore, making the wellbore easier to fracture.

3.3. Effect of Different Rock Bedding Dip

In this section, a horizontal well drilled in transversely isotropic reservoir is assumed. The bedding plane is parallel to the well axis but dipping at different angles. The effects of different rock bedding dip angle on the pore pressure, stress distribution and possibility of fracture initiation are studied.

3.3.1. Problem Statement

A horizontal well is drilled along the direction of minimum horizontal in-situ stress in transversely isotropic reservoir. The isotropic plane (see Fig. 3.93) is parallel to the well axis but dipping at different angles. The borehole radius is R=0.1 m.

The loading and geometry are shown in Fig. 3.94. The definition and notation of coordinate systems are the same as described before. The in-situ stresses σ_H, σ_h, σ_v are defined in global coordinate system and thus are also denoted as σ_x^g, σ_y^g, σ_z^g.

The well coordinate system, which denotes the well orientation, is rotated from global coordinate system position following the steps described in section 2.1.6: Assume the well coordinate system initially coincide with the global coordinate system. In first step, rotate the initial well coordinate system 90° about its z-axis to get a new well coordinate system (WCS'). In second step, rotate the new well coordinate system 90° about its x axis to get another new well coordinate system (WCS''). The in situ stresses are converted to the well coordinate system and denoted as σ_x^g, σ_y^g, σ_z^g, σ_{xy}^g, σ_{yz}^g, σ_{zx}^g.

Similarly, the material coordinate system is rotated a dip angle ϕ_{dip} (which is the parameter in this section) about its x axis from global coordinate system.

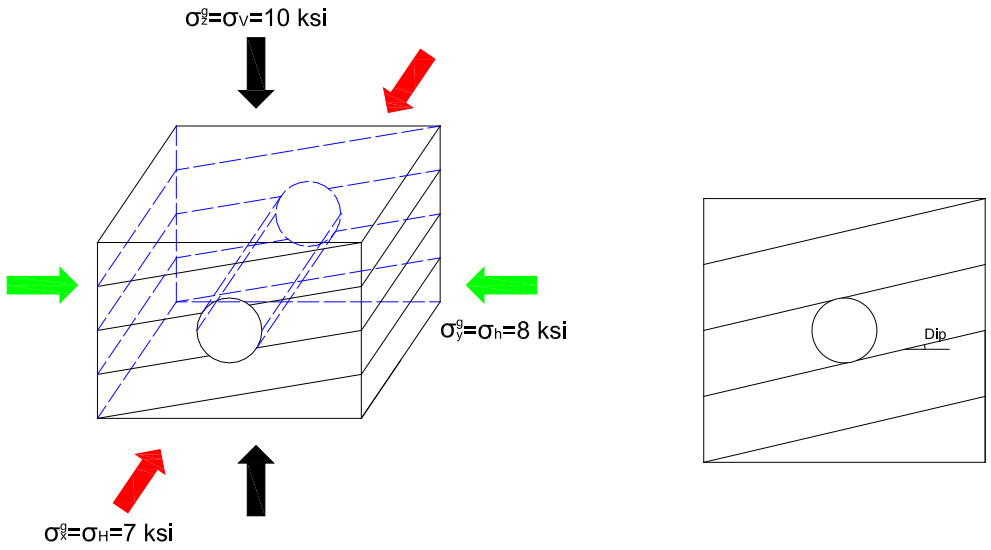

Fig. 3.93 Case 9-12: horizontal well and rock bedding position

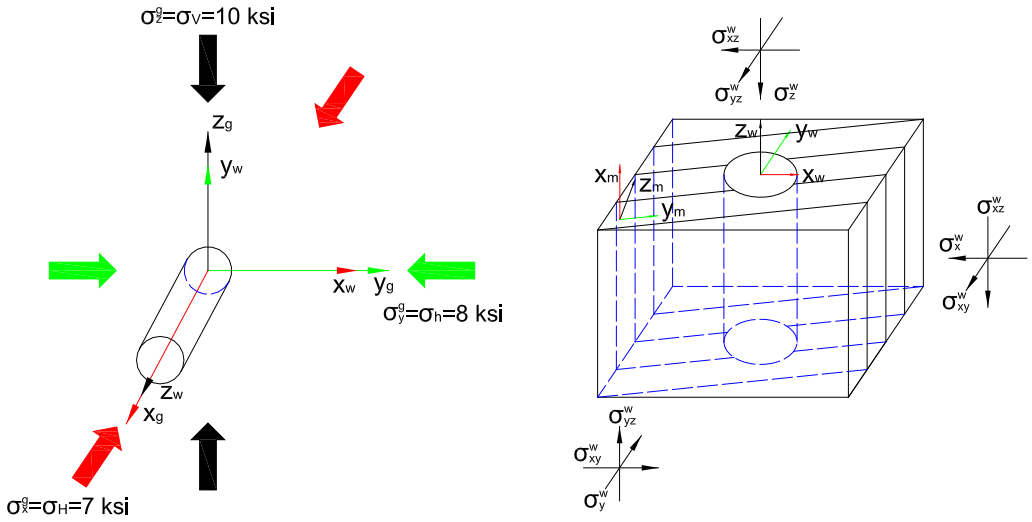

Fig. 3.94 Case 9-12: definition sketch of an horizontal borehole problem

To study the effects of bedding plane dipping, four cases are simulated in this section. In Case 9, the bedding plane is horizontal. In Case 10, the bedding plane dip is 30°. In Case 11, the bedding plane dip is 60°. In Case 12, the bedding plane is vertical (dip is 90°).

The common reservoir properties in four cases are presented as follows:

Angles rotating about z, x, y axes sequentially to transform global coordinate system to well coordinate system: $\phi_{w1}=90°$, $\phi_{w2}=90°$, $\phi_{w3}=0°$

Initial state (in global coordinate system):

- Initial Pore Pressure: $p_0=6$ ksi
- In-situ Stresses: $\sigma_H=8$ ksi, $\sigma_h=7$ ksi, $\sigma_v=10$ ksi
- Mud Pressure: $p_{mud}=8$ ksi
- Fluid viscosity: $\mu=0.001$Pa.s

Transversely isotropic rock properties (in material coordinate system):

- Permeability: $K_x=K_y=1.0e\text{-}6$ darcy, $K_z=1.0e\text{-}7$ darcy ($K_h/K_v=10$)
- Young's Modulus: $E_x=E_y=4.2e3$ ksi, $E_z=1.4e3$ ksi ($E_h/E_v=3$)
- Poisson's Ratio: $\nu_{xy}=\nu_{yz}=\nu_{zx}=0.25$
- Shear Modulus: $G_{xy}=1.68e3$ ksi, $G_{yz}=G_{zx}=0.56e3$ ksi
- Biot Coefficient: $\alpha_x=\alpha_y=0.332$, $\alpha_z=0.599$
- Biot Modulus: $M=2.78e3$ ksi

Angles rotating about z, x, y axes sequentially to transform global coordinate system to material coordinate system in four cases are listed as follows:

- Case 9, dip=0°: $\phi_{m1}=0°$, $\phi_{m2}=0°$, $\phi_{m3}=0°$
- Case 10, dip=30°: $\phi_{m1}=0°$, $\phi_{m2}=30°$, $\phi_{m3}=0°$
- Case 11, dip=60°: $\phi_{m1}=0°$, $\phi_{m2}=60°$, $\phi_{m3}=0°$
- Case 12, dip=90°: $\phi_{m1}=0°$, $\phi_{m2}=90°$, $\phi_{m3}=0°$

3.3.2. Results

Pore pressure, Biot's effective stress and total stress in different directions (tangential, radial and z-direction) near the wellbore and tangential Terzaghi's effective stress around wellbore at three time steps (1 second, 30 minutes and 3 days) from all four cases are presented in Fig. 3.95-Fig. 3.150.

3.3.2.1. Case 9: dip=0°

Case 9 is the base of all four cases. Case 10, 3 and 4 is compared to Case 9 to study the effect of different bedding plane dips.

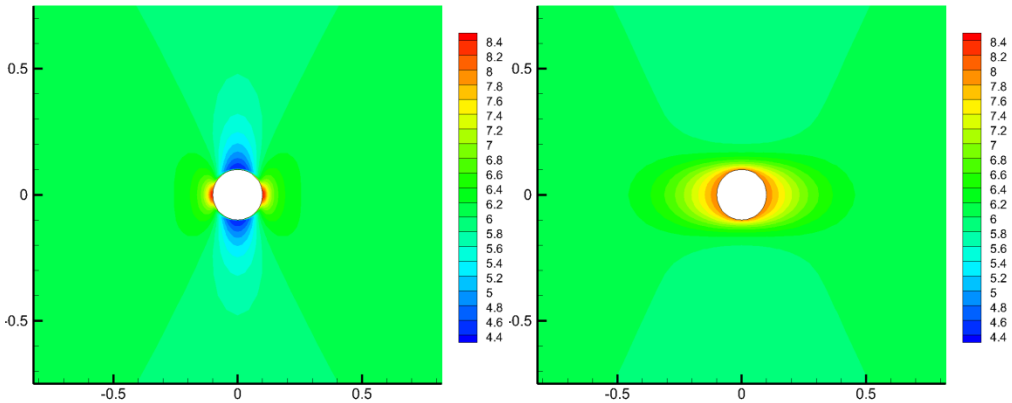

(a) t=1 second **(b) t=30 minutes**

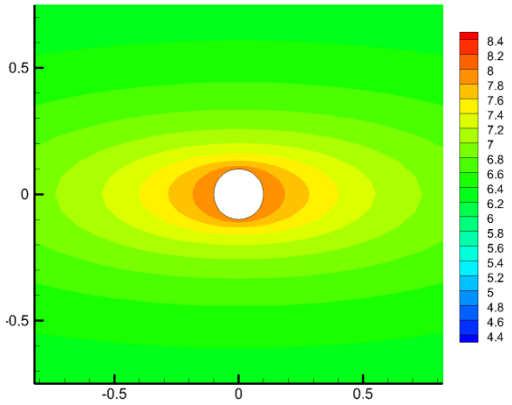

(c) t=3 days

Fig. 3.95 Case 9: pore pressure distribution

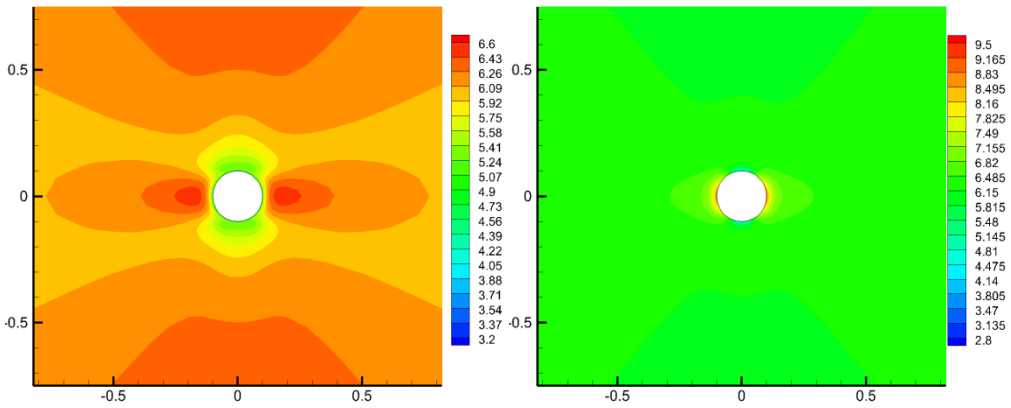

(a) Radial Stress **(b) Tangential Stress**

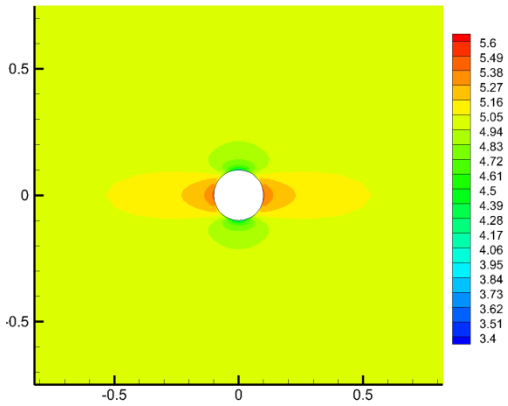

(c) Z Direction Stress

Fig. 3.96 Case 9: Biot's effective stress distribution at t=1 second

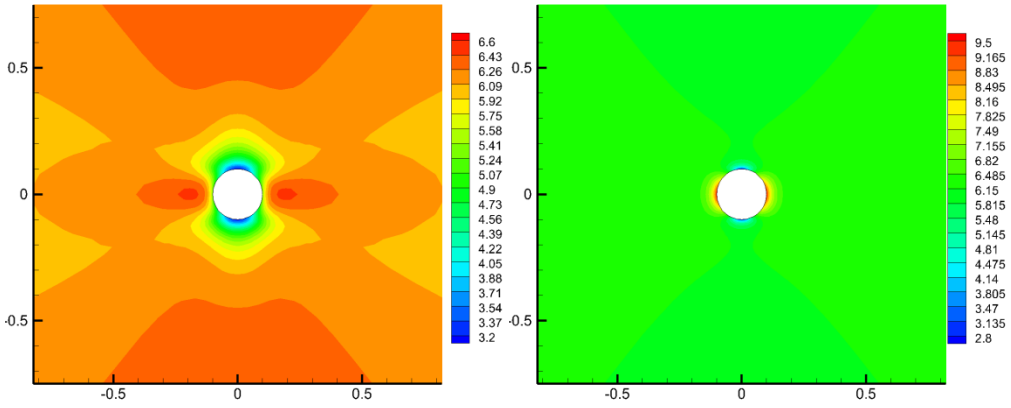

(a) Radial Stress **(b) Tangential Stress**

Fig. 3.97 Case 9: Biot's effective stress distribution at t=30 minutes

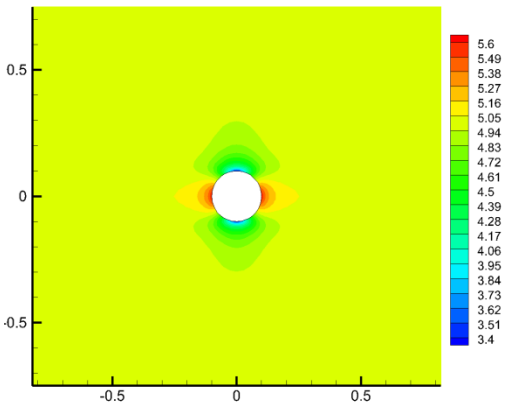

(c) Z Direction Stress

Fig. 3.97 Continued

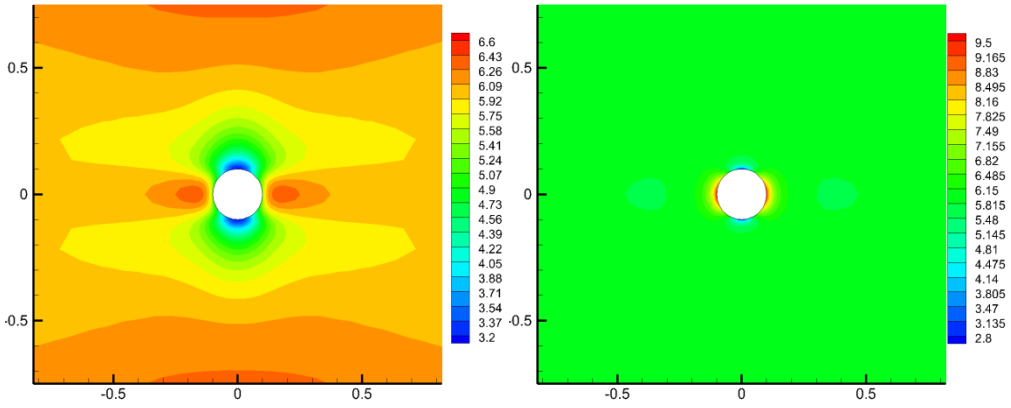

(a) Radial Stress **(b) Tangential Stress**

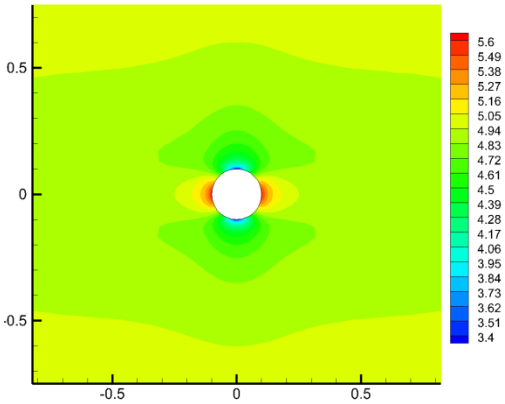

(c) Z Direction Stress

Fig. 3.98 Case 9: Biot's effective stress distribution at t=3 days

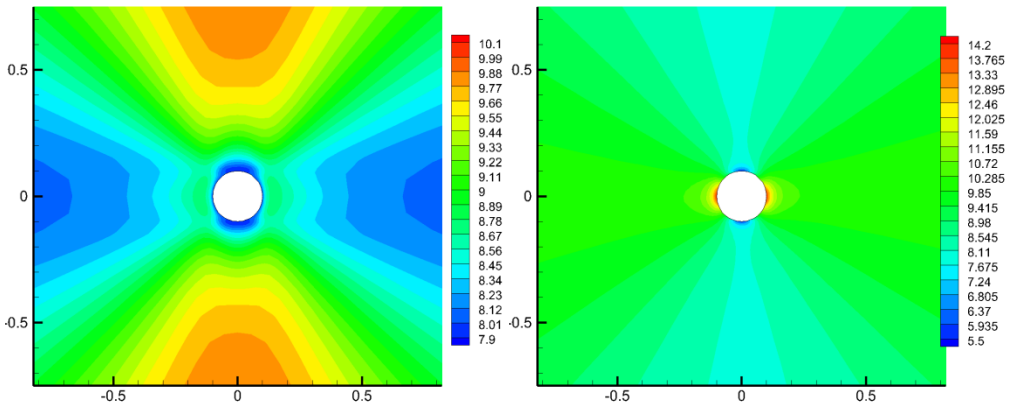

(a) Radial Stress **(b) Tangential Stress**

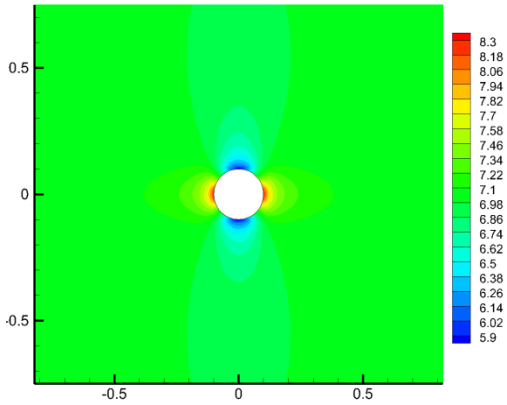

(c) Z Direction Stress

Fig. 3.99 Case 9: total stress distribution at t=1 second

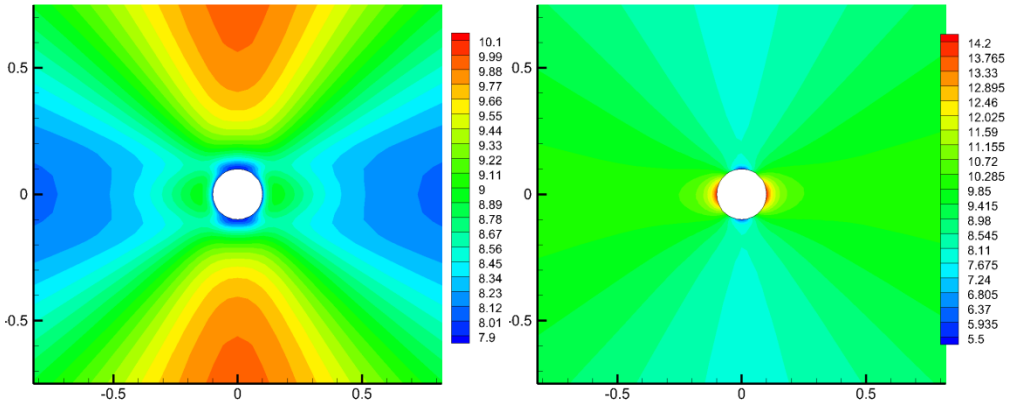

(a) Radial Stress **(b) Tangential Stress**

Fig. 3.100 Case 9: total stress distribution at t=30 minutes

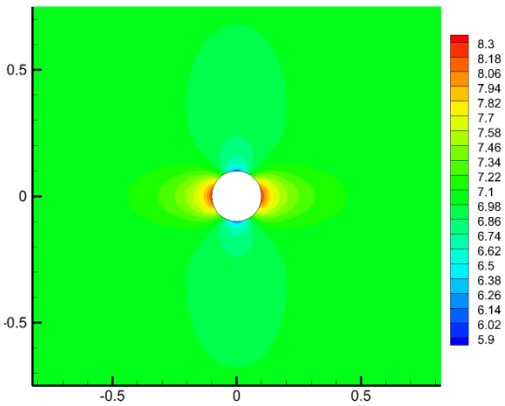

(c) Z Direction Stress

Fig. 3.100 Continued

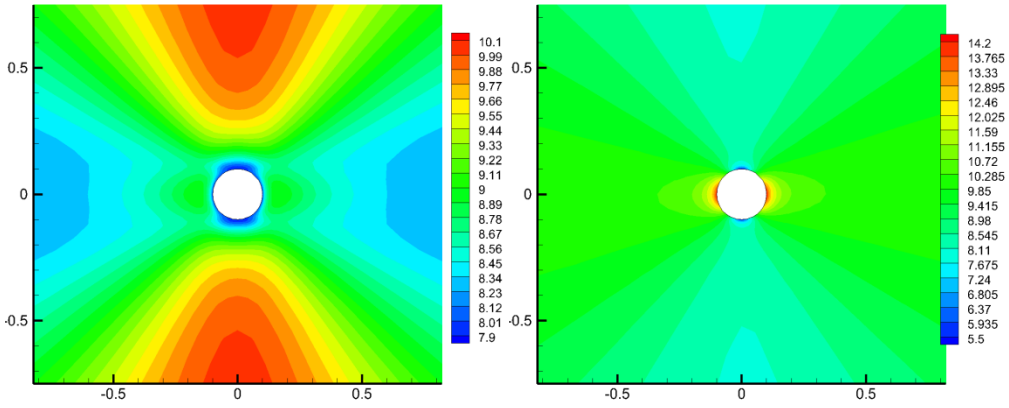

(a) Radial Stress **(b) Tangential Stress**

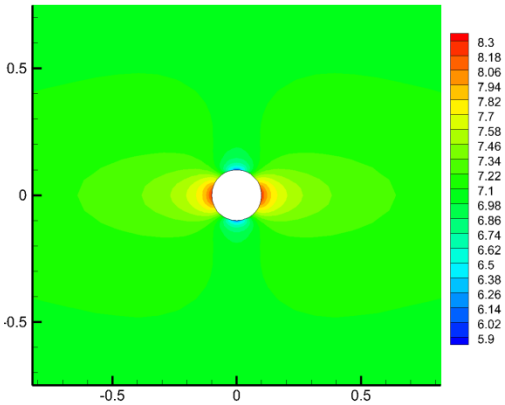

(c) Z Direction Stress

Fig. 3.101 Case 9: total stress distribution at t=3 days

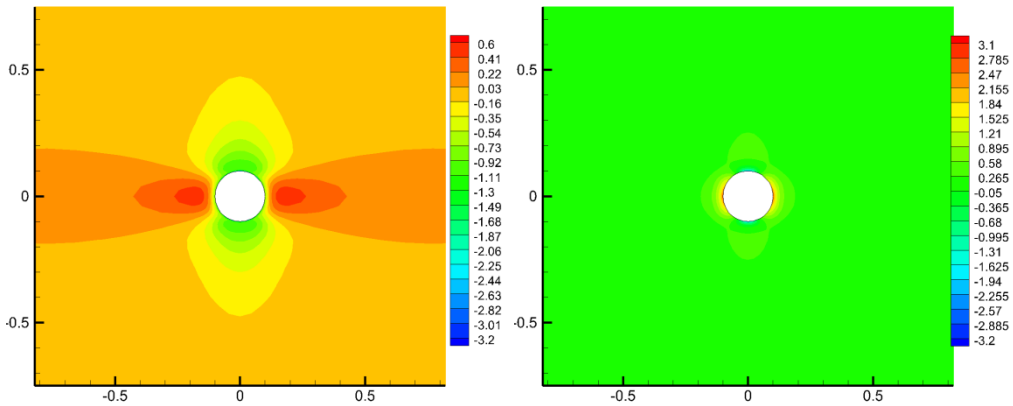

(a) Radial Stress **(b) Tangential Stress**

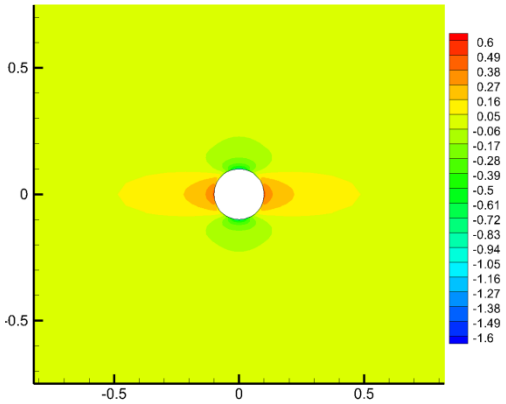

(c) Z Direction Stress

Fig. 3.102 Case 9: induced Biot's effective stress distribution at t=1 second

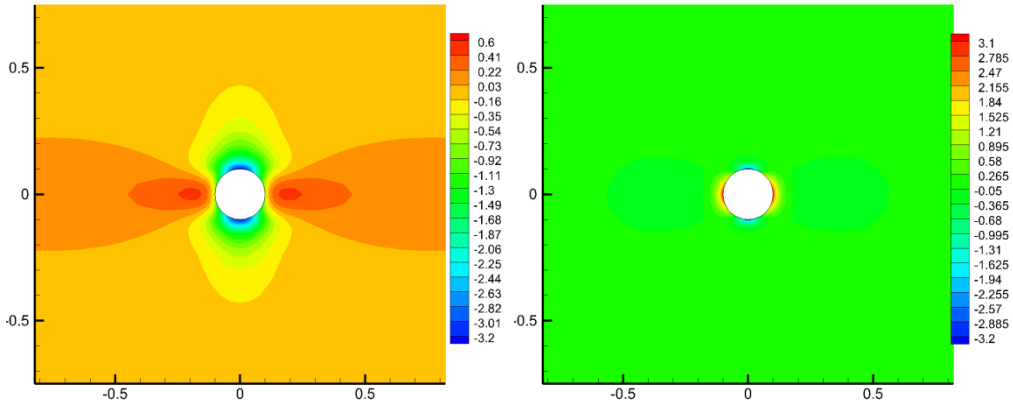

(a) Radial Stress **(b) Tangential Stress**

Fig. 3.103 Case 9: induced Biot's effective stress distribution at t=30 minutes

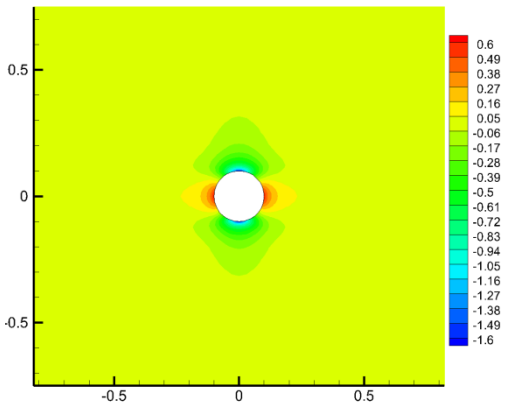

(c) Z Direction Stress

Fig. 3.103 Continued

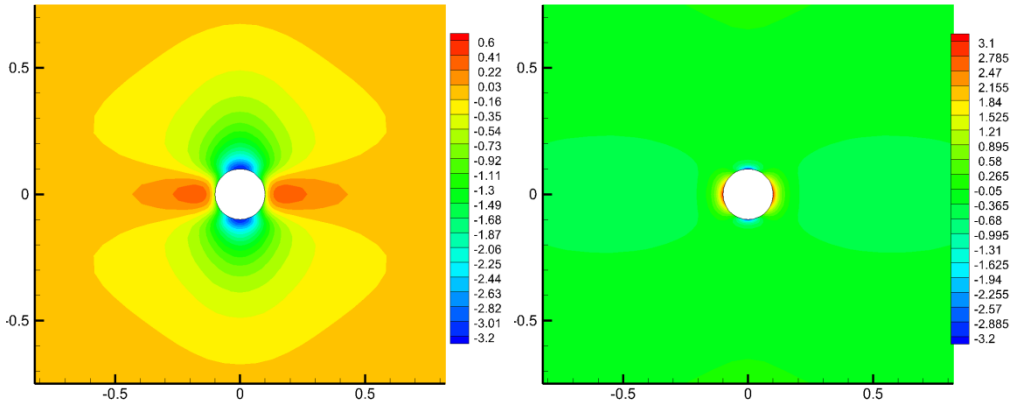

(a) Radial Stress **(b) Tangential Stress**

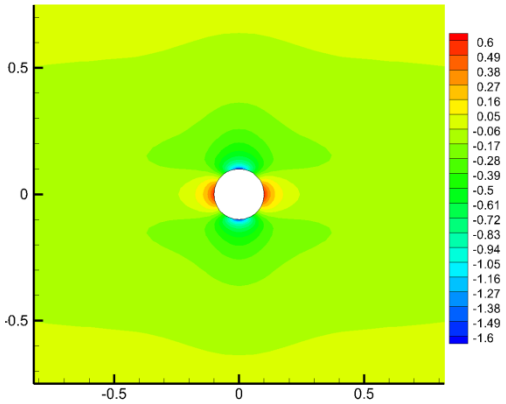

(c) Z Direction Stress

Fig. 3.104 Case 9: induced Biot's effective stress distribution at t=3 days

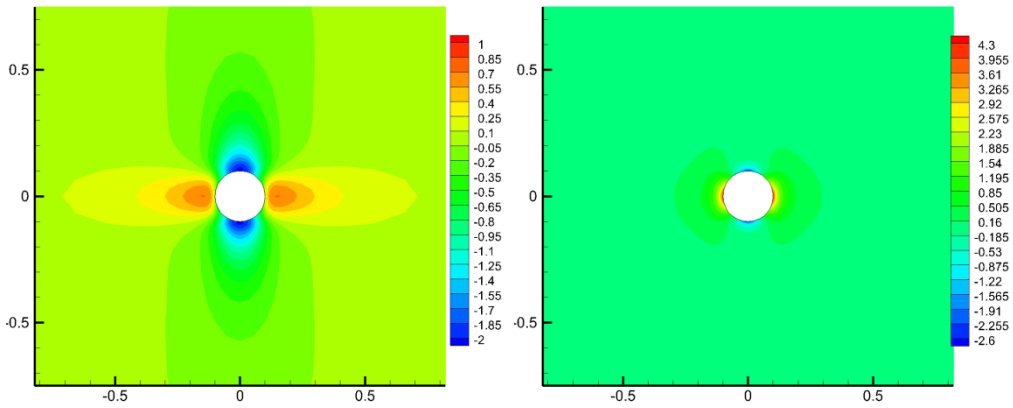

(a) Radial Stress **(b) Tangential Stress**

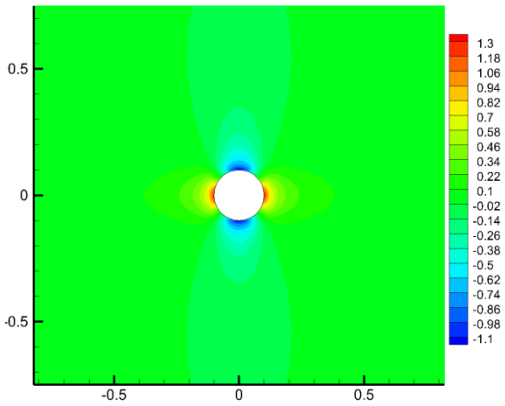

(c) Z Direction Stress

Fig. 3.105 Case 9: induced total stress distribution at t=1 second

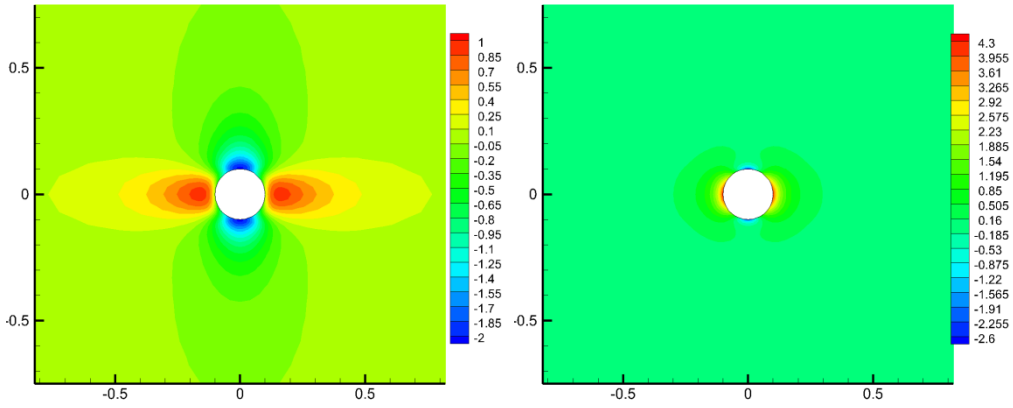

(a) Radial Stress **(b) Tangential Stress**

Fig. 3.106 Case 9: induced total stress distribution at t=30 minutes

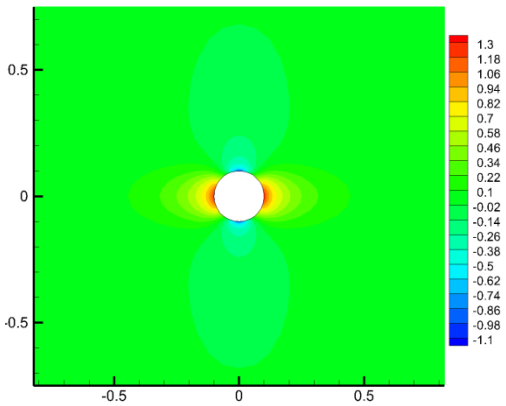

(c) Z Direction Stress

Fig. 3.106 Continued

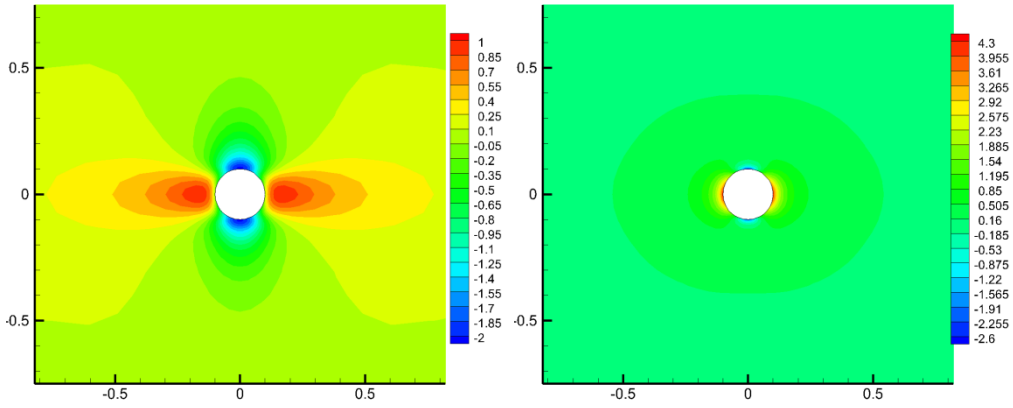

(a) Radial Stress **(b) Tangential Stress**

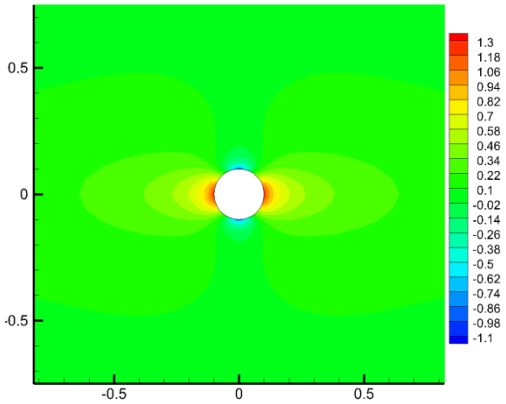

(c) Z Direction Stress

Fig. 3.107 Case 9: induced total stress distribution at t=3 days

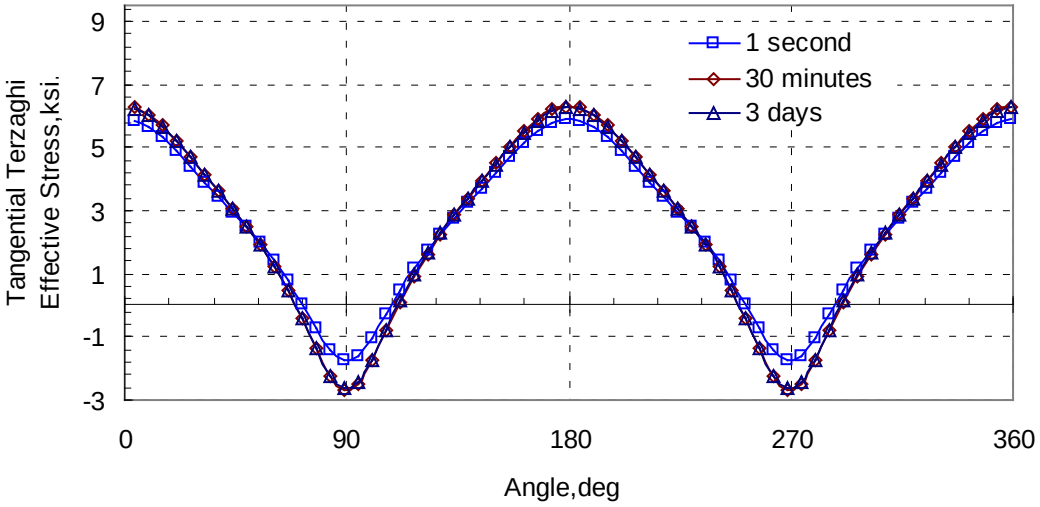

Fig. 3.108 Case 9: tangential Terzaghi's effective stress around wellbore

3.3.2.2. Case 10: dip=30°

Compared to Case 9, Case 10 shows the effect of 30° bedding plane.

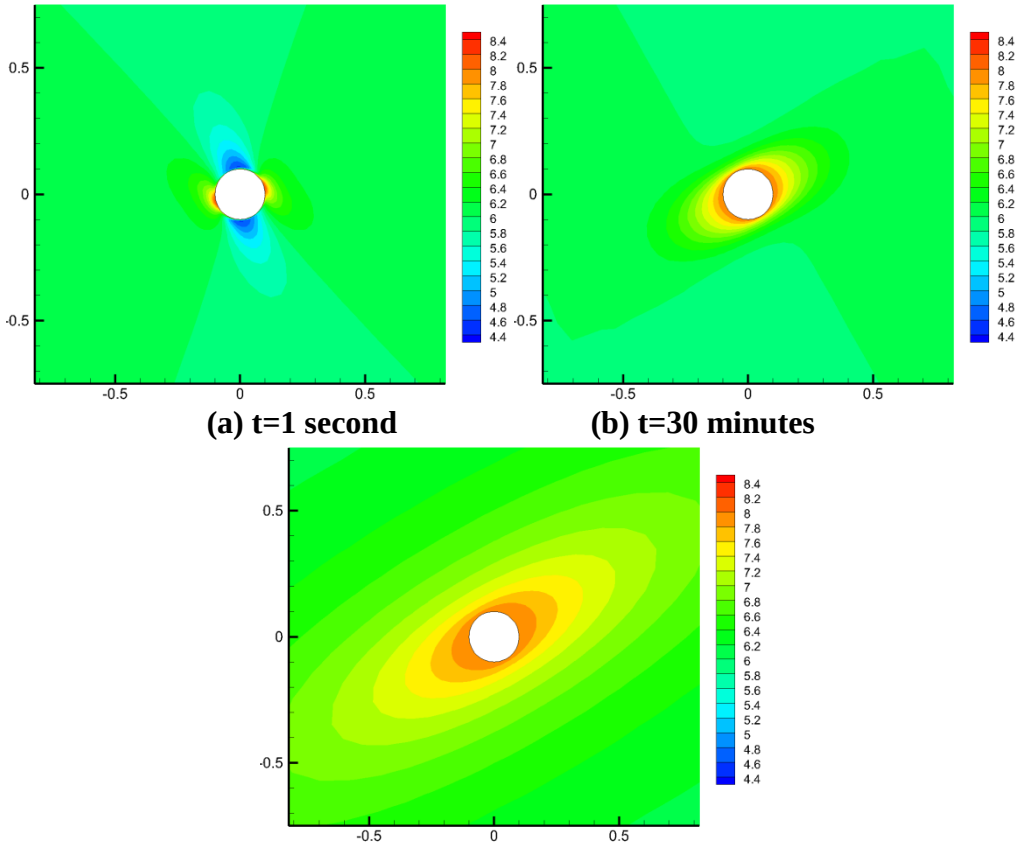

(a) t=1 second **(b) t=30 minutes**

(c) t=3 days

Fig. 3.109 Case 10: pore pressure distribution

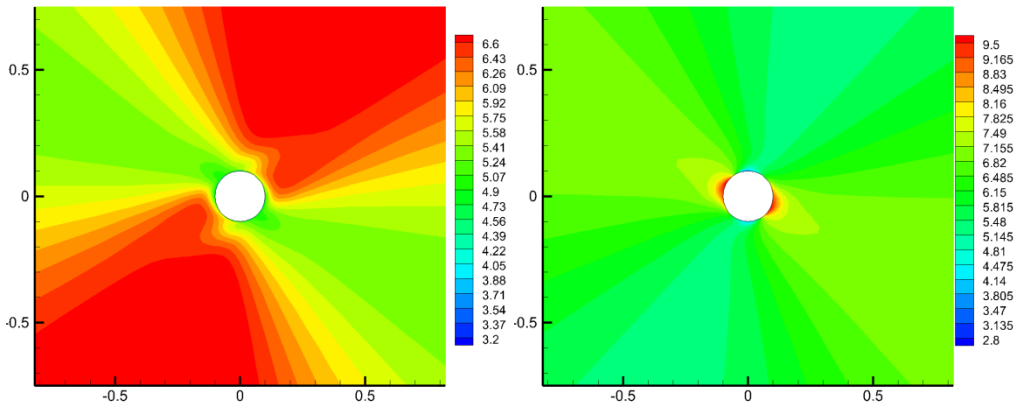

(a) Radial Stress **(b) Tangential Stress**

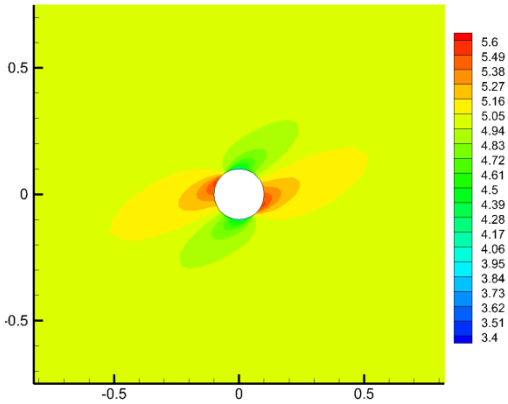

(c) Z Direction Stress

Fig. 3.110 Case 10: Biot's effective stress distribution at t=1 second

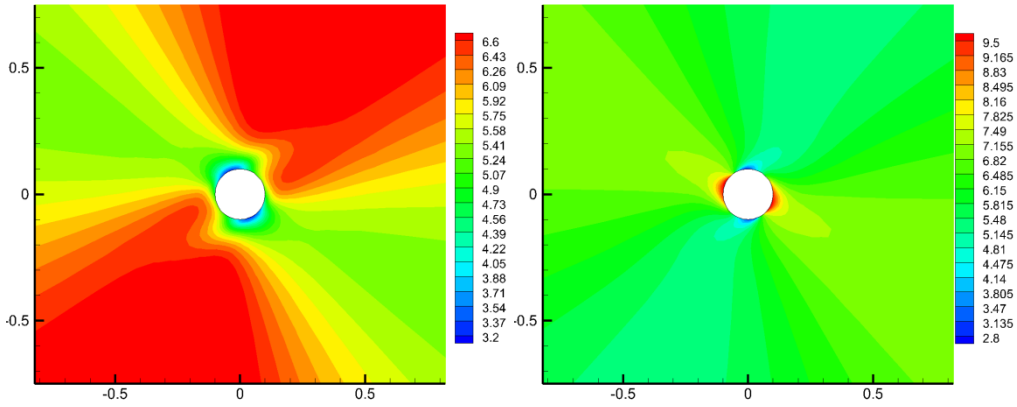

(a) Radial Stress **(b) Tangential Stress**

Fig. 3.111 Case 10: Biot's effective stress distribution at t=30 minutes

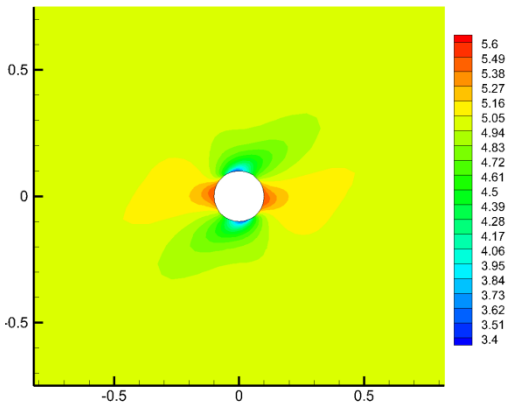

(c) Z Direction Stress

Fig. 3.111 Continued

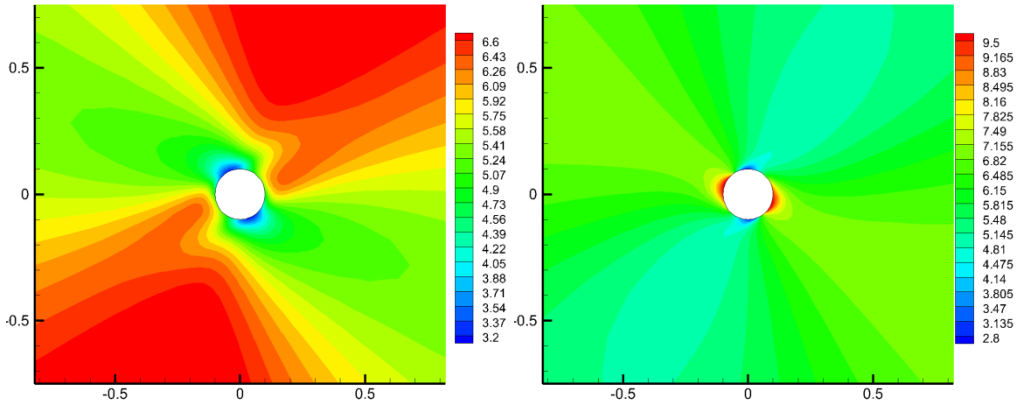

(a) Radial Stress **(b) Tangential Stress**

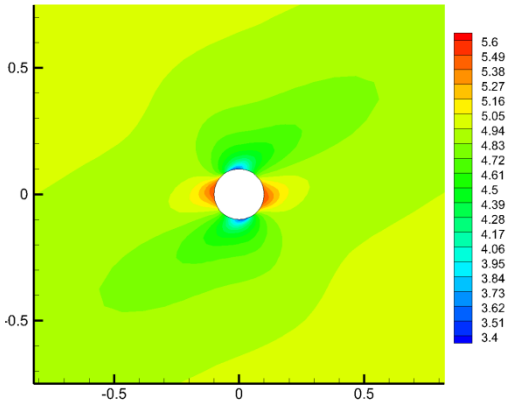

(c) Z Direction Stress

Fig. 3.112 Case 10: Biot's effective stress distribution at t=3 days

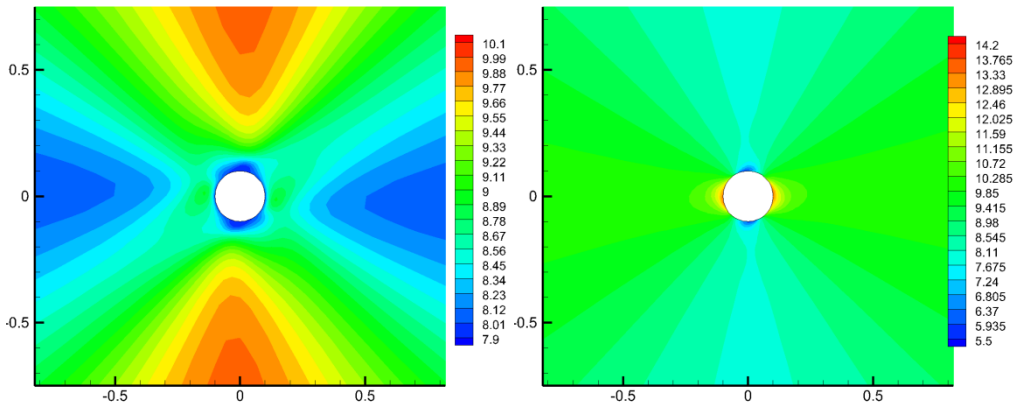

(a) Radial Stress **(b) Tangential Stress**

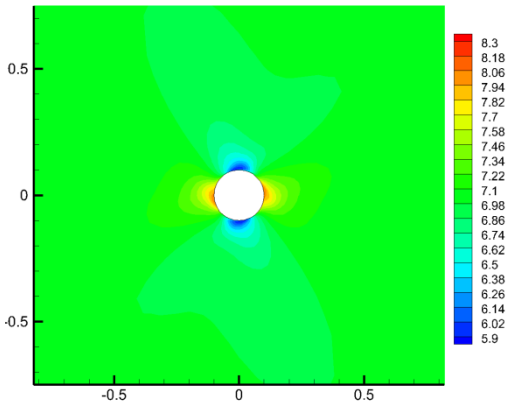

(c) Z Direction Stress

Fig. 3.113 Case 10: total stress distribution at t=1 second

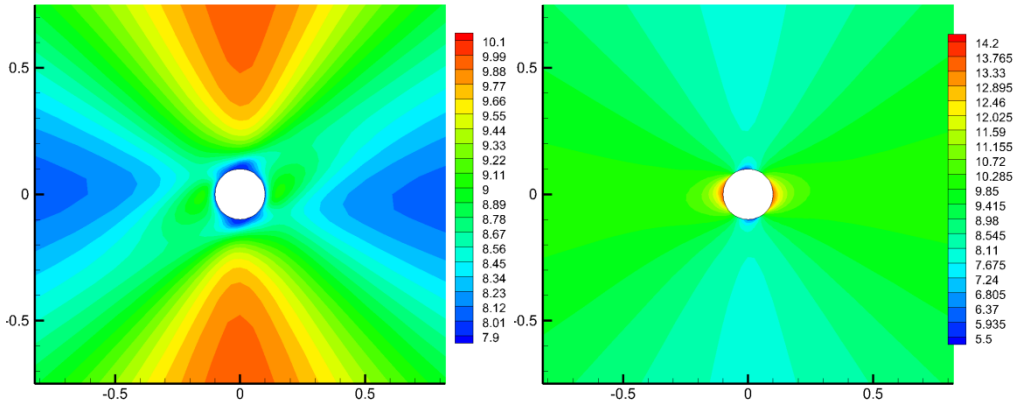

(a) Radial Stress **(b) Tangential Stress**

Fig. 3.114 Case 10: total stress distribution at t=30 minutes

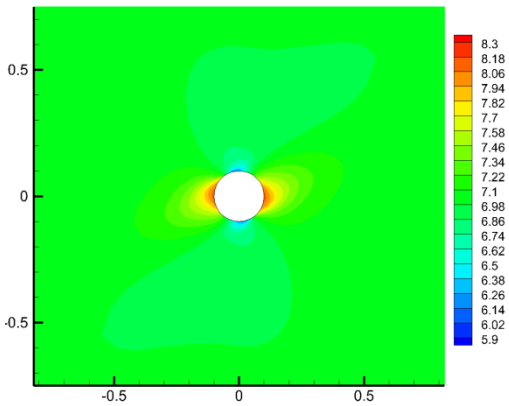

(c) Z Direction Stress

Fig. 3.114 Continued

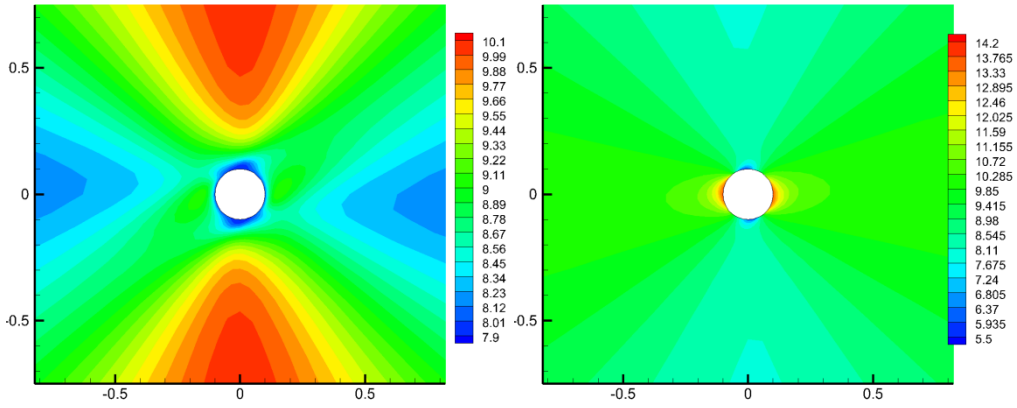

(a) Radial Stress **(b) Tangential Stress**

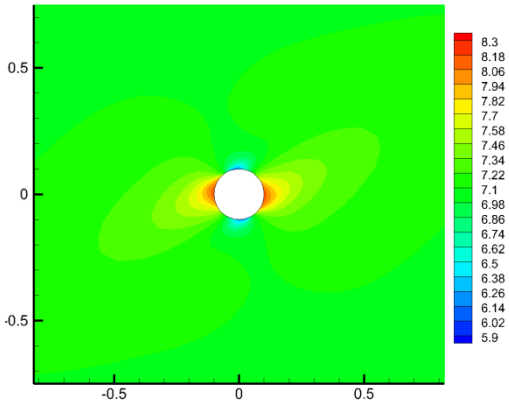

(c) Z Direction Stress

Fig. 3.115 Case 10: total stress distribution at t=3 days

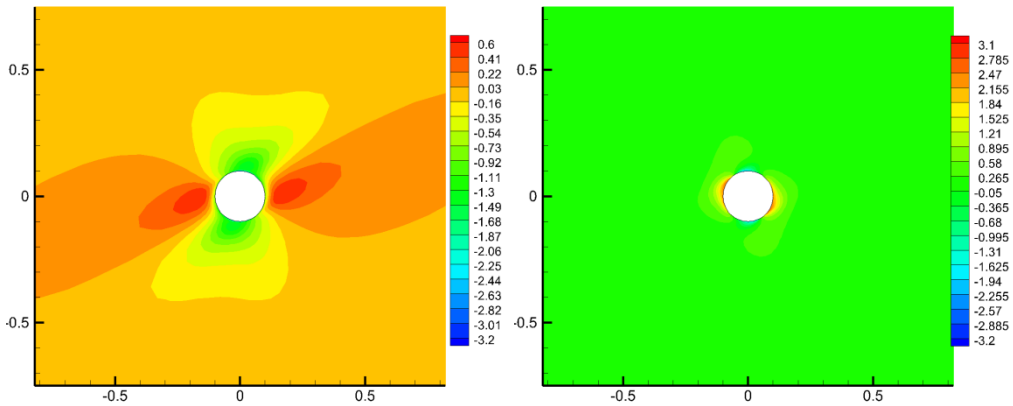

(a) Radial Stress **(b) Tangential Stress**

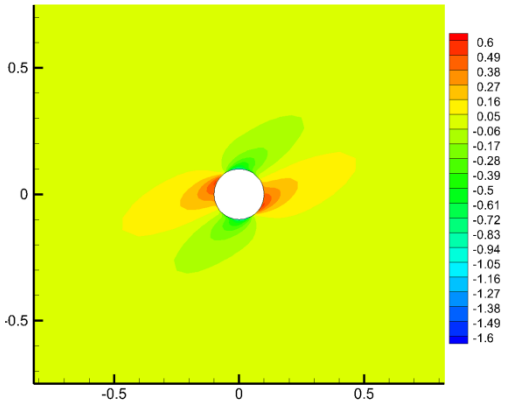

(c) Z Direction Stress

Fig. 3.116 Case 10: induced Biot's effective stress distribution at t=1 second

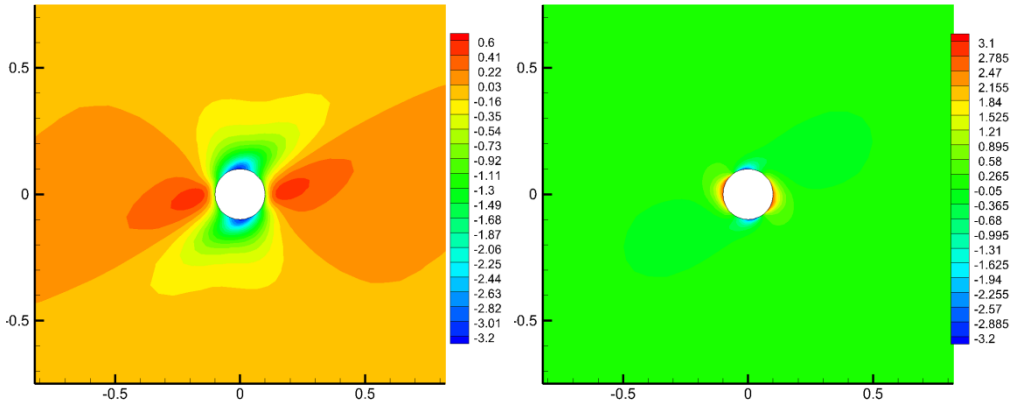

(a) Radial Stress **(b) Tangential Stress**

Fig. 3.117 Case 10: induced Biot's effective stress distribution at t=30 minutes

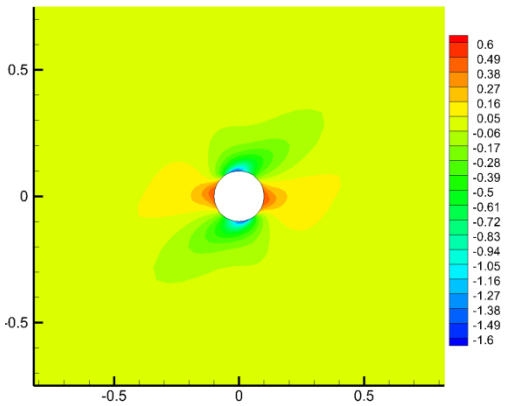

(c) Z Direction Stress

Fig. 3.117 Continued

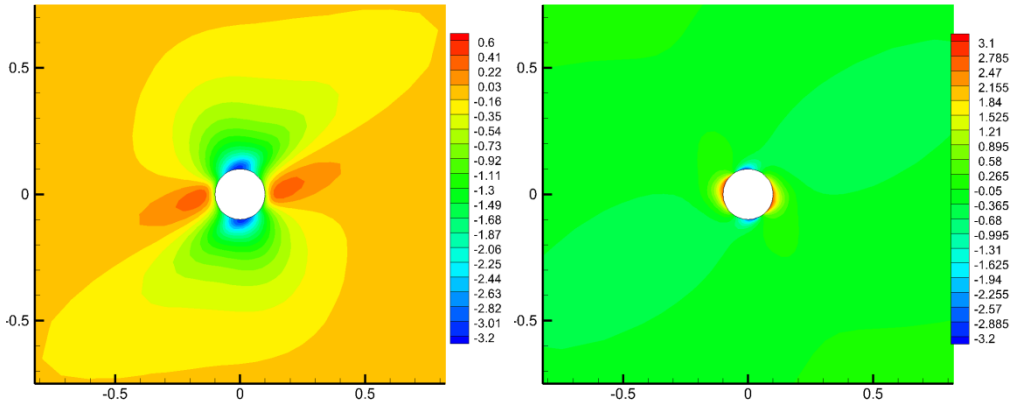

(a) Radial Stress **(b) Tangential Stress**

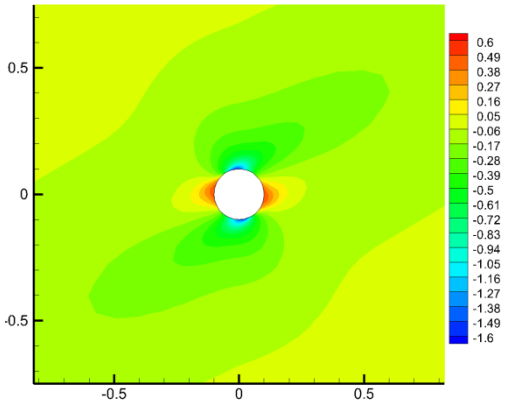

(c) Z Direction Stress

Fig. 3.118 Case 10: induced Biot's effective stress distribution at t=3 days

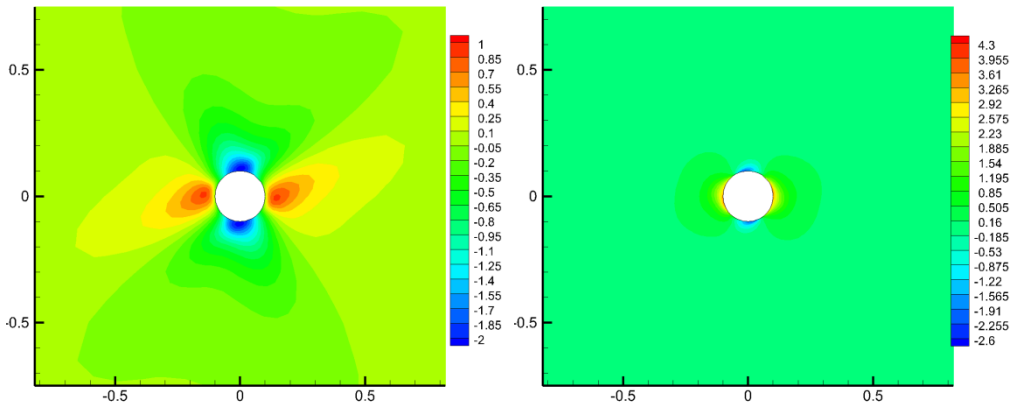

(a) Radial Stress **(b) Tangential Stress**

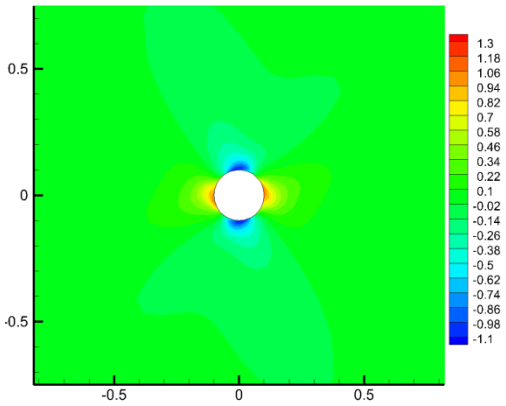

(c) Z Direction Stress

Fig. 3.119 Case 10: induced total stress distribution at t=1 second

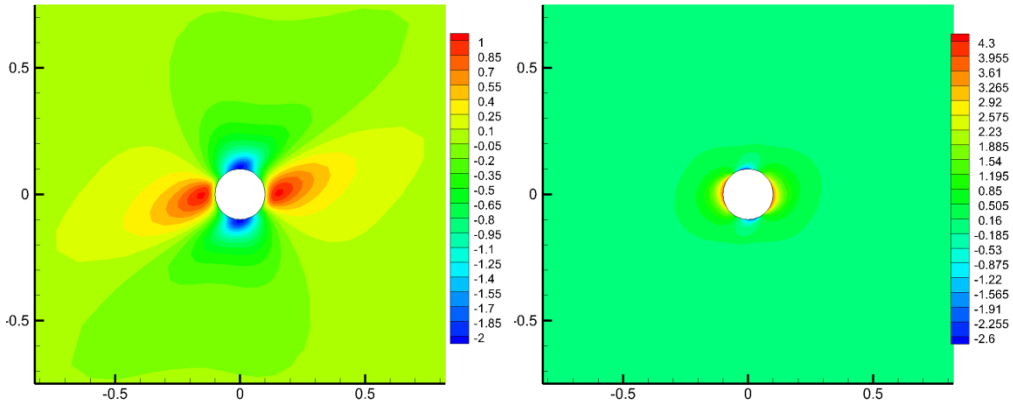

(a) Radial Stress **(b) Tangential Stress**

Fig. 3.120 Case 10: induced total stress distribution at t=30 minutes

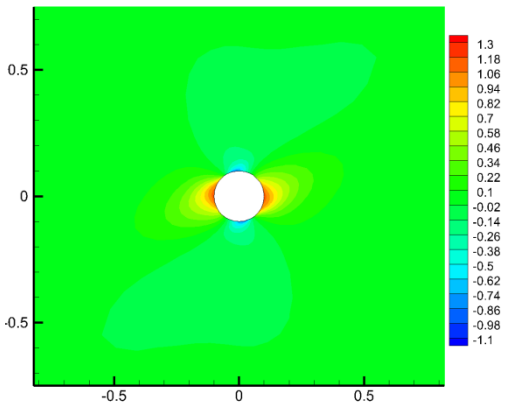

(c) Z Direction Stress

Fig. 3.120 Continued

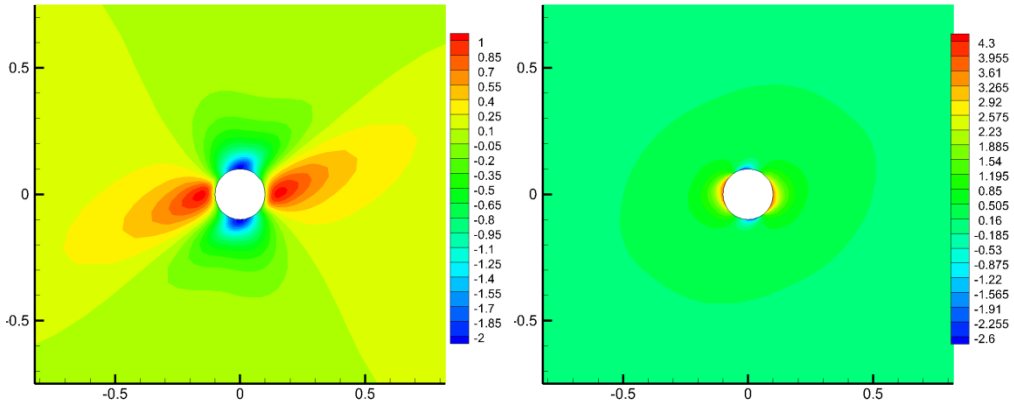

(a) Radial Stress **(b) Tangential Stress**

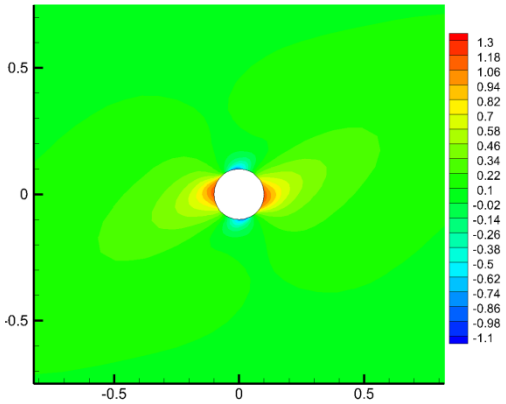

(c) Z Direction Stress

Fig. 3.121 Case 10: induced total stress distribution at t=3 days

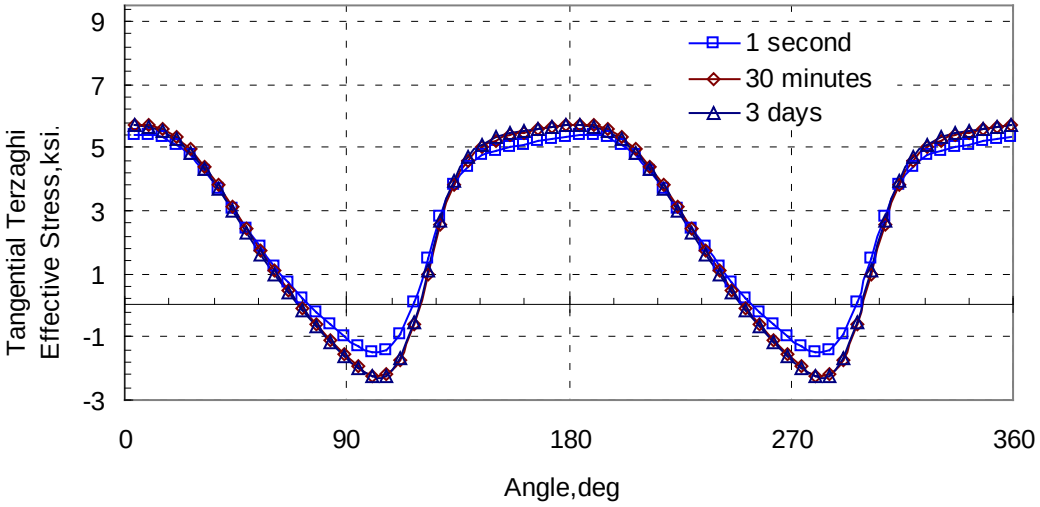

Fig. 3.122 Case 10: tangential Terzaghi's effective stress around wellbore

3.3.2.3. Case 11: dip=60°

Compared to Case 9, Case 12 shows the effect of 60° bedding plane.

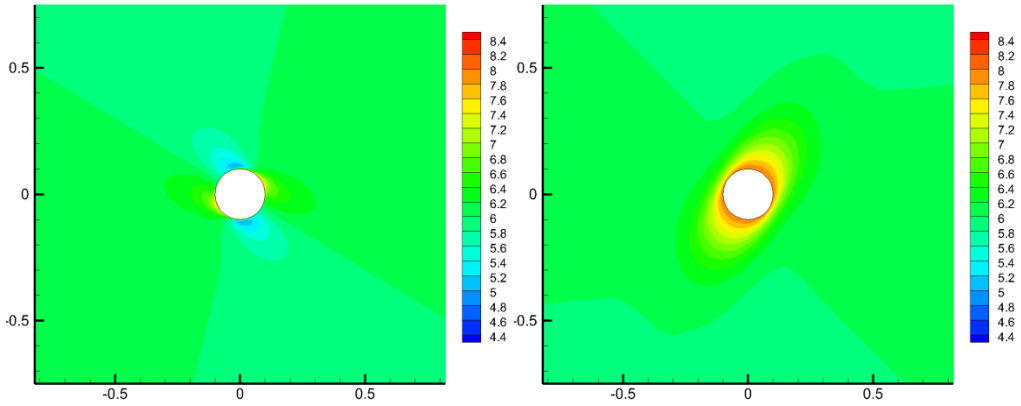

(a) t=1 second **(b) t=30 minutes**

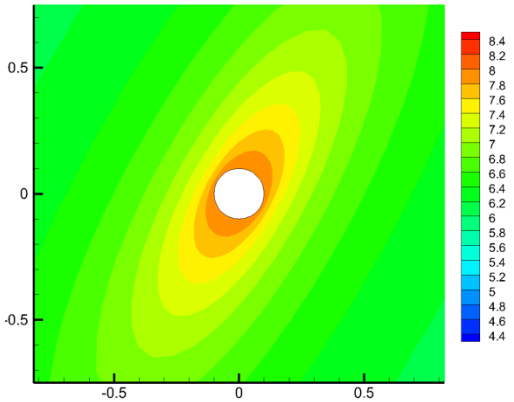

(c) t=3 days

Fig. 3.123 Case 11: pore pressure distribution

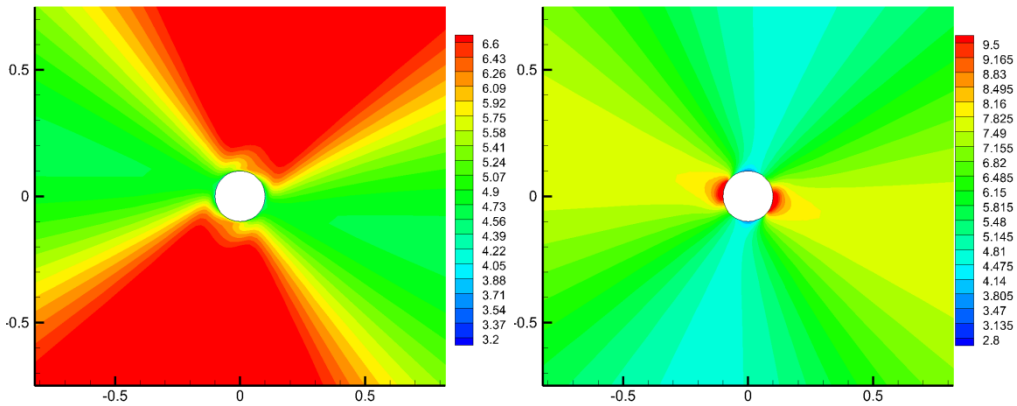

(a) Radial Stress **(b) Tangential Stress**

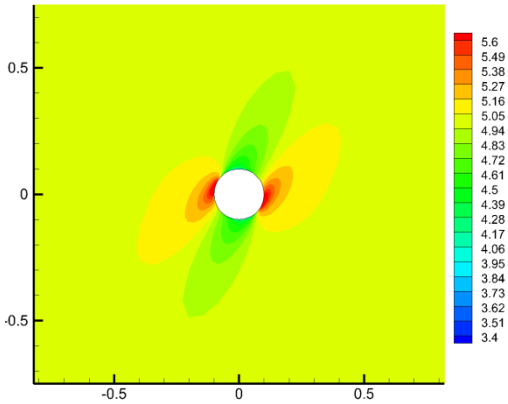

(c) Z Direction Stress

Fig. 3.124 Case 11: Biot's effective stress distribution at t=1 second

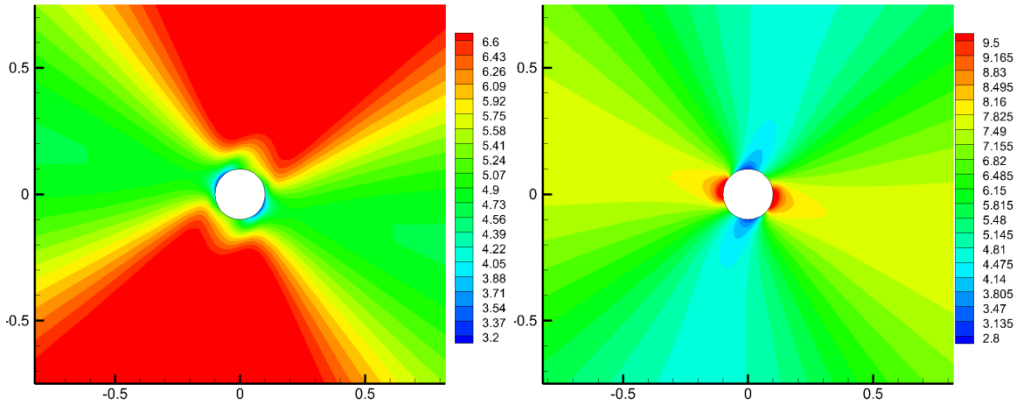

(a) Radial Stress **(b) Tangential Stress**

Fig. 3.125 Case 11: Biot's effective stress distribution at t=30 minutes

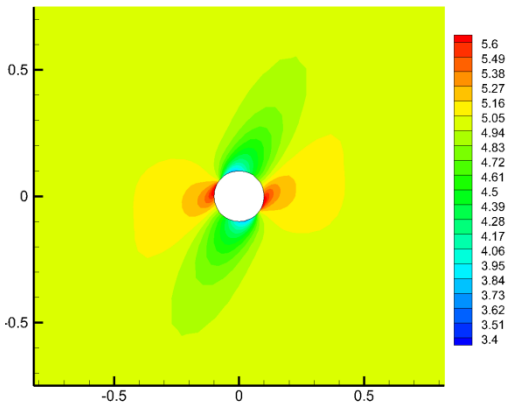

(c) Z Direction Stress

Fig. 3.125 Continued

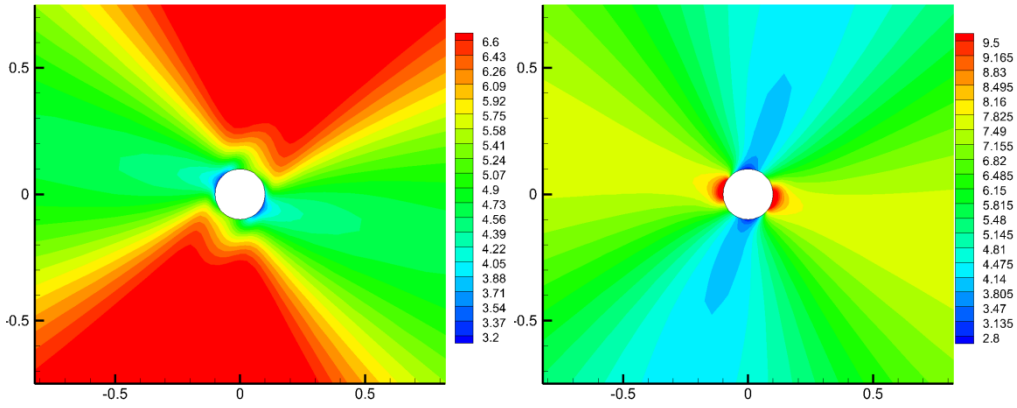

(a) Radial Stress **(b) Tangential Stress**

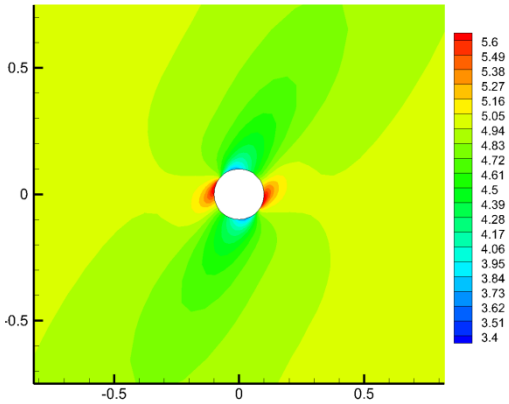

(c) Z Direction Stress

Fig. 3.126 Case 11: Biot's effective stress distribution at t=3 days

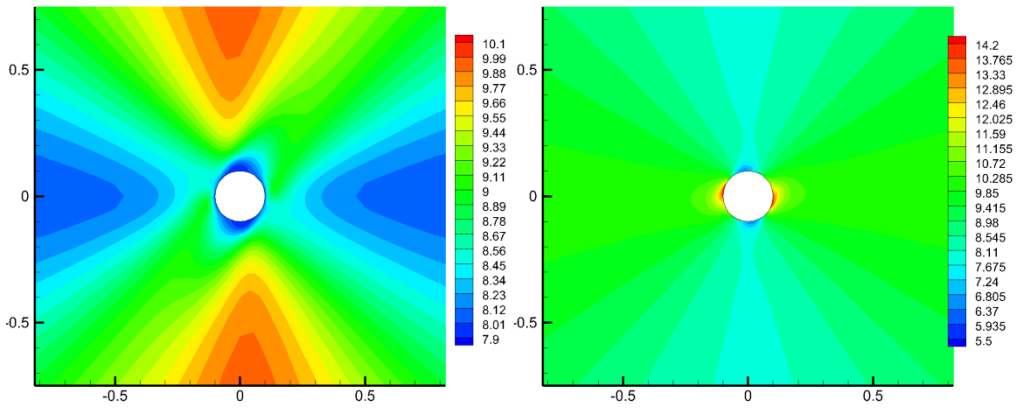

(a) Radial Stress **(b) Tangential Stress**

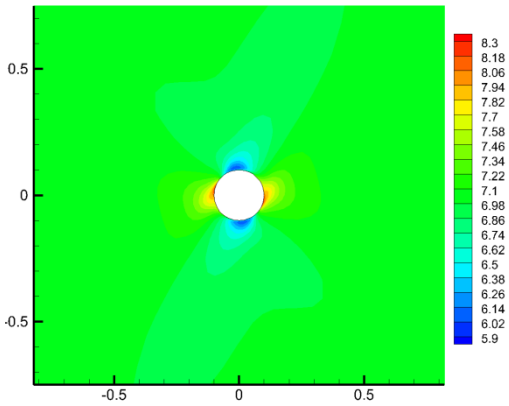

(c) Z Direction Stress

Fig. 3.127 Case 11: total stress distribution at t=1 second

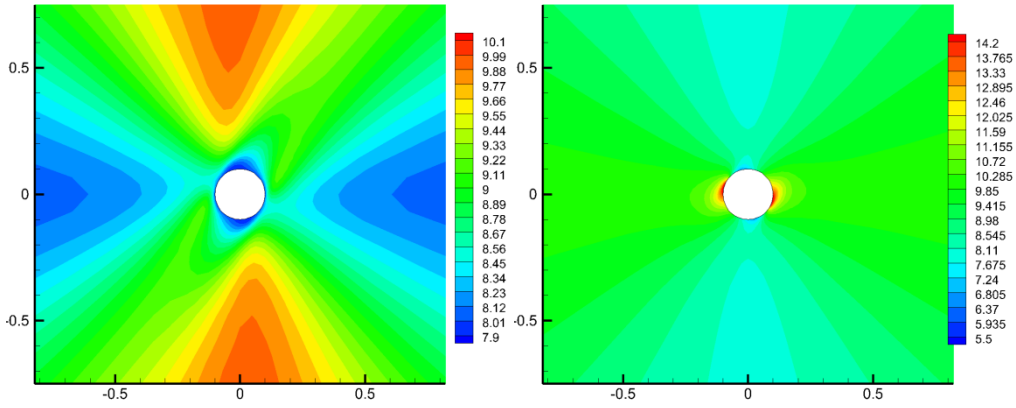

(a) Radial Stress **(b) Tangential Stress**

Fig. 3.128 Case 11: total stress distribution at t=30 minutes

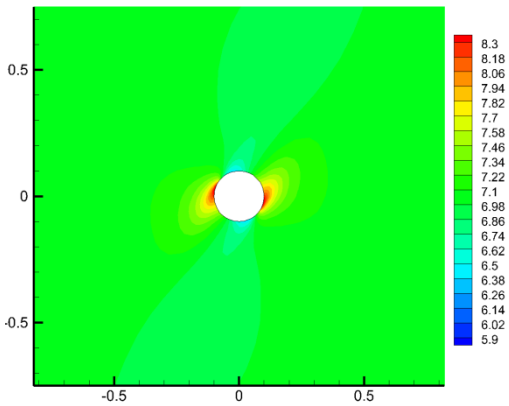

(c) Z Direction Stress

Fig. 3.128 Continued

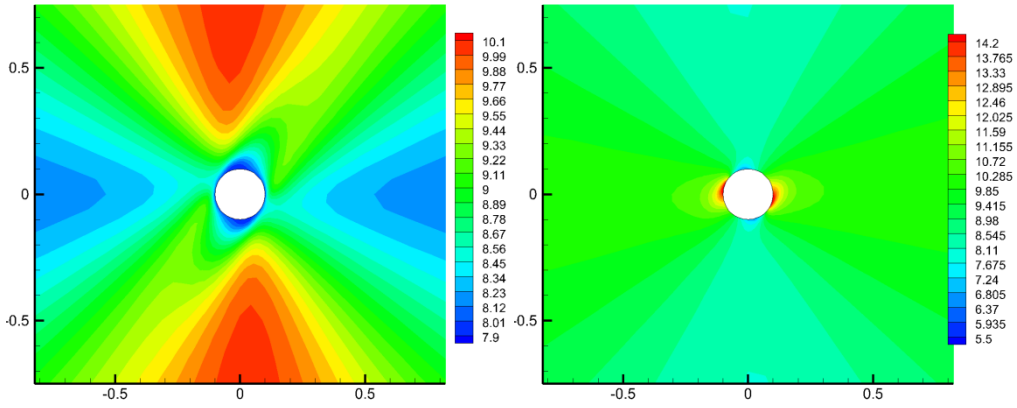

(a) Radial Stress **(b) Tangential Stress**

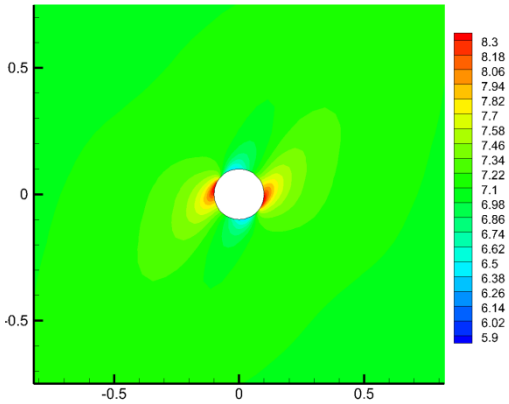

(c) Z Direction Stress

Fig. 3.129 Case 11: total stress distribution at t=3 days

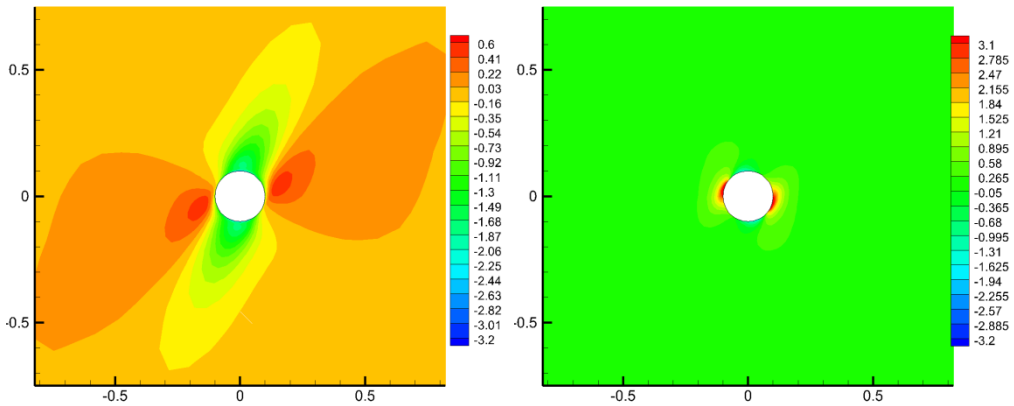

(a) Radial Stress **(b) Tangential Stress**

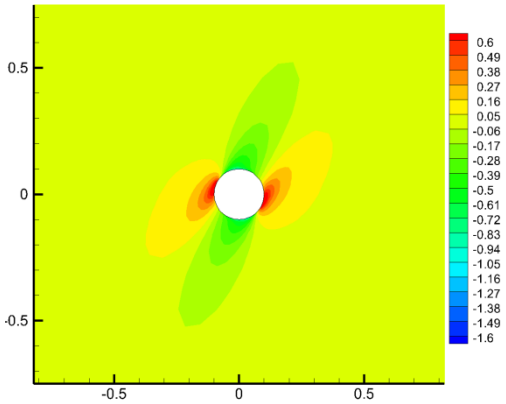

(c) Z Direction Stress

Fig. 3.130 Case 11: induced Biot's effective stress distribution at t=1 second

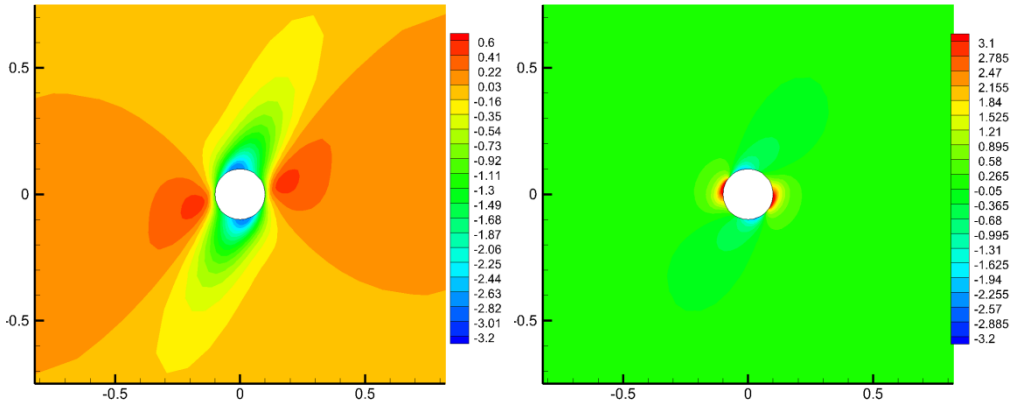

(a) Radial Stress **(b) Tangential Stress**

Fig. 3.131 Case 11: induced Biot's effective stress distribution at t=30 minutes

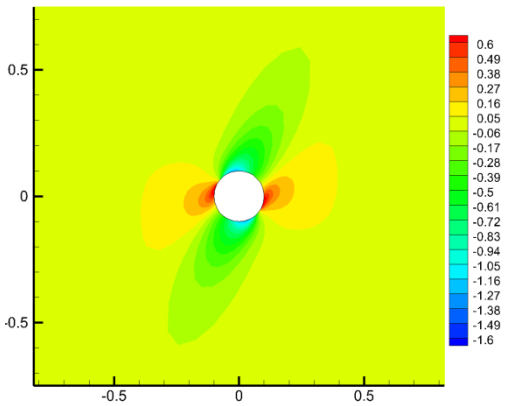

(c) Z Direction Stress

Fig. 3.131 Continued

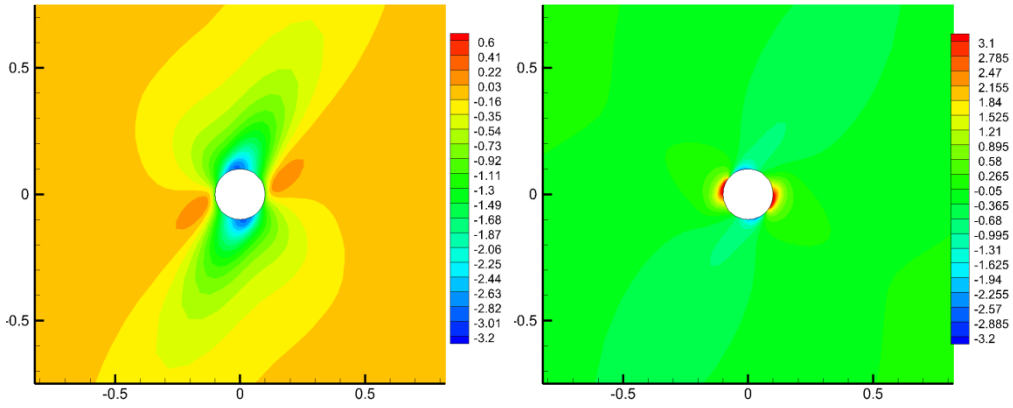

(a) Radial Stress **(b) Tangential Stress**

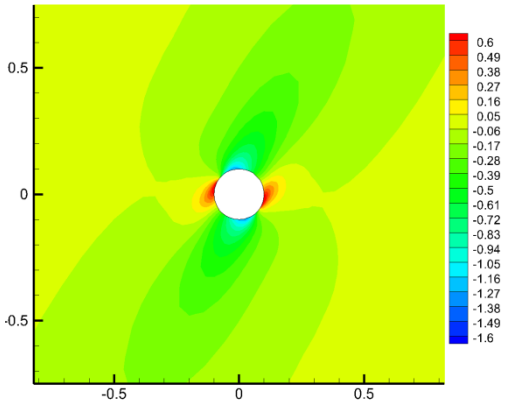

(c) Z Direction Stress

Fig. 3.132 Case 11: induced Biot's effective stress distribution at t=3 days

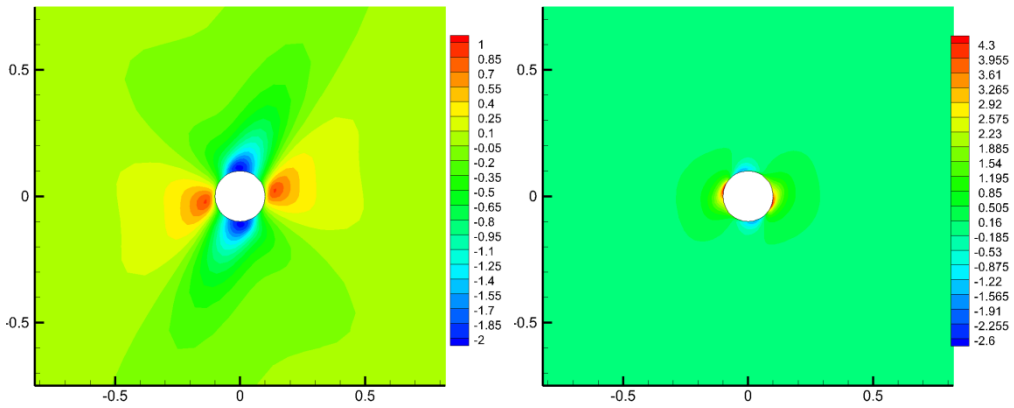

(a) Radial Stress **(b) Tangential Stress**

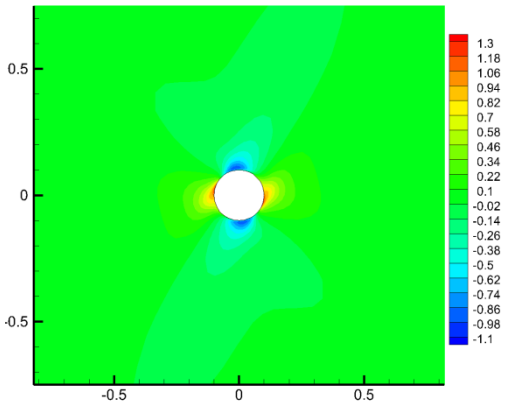

(c) Z Direction Stress

Fig. 3.133 Case 11: induced total stress distribution at t=1 second

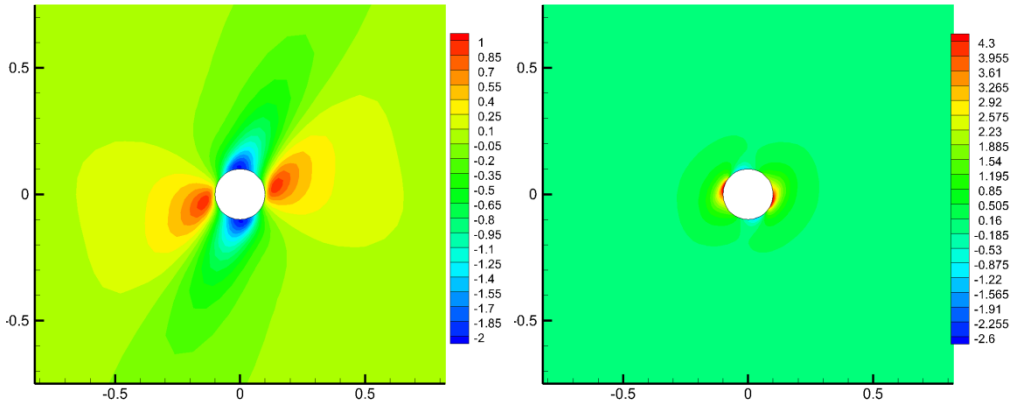

(a) Radial Stress **(b) Tangential Stress**

Fig. 3.134 Case 11: induced total stress distribution at t=30 minutes

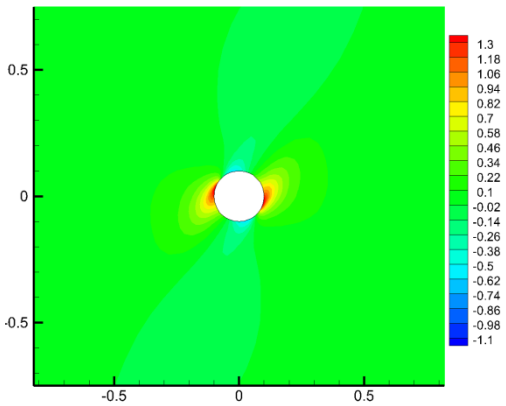

(c) Z Direction Stress

Fig. 3.134 Continued

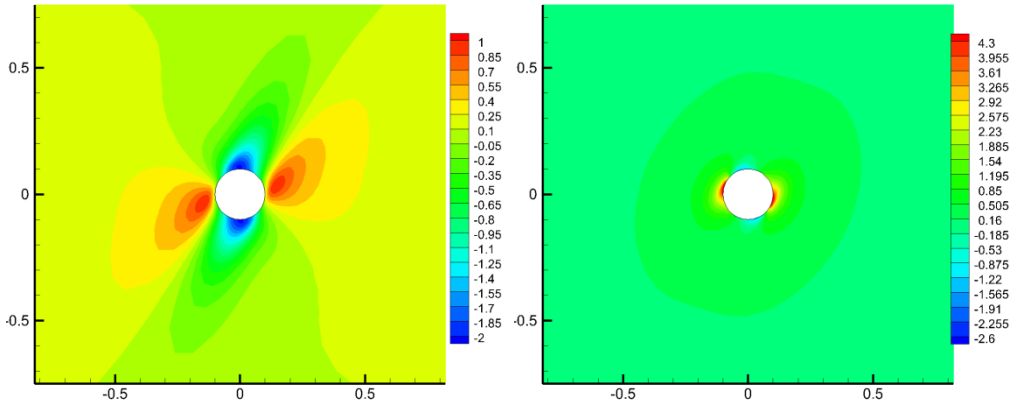

(a) Radial Stress **(b) Tangential Stress**

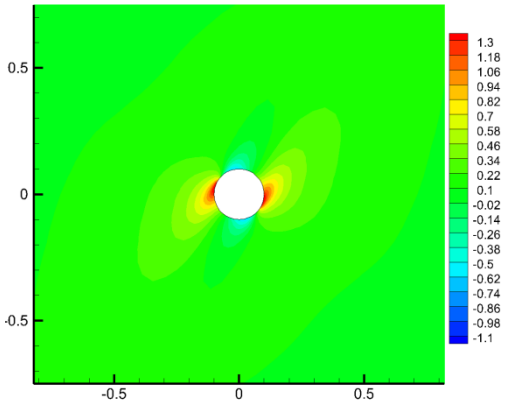

(c) Z Direction Stress

Fig. 3.135 Case 11: induced total stress distribution at t=3 days

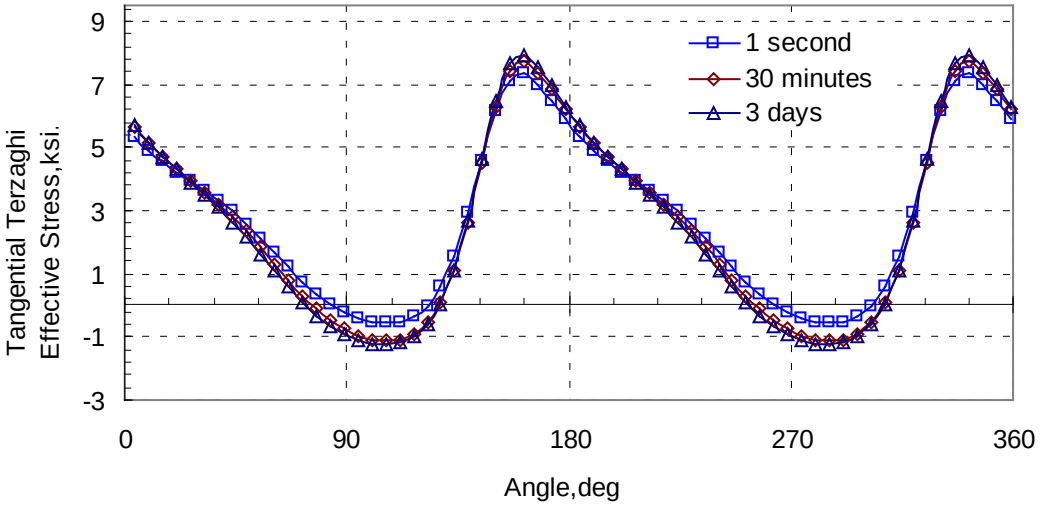

Fig. 3.136 Case 11: tangential Terzaghi's effective stress around wellbore

3.3.2.4. Case 12: dip=90°

Compared to Case 9, Case 12 shows the effect of vertical bedding plane.

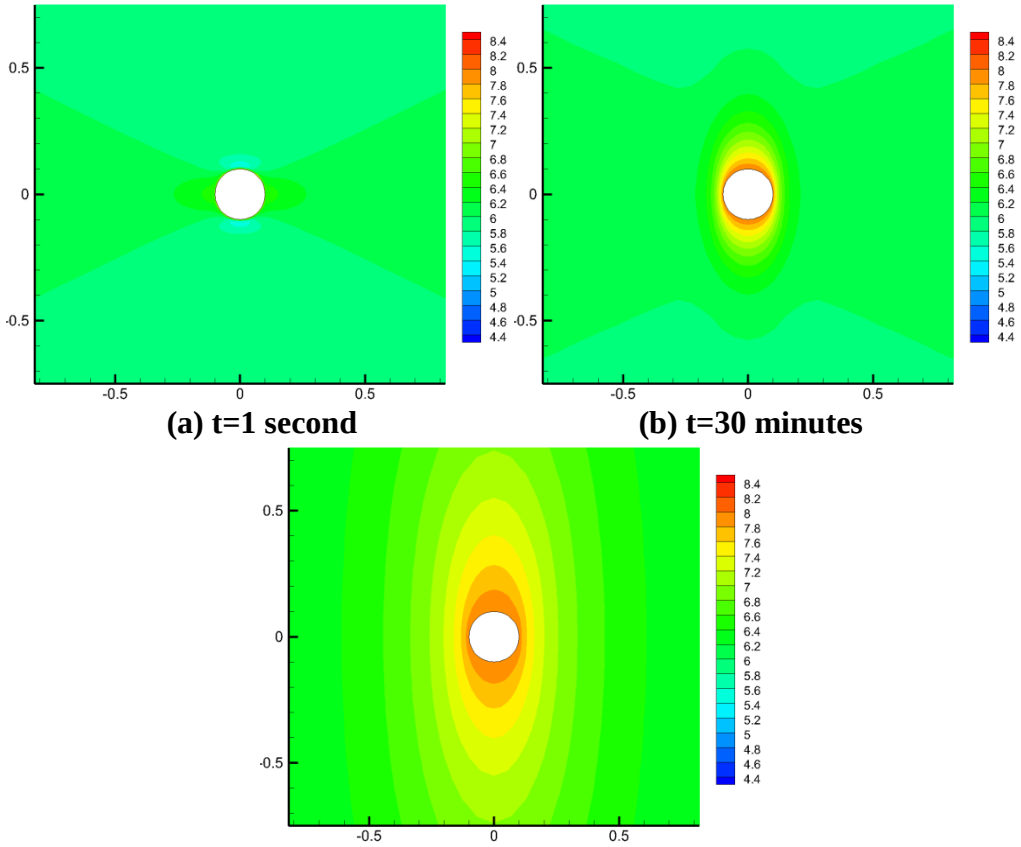

(a) t=1 second **(b) t=30 minutes**

(c) t=3 days

Fig. 3.137 Case 12: pore pressure distribution

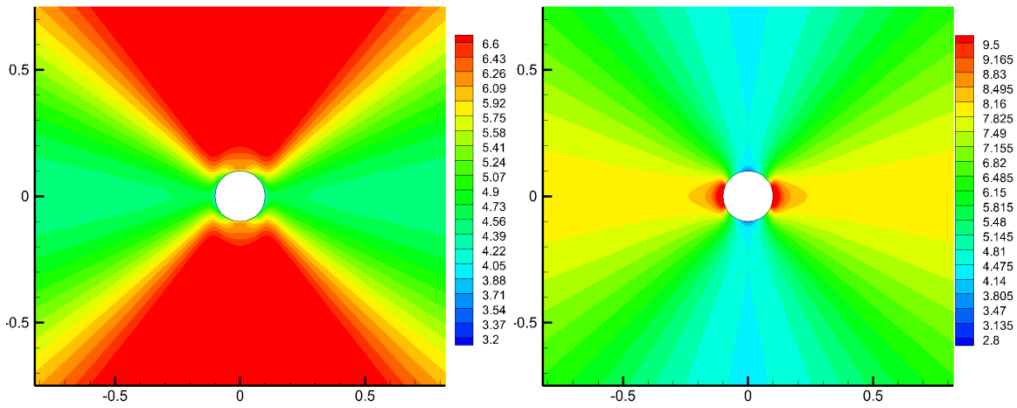

(a) Radial Stress **(b) Tangential Stress**

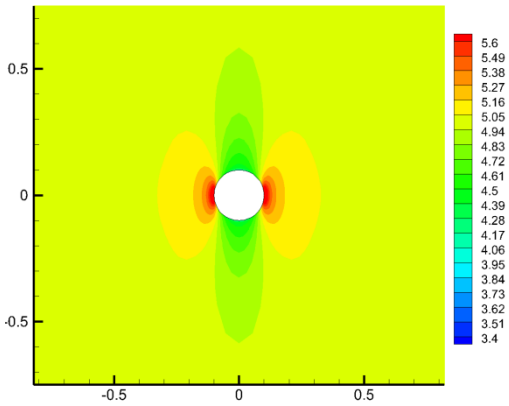

(c) Z Direction Stress

Fig. 3.138 Case 12: Biot's effective stress distribution at t=1 second

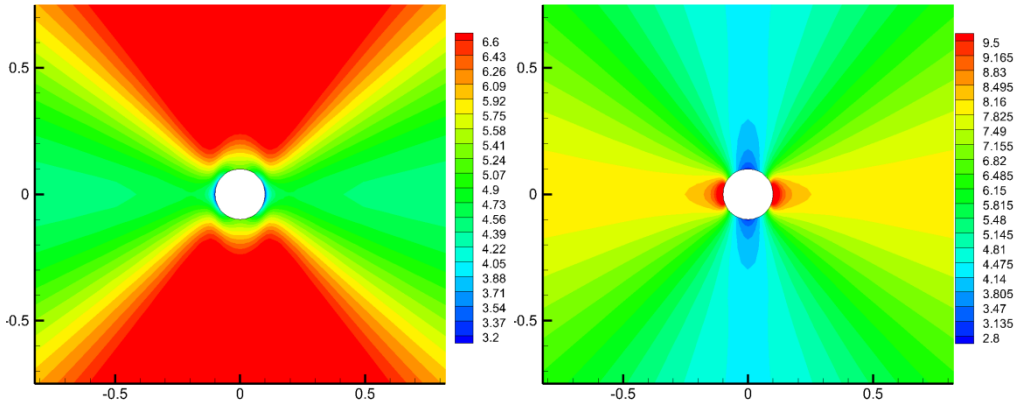

(a) Radial Stress **(b) Tangential Stress**

Fig. 3.139 Case 12: Biot's effective stress distribution at t=30 minutes

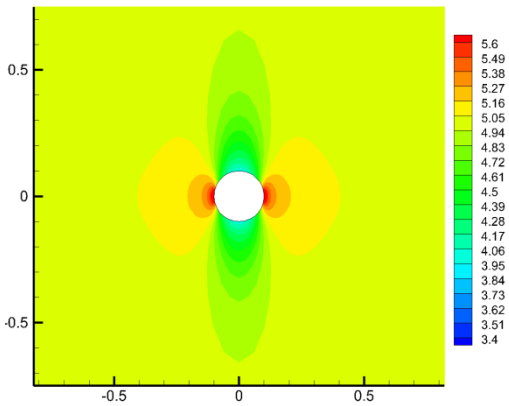

(c) Z Direction Stress

Fig. 3.139 Continued

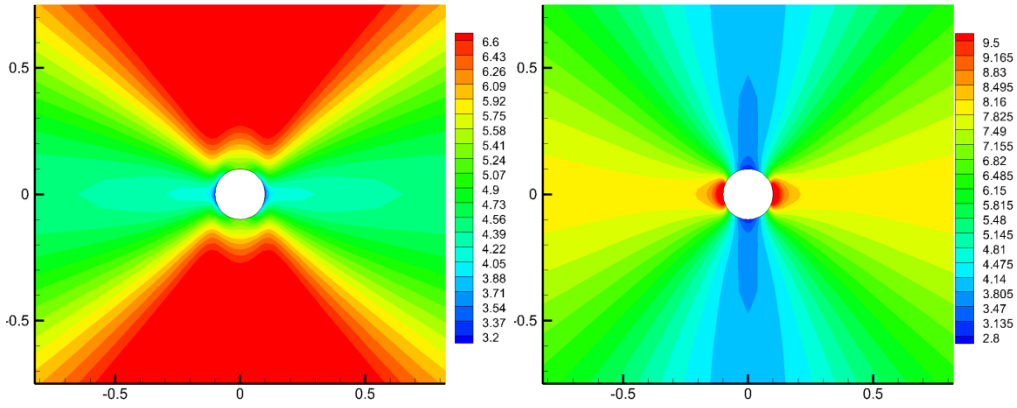

(a) Radial Stress **(b) Tangential Stress**

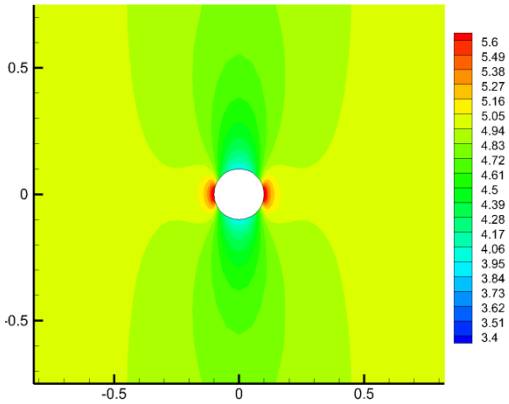

(c) Z Direction Stress

Fig. 3.140 Case 12: Biot's effective stress distribution at t=3 days

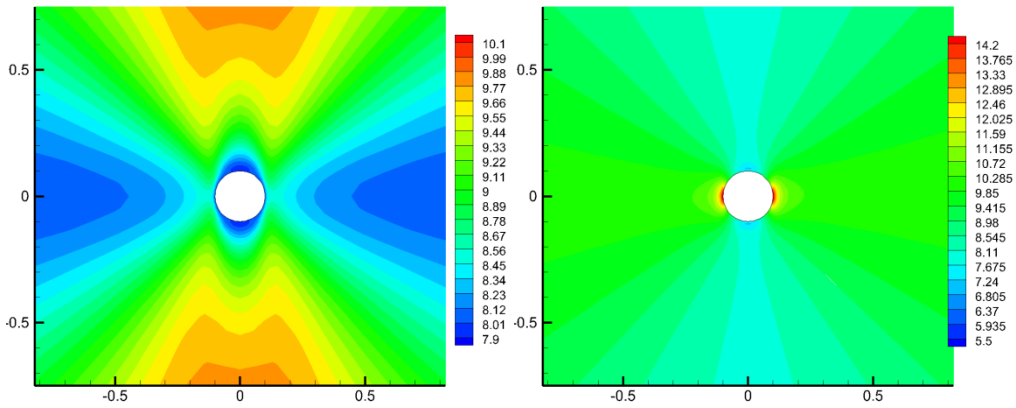

(a) Radial Stress **(b) Tangential Stress**

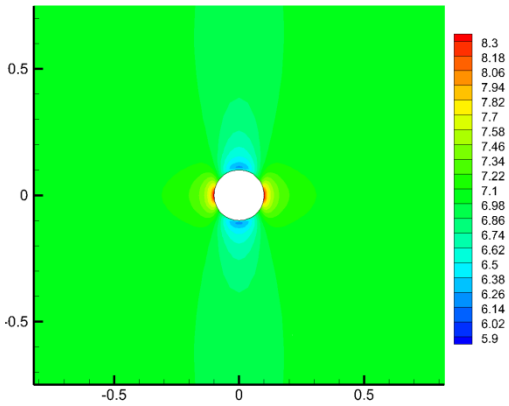

(c) Z Direction Stress

Fig. 3.141 Case 12: total stress distribution at t=1 second

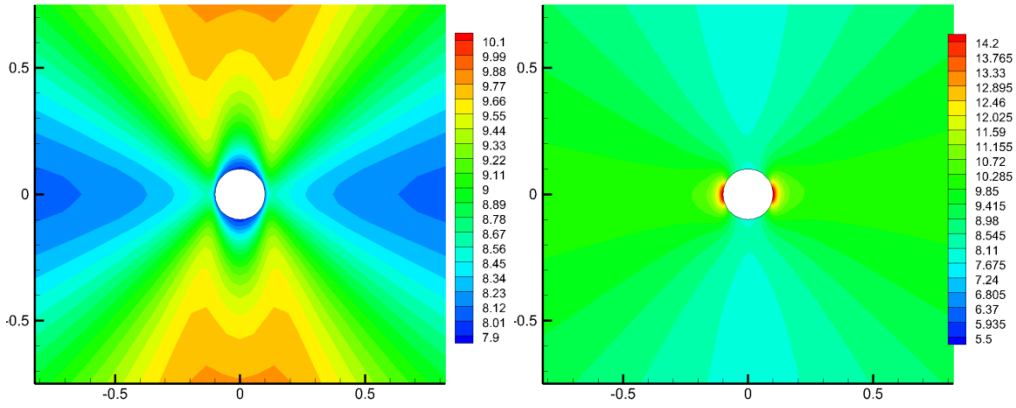

(a) Radial Stress **(b) Tangential Stress**

Fig. 3.142 Case 12: total stress distribution at t=30 minutes

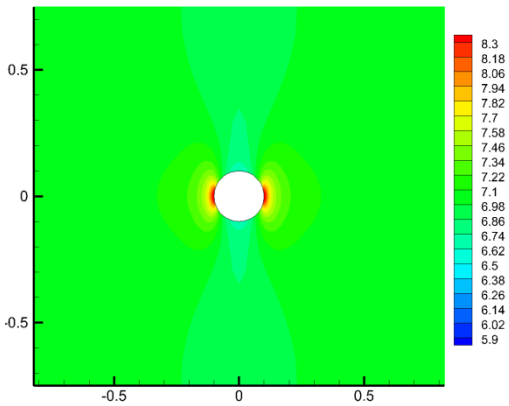

(c) Z Direction Stress

Fig. 3.142 Continued

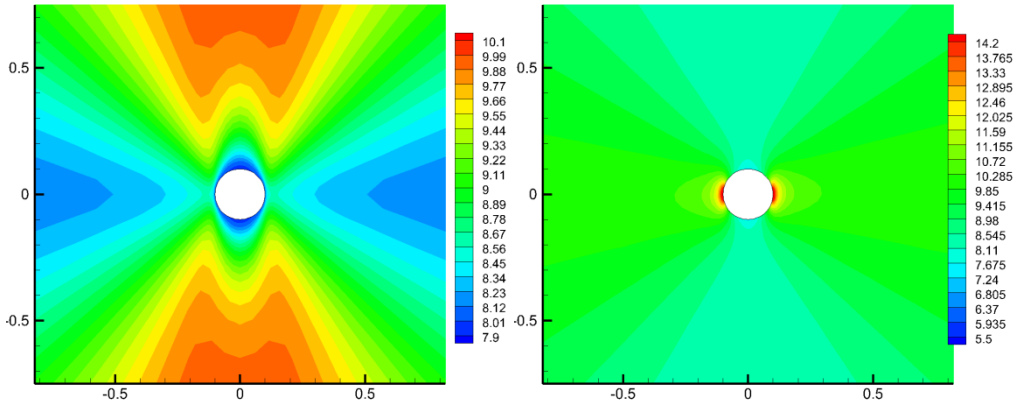

(a) Radial Stress **(b) Tangential Stress**

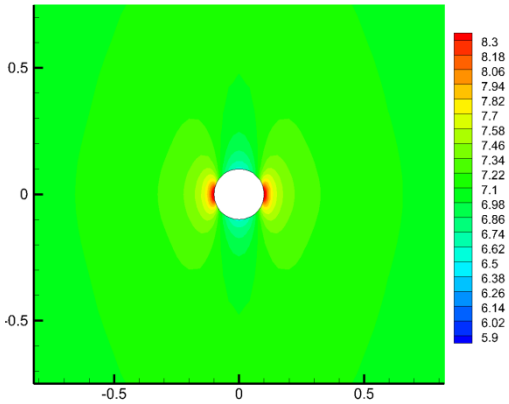

(c) Z Direction Stress

Fig. 3.143 Case 12: total stress distribution at t=3 days

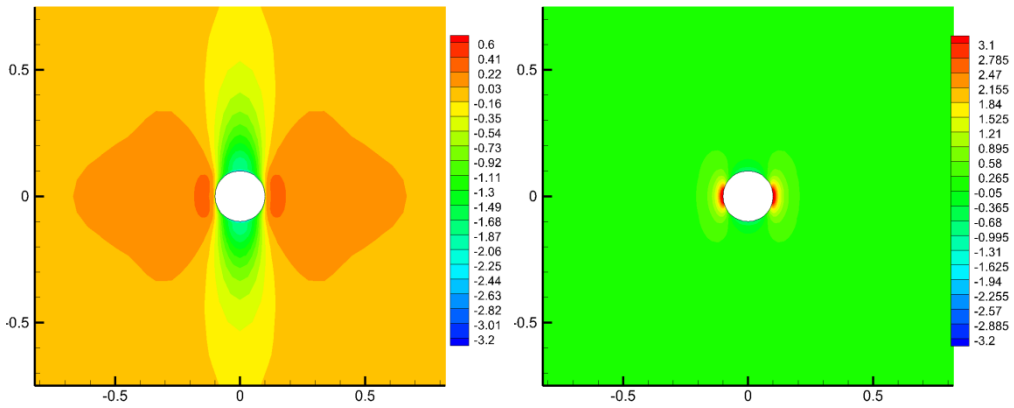

(a) Radial Stress **(b) Tangential Stress**

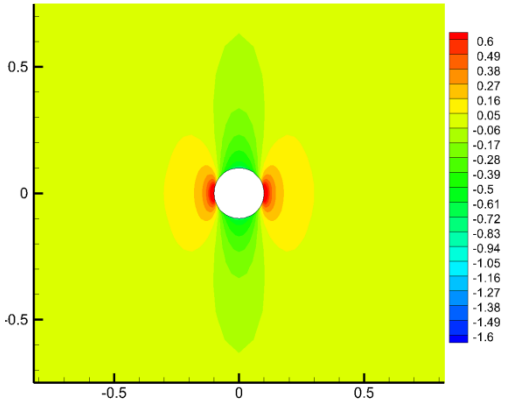

(c) Z Direction Stress

Fig. 3.144 Case 12: induced Biot's effective stress distribution at t=1 second

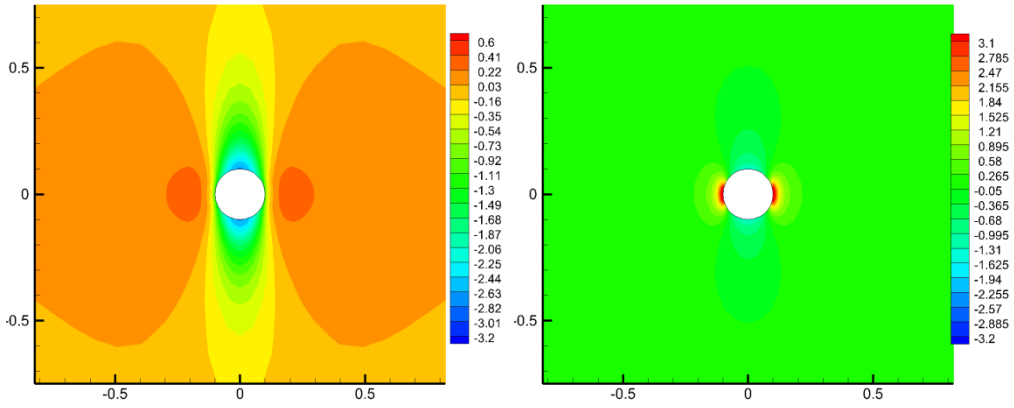

(a) Radial Stress **(b) Tangential Stress**

Fig. 3.145 Case 12: induced Biot's effective stress distribution at t=30 minutes

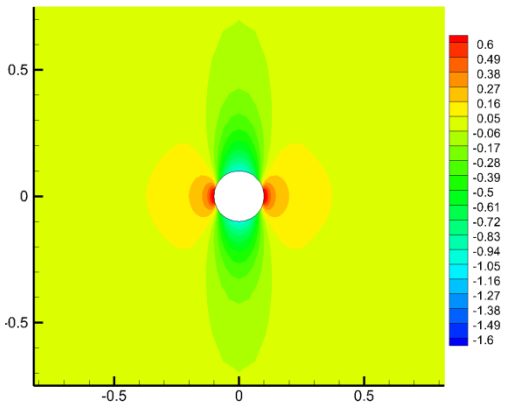

(c) Z Direction Stress

Fig. 3.145 Continued

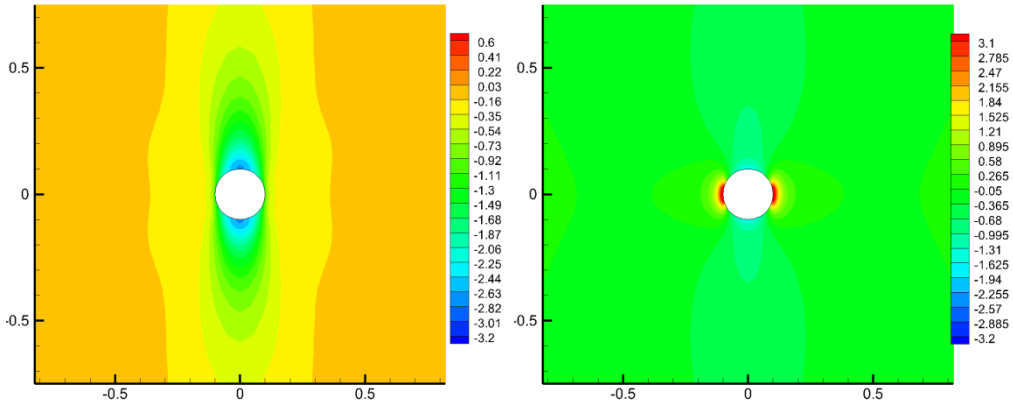

(a) Radial Stress **(b) Tangential Stress**

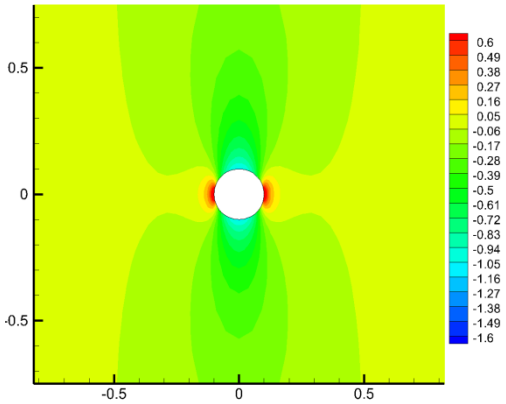

(c) Z Direction Stress

Fig. 3.146 Case 12: induced Biot's effective stress distribution at t=3 days

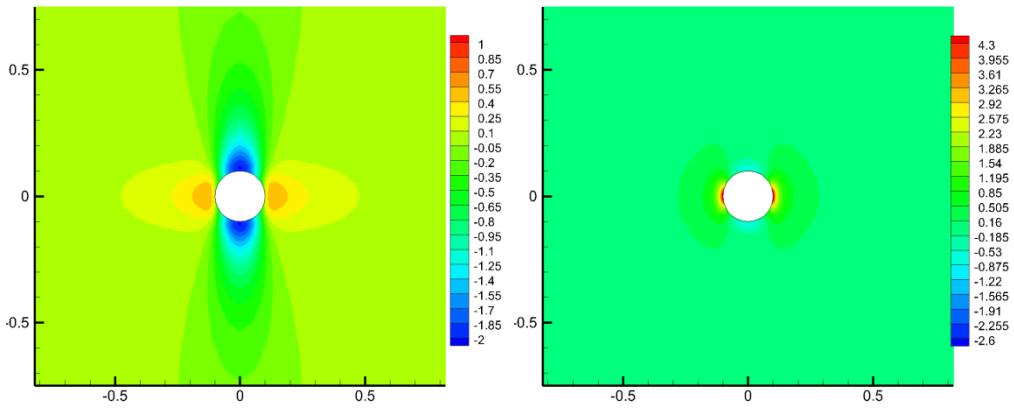

(a) Radial Stress **(b) Tangential Stress**

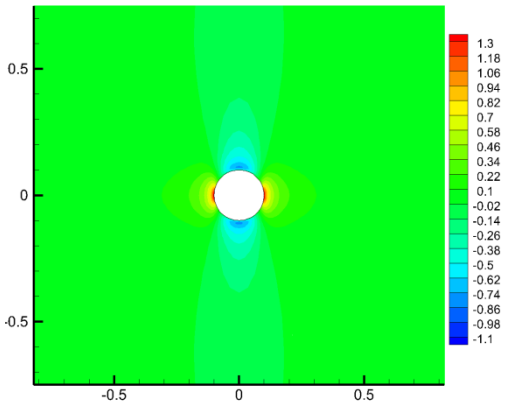

(c) Z Direction Stress

Fig. 3.147 Case 12: induced total stress distribution at t=1 second

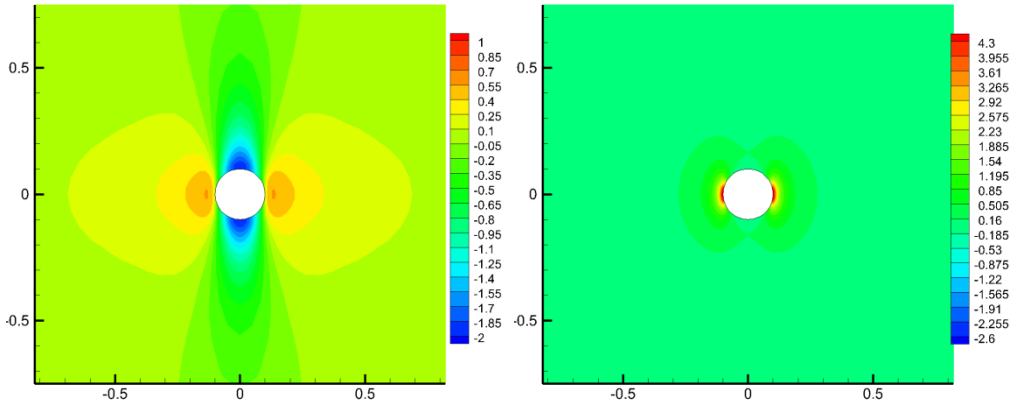

(a) Radial Stress **(b) Tangential Stress**

Fig. 3.148 Case 12: induced total stress distribution at t=30 minutes

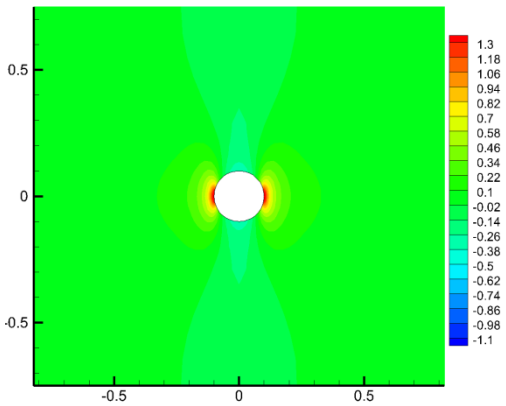

(c) Z Direction Stress

Fig. 3.148 Continued

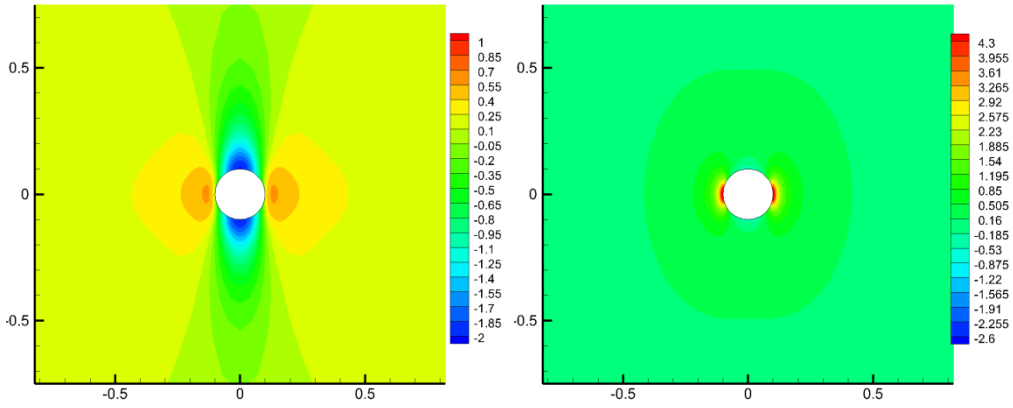

(a) Radial Stress **(b) Tangential Stress**

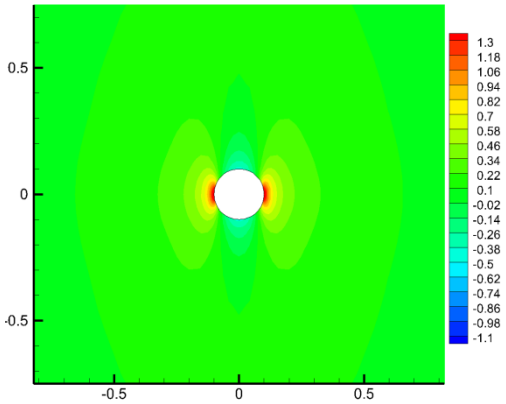

(c) Z Direction Stress

Fig. 3.149 Case 12: induced total stress distribution at t=3 days

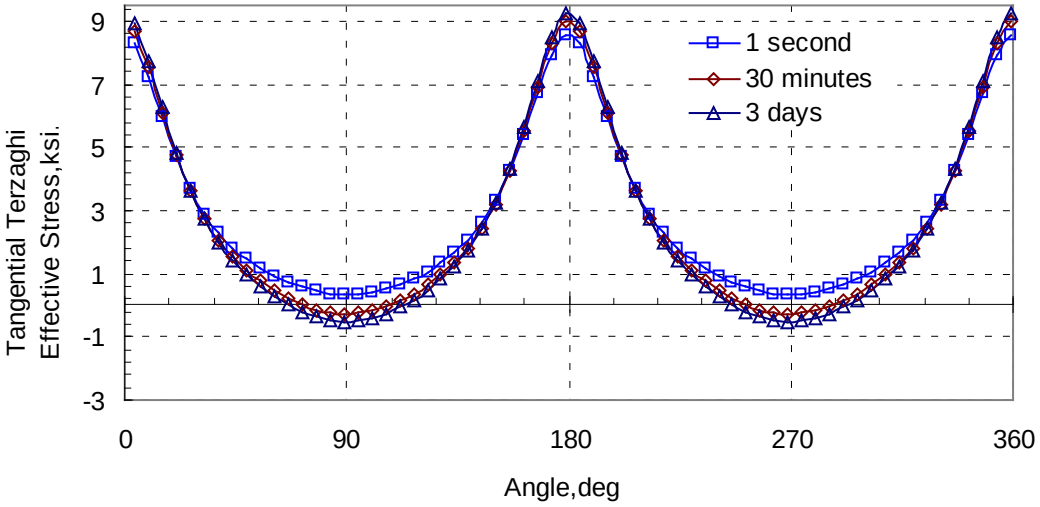

Fig. 3.150 Case 12: tangential Terzaghi's effective stress around wellbore

3.3.3. Summary

Comparing Case 10, 3 and 4 with Case 9, we found some interesting results discussed as follows.

Both the short-term and long-term pore pressure distributions are significantly influenced by the direction of bedding plane. For the short term, due to the excavation of the wellbore, the high pore pressure area appears in the horizontal direction on the wellbore wall and turns parallel to the bedding plane inside the wellbore wall. The low pore pressure area appears in the vertical direction on the wellbore wall and turns perpendicular to the bedding plane inside the wellbore wall. As the rock bedding plane rotates from the horizontal direction to the vertical direction, the pore pressure becomes more and more evenly distributed around the wellbore. For the long term, as the rock bedding plane rotates from the horizontal direction to the vertical direction, the pore pressure distribution remains the same shape but rotates with the bedding plane.

The induced total stress and the induced effective stress distributions are also influenced by the direction of bedding plane. The stress increasing area appears in the horizontal direction near the wellbore wall and turns parallel to the bedding plane inside the wellbore wall. The stress decreasing area appears in the vertical direction on the wellbore wall and also turns parallel to the bedding plane but in an opposite direction inside the wellbore wall. In other words, the induced stress distributions "rotate" in correspondence with the rock bedding plane.

Since the actual stresses can be treated as a superposition of induced stresses and initial in-situ stresses, the actual total stress and effective stress distributions exhibit

similar "rotation" phenomena as exhibited in induced stress distributions when the rock bedding plane rotates from the horizontal direction to the vertical direction. Notice that this "rotation" phenomena is usually more significant around the wellbore (see the actual total stress distributions in Fig. 3.113-Fig. 3.115 and Fig. 3.127-Fig. 3.129). Two possible reasons can account for this: the in-situ stresses are constant and their distributions do not "rotate" with the bedding plane angle; the induced stresses around wellbore are more significant than far field.

Due to the "rotation" phenomena, the shape of the tangential Terzaghi's effective stress around the wellbore also changes. Both the minimum value and its position alter with the rotation of rock bedding plane. This means different fracture initiation potential and position under different rock bedding orientation.

In summary, the study shows that the effect of bedding plane direction cannot be neglected. The pore pressure and stress distributions tend to "rotate" in correspondence with the rock bedding plane. The fracture initiation potential and position will alter when rock bedding orientation varies.

4. CONCLUSION AND SUMMARY

The principle of generalized plane-strain finite element formulation of anisotropic poroelastic problems is explained and a finite element model is developed from a plane-strain isotropic poroelastic model. Two numerical examples are simulated and the finite element results are compared with a closed form solution and another FE program. The validity of the developed finite element model is demonstrated. Using the validated finite element model, sensitivity analysis is carried out to evaluate the effects of transverse isotropy ratios, well azimuth, and rock bedding dip on pore pressure distribution, total and effective stress distribution and possibility of fracture initiation. The study shows following conclusions.

The short term pore pressure distribution is sensitive to E_v/E_h ratio, while the long term pore pressure distribution is only sensitive to K_v/K_h ratio. Restrained by equilibrium condition, the total stress distribution generally is not very sensitive to transverse isotropy ratios. The effective stress and fracture initiation are very sensitive to E_v/E_h ratio. ν_v/ν_h ratio only has large effect on z-direction stress.

The effect of well azimuth cannot be neglected. As the well rotates from minimum horizontal in-situ stress to maximum horizontal in-situ stress, the pore pressure and stress distributions tend to be more unevenly distributed around the wellbore, making the wellbore easier to fracture.

The effect of bedding plane direction cannot be neglected. The pore pressure and stress distributions tend to "rotate" in correspondence with the rock bedding plane. The fracture initiation potential and position will alter when rock bedding orientation varies.

REFERENCES

Aadnoy, B.S., 1989. Stresses around horizontal boreholes drilled in sedimentary rocks. Journal of Petroleum Science and Engineering, v. 2, p. 349-360.

Abousleiman, Y., Cui, L., 1998. Poroelastic solutions in transversely isotropic media for wellbore and cylinder. International Journal of Solids and Structures, v. 35, p. 4905-4929.

Amadei, B., 1983. Rock anisotropy and the theory of stress measurements. Springer-Verlag, New York.

Bai, M., Abousleiman, Y., Cui, L., Zhang, J., 1999. Dual-porosity poroelastic modeling of generalized plane strain. International Journal of Rock Mechanics and Mining Sciences, v. 36, p. 1087-1094.

Chen, G., Chenevert, M.E., Sharma, M.M., and Yu, M., 2003. A study of wellbore stability in shales including poroelastic, chemical, and thermal effects. Journal of Petroleum Science and Engineering, v. 38, p. 167-176.

Cheng, A.H.D., 1997. Material coefficients of anisotropic poroelasticity. International Journal of Rock Mechanics and Mining Sciences, v. 34, p. 199-205.

Cheng, A.H.D., 1998. On generalized plane strain poroelasticity. International Journal of Rock Mechanics and Mining Sciences, v. 35, p. 183-193.

Cheng, A.H.D., Abousleiman, Y., and Roegiers, J.C., 1993. Review of some poroelastic effects in rock mechanics. International Journal of Rock Mechanics and Mining Sciences & Geomechanics Abstracts, v. 30, p. 1119-1126.

Cui, L., Cheng, A.H.D., and Abousleiman, Y., 1997a. Poroelastic solution for an inclined borehole. Journal of Applied Mechanics, v. 64, p. 32-38.

Cui, L., Cheng, A.H.D., Kaliakin, V.N., Abousleiman, Y., and Roegiers, J.C., 1996. Finite element analyses of anisotropic poroelasticity: a generalized Mandel's problem and an inclined borehole problem. International Journal for Numerical and Analytical Methods in Geomechanics, v. 20, p. 381-401.

Cui, L., Kaliakin, V.N., Abousleiman, Y., and Cheng, A.H.D., 1997b. Finite element formulation and application of poroelastic generalized plane strain problems. International Journal of Rock Mechanics and Mining Sciences, v. 34, p. 953-962.

Detournay, E., and Cheng, A.H.D., 1988. Poroelastic response of a borehole in a non-hydrostatic stress field. International Journal of Rock Mechanics and Mining Sciences & Geomechanics Abstracts, v. 25, p. 171-182.

Detournay, E., Cheng, A.H.D., Roegiers, J.C., and McLennan, J.D., 1989. Poroelasticity considerations in in-situ stress determination by hydraulic fracturing. International Journal of Rock Mechanics and Mining Sciences & Geomechanics Abstracts, v. 26, p. 507-513.

Ghassemi, A., Diek, A., and Roegiers, J.C., 1998. A solution for stress distribution around an inclined borehole in shale. International Journal of Rock Mechanics and Mining Sciences, v. 35, p. 538-540.

Hoang, S.K., and Abousleiman, Y.N., 2010. Poroviscoelasticity of transversely isotropic cylinders under laboratory loading conditions. Mechanics Research Communications, v. 37, p. 298-306.

Kaewjuea, W., Senjuntichai, T., and Rajapakse, R.K.N.D., 2011. Poromechanical response of a finite elastic cylinder under axisymmetric loading. International Journal of Solids and Structures, v. 48, p. 346-356.

Kirsch. 1898. The theory of elasticity and the need of the strength of materials. Journal of the Association of German Engineers 42: 797-807.

Lekhnitskii, S.G. 1963. Theory of elasticity of an anisotropic elastic body, original edition. Holden Day Inc., San Fransisco.

Lekhnitskii, S.G. 1981. Theory of elasticity of an anisotropic body, original edition. Mir Publications, Moscow.

Obert, L., Duvall, Wilbur I., 1967. Rock mechanics and the design of structures in rock. Wiley, New York.

Rémond, A., and Naili, S., 2005. Transverse isotropic poroelastic osteon model under cyclic loading. Mechanics Research Communications, v. 32, p. 645-651.

Smith, I.M., Griffiths, D. V., 2004. Programming the finite element method. John Wiley & Sons, Hoboken, N.J.

Tao, Q., and Ghassemi, A., 2010. Poro-thermoelastic borehole stress analysis for determination of the in situ stress and rock strength. Geothermics, v. 39, p. 250-259.

Tran, M.H., and Abousleiman, Y.N., 2013. Anisotropic porochemoelectroelastic Mandel's problem solutions for applications in reservoir modeling and laboratory characterization. Mechanics Research Communications, v. 47, p. 89-96.

Zhang, J., 2013. Borehole stability analysis accounting for anisotropies in drilling to weak bedding planes. International Journal of Rock Mechanics and Mining Sciences, v. 60, p. 160-170.

Zhou, X., and Ghassemi, A., 2009. Finite element analysis of coupled chemo-poro-thermo-mechanical effects around a wellbore in swelling shale. International Journal of Rock Mechanics and Mining Sciences, v. 46, p. 769-778.

APPENDIX A.

UPGRADE FE PROGRAM FROM PLANE-STRAIN

TO GENERALIZED PLANE STRAIN

The finite element model used in this study is developed from a plane-strain isotropic poroelastic model. In this section, the steps to develop a generalized plane strain program from plane strain program is briefly discussed.

A.1. Add Displacement in Z Direction as a New DoF

As described before, displacement in Z direction is zero for plane strain problems while displacement in Z direction is non-zero but irrelevant to Z in generalized plane strain problems. A new DoF, displacement in Z direction must be added on each node. The number of Dofs on each element and total number of Dofs are thus changed.

Mechanical DoFs on each element in plane strain problems are:

$$[\hat{u}]_{3n_u\times 1} = [\hat{u}_x^1, \hat{u}_y^1, \hat{u}_x^2, \hat{u}_y^2 ..., \hat{u}_x^{n_u}, \hat{u}_y^{n_u}]^T,$$

Mechanical DoFs on each element in generalized plane strain problems are:

$$[\hat{u}]_{3n_u\times 1} = [\hat{u}_x^1, \hat{u}_y^1, \hat{u}_z^1, \hat{u}_x^2, \hat{u}_y^2, \hat{u}_z^2, ..., \hat{u}_x^{n_u}, \hat{u}_y^{n_u}, \hat{u}_z^{n_u}]^T,$$

$\hat{u}_x^i, \hat{u}_y^i, \hat{u}_z^i$ are the x, y, z displacements of node i in a given element,

n_u is the number of nodes with displacement DOFs in a given element.

Pore pressure Dofs still remain the same in generalized plane strain problems.

A.2. Modify shape function matrix, stress-strain matrix and pore pressure derivative matrix

There is one more Dof on each node in generalized plane strain problem and all the DoFs are irrelevant to time. As a result, the shape function matrix [S], stress-strain matrix [B_u] and pore pressure derivative matrix [B_p] in plane strain problem need to be modified to accommodate generalized plane strain problems

A.2.1. Shape function matrix for displacement and pore pressure

Due to the change of the number of DoFs, the dimension of shape function matrix also changes in generalized plane strain problem.

Shape function matrix for displacements in plane strain problems is:

$$[S_u]_{2\times 2n_u} = \begin{bmatrix} N_u^1 & 0 & N_u^2 & 0 & \dots & N_u^{n_u} & 0 \\ 0 & N_u^1 & 0 & N_u^2 & \dots & 0 & N_u^{n_u} \end{bmatrix},$$

Shape function matrix for displacements [S] in generalized plane strain problems is:

$$[S_u]_{3\times 3n_u} = \begin{bmatrix} N_u^1 & 0 & 0 & N_u^2 & 0 & 0 & \dots & N_u^{n_u} & 0 & 0 \\ 0 & N_u^1 & 0 & 0 & N_u^2 & 0 & \dots & 0 & N_u^{n_u} & 0 \\ 0 & 0 & N_u^1 & 0 & 0 & N_u^2 & \dots & 0 & 0 & N_u^{n_u} \end{bmatrix},$$

N_u^i is the shape function on node i for displacements discretization.

In generalized plane strain problems, the shape function matrix has the same pattern as in 3D problems. However, because the DoFs are irrelevant of Z, we should use the same shape function as in plane strain problems. DO NOT use shape functions for 3D problems.

Shape function matrix for pore pressure in plane strain problems and generalized plane strain problems remains the same:

$$[S_p]_{1\times n_p} = [N_p^1, N_p^2, ..., N_p^{n_p}],$$

N_p^i is the shape function on node i for pore pressure discretization. Similarly, we should use the same shape function as in plane strain problems.

A.2.2. Stress-strain matrix and pore pressure derivative matrix

Due to the change of DoFs, the dimension and pattern of stress-strain matrix also change in generalized plane strain problem.

Stress-strain matrix in plane strain problems is:

$$[B_u]_{3\times 2n_u} = \begin{bmatrix} \frac{\partial N_u^1}{\partial x} & & \frac{\partial N_u^2}{\partial x} & & \cdots & \frac{\partial N_u^{n_u}}{\partial x} & \\ & \frac{\partial N_u^1}{\partial y} & & \frac{\partial N_u^2}{\partial y} & \cdots & & \frac{\partial N_u^{n_u}}{\partial y} \\ \frac{\partial N_u^1}{\partial y} & \frac{\partial N_u^1}{\partial x} & \frac{\partial N_u^2}{\partial y} & \frac{\partial N_u^2}{\partial x} & \cdots & \frac{\partial N_u^{n_u}}{\partial y} & \frac{\partial N_u^{n_u}}{\partial x} \end{bmatrix}$$

Stress-strain matrix in 3D problems is:

$$[B_u]_{6\times 3n_u}=\begin{bmatrix} \frac{\partial N_u^1}{\partial x} & & & \frac{\partial N_u^2}{\partial x} & & & \cdots & \frac{\partial N_u^{n_u}}{\partial x} & 0 & 0 \\ & \frac{\partial N_u^1}{\partial y} & & & \frac{\partial N_u^2}{\partial y} & & \cdots & 0 & \frac{\partial N_u^{n_u}}{\partial y} & 0 \\ & & \frac{\partial N_u^1}{\partial z} & & & \frac{\partial N_u^2}{\partial z} & \cdots & 0 & 0 & \frac{\partial N_u^{n_u}}{\partial z} \\ \frac{\partial N_u^1}{\partial y} & \frac{\partial N_u^1}{\partial x} & & \frac{\partial N_u^2}{\partial y} & \frac{\partial N_u^2}{\partial x} & & \cdots & \frac{\partial N_u^{n_u}}{\partial y} & \frac{\partial N_u^{n_u}}{\partial x} & 0 \\ & \frac{\partial N_u^1}{\partial z} & \frac{\partial N_u^1}{\partial y} & & \frac{\partial N_u^2}{\partial z} & \frac{\partial N_u^2}{\partial y} & \cdots & 0 & \frac{\partial N_u^{n_u}}{\partial z} & \frac{\partial N_u^{n_u}}{\partial y} \\ \frac{\partial N_u^1}{\partial z} & & \frac{\partial N_u^1}{\partial x} & \frac{\partial N_1^x}{\partial z} & & \frac{\partial N_u^2}{\partial x} & \cdots & \frac{\partial N_u^{n_u}}{\partial z} & 0 & \frac{\partial N_u^{n_u}}{\partial x} \end{bmatrix}$$

Note that N_u^i is independent of z, so $\frac{\partial N_u^i}{\partial z}=0$, stress-strain matrix in generalized plane strain problems is:

$$[B_u]_{6\times 3n_u}=\begin{bmatrix} \frac{\partial N_u^1}{\partial x} & & & \frac{\partial N_u^2}{\partial x} & & & \cdots & \frac{\partial N_u^{n_u}}{\partial x} & 0 & 0 \\ & \frac{\partial N_u^1}{\partial y} & & & \frac{\partial N_u^2}{\partial y} & & \cdots & 0 & \frac{\partial N_u^{n_u}}{\partial y} & 0 \\ & & 0 & & & 0 & \cdots & 0 & 0 & 0 \\ \frac{\partial N_u^1}{\partial y} & \frac{\partial N_u^1}{\partial x} & & \frac{\partial N_u^2}{\partial y} & \frac{\partial N_u^2}{\partial x} & & \cdots & \frac{\partial N_u^{n_u}}{\partial y} & \frac{\partial N_u^{n_u}}{\partial x} & 0 \\ & 0 & \frac{\partial N_u^1}{\partial y} & & 0 & \frac{\partial N_u^2}{\partial y} & \cdots & 0 & 0 & \frac{\partial N_u^{n_u}}{\partial y} \\ 0 & & \frac{\partial N_u^1}{\partial x} & 0 & & \frac{\partial N_u^2}{\partial x} & \cdots & 0 & 0 & \frac{\partial N_u^{n_u}}{\partial x} \end{bmatrix}$$

Comparing above three matrices, it is obvious that: the pattern of stress-strain matrix in generalized plane strain problems is the same as in 3D problems. The subroutine "beemat" to assemble the $[B_u]$ matrix from derivatives of the shape functions for 3D problem still works for generalized plane strain problems.

Pore pressure derivative matrix in 3D problems is:

$$[B_p]_{3\times n_p} = \begin{bmatrix} \frac{\partial N_p^1}{\partial x} & \frac{\partial N_p^2}{\partial x} & \cdots & \frac{\partial N_p^{n_p}}{\partial x} \\ \frac{\partial N_p^1}{\partial y} & \frac{\partial N_p^2}{\partial y} & \cdots & \frac{\partial N_p^{n_p}}{\partial y} \\ \frac{\partial N_p^1}{\partial z} & \frac{\partial N_p^2}{\partial z} & \cdots & \frac{\partial N_p^{n_p}}{\partial z} \end{bmatrix}$$

Pore pressure derivative matrix in plane strain problems is:

$$[B_p]_{3\times n_p} = \begin{bmatrix} \frac{\partial N_p^1}{\partial x} & \frac{\partial N_p^2}{\partial x} & \cdots & \frac{\partial N_p^{n_p}}{\partial x} \\ \frac{\partial N_p^1}{\partial y} & \frac{\partial N_p^2}{\partial y} & \cdots & \frac{\partial N_p^{n_p}}{\partial y} \end{bmatrix}$$

Note that N_p^i are independent of z, so $\frac{\partial N_p^i}{\partial z}=0$, pore pressure derivative matrix in generalized plane strain problems is:

$$[B_p]_{3\times n_p} = \begin{bmatrix} \frac{\partial N_p^1}{\partial x} & \frac{\partial N_p^2}{\partial x} & \cdots & \frac{\partial N_p^{n_p}}{\partial x} \\ \frac{\partial N_p^1}{\partial y} & \frac{\partial N_p^2}{\partial y} & \cdots & \frac{\partial N_p^{n_p}}{\partial y} \\ 0 & 0 & \cdots & 0 \end{bmatrix}$$

Because $\frac{\partial N_p^i}{\partial z}=0$ and $\frac{\partial N_u^i}{\partial z}=0$, the subroutine "shape_der" to calculate derivatives of the shape functions needs to be modified to accommodate generalized plane strain problems.

APPENDIX B.

FAILURE CRITERIA FOR ROCKS

Two types of failure may occur in rock: shear failure and tensile failure.

B.1. Shear Failure

Mohr-Coulomb failure criterion and Drucker-Prager failure criterion are two widely used shear failure criterion in geomechanics.

- Mohr-Coulomb Failure Criterion

The Mohr-Coulomb failure criterion can be expressed as:

$\tau \le [\tau] = \sigma \tan(\phi) + c$ (compression positive)

where

$[\tau]$ is the shear strength,

τ is the shear stress,

σ is the normal stress,

c is the cohesion,

ϕ is the internal friction angle.

From Mohr's circle, τ and σ can be expressed in principal stress when $\tau = [\tau] = \sigma \tan(\phi) + c$:

$$\sigma = \frac{\sigma_1 + \sigma_3}{2} - \frac{\sigma_1 - \sigma_3}{2} \sin\phi$$

$$\tau = \frac{\sigma_1 - \sigma_3}{2} \cos\phi$$

- Drucker-Prager Failure Criterion

The Drucker-Prager failure criterion can be expressed as:

$f_{DP} = \sqrt{J_2} - \alpha I_1 - k$ (compression positive)

where

f_{DP} is the failure function, f_{DP}>0 means shear failure.

I_1 is the first stress invariant,

J_2 is the second deviatoric stress invariant,

α and k are material constants.

I_1 and J_2 can be expressed in principal stress:

$$I_1 = \sigma_1 + \sigma_2 + \sigma_3$$

$$J_2 = \sqrt{\frac{1}{6}[(\sigma_1 - \sigma_2)^2 + (\sigma_2 - \sigma_3)^2 + (\sigma_1 - \sigma_3)^2]}$$

α and k can be expressed in terms of cohesion (c) and internal friction angle (ϕ) [Drucker and Prager, 1952]:

$$\alpha = \frac{\sin\phi}{\sqrt{3}\sqrt{3 + \sin^2\phi}}$$

$$k = \frac{\sqrt{3}c\cos\phi}{\sqrt{3 + \sin^2\phi}}$$

In this study, the Drucker-Prager failure criterion is used. α and k are calculated from c and ϕ in Mohr-Coulomb failure criterion.

A shear failure safety factor is introduced in this study:

$$SF_{sh}=\frac{k}{\sqrt{J_2}-\alpha I_1}=\frac{k}{f_{DP}+k}$$

When $0< SF_{sh} <1$, shear failure occurs.

Note: SF_{sh} may less than zero when deviatoric stress is very small comparing to isotropic stress

B.2. Tension Failure (Tension Cut-off)

In case of the stress go to the tensile regime a tension cut-off value, the tensile strength, must be specified. The tensile failure occurs when the tensile stress exceeds this specified value:

$\sigma_3 < T$ (compression positive)

where

σ_3 is the minimum principal stress,

T is the tensile strength.

A tension failure safety factor is introduced in this study:

$$SF_t=\frac{T}{\sigma_3}$$

When $0< SF_t <1$, tension failure occurs.

Note: SF_t may less than zero when σ_3 is still in compression.